Identification of autophagy-modulating natural products and derivatives for the elimination of therapy-resistant tumor cells

Inaugural-Dissertation

zur Erlangung des Doktorgrades
der Mathematisch-Naturwissenschaftlichen Fakultät
der Heinrich-Heine-Universität Düsseldorf

vorgelegt von

Jana Deitersen

aus Essen

Düsseldorf, Mai 2020

aus dem Institut für Molekulare Medizin I

der Heinrich-Heine-Universität Düsseldorf

Gedruckt mit der Genehmigung der

Mathematisch-Naturwissenschaftlichen Fakultät der

Heinrich-Heine-Universität Düsseldorf

Referent: Univ.-Prof. Dr. Björn Stork

Koreferent: Univ.-Prof. Dr. Peter Proksch

Tag der mündlichen Prüfung in englischer Sprache:

Eidesstattliche Erklärung

Ich versichere an Eides statt, dass die Dissertation von mir selbständig und ohne unzulässige fremde Hilfe unter Beachtung der „Grundsätze zur Sicherung guter wissenschaftlicher Praxis an der Heinrich-Heine-Universität Düsseldorf“ erstellt worden ist. Die vorliegende Arbeit wurde von mir selbständig verfasst und keine anderen als die angegebenen Hilfsmittel verwendet. Alle wörtlich oder inhaltlich übernommenen Stellen habe ich als solche gekennzeichnet. Zudem versichere ich, dass ich die vorliegende Dissertation nur in diesem und keinem anderen Promotionsverfahren eingereicht habe und diesem kein früheres Promotionsverfahren vorausgegangen ist.

_____ _____

Ort, Datum Jana Deitersen

一步一个脚印。

Ein Schritt, ein Fußabdruck.

Acknowledgement

Mein besonderer Dank gilt meinem Doktorvater Prof. Dr. Björn Stork für die hervorragende fachliche Betreuung, angeregte Diskussionen und Anleitung zur wissenschaftlichen Selbstständigkeit. Jemanden zum Mentor zu haben, dessen geistige Wahlheimat Gelsenkirchen ist, hat mir meinen Ruhrpott ins Rheinland gebracht.

Weiterhin danke ich meinem Zweitgutachter Prof. Peter Proksch für die Begutachtung dieser Arbeit und darüber hinaus für seine überragende Expertise auf dem Gebiet der Naturstoffe, seine chinesischen Kontakte und uneingeschränkte Passion für unsere gemeinsamen Kooperationsprojekte.

Großer Dank gilt auch Prof. Sebastian Wesselborg, an dessen Institut für Molekulare Medizin I ich diese Arbeit angefertigt habe. Das wertvollste Inventar seines Instituts sind die Kolleginnen und Kollegen, die mir Wegbegleiter, Familienersatz und Freunde sind, und ohne diese die vorliegende Arbeit nicht möglich gewesen wäre. Danke, thank you, 谢谢, gracias!

Diese Arbeit war ein Teilprojekt eines interdisziplinären Graduiertenkollegs, in welchem pharmazeutische, chemische, biologische und medizinische Expertise zusammengefunden hat. Daher möchte ich mich bei allen Kolleginnen und Kollegen des GRK2158, dessen Koordinatorin Martina Holz und der DFG für die Förderung bedanken. Weiterer Dank gilt allen Kooperationspartnern und Co-Autoren, welche in Abschnitt 4 ausdrücklich erwähnt werden.

Mille grazie a Maria Chiara Monti e le sue ragazze per l'ospitalità, per darmi il benvenuto nel tuo laboratorio e famiglie. Grazie cucciolotte!

Die Motivation für diese Doktorarbeit entstammt hauptsächlich einer inhärenten Neugier, für deren Förderung ich im Besonderen fähigen Professoren, Lehrern und Erziehern danken möchte. Ausschlaggebend dabei waren meine Eltern, Petra und Dirk, die mich gelehrt haben, Fragen zu stellen bis niemand eine Antwort weiß und Fragen zu beantworten bis niemand mehr fragt.

Für die Geduld, das Verständnis, und Toleranz möchte ich meiner gesamten Familie und meinen Freunden danken. Besonders danke ich Daniel, der mich geduldig mit der Wissenschaft geteilt hat, sich viele Laborgeschichten anhören musste und alle meiner wissenschaftlichen Texte Korrektur gelesen hat. Er hat mich motiviert, wenn meine Leidenschaft zur Wissenschaft mehr Leiden als Wissen geschaffen hat.

Zu guter Letzt bedanke ich mich bei allen Forscherinnen und Forschern, auf deren Arbeiten ich aufbauen konnte und die maßgeblich zur Naturstoff- und Autophagieforschung durch die Etablierung von Methoden und Aufklärung von Signalwegen beigetragen haben.

Abbreviations

3-MA	3-methyladenine
5-LO	5-lipo-oxygenase
ACAT1	acetyl-CoA acetyltransferase, see THIL
ACON	aconitate hydratase
ADP	Adenosine diphosphate
AKT	RAC-alpha serine/threonine-protein kinase
AMP	Adenosine monophosphate
AMPK	5'-AMP-activated protein kinase
AP-MS	affinity purification prior to mass spectrometry analysis
ATG	autophagy-related
ATP	Adenosine triphosphate
BAK	BCL-2 antagonist/killer
BAX	BCL-2-associated X protein
BCL-2	B-cell lymphoma 2
Bcl-2-L-13	Bcl-2-like protein 13
BRCA1	Breast Cancer 1
CALCOCO2	calcium-binding and coiled-coil domain-containing protein 2, see NBR1
CCCP	carbonyl cyanide m-chlorophenyl hydrazone
CDDP, also CisPt	cisplatin
CMA	chaperone-mediated autophagy
CPS1	carbamoyl-phosphate synthase 1
(H)CQ	(hydroxy)chloroquine
DARTS	Drug affinity response target stability
ER	endoplasmic reticulum
ERBB2	Receptor tyrosine-protein kinase erbB-2, see HER2
FKBP12	FK506 binding protein 12
FRB	FKBP12-rapamycin binding
FUNDC1	FUN14 domain-containing protein 1
GABARAP	γ-amino-butyric acid receptor-associate protein
GATE-16	Golgi-associated ATPase enhancer of 16 kDa
GFP/RFP	green/red fluorescent protein
HER2	human epidermal growth factor receptor 2
HS71A	heat shock 70 kDa protein 1A
HS90A	heat shock protein HSP 90α
HSC70, hsc70	heat shock-cognate protein of 70 kDa
LC3	Microtubule-associated proteins 1A/1B light chain 3
LIR	LC3-interacting region
log P	octanol-water partition coefficient
mPGES-1	microsomal prostaglandin E2 synthase-1
mTOR	Mammalian/mechanistic target of rapamycin
mTORC1/2	Mammalian/mechanistic target of rapamycin complex 1/2
NAD(P)H	reduced Nicotinamide adenine dinucleotide (phosphate)
NBR1	next to BRCA1 gene 1 protein
NDP52	nuclear dot protein 52
NIH	National Institutes of Health
NIX	BCL-2/adenovirus E1B 19 kDa protein-interacting protein 3-like
NQO1	NAD(P)H dehydrogenase [quinone] 1, formerly called DT diaphorase
OMA1	Overlapping with the m-AAA protease 1 homolog
OPA1	Optic atrophy protein 1
OPTN	optineurin
p62/SQSTM1	protein of 62 kDa, also Sequestosome-1
PAINS	pan-assay interference compounds
PARL	presenilin-associated rhomboid-like protease
PI	phosphatidylinositol
PI3K	phosphatidylinositol 3-kinase
PI3P	phosphatidylinositol 3-phosphate
PINK1	PTEN-induced putative kinase protein 1
PTEN	phosphatidylinositol 3,4,5-trisphosphate 3-phosphatase
PYGB, also bGP	glycogen phosphorylase
RAB1B1	Ras-related protein Rab-1B
RB1CC1	RB1-inducible coiled-coil protein 1
ROS	reactive oxygen species
shRNA	short/small hairpin ribonucleic acid
SNAP	synaptosomal-associated protein
SNARE	soluble N-ethylmaleimide-sensitive-factor attachment receptor
SOD2	mitochondrial superoxide dismutase
STAT3, Stat3	Signal transducer and activator of transcription 3
TAX1	transient axonal glycoprotein 1
TAX1BP1	TAX1-binding protein 1
THIL, also ACAT1	Thiamine-monophosphate kinase
TIM	translocase of inner membrane
t-LiP-MRM	targeted limited proteolysis
TOM	translocase of outer membrane
vATPase	vacuolar ATPase
VDAC1	voltage-dependent anion-selective channel protein 1
Vps34	vacuolar protein sorting 34
WIPI	WD repeat domain phosphoinositide-interacting protein

Amino acids

Amino acid	Single letter code
Alanine	A
Cysteine	C
Aspartic acid	D
Glutamic acid	E
Phenylalanine	F
Glycine	G
Histidine	H
Isoleucine	I
Lysine	K
Leucine	L
Methionine	M
Asparagine	N
Proline	P
Glutamine	Q
Arginine	R
Serine	S
Threonine	T
Valine	V
Tryptophan	W
Tyrosine	Y

Table of Contents

Summary

Autophagy is an evolutionary conserved intracellular degradation pathway for the elimination of long-lived or misfolded proteins, aggregates, pathogenic particles or entire organelles. During macroautophagy (in this thesis referred to as autophagy), double-membrane autophagosomes isolate harmful intracellular components, which then become degraded into macronutrients within the lysosome. Thereby, autophagy is involved in a plethora of human diseases such as cancer.

Basal autophagy in our bodily cells aims to prevent tumorigenesis by removing potential threat. In cancer cells, autophagy protects from nutrient starvation and genotoxic stress during chemotherapy. Inhibition of autophagy was shown to re-sensitize cancer cells to the lethal effects of chemotherapy, radiotherapy and targeted therapies, while also enhanced induction of autophagy could aid anti-cancer therapy by driving cancer cells into an autophagic cell death. So far, multiple clinical trials reported benefits of combinational therapies of approved drugs with autophagy modulators to overcome therapy-resistance. However, most known modulators of autophagy target additional pathways and create a need for novel more specific compounds. Among a natural compound library, we therefore searched for novel drugs or lead structures to modulate autophagy and/or overcome therapy-resistance.

We identified several natural compounds that were able to induce or inhibit autophagy, among which we focused on the phloroglucinyl-pyrone arzanol and a class of hydroxyanthraquinones. We investigated their modes of action, and characterized arzanol in detail. Interestingly, arzanol not only inhibited autophagic flux, it also caused mitochondrial damage by targeting mitochondrial oxidoreductases. In this, we attribute the observed formation of immature autophagosomes to the induction of mitophagy. Its cytotoxic effects reduced cancer cell viability both in cisplatin-sensitive and -resistant bladder carcinoma cells and further sensitized these cancer cells against first-line treatment with cisplatin.

Among the natural compound library, we further identified phomoxanthone A, a compound that is known to sensitize therapy-resistant cancer cells to cisplatin. We investigated its mode of action and designated it as potent mitotoxin, inducing the fragmentation of the inner mitochondrial membrane. In addition, we propose the urea cycle enzyme CPS1 as a novel target of phomoxanthone A.

In this thesis, we discuss the structures and activities of phomoxanthone A, arzanol, and hydroxyanthraquinones, and provide vital information for their use in further anti-cancer drug development.

Zusammenfassung

Autophagie ist ein evolutionär konservierter, intrazellulärer Abbauweg zur Eliminierung langlebiger oder fehlgefalteter Proteine, Aggregate, pathogener Partikel oder ganzer Organellen. Während der Makroautophagie (in dieser Dissertation als Autophagie bezeichnet) isolieren Autophagosomen schädliche intrazelluläre Komponenten, die dann innerhalb des Lysosoms zu Makronährstoffen abgebaut werden. Dabei ist die Autophagie an einer Vielzahl menschlicher Krankheiten wie Krebs beteiligt. Die basale Autophagie in unseren Körperzellen zielt darauf ab, die Tumorentstehung zu verhindern, indem potenzielle Bedrohungen beseitigt werden. In Krebszellen schützt die Autophagie während der Chemotherapie vor Nährstoffmangel und genotoxischem Stress. Es wurde gezeigt, dass die Hemmung der Autophagie Krebszellen für die tödlichen Auswirkungen von Krebstherapien erneut sensibilisiert. Jedoch könnte auch eine verstärkte Induktion der Autophagie die Krebstherapie unterstützen, indem Krebszellen in einen autophagischen Zelltod getrieben werden. Bisher berichteten mehrere klinische Studien Vorteile von Kombinationstherapien zugelassener Arzneimittel mit Autophagie-Modulatoren zur Überwindung von Therapieresistenzen. Die meisten bekannten Modulatoren der Autophagie zielen jedoch auf zusätzliche Signalwege ab und erfordern daher neue spezifischere Verbindungen. In einer Bibliothek von Naturstoffen suchten wir daher nach neuartigen Medikamenten oder Leitstrukturen, um die Autophagie zu modulieren und / oder Therapieresistenzen zu überwinden.

Wir identifizierten mehrere natürliche Verbindungen, die Autophagie induzieren oder hemmen konnten, darunter das Phloroglucinylpyron Arzanol und eine Klasse von Hydroxyanthrachinonen. Wir untersuchten ihre Wirkmechanismen und charakterisierten Arzanol im Detail. Interessanterweise hemmte Arzanol nicht nur die autophagische Abbaurate, sondern verursachte auch mitochondriale Schäden, indem es auf mitochondriale Oxidoreduktasen abzielte. Dabei führen wir die beobachtete Bildung unreifer Autophagosomen auf die Induktion der Mitophagie zurück. Die zytotoxische Wirkung von Arzanol verringerte die Lebensfähigkeit von Krebszellen, und sensibilisierte Krebszellen zudem gegen eine Erstbehandlung mit Cisplatin.

In der Naturstoff-Bibliothek haben wir außerdem Phomoxanthon A identifiziert, eine Verbindung, von der bekannt ist, dass sie therapieresistente Krebszellen gegenüber Cisplatin sensibilisieren kann. Wir untersuchten seine Wirkungsweise und identifizierten Phomoxanthon A als starkes Mitotoxin, das die Fragmentierung der inneren Mitochondrienmembran induziert. Zusätzlich schlagen wir das Harnstoffzyklusenzym CPS1 als neues Ziel von Phomoxanthon A vor. In dieser Arbeit diskutieren wir die Strukturen und Aktivitäten von Phomoxanthon A, Arzanol und Hydroxyanthrachinonen und liefern wichtige Informationen für ihre Verwendung bei der weiteren Entwicklung von Krebsmedikamenten.

1 Introduction

1.1 Background and scope of this dissertation

Life is a cycle of coming into being and passing away. From the smallest molecule to the biggest life forms, vanishment is just as much of importance as emergence, and its regulation must be finely tuned in order to establish balance. Autophagy is a lysosomal degradation process maintaining the balance of organelles, proteins, and nutrients inside eukaryotic cells. It contributes to the waste removal of damaged or long-lived proteins and organelles, and at the same time recycles them into new sources of energy in form of macronutrients. Because of this crucial pro-survival role, autophagic dysfunction is related to a number of human pathologies such as neurodegenerative diseases, heart diseases, infections, aging and cancer.

While the complex molecular mechanism of autophagy in human cells is still being discovered, small compound modulators of autophagy are being employed in order to identify novel **a**u**t**opha**g**y-related (ATG) target proteins and for treating autophagy-related diseases. Especially cancer research benefitted from advancements in autophagy and today the National Institutes of Health (NIH) lists 75 clinical trials combining autophagy and cancer treatment, including one phase III clinical trial administering the autophagy inhibitor chloroquine (CQ) (https://clinicaltrials.gov/ on 13th April, 2020). In recent years, researchers identified many successful treatment combinations of autophagy modulators enhancing chemotherapy efficacy, but also faced frustrating off-target effects. Now, the field of autophagy modulators in cancer treatment is resurgent [1].

'There's a revitalized interest clinically […]. But I don't think you're going to maximally know what can be done by inhibiting this pathway unless we get better chemical matter.'

Alec Kimmelman [1],

radiation oncologist at New York University and co-founder of Vescor

Nature is a highly creative and nearly inexhaustible source of novel small molecule compounds with bioactive properties. Especially in evolutionary stressed niches such as oceans and meadows, you can find a plentitude of secondary metabolites. Our idea is to find and characterize novel autophagy-modulating natural products and derivatives and identify lead structures to eliminate wild type but most important therapy-resistant tumor cells.

1.2 A short history of intracellular waste removal

For cells to maintain a healthy intracellular homeostasis of organelles, proteins and nutrients, they also require a well-balanced and cargo-specific system of intracellular waste disposal. One highly evolutionary conserved mechanism of waste removal is the ubiquitin-proteasome pathway. It consists of the ubiquitin-dependent tagging of misfolded, damaged, long-lived or unneeded proteins by E1 (ubiquitin-activating), E2 (ubiquitin-conjugating) and E3 (ubiquitin-ligating) enzymes, and the subsequent endoproteolytic degradation of ubiquitin-tagged proteins within a multi-protein complex of proteases [2]. In 2004, the discovery of the ubiquitin-mediated protein degradation was awarded with the Nobel Prize in Chemistry to Aaron Ciechanover, Avram Hershko and Irwin Rose [3, 4, 5]. They were among the most successful researchers interested in organized intracellular removal, defying the trend of protein synthesis research at that time. The proteasomal pathway they discovered effectively rids the cells from proteins, but it cannot deplete entire multi-protein complexes or organelles.

Already decades before the discovery of the proteasomal pathway in the late 70s and early 80s, researchers started to notice intracellular dense bodies containing both semi-digested organelles and lysosomal hydrolases [6, 7]. After the Nobel Prize winning discovery of the lysosome by Christian de Duve in 1955, the development of electron microscopy lead to the first deeper understanding of organelle degradation [de Duve, 1966]. In 1961, microscopy experts Ashford and Porter identified perinuclear dense bodies in glucagon-treated perfusions of rat liver containing cytoplasmic components [8]. They called these dense bodies ‘foci of autolysis’. In the years after, various inducing stimuli and targeted organelles of ‘autolysis’ were identified. They were presented at the Ciba Foundation symposium on lysosomes in 1963, where Novikoff proposed the term ‘cytolysomes’ for his observation of acid-phosphatase-positive structures containing cytoplasmic components such as mitochondria and endoplasmic reticulum (ER) membranes. In order to distinguish endocytosis-related (‘heterophagic’) from purely intracellular functions of lysosomes, Christian de Duve established the term ‘autophagic’ derived from the Ancient Greek αὐτόφαγος (*autóphagos*) meaning self-eating, and proposed the term ‘autophagic vacuoles’ for Novikoff’s ‘cytolysosomes’. De Duve prevailed and the field of autophagy research was born.

It should take another few decades until the most important autophagy marker microtubule-associated protein 1 light chain 3 (LC3) was identified and its mode of action was revealed [9]. Strikingly, despite its low similarity in amino acid sequence, LC3 is considered an ubiquitin-like protein that tags autophagic cargo and facilitates autolysosomal degradation quite similar to the proteasomal pathway for protein removal.

1.3 Morphology and molecular pathway of autophagy

Autophagy is an evolutionary conserved pathway, which was presumably used by unicellular organisms as a means of obtaining macronutrients in times of starvation. In higher eukaryotes, the role of autophagy in removal of dispensable or harmful cargo has additionally gained in importance. Almost at the same time as the introduction of autophagy research, selective autolysosomal degradation of damaged organelles was proposed in addition to nonselective bulk degradation. Since then, a multitude of different specific subtypes of autophagy was observed and classified, each named a portmanteau from the impacted cargo and the suffix '-phagy': Aggrephagy (protein aggregates) [10, 11], chlorophagy (chloroplasts) [12], ERphagy/reticulophagy (ER fragments) [13], ferritinophagy (ferritin) [14], glycophagy (glycogen) [15], granulophagy (stress granules) [16], lipophagy (lipid droplets) [17], mitophagy (mitochondria) [18, 19], myelinophagy (myelin) [20], nucleophagy (nucleic parts) [21, 22], pexophagy (peroxisomes) [23], proteaphagy (proteasome) [24], ribophagy (ribosomes) [25], xenophagy (bacteria and other pathogens) [26, 27], or zymophagy (zymogen granules) [28, 29].

In addition, three distinct morphological modes of mammalian autophagy were observed and classified. Microautophagy describes the direct uptake of cargo into the final vesicles. During microautophagy in yeast, intracellular cargo is directly engulfed by invaginations of the lysosome, whereas mammalian microautophagy involves late endosome/multivesicular bodies. Microautophagy has been proposed to degrade both bulk cytoplasmic contents, and selected proteins or organelles that are recruited to the vesicular outer membrane by microautophagic receptors. In contrast, during chaperone-mediated autophagy (CMA), specific substrate proteins with the pentapeptide motif KFERQ are escorted to the lysosomal membrane by the cytosolic chaperone heat shock-cognate protein of 70 kDa (HSC70) and co-chaperones [30]. CMA-target proteins are then transported across the lysosomal membrane via lysosome-associated membrane glycoprotein 2 (LAMP2A). The third mode of autophagy has its origin the late 60s to early 70s, when researchers were able to discriminate autophagosome and autolysosome. These two vesicular morphologies distinguish macroautophagy from chaperone-mediated and microautophagy. Since then, macroautophagy remains the most frequently researched mode of autophagy and is therefore often (also in this thesis) referred to as autophagy.

The morphological pathway of (macro-)autophagy has been categorized into chronological steps: initiation of autophagy, elongation of the initiation membrane, maturation of the autophagosome, fusion of autophagosome and lysosome, and degradation of autophagic cargo within the autolysosome. Among all species, autophagy is best characterized in yeast although many orthologs and analogs of *ATG* genes can be found in mammals. For instance, Unc-51-like kinase 1 (ULK1) is one of five human homologues to yeast Atg1 (originally known as Apg1), which was identified in a screening

as the first known autophagy-defective mutant strain of *Saccharomyces cerevisiae* [31, 32, 33]. This screening by Tsukada and Ohsumi revealed the first 15 APG (ATG) genes, which was awarded in 2016 with the Nobel Price for Physiology or Medicine to Yoshinori Ohsumi.

From yeast to humans, six functional groups have been classified as the core autophagic machinery hierarchically coordinating the formation of the autophagosome: (i) the initiating Atg1 complex (ULK1 complex in humans), (ii) the phosphatidylinositol (PI) 3-kinase (PI3K) complex, (iii) the Atg2-Atg18 complex (WD repeat domain phosphoinositide-interacting protein [WIPI] complex in humans), (iv) Atg9 (ATG9A in humans), (v) the Atg12—Atg5-Atg16 conjugation system (ATG12—ATG5-ATG16L complex in humans), (vi) the Atg8—PE conjugation system (LC3—PE conjugation system in humans) [34].

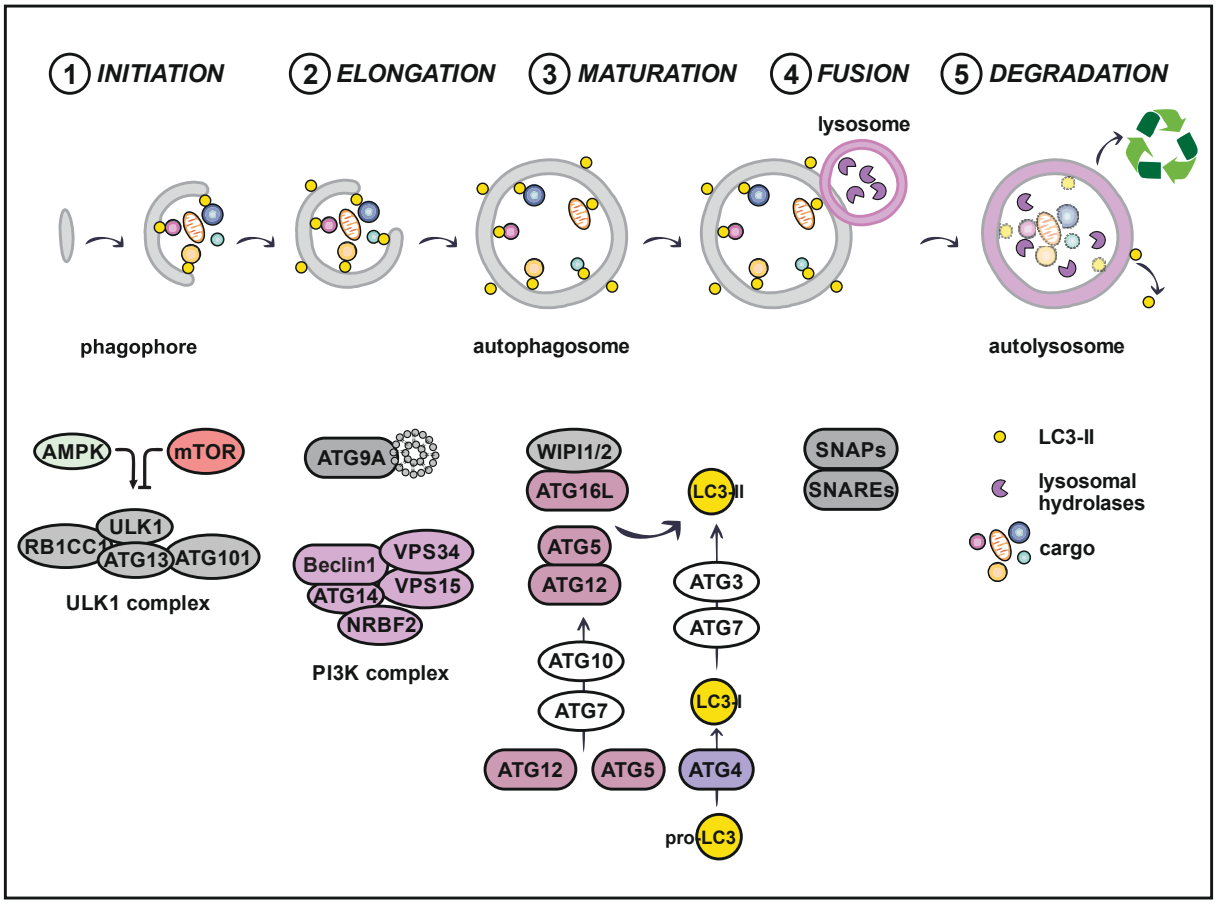

Figure 1. The core autophagic machinery.
Upon autophagic stimuli, AMPK associates and mTOR dissociates from ULK1, activating the ULK1 complex, which triggers phagophore initiation. Vesicle-bound ATG9A and the PI3K complex are recruited to the phagophore, where the class III PI3 kinase VPS34 generates PI3P that in turn recruits WIPI1/2. LC3 is expressed as pro-protein that is cleaved by ATG4 to become cytosolic LC3-I exposing a C-terminal glycine. At the phagophore, WIPI1/2 recruits ATG16L which it is involved in the lipidation of LC3 together with ATG7, ATG3, and ATG12—ATG5. Lipidated LC3-II coats the phagophore, where it binds to autophagic cargo via receptors. After autophagosome maturation, most complexes dissociate from the membrane. During fusion, the SNAP/SNARE proteins tether the autophagosome to the lysosome, resulting in an autolysosome. In a last step, lysosomal hydrolases degrade the intralysosomal cargo and receptors and allocate them as new macromolecules for the cell metabolism. Outer membrane-bound LC3-II is cleaved off again.

Autophagy can be initiated by many stimuli, which include amino acid or glucose starvation, growth factor withdrawal, hypoxia, DNA damage, intracellular pathogens, protein aggregation or damaged organelles [35]. Mammalian/mechanistic target of rapamycin (mTOR) acts as sensor for growth factors and nutrient supply in two functionally distinct kinase complexes (mTORC1 and mTORC2) [36, 37]. Upon nutrient supply, mTORC1 phosphorylates both ULK1 and ATG13 of the ULK1 complex leading to its inactivation [38, 39, 40]. In response to nutrient withdrawal, growth factor deprivation or rapamycin treatment, mTORC1 dissociates from the ULK1 complex, allowing ULK1 to auto-phosphorylate and trans-phosphorylate ATG13 and RB1-inducible coiled-coil protein 1 (RB1CC1) [41, 39, 42, 43]. Another energy-sensing kinase, 5'-AMP-activated protein kinase (AMPK), is activated by a low ATP:AMP ratio or downstream of Ca^{2+} signaling and growth factor pathways; it phosphorylates Raptor and thereby inactivates mTORC1, while it also directly phosphorylates and activates ULK1. Different from yeast where Atg1 and Atg13 actively associate upon starvation, the ULK1 complex in vertebrates is considered to be constitutively assembled and mainly governed by its phosphorylation status [41, 39]. The activated ULK1 complex translocates together with the PI3K complex to the site of autophagosome formation, where the PI3K class III generates phosphatidylinositol 3-phosphate (PI3P) to recruit PI3P-binding effectors such as WIPI, and double FYVE domain containing protein (DFCP) [44, 45]. In vertebrates, ER-mitochondria-contact sites form evaginations termed omegasomes, which evolve into isolation membranes (alias phagophores) that later on mature into autophagosomes [46, 47, 48]. However, different lipid sources contribute to the autophagosomal membrane and are currently debated.

The ATG12—ATG5-ATG16L complex is recruited to the outer surface of the initiation membrane by the interaction of WIPI2 and ATG16L1 [49]. The ubiquitin-like LC3 belongs to the Atg8-family proteins that comprises the subfamilies of microtubule-associated protein 1 light chain 3 (MAP1LC3) proteins, and γ-amino-butyric acid receptor-associate protein (GABARAP), and (iii) Golgi-associated ATPase enhancer of 16 kDa (GATE-16) [50]. The MAP1LC3 subfamily includes MAP1LC3A, MAP1LC3B, MAP1LC3C, and MAP1LC3B2, of which MAP1LC3B is the best characterized. It is C-terminally cleaved after synthesis as pro-protein and locates to the cytosol as truncated LC3-I [9]. After the initiation of autophagy, LC3-I is conjugated to phosphatidylethanolamine (PE) in an E1/E2/E3-like fashion by ATG7, ATG3 and the ATG12—ATG5-ATG16L complex [51, 52, 53]. Lipid-bound LC3-II integrates into the inner and outer autophagosomal membrane, where it serves as an anchor for downstream proteins and autophagic cargo. Many ATGs as well as specific autophagic receptors such as Sequestosome-1 (p62/SQSTM1), BCL2/adenovirus E1B 19 kDa protein-interacting protein 3-like (BNIP3L, also NIX), FUN14 domain-containing protein 1 (FUNDC1) or optineurin (OPTN) bind LC3 via their LC3-interacting region (LIR) motif [W/F/Y]xx[L/I/V] [54].

After full closure of the matured autophagosome, most ATGs depart from the outer autophagosomal surface while inner membrane-bound autophagy receptors keep the autophagic cargo engulfed. These receptors, together with their cargo, are degraded by lysosomal hydrolases after fusion of autophagosome and lysosome, which is facilitated by synaptosomal-associated proteins (SNAPs) and soluble N-ethylmaleimide-sensitive-factor attachment receptors (SNAREs) [55]. Autophagic receptors such as LC3 therefore serve as markers for autophagic flux assays. Common autophagy assays include immunoblot analysis of endogenous LC3-II, or flow cytometric and fluorescence microscopic analysis of fluorophore-tagged LC3 [56]. Decreasing signal of single-fluorophore-tagged GFP-LC3 or mCitrine-LC3 correlates to its pH-dependent quenching or lysosomal degradation and indicates a successful autophagic flux [57]. Another construct, RFP-GFP-LC3, is based on the combined yellow tandem fluorescence of GFP and RFP in autophagosomes and can help to discriminate red only autolysosomes due to a higher stability of RFP over GFP in the lysosome [58]. The latest state of the art construct, GFP-LC3-RFP-LC3ΔG, carries an internal flux control; after synthesis, the construct is cleaved by ATG4 into equimolar amounts of GFP-LC3, which can be monitored as described above, and RFP-LC3ΔG, which cannot be lipidated or integrated into the membrane [59].

1.4 Mitophagy

As mentioned in chapter 1.3, cells can use autophagy to degrade a variety of different and specific cargo such as organelles. Mitophagy describes the autophagic engulfment and degradation of mitochondria.

During the maturation of red blood cells (erythropoiesis), reticulocytes rely on mitophagy for mitochondrial clearance [60, 61]. The mitochondrial outer membrane protein NIX serves as a mitophagy receptor in reticulocytes by recruiting the Atg8-family protein GABARAP-L1 to the dispensable mitochondria [62, 63, 64]. In addition to developmentally induced mitophagy, stress stimuli such as mitotoxin exposure, respiratory chain uncoupling, and loss of membrane potential induce mitophagy. Mitochondria are a network of dynamic elongated tubes that are constantly subjected to fusion and fission [65]. During mitochondrial quality control, damaged mitochondria are prevented from fusion with the network and the isolated organelles are subjected to mitophagy [66]. A key component linking mitochondrial quality control and mitophagy is the phosphatidylinositol 3,4,5-trisphosphate 3-phosphatase and dual-specificity protein phosphatase (PTEN)-induced putative kinase protein 1 (PINK1)/Parkin pathway: With its N-terminal mitochondrial localization sequence, PINK1 is constitutively imported into healthy mitochondria where it spans across the membranes via translocase of outer membrane (TOM) and translocase of inner membrane (TIM). At the inner

mitochondrial membrane, the N-terminus of PINK1 is cleaved by presenilin-associated rhomboid-like protease (PARL), preparing PINK1 for proteasomal degradation. Damaged mitochondria are not able to import PINK1 into the inner mitochondrial membrane, causing PINK1 to accumulate on the outer mitochondrial membrane, where it phosphorylates ubiquitin and recruits the ubiquitin-ligase Parkin [67, 68]. Parkin-dependent ubiquitination of mitochondrial surface proteins such as voltage-dependent anion-selective channel protein 1 (VDAC1), a component of the mitochondrial permeability transition pore, serves as a binding substrate for mitophagic receptors [69]. Receptors such as p62/SQSTM1, next to BRCA1 gene 1 protein (NBR1), nuclear dot protein 52 (NDP52, also calcium-binding and coiled-coil domain-containing protein 2 [CALCOCO2]), OPTN, and transient axonal glycoprotein 1 (TAX1)-binding protein 1 (TAX1BP1) then bind LC3 via their LIR domains and recruit the autophagic machinery to construct an autophagosomal membrane around the damaged and isolated mitochondrion [70].

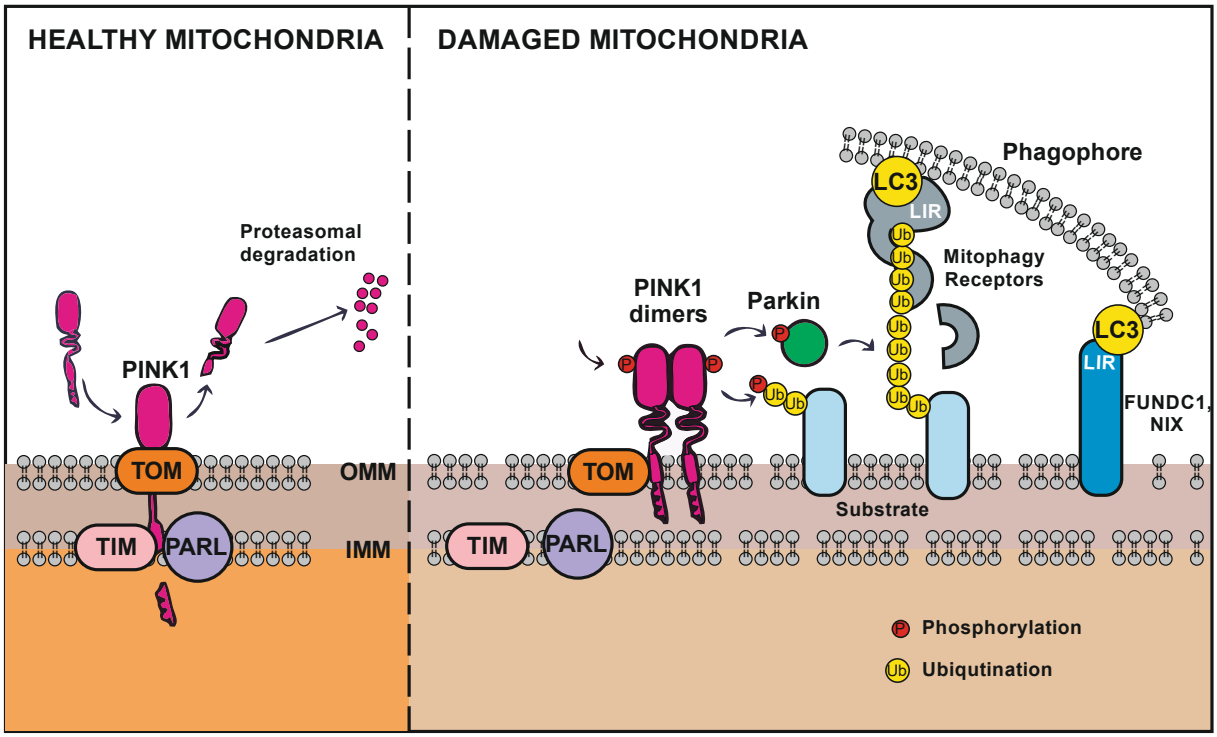

Figure 2. Initiation of mitophagy by damaged mitochondria.
In healthy mitochondria (left panel), PINK1 is imported via importers TOM and TIM to be processed by the protease PARL in the inner mitochondrial membrane (IMM), resulting in the release and proteasomal degradation of PINK1. In damaged mitochondria (right panel), PINK1 accumulates and dimerizes at the outer mitochondrial membrane (OMM), where it activates through autophosphorylation. PINK1 then activates Parkin, which ubiquitinates mitochondrial substrates such as VDAC1. Mitophagy receptors such as p62/SQSTM1, NDP52, OPTN or TAX1BP1 bind the ubiquitinated substrates and recruit LC3. FUNDC1 and NIX bind LC3 via their LIR domain.

Other mitophagy receptors are directly incorporated into mitochondrial membrane, where they support mitochondrial quality and dynamics upon physiological conditions. Bcl-2-like protein 13 (Bcl-2-L-13), a functional homologue to yeast Atg32, regulates mitochondrial fission in healthy cells

and recruits LC3 and ULK1 upon mitochondrial damage [71, 72, 73, 74]. Another LC3-binding mitophagy receptor is FUN14 domain-containing protein 1 (FUNDC1), which is regulated by hypoxia-induced factors and coordinates mitochondrial fusion and fission via interaction with Optic atrophy protein 1 (OPA1) [75, 76, 56]. As a key protein for mitochondrial fusion, OPA1 is proteolytically cleaved into its shorter forms by the metalloendopeptidase overlapping with the m-AAA protease 1 homolog (OMA1) subsequent to mitochondrial damage such as the loss of the mitochondrial membrane potential or low amounts of ATP generated during oxidative phosphorylation of the respiratory chain complexes [77, 78]. Fragmented OPA1 prevents mitochondrial fusion of the damaged organelles and isolates them for autophagic degradation. Ongoing stress, however, results in complete loss of long OPA1 forms and induces cristae remodeling as well as the release of cytochrome c, which in turn induces intrinsic apoptosis [79, 80, 81]. The different functions of OPA1 show the intricate molecular coordination of mitochondrial quality control, mitophagy, and apoptosis-related cell death.

1.5 Autophagy and Apoptosis

Apoptosis is a caspase-dependent cell death pathway that is induced either extrinsically via death receptors or intrinsically via mitochondrial membrane permeabilization. Both routes lead to an irreversible cascade of cysteine-dependent aspartate-directed proteases (short caspases) cleaving intracellular proteins, which results in the formation of apoptotic bodies and their clearance by macrophages. A major common regulator of autophagy and apoptosis is oxidative stress. Reactive oxygen species (ROS) are free radicals with function as signaling molecules, in the promotion of mutations and genetic instability, and during the induction of apoptosis [82, 83, 84]. Especially superoxide, which is intrinsically produced by mitochondrial respiratory chain complexes I and III, is involved in the initiation of autophagy during starvation [85]. Excessive ROS can induce mitochondrial damage e.g. via lipid hydroperoxides or oxidation of membrane protein thiols [86, 87, 88]. ROS-induced mitochondrial damage can then in early stages induce mitophagy, or induce apoptosis after prolonged damage. Of note, many chemotherapeutics but also natural compounds like the anthraquinone emodin induce ROS and thereby trigger cell death in cancer cells [89, 90].

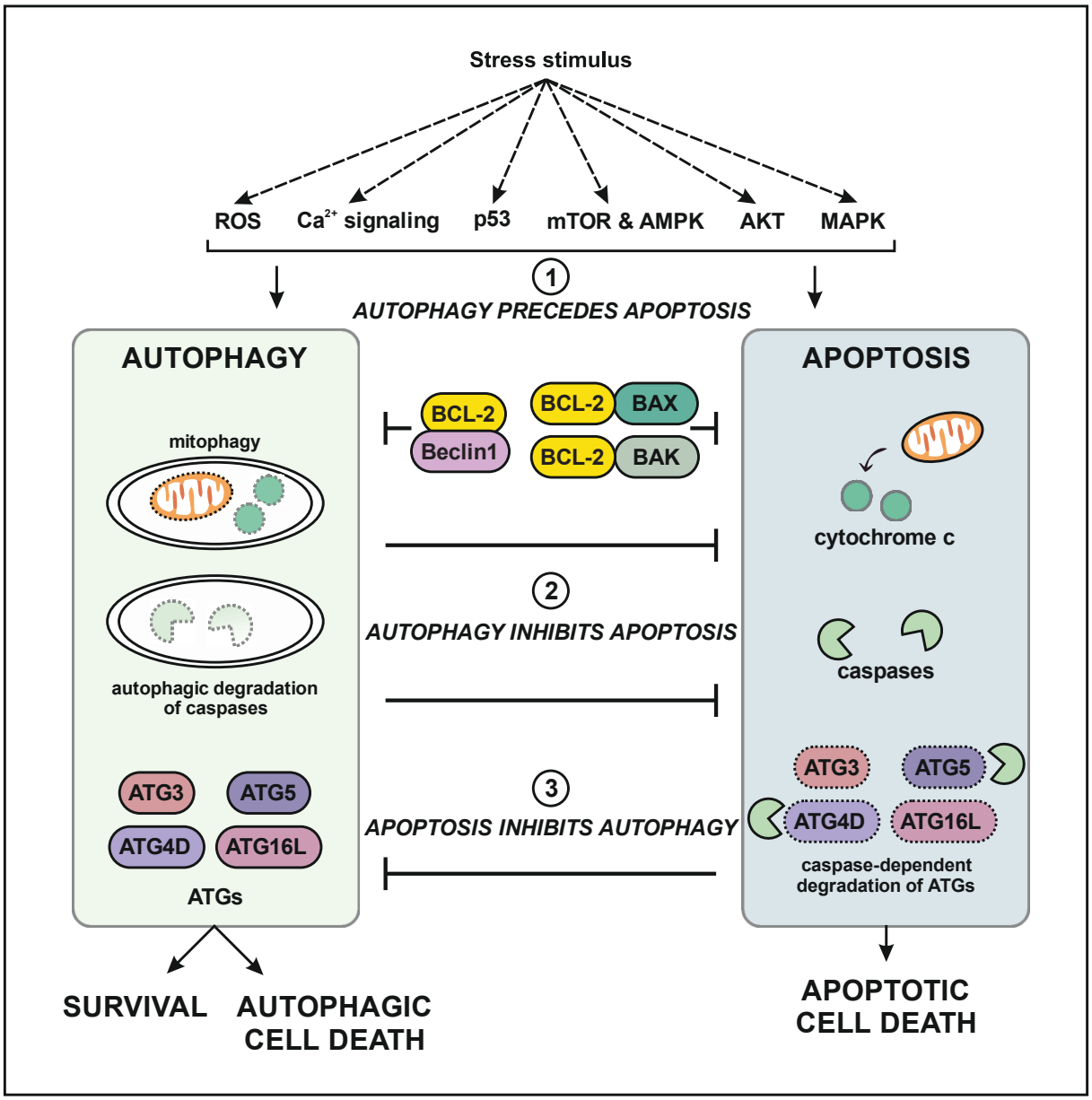

Figure 3. Cross talk between autophagy and apoptosis.
Stress stimuli induce autophagy and apoptosis via common signaling pathways. Upon acute stress, autophagy can be induced as means of survival. Chronic or severe stress induces apoptosis via cytochrome c release from the mitochondria (intrinsic apoptosis pathway) and caspase activity. In this first scenario, autophagy precedes apoptosis. The inhibitory protein BCL-2 is bound to pro-apoptotic BAX/BAK or pro-autophagic Beclin1, giving BCL-2 an anti-autophagic and/or anti-apoptotic role. In a second scenario, autophagy inhibits apoptosis via degradation of damaged mitochondria prior to the induction of the intrinsic apoptosis pathway and degradation of caspases. In a third scenario, apoptosis inhibits autophagy via caspase-dependent degradation of ATGs. By fine-tuning these two pathways, cells can respond adequately to stress stimuli and promote cell survival, or cell death.

As in the case of prolonged mitochondrial damage, autophagy as a means of cell survival often precedes apoptotic cell death. Although these two cell fates are very distinct from another, they have many molecular overlaps coordinating the timeline of intracellular risk assessment. Factors such as p53, ER stress, Ca^{2+} signaling, regulation of mTOR via AMPK, phosphatidylinositol 3-kinase (PI3K), RAC-alpha serine/threonine-protein kinase (also termed AKT), or the mitogen-activated protein kinase-

pathway, are involved in both autophagy and apoptosis [91]. During early acute stress, the initiation of autophagy can result in autophagy-dependent inhibition of apoptosis. This is mediated by autophagic degradation of pro-apoptotic factors such as the mitophagic degradation of damaged mitochondria, or the autophagic degradation of caspases [92, 93, 94]. The family of B-cell lymphoma 2 (Bcl-2) proteins comprises more than a dozen proteins that act as pro- and/or anti-apoptotic regulators. The eponymous member of this protein family, BCL-2, is an anti-apoptotic and anti-autophagic protein that acts via inhibitory binding to either pro-apoptotic BCL-2-associated X protein (BAX) and BCL-2 antagonist/killer (BAK), or the pro-autophagic Beclin-1. Upon stress, BCL-2 dissociates from Beclin-1 allowing it to assemble with the PI3K complex to conduct autophagy. Similarly, BCL-2 dissociates from BAX and BAK, which regulate the stress-induced formation of a mitochondrial outer membrane pore to release mitochondrial proteins such as cytochrome c into the cytosol and induce apoptosis [95]. Activated apoptosis, however, can also inhibit autophagy via proteolytic cleavage of ATGs by activated caspases. Interestingly, pharmacological inhibition of apoptosis is associated with ATG7-, ATG5- and Beclin-1-dependent autophagic cell death [96, 97]. Similarly, autophagic cell death was induced via ER stress in apoptosis-incompetent cells [98, 99]. The term 'autophagic cell death', however, is often used misleadingly and fails to distinguish actual autophagic cell death from autophagy-accompanied cell death. In order to clear misconceptions, in 2012 the Nomenclature Committee on Cell Death proposed a set of recommendations for the definition of autophagic cell death. These include that phenotypes have to involve ATG genes, observed effects have to be susceptible to pharmaceutic or genetic inhibition of the autophagic pathway, and studies should involve knockdowns of at least two essential autophagic genes [100]. Therefore, although in literature there are many cases termed autophagic cell death, some of them could be cases of apoptotic or necroptotic cell death accompanied by autophagy.

1.6 Autophagy and Cancer

In 2011, Hanahan and Weinberg added autophagy as modulator of tumor cell survival and death to the category of "Resisting Cell Death" within the hallmarks of cancer [101]. In addition, autophagy is connected to the other hallmarks such as energetics, proliferation, inflammation, invasion and metastasis, angiogenesis, genome instability, and mutation [102, 103, 104, 105, 106]. Overall, autophagy is involved in cancer prevention, tumorigenesis and chemotherapy. Due to its tumor-suppressive and tumor-promoting roles, autophagy is frequently referred to as a 'double-edged sword' in cancer research.

Upon physiological conditions, basal autophagy maintains intracellular homeostasis and clears oncogenic factors such as misfolded proteins, ROS or damaged organelles. Defects in basal autophagy are associated with tumorigenesis, e.g. heterozygous knockout of *BECN1* reduced autophagic flux and

caused spontaneous malignancies in mice [107]. Similarly, analysis of large cancer datasets revealed a correlation of decreased *BECN1* expression and increased aggressiveness with poor prognosis in breast cancer [108]. In contrast, ectopic overexpression of *BECN1* in autophagy-defective cells induced autophagy while reducing proliferation and tumor growth [109].

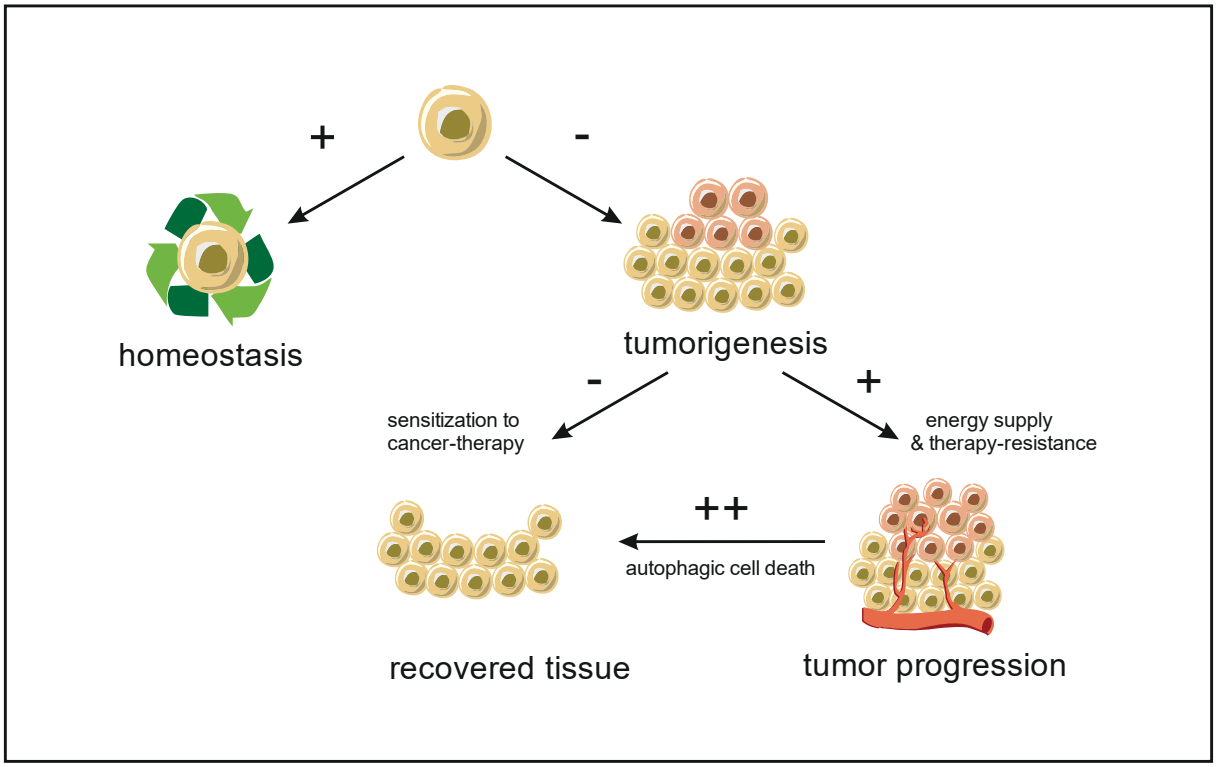

Figure 4. The dual role of autophagy in cancer.
Basal autophagy in body cells maintains a healthy homeostasis, while loss of ATGs can induce tumorigenesis. Autophagy in cancer cells contributes to their energy supply and therapy-resistance, and thereby promotes tumor progression. Inhibition of autophagy can therefore sensitize malignant cells to cancer-therapy. The enhanced induction of autophagy could force cancer cells into an autophagic death. Both, inducers and inhibitors of autophagy are promising new classes of anti-cancer drugs.

As survival pathway, autophagy is considered tumor-promoting in established tumors. Autophagy was observed in hypoxic regions of tumors where it contributed to the metabolism and survival of malignant cells [110]. In some cases of cancer, inhibition of autophagy successfully re-sensitized resistant cancer cells to chemotherapy, e.g. LC3 knockdown via shRNA suppressed treatment-induced autophagy in breast cancer and sensitized the cancer cells to the receptor tyrosine-protein kinase erbB-2 (also HER2) monoclonal antibody trastuzumab [111]. Increased pharmacodynamic efficacies due to combinational treatment of chemotherapeutics and autophagy inhibitors resulted in the hypothesis that autophagy largely contributes to chemotherapy-resistance [112, 113, 114, 115]. Inhibition of autophagy was shown to sensitize cancer cells to the lethal effects of various cancer therapies, including chemotherapy, radiotherapy and targeted therapies [116, 117, 118]. Combinational therapies of approved drugs with autophagy modulators overcame therapy-resistant tumor cell survival [119, 120]; especially the combination of inducers of metabolic stress with autophagy inhibitors promise better efficacies against

cancer [121]. As most studies regarding autophagy inhibitors and chemotherapeutics are carried out in cell culture settings, co-culture experiments suggest additional tumor-promoting effects by autophagy induction in tumor-adjacent tissue. In vivo, inhibition of autophagy has however shown difficult due to the dependence of immune cells on autophagy. The induced deficiency of immunogenic signaling could contraindicate the use of autophagy inhibitors in some clinical settings [122]

In addition to many clinical trials investigating autophagy inhibitors as novel anti-cancer drugs, induction of autophagic cell death by autophagy inducers presents an alternative therapeutic strategy. The basic assumption is that uncontrolled autophagy is self-limited and continues until essential components for cell survival are degraded, leading to autophagic cell death. Due to its close connection to other cell death pathways, the actual contribution of autophagy in reported cases of autophagic cell death is highly debated (see chapter 1.5). Ceramide, for example, was reported to induce apoptosis-independent autophagic cell death in malignant glioma cells via Bcl-2/adenovirus E1B 19 kDa-interacting protein 3 (BNIP3) [123]. However, it is also known that ceramide induces necrosis as an alternative cell death pathway [124]. Similarly, obatoclax (GX15-070) was reported to induce cell death via both ATG5-dependent autophagy and BAK-dependent apoptosis in human acute lymphoblastic leukemia cells [125]. In apoptosis-incompetent cells, Bonapace et al. confirmed obatoclax-induced ATG-dependent cell death. However, further analysis led them to the discovery of autophagy-dependent necroptosis during treatment with obatoclax [126]. Basit et al. who verified that the obatoclax-induced cell death is dependent on autophagy-related proteins, observed that the assembly of the necrosome is ATG-dependent [127]. These cases highlight how important it is to distinguish ‘non-apoptotic cell death’ from ‘autophagic cell death’. Our group recently investigated in detail, how autophagy and necrosis are related, and found a reciprocal impact of autophagy-related and necrosis-related kinases (chapters 3.2.3 and 3.2.4).

Autophagy can therefore protect cancer cells from death, but also serve as backup pathway for cell death in cancer cells with high apoptotic threshold; however, systemically undesired necrosis can also be involved. As a result, the pharmacological modulation of autophagy is largely dependent on the genetic background of the cancer cell and its developmental stage.

1.7 Natural compounds in drug discovery

Clinical drug discovery implies distinct research steps from the problem of a disease until the solution in form of a marketable and approved drug [128]. After disease and target identification, large screenings aim to identify hit compounds targeting the protein or pathway of choice. In this phase, non-functional compounds are ruled out, and often both hit compounds and false positive pan-assay interference

compounds (PAINS) remain. PAINS are compounds that interfere with high-throughput assays due to their high chemical reactivity, fluorescence or color, function as chelators, aggregators or redox cycling compounds. Therefore, hits have to be confirmed in confirmatory testing and secondary screenings to investigate their robustness and efficacy. Still, biochemically promiscuous compounds as well as compounds with biochemically promiscuous targets can remain among hits and often complicate the hit-to-lead process. During lead optimization, confirmed compounds are tested and if necessary, chemically optimized with regard to good pharmacokinetic properties such as absorption, distribution, metabolism, excretion, and toxicity. Chemists are thereby often guided by Lipinski's rule, which recommends criteria of less than five hydrogen bond donors within a compound, less than ten hydrogen bond acceptors, a molecular mass less than 500 Daltons and a octanol-water partition coefficient (log P) lower than five [129]. In the presence of new data on clinically approved drugs, 'Lipinski's rule of five' is debated. Still, compounds that display features far from the rule often fail in clinical trials due to low absorption or stability. Optimized leads, however, go through clinical trials and—if successful—become approved, patented and marketed.

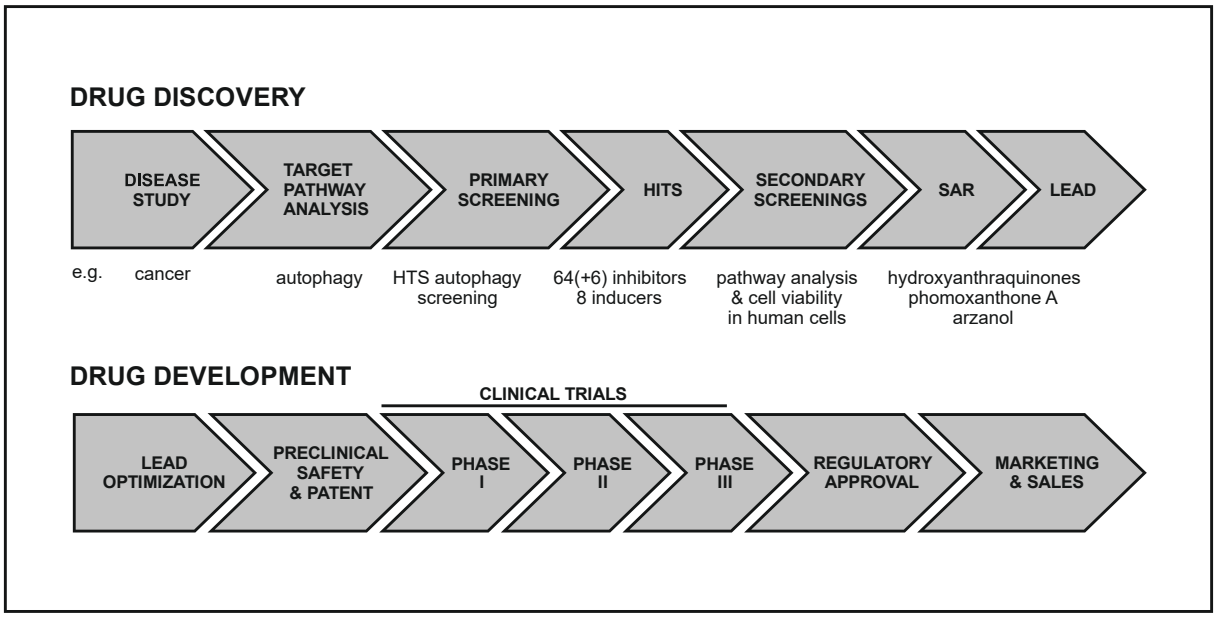

Figure 5. Stages of drug discovery and drug development from disease to its treatment.
In this thesis, we emulate anti-cancer drug discovery by screening for modulators of autophagy among a natural compound library.

Historically, natural compounds have proven very successful in drug discovery and yielded a wide range of drugs from antibiotics to antimalarial drugs and chemotherapeutics against cancer [130]. Through evolution, bioactive natural compounds accumulated in almost inexhaustible quantities in nature. By environmental pressure, they gained an often non-synthesizable complexity and a high degree of stereochemistry, while targeting evolutionary conserved pathways such as apoptosis or autophagy [131, 132]. After almost a century of successful drug discovery among natural compounds,

researchers and pharma companies turned to synthetic compounds during the era of high-throughput screenings. While natural compounds are endangered by extinction rates, and depend on seasonal and environmental availability, synthetic compounds can be consistently manufactured in laboratories. These structurally simpler synthetic compounds are more susceptible to derivatization, conform in higher numbers to the Lipinski's rule, and promise fast structure and target discovery. Natural compounds, on the other hand, often remained impure after isolation, their structural complexity consumed valuable time for characterization, and their patentability is uncertain in some countries. Today, recent advances in genomics, bioinformatics and synthetic biology improve our understanding of natural compound biosynthesis and allow semi-synthetic approaches [133, 134, 135]. Most importantly, the current medical challenges of anti-cancer and antibiotic drug-resistances urge the researchers to consider all possible resources for drug discovery [131].

1.8 Natural compounds as autophagy modulators in cancer

As autophagy gains clinical relevance, researchers investigate compounds to identify novel pharmacological modulators of autophagy. So far, the majority of publications addressing the role of natural compounds in autophagy reports phenotypic accumulation of autophagosomes or changes in the autophagic flux. In this, natural compound-induced autophagy is often accompanied by an induction of apoptosis, while the mechanistic targets of these compounds remain undiscovered.

In addition to novel natural compounds however, there are also better understood and established inducers and inhibitors of autophagy such as mTOR inhibitors, AMPK activators, or class I PI3K inhibitors. Among the first generation of pharmacological inducers of autophagy was the mTOR inhibitor rapamycin. It was first isolated from the bacterium *Streptomyces hygroscopicus* found in the soil of Rapa Nui on the Easter Island. Rapamycin induces autophagy by dual binding to the peptidyl-prolyl cis-trans isomerase FKBP12 and the FKBP12-rapamycin binding (FRB) domain of mTOR, inactivating mTORC1 [136, 137]. In contrast, mTORC2 is rather insensitive to rapamycin treatment and is only inhibited after chronic exposure [138, 139, 140]. Of note, mTOR is a protein target upstream of autophagy, but also upstream of cell growth and cell proliferation. Due to their inhibition of T-cell proliferation, rapamycin (also sirolimus/Rapamune®) and the rapamycin analog (rapalog) everolimus are approved as immunosuppressants during transplantations. Everolimus is further approved against advanced breast cancer, neuroendocrine tumors of pancreatic origin, and renal cell carcinoma. Temsirolimus is another rapalog and can be prescribed against renal cell carcinoma, whereas another rapalog, ridaforolimus, is still in its experimental phase. Rapalogs represent the first generation of mTOR inhibitors, but side effects such as hyperlipidemia and hyperglycemia led to the investigation of

second generation mTOR inhibitors including ATP-competitive mTOR kinase inhibitors and dual mTOR/PI3K inhibitors [141, 142].

Torin1 and torin2 are ATP-competitive mTOR kinase inhibitors that were chemically developed from a quinoline derivative found in a high-throughput screening of kinase inhibitors and potential ATP binding pocket-related heterocycles [143, 144]. ATP-competitive mTOR kinase inhibitors like torin2 or a class of pyrazolopyrimidines inhibit the catalytic activity of both mTORC1 and mTORC2, while also blocking the PI3K/AKT pathway [145, 146]. The anti-cancer success of torin2 and the discovery of feedback loops between mTOR and PI3K/AKT led to the development of dual PI3K/mTOR inhibitors such as dactolisib (NVP-BEZ235), SF1126, and PF-04691502 that were investigated in clinical trials against advanced cancer [142]. Pharma companies developed these compounds in a structure-based discovery approach, whereby dactolisib is a derivative of imidazoquinoline, and SF1126 derived from the PI3K inhibitor LY294002 that derived from the flavonoid quercetin [147]. Like the rapalogs, also torin2 and dactolisib induce autophagy and suppress cancer cell growth [148, 149, 150]. As for the dual inhibitors, recent approaches successfully include a combination with autophagy inhibitors to further improve anti-cancer efficacy [151, 152, 153].

Inhibitors of mTOR conclude a successful journey of anti-cancer drug development from the identification of a parent natural compound via decades of basic research to its derivatization and market approval. Another way to develop new anti-cancer drugs can be achieved by repurposing drugs that are already approved for other diseases. Decades of research data and already successfully passed clinical trials are advantages in this regard. One such compound is the anti-diabetic drug metformin. Metformin is a galegine derivative isolated from the European medicinal plant *Galega officinalis* that acts as inducer of autophagy [154]. This compound is used for decades in the treatment of diabetes type 2, while cohorts have shown that is associated with a lower risk of developing cancer [155, 156]. Its function as hypoglycemic drug led to the discovery of metformin-induced activation of AMPK [157]. While several researchers described the induction of autophagy by metformin via AMPK activation, its exact mechanistic target has not been found yet [158, 159, 160]. In addition to AMPK, metformin also acted via downregulation of signal transducer and activator of transcription 3 (Stat3), a transcription factor of Bcl-2 [161]. Thereby, it induced autophagy but also apoptosis in esophageal squamous carcinoma cells, a finding that is consistent with several clinical trials that currently investigate metformin as anti-cancer drug (www.clinicaltrials.gov).

In addition to natural compound-based inducers of autophagy, there are also inhibitors of autophagy used in clinical trials and approved as anti-cancer drugs. Chloroquine (CQ) and its derivative hydroxychloroquine (HCQ) are the most studied compounds in this regard. It is a chemical derivative of quinine, a 4-aminoquinoline isolated from *Cinchona officinalis*. After indigenous people of South

America used the bark of the lojabark tree against fever, Europeans imported it and developed quinine into an anti-malarial drug [162]. In 1949, the FDA approved chloroquine under the name 'aralen' as anti-malarial treatment, and in 2020, it entered clinical trials as anti-viral compound against the SARS-CoV-2 virus. While many modes of action have been proposed for chloroquine, still no molecular target was agreed on. Early on, chloroquine was proposed to target the parasitophorous food vacuole that parasites of the group *Plasmodium* form during malaria after entering human red blood cells. Chloroquine was proposed to raise the intra-vacuolar pH, and thereby inhibit vacuolar proteases and starve the trophozoite [163]. Similarly, chloroquine inhibits vacuoles such as the lysosome in mammalian cells and blocks late stage autophagy [164, 165]. It was further shown that chloroquine acts via the PI3K/Akt/mTOR- and p53 signaling-pathways to reduce cell growth of tumor cells [166]. Despite chloroquine-related renal and ocular toxicity, chloroquine is used as potential anti-cancer drug in several pre-clinical settings and clinical trials both as monotherapy and in combination with cisplatin and other chemotherapeutics [167, 168, 169, 170].

Another late stage inhibitor of autophagy is bafilomycin A_1, a macrolide antibiotic produced by the family of *Streptomycetaceae* [171]. Within the lysosomal membrane, bafilomycin A_1 binds to the proteolipid ring of the V_0 domain of the vacuolar ATPase (vATPase), and inhibits its proton pump activity [172]. Without vATPase activity, lysosomes cannot maintain their low pH needed for the activity of the lysosomal enzymes, which prevents damaged lysosomes from fusion with autophagosomes [173]. Although the vATPase contributes to cancer growth, metastasis, and drug resistance, the pronounced cytotoxic properties of bafilomycin A_1 prevented further in vivo experiments and clinical trials [174]. Nevertheless, bafilomycin is a much used and very potent inhibitor of autophagy in basic research. Other inhibitors of autophagy include the PI3K inhibitors wortmannin and 3-methyladenine [175, 176]. While the fungal steroid-derived wortmannin is a pan inhibitor of class I, II and III PI3 kinases, 3-methyladenine (3-MA) seems to be more specific for vacuolar protein sorting 34 (Vps34), the only known class III PI3K so far that is also involved in autophagy [176, 177]. Seglen and Gordon first identified 3-MA as an inhibitor of autophagy, when they observed its inhibitory effect on intracellular protein degradation but not on protein synthesis, or intracellular ATP levels [178]. More recently, 3-MA was shown to have differential temporal effects on class I and class III PI3 kinases, which could explain how it suppresses starvation-induced autophagy but promotes autophagy under nutrient-rich conditions [179]. A more specific inhibitor of class III PI3K was developed by chemical optimization of tetrahydropyrimidopyrimidinones, which were potent hits in a high-throughput cell image-based screening for novel autophagy modulators [180]. SAR405 (compound 22) was identified by Pasquier et al. as a very potent Vps34 inhibitor with good pharmacological properties [181]. While SAR405 inhibited Vps34 kinase activity and prevented autophagy, it also reduced tumor growth in mouse xenografts of head and neck cancer [182, 183].

All these compounds suggest that autophagy is an impactful pathway to target in anti-cancer therapy, however they also make clear that there is so far no ATG-specific natural pharmacological modulator. Due to multiple targets or unknown modes of actions, these compounds make it hard to assess the impact of autophagy in anti-cancer treatment and reveal the urgent demand for novel specific modulators of autophagy.

2 Aims of this work

The two main aims of this dissertation were the identification of autophagy-modulating natural products and the elimination of therapy-resistant cancer. Thereby, this dissertation addresses the questions if natural compounds modulate autophagy, how they modulate autophagy, and if one can use these natural compounds to combat therapy-resistant cancer in mono- or combinational therapy. These aims are addressed in several collaboration projects that were published or are prepared for publication. The corresponding manuscripts can be found in the appendix to this dissertation. All projects resumed in this dissertation resemble early steps in drug discovery from screening to early SAR studies in order to propose a lead structure for future optimization.

The approaches to identify novel modulators of autophagy included a high-throughput LC3-based screening of an in house natural compound library in murine fibroblasts, and the establishment of a secondary orthogonal screening based on state of the art autophagy markers in human cancer cells. This thesis focusses on the characterization of the modes of action of selected natural compound hits i.e. hydroxyanthraquinones, arzanol, and phomoxanthone A.

Approaches to overcome therapy resistance were investigated in a model of cisplatin-resistant bladder carcinoma cell line. We tested the impact of autophagy modulators on cisplatin efficacy in a proof-of-principle project with known compounds, prior to according investigations using arzanol.

3 Summary of publications

3.1 Publications within the scope of this dissertation

The full original texts of these manuscripts are in the appendix of this dissertation.

3.1.1 Publication 1

Targeting urothelial carcinoma cells by combining cisplatin with a specific inhibitor of the autophagy-inducing class III PtdIns3K complex

David Schlütermann, Margaretha A. Skowron, Niklas Berleth, Philip Böhler, Jana Deitersen, Fabian Stuhldreier, Nora Wallot-Hieke, Wenxian Wu, Christoph Peter, Michèle J. Hoffmann, Günter Niegisch, Björn Stork

Urologic Oncology: Seminars and Original Investigations, volume 36, issue 4, pages 160.e1-160.e13, April 2018

DOI: 10.1016/j.urolonc.2017.11.021

Urothelial carcinoma are a common form of cancer often progressing into metastatic diseases with poor prognosis. Routinely, platinum-based chemotherapy is employed for the treatment of urothelial carcinoma. The resistance of cancer cells to cisplatin treatment impairs its therapeutic success. In recent years, the role of autophagy as pro-survival pathway has also been shown to act tumor-promoting. Autophagy enables cell survival by providing nutrients especially in hypoxic niches such as in tumors and additionally supports chemoresistance in cancer cells. Therefore, we modulated autophagy using the small compounds chloroquine, 3-methyladenine, and SAR405 in order to sensitize bladder cancer cells to cisplatin treatment. Interestingly, cisplatin-resistant urothelial carcinoma cells display up-regulated amounts of autophagy-related proteins and both cisplatin-resistant and –sensitive urothelial carcinoma cells could be sensitized to cisplatin treatment upon inhibition of autophagy.

Author contribution:

The author of this dissertation contributed several ideas and suggestions to the project and gave technical support with immunoblotting and statistical analyses. Relative contribution: about 5%.

3.1.2 Publication 2

Anthraquinones and autophagy–Three rings to rule them all?

Jana Deitersen, Dina H. El-Kashef, Peter Proksch, Björn Stork

Bioorganic and Medicinal Chemistry, Volume 27, Issue 20, 115042, October 2019.

DOI: 10.1016/j.bmc.2019.115042

Anthraquinones are a class of tricyclic natural compounds that can be isolated from plants of the genus *Rheum* and are an integral part of traditional Chinese medicine. In recent years, the anti-cancer effect of different anthraquinone derivatives has been highlighted and their impact on both apoptosis and autophagy has been partially researched. While apoptosis is a cell death pathway induced by cytotoxic concentrations of drugs, autophagy is rather understood as a pro-survival pathway triggered by sublethal drug concentrations. Due to the dependency on autophagy within several cancer cell lines and its contribution to chemotherapy resistance, autophagy is of particular interest to cancer research. Among the anthraquinone derivatives being debated as potential new chemotherapeutic are emodin, aloe emodin, rhein, physcion, chrysophanol and altersolanol A. They modulate autophagy via diverging pathways, such as the PI3K/AKT/mTOR-axis, formation of reactive oxygen species and the transcription of autophagy-related proteins, each exhibiting different cell line specific modes of action. In this manuscript, we gathered data about anthraquinone-sensitive, autophagy-related pathways from multilingual publications and discuss the structure-activity relationship of the selected anthraquinone derivatives. We conclude the importance of a three-ring system including two para-keto groups at the central ring, and hydroxylation of positions C1, C3 and C8 for their bioactivity and emphasize the potential of autophagy-modulating anthraquinones as novel chemotherapeutic drugs.

Author contribution:

The author of this dissertation wrote the manuscript, made all graphics and performed flow cytometry analyses for figure 3. Relative contribution: about 70%.

3.1.3 Publication 3

High-throughput screening for natural compound-based autophagy modulators reveals novel chemotherapeutic mode of action for arzanol

Jana Deitersen, Fabian Stuhldreier, Sara Ceccacci, David Schlütermann, Lena Berning, Wenxian Wu, Yadong Sun, Niklas Berleth, Maria José Mendiburo, Sabine Seggewiß, Maria Chiara Monti, Peter Proksch, Björn Stork

Manuscript in preparation.

The pharmacological modulation of autophagy can aid chemotherapy by sensitizing cancer cells towards approved drugs and overcoming chemoresistance. Recent translational data on autophagy modulators show promising results in reducing tumor growth and metastasis, but also reveal a need for more specific compounds and novel lead structures. Here, we searched for such autophagy-modulating compounds in a high-throughput screening of an in-house natural compound library. We successfully identified novel inducers and inhibitors of the autophagic pathway. Among these, we identified arzanol as autophagy-modulating drug that is able to sensitize RT-112 bladder cancer cells towards cisplatin (CDDP). Its anticancer activity was further confirmed in monotherapy against both CDDP-sensitive and -resistant bladder cancer cells. We determine arzanol as novel mitotoxin, inducing the fragmentation of mitochondrial membranes, and identified mitochondria-associated quinone-binding oxidoreductases as new targets. Surprisingly, we observed a reduction of the size of autophagosomes and a pronounced accumulation of p62/SQSTM1 in response to arzanol treatment. We therefore speculate that arzanol acts both as inducer of early autophagosome biogenesis and as inhibitor of late autophagy events, deeming arzanol a valuable tool for autophagy research and cancer therapy.

Author contribution:

The author of this dissertation designed the experiments, performed flow cytometry analyses, microscopy and cell viability assays, performed the NQO1 activity assay and immunoblot analyses, and prepared samples for AP-MS and DARTS. They also analyzed and interpreted the data and wrote the manuscript. Relative contribution: about 70%.

3.1.4 Publication 4

The mycotoxin phomoxanthone A disturbs the form and function of the inner mitochondrial membrane

Philip Böhler, Fabian Stuhldreier, Ruchika Anand, Arun Kumar Kondadi, David Schlütermann, Niklas Berleth, Jana Deitersen, Nora Wallot-Hieke, Wenxian Wu, Marian Frank, Hendrik Niemann, Elisabeth Wesbuer, Andreas Barbian, Tomas Luyten, Jan B. Parys, Stefanie Weidtkamp-Peters, Andrea Borchardt, Andreas S. Reichert, Aida Peña-Blanco, Ana J. García-Sáez, Samuel Itskanov, Alexander M. van der Bliek, Peter Proksch, Sebastian Wesselborg, Björn Stork

Cell Death and Disease, 19;9(3):286, February 2018.

DOI: 10.1038/s41419-018-0312-8

Phomoxanthone A is a natural compound, which can be isolated from the endophytic fungus *Phomopsis longicolla*. It is a homodimer of two symmetrical C-4,4'-linked acetylated tetrahydroxanthones with prominent anti-bacterial function. Further, it has been shown to induce rapid apoptosis in human cancer cell lines at lower micromolar concentrations. This manuscript reveals for the first time the mode of action of phomoxanthone A in the induction of apoptosis. Targeting the inner mitochondrial membrane, phomoxanthone A inhibits the electron transport chain activity and cellular respiration. It rapidly leads to the depolarization of the mitochondrial membrane and the disruption of cristae within the mitochondria. Independently from the canonical mitochondrial fission and fusion mediators dynamin-1-like protein (DNM1L, also DRP1) and OPA1, phomoxanthone A causes a collapse of the mitochondrial network structure and a release of both pro-apoptotic proteins and the second messenger Ca^{2+} from the mitochondria. Acting as a mitochondrial toxin, it bears a novel mode of action that might prove a useful tool to study mitochondria in future research.

Author contribution:

The author of this dissertation contributed several ideas and suggestions to the project and gave technical support with flow cytometry and cloning. Relative contribution: about 5%.

3.1.5 Publication 5

Carbamoyl-phosphate synthase 1 as a novel target of phomoxanthone A, a bioactive fungal metabolite

Sara Ceccacci, Jana Deitersen, Matteo Mozzicafreddo, Elva Morretta, Peter Proksch, Sebastian Wesselborg, Björn Stork, Maria Chiara Monti

Manuscript under revision at Biomolecules.

Phomoxanthone A, a bioactive xanthone dimer isolated from the endophytic fungus *Phomopsis sp*., is a mitochondrial toxin weakening cellular respiration and electron transport chain activity by a rapid fragmentation of the mitochondrial network structure. To fully address its mechanism of action, a multi-disciplinary strategy has been developed and applied for identifying novel targets of phomoxanthone A. Drug affinity response target stability (DARTS) and targeted limited proteolysis (t-LiP-MRM) point to the identification of carbamoyl-phosphate synthase 1 (CPS1) as a major phomoxanthone A target in mitochondria. We give detailed insights into the ligand/target interaction sites by molecular docking studies and observe an unexpected phomoxanthone A-dependent stimulation of carbamoyl-phosphate synthase 1 activity. Thus, we discuss how xanthones can be regarded as promising new lead structures for drug development in CPS1-related hyperammonemia.

Author contribution:

The author of this dissertation contributed several ideas and suggestions to the project and purified mitochondria, which served as sample for all target identification and validation experiments. Relative contribution: about 10%.

3.2 Publications beyond the scope of this dissertation

The author of this dissertation contributed to several additional publications during her doctorate. As these publications are beyond the scope of this dissertation, they are not attached to this work.

3.2.1 Publication 6

Systematic analysis of ATG13 domain requirements for autophagy induction

Nora Wallot-Hieke, Neha Verma, David Schlütermann, Niklas Berleth, Jana Deitersen, Philip Böhler, Fabian Stuhldreier, Wenxian Wu, Christoph Peter, Sabine Seggewiss, Holger Gohlke, Noboru Mizushima, Björn Stork

Autophagy. 2018;14(5):743-763, March 2018.

DOI: 10.1080/15548627.2017.1387342

Author contribution:

The author of this dissertation gave technical support, discussed the results and commented on the manuscript. Relative contribution: about 2%.

3.2.2 Publication 7

A systems study reveals concurrent activation of AMPK and mTOR by amino acids

Piero Dalle Pezze, Stefanie Ruf, Annika G. Sonntag, Miriam Langelaar-Makkinje, Philip Hall, Alexander M. Heberle, Patricia Razquin Navas, Karen van Eunen, Regine C. Tölle, Jennifer J. Schwarz, Heike Wiese, Bettina Warscheid, Jana Deitersen, Björn Stork, Erik Fäßler, Sascha Schäuble, Udo Hahn, Peter Horvatovich, Daryl P. Shanley, Kathrin Thedieck

Nature Communications, volume 7, Article number: 13254, November 2016.

DOI: 10.1038/ncomms13254

Author contribution:

The author of this dissertation generated the ULK1 wild type and ULK1-S758E-expressing ULK1/2 double knockout murine embryonic fibroblasts, and commented on the manuscript. Relative contribution: about 2%.

3.2.3 Publication 8

The autophagy-initiating kinase ULK1 controls RIPK1-mediated cell death

Wenxian Wu, Xiaojing Wang, Niklas Berleth, Jana Deitersen, Nora Wallot-Hieke, Philip Böhler, David Schlütermann, Fabian Stuhldreier, Jan Cox, Katharina Schmitz, Sabine Seggewiß, Christoph Peter, Gary Kasof, Anja Stefanski, Kai Stühler, Astrid Tschapek, Axel Gödecke, Björn Stork

Cell Reports. 31(3):107547, April 2020

doi: 10.1016/j.celrep.2020.107547.

Author contribution:

The author of this dissertation gave technical and statistical support, discussed the results and commented on the manuscript. Relative contribution: about 5%.

3.2.4 Publication 9

TNF-induced necroptosis initiates early autophagy events via RIPK3-dependent AMPK activation and inhibits late autophagy via cleavage of STX17

Wenxian Wu, Xiaojing Wang, Yadong Sun, Niklas Berleth, Jana Deitersen, David Schlütermann, Fabian Stuhldreier, Nora Wallot-Hieke, Maria José Mendiburo, Christoph Peter, Ann Kathrin Bergmann, Björn Stork

Manuscript in preparation

Author contribution:

The author of this dissertation gave technical and statistical support, discussed the results and commented on the manuscript. Relative contribution: about 5%.

4 Conclusion & Discussion

Discovering novel drug candidates for anti-cancer research is crucial. In this, understanding the modes of action of hit compounds is important in order to assess potential target- or off-target-related side effects and gather information for chemical derivatization. This work describes the early drug discovery approach to find novel modulators of autophagy and identify mechanisms by which chemotherapeutic resistance can be overcome in cancer cells. Within the work of this dissertation, the first achieved milestone was the successful identification of several novel autophagy-modulating compounds, including a subclass of hydroxyanthraquinones and arzanol. As second milestone, we identified several new pharmacological approaches to overcome therapy-resistance in cancer cells, including re-sensitization of bladder carcinoma cells using autophagy inhibitors, and inducing mitochondrial damage via monotherapy of phomoxanthone A or arzanol.

In a proof-of-principle manuscript, we investigated if and how the modulation of autophagy affects the efficacy of cisplatin (CDDP or CisPt) in sensitive and resistant urothelial carcinoma cells. According to The European Association of Urology, cisplatin is applied as first-line treatment in many cases of advanced or metastatic urothelial carcinoma [184]. While only 50% to 62% of patients with advanced transitional-cell carcinoma responded to a first-line combination chemotherapy of methotrexate, vinblastine, adriamycine, and cisplatin, refractory bladder cancer had an overall response rate of 14% for single drug and 32% for doublet chemotherapy in second-line treatment [185, 186]. One approach to combat this poor prognosis is the identification of novel drugs for single or combination treatment. Many studies report that the modulation of autophagy (both inhibition and induction) was able to sensitize therapy-resistant cells to cisplatin-induced cell death in different cancer settings [187, 188, 189, 190, 191, 192, 193]. Although most of these publications studied the effect of small molecules with rather broad pharmaceutical implications such as mTOR inhibitors or chloroquine, ATG knockdown studies were able to confirm the specific impact of autophagy on cisplatin-resistance [194, 195, 196, 197]. In line with these data, we found autophagy-related proteins were up-regulated in cisplatin-resistant versus sensitive urothelial carcinoma cells, and we proved that synergistic effects of autophagy-inhibitors SAR405, 3-MA or chloroquine with cisplatin sensitized resistant cancer cells towards second-line therapy [119]. We characterized autophagy as an appropriate target pathway in cisplatin therapy-resistance (chapter 3.1.1), and went on to identify novel modulators of autophagy.

4.1 Identification of autophagy-modulating natural compounds

In order to identify novel modulators, we performed fluorescence-based flow cytometric autophagy screenings of more than 300 natural compounds. To exclude PAINS among our hits, the majority of compounds was screened for cytotoxicity in different cancer cell lines, immune cells, and pathogens (*Toxoplasma gondii*, *Mycobacterium tuberculosis,* and *Escherichia coli*) within our collaboration network. In a prior small scale screening, we identified a class of anthraquinones, of which six derivatives namely 1'-deoxyrhodoptilometrin-6-O-sulfate, 1'-deoxyrhodoptilometrin, altersolanol A, emodin, skyrin, and biemodin acted as inhibitors of starvation-induced autophagy (chapter 3.1.2) [90]. Our data confirm anti-autophagic effects of emodin observed by other groups, which propose multiple pathways as well as emodin-dependent ROS scavenging as modes of action (reviewed in [90]). In contrast, to our knowledge, we are the first group to report autophagy-modulating properties of the other hydroxyanthraquinone derivatives including altersolanol A.

In addition to these anthraquinones, our large scale screening uncovered 64 inhibitors of starvation-induced autophagy, thereof five inhibitors of basal autophagy (aaptamine, stemphyltoxin I, manzamine J N-oxid, secalonic acid F and kuanoniamin D) (chapter 3.1.3). Among the most potent inhibitors of autophagy were wortmannin A (see wortmannin, chapter 1.8) and wortmannin C, a derivative with the furan-group substituted by an amine-group, which should not to be confused with the nomenclature of Fu et al. [198]. To find the well-known autophagy inhibitor wortmannin among our blinded screening proofed the reliability of our settings. We further identified eight potential autophagy inducers, of which enniatin A1, the lignans (-)-arctigenin and (-)-matairesinol, and 4,6 dibromo-2-(2',4'-dibromophenoxy)phenol are sole inducers, whereas beauvericin J, enniatin B1, pergularinin and viriditoxin acted pro-autophagic upon full medium but inhibitory during starvation, which could be related to their cytotoxicity. Phomoxanthone A displayed similar dual properties in the first run of the screening, but lost its effect in the replication due to a freezing-dependent compound instability, which we prevented in subsequent studies of phomoxanthone A.

Biochemically, phomoxanthone A is a putative derivative of emodin in the biosynthetic pathway from C_{16} polyketides to 4,4'-linked xanthones via oxidative ring-scission and subsequent decarboxylative cyclisation of the monodictyphenone [199]. In a cancer setting, Rönsberg et al. reported that phomoxanthone A is able to induce apoptosis in the otherwise highly apoptosis-resistant Burkitt lymphoma cell line DG-75. This cell line is deficient for BAK, BAX and BCL-2, indicating a mode of action for phomoxanthone A that bypasses BCL-2-dependent intrinsic apoptosis [200, 201]. Intrigued by its strong anti-cancer properties, we investigated the mode of action of phomoxanthone A, and found that phomoxanthone A induces rapid mitochondrial damage characterized by mitochondrial depolarization and a strong release of mitochondrial Ca^{2+} (chapter 3.1.4) [202]. In contrast to uncouplers like carbonyl

cyanide m-chlorophenyl hydrazone (CCCP), phomoxanthone A-treated mitochondria exhibited only low rates of electron transport chain activity and cellular respiration, which indicated an unknown mechanism of inducing mitochondrial damage. In line with this hypothesis, only the inner mitochondrial membrane was fragmented, but still pro-apoptotic proteins were released to induce apoptosis. Confirming our observations, Wang et al. witnessed the depolarization of the mitochondrial membrane potential, and an increase in intracellular Ca^{2+} in cisplatin-sensitive and -resistant cells [203]. Using in silico analysis, they show how phomoxanthone A can incorporate into the inner mitochondrial membrane, where it might act as proton shuttle to disrupt the proton gradient. Although their concept fits to the rapid depolarization of mitochondria within a few minutes after phomoxanthone A treatment, phomoxanthone A does not seem to act like a typical uncoupler of the mitochondrial membrane. Its substantially different mode of action compared to the standard uncoupler CCCP led us to speculate on an additional protein target for phomoxanthone A. Therefore, In our studies of isolated mitochondria, acetyl-CoA acetyltransferase (THIL), aconitate hydratase (ACON), heat shock 70 kDa protein 1A (HS71A), and carbamoyl-phosphate syntase-1 (CPS1) were identified as protein targets of phomoxanthone A in targeted-Limited Proteolysis-Multiple Reaction Monitoring (t-LiP-MRM) (publication 3.1.5). In silico analysis mapped the binding interfaces of phomoxanthone A on the protein surface of CPS1, where it increases at high concentrations the enzymatic activity. CPS1 is a mitochondrial protein that combines ammonia, bicarbonate and ATP to carbamoyl phosphate, which ultimately enters the urea cycle. So far, we have not investigated if and how phomoxanthone A-induced imbalance in CPS1 activity could affect mitochondrial damage. The mode of action for phomoxanthone A might be pleiotropic and include both protein- and membrane-binding properties.

In an orthogonal secondary screening of the natural compound library in human cells, we found arzanol as most potent compound inducing the accumulation of the autophagic markers p62/SQSTM1 and LC3-II upon starvation (publication 3.1.3). Consistent with these data, we observed an early accumulation of ATG16L1 and an accumulation of LC3-positive immature autophagosomes in response to arzanol treatment in starved HeLa cells. After excluding ROS generation or scavenging as mode of action, we investigated arzanol-induced mitochondrial damage and observed the fragmentation of both inner and outer mitochondrial membranes. In addition, markers for mitochondrial damage such as PINK1 accumulation, ubiquinated Parkin, or cleavage of OPA1, were elevated upon arzanol treatment. Using affinity purification and DARTS for target identification, we found several new molecular targets for arzanol that involve quinone-binding oxidoreductases inter alia of the respiratory chain complex III. We propose a mode of action for arzanol that comprises the inhibition of oxidoreductases of the respiratory chain, leading to mitochondrial damage. We present a hypothesis by which arzanol-induced mitochondrial damage causes the initial induction of mitophagy as a survival response. We speculate that failure of autophagosome maturation, leading to accumulation of LC3-II

and p62/SQSTM1, is caused either by prolonged mitochondrial damage and the induction of cell death, or by another autophagy-related arzanol target such as Ras-related protein Rab-1B (RAB1B), or heat shock protein HSP 90-alpha (HS90A). Ultimately, we designate arzanol as a novel mitotoxin and inhibitor of autophagy. In this, we are the first group to show an impact of arzanol on autophagy and/or mitochondria.

4.2 Elimination of therapy-resistant cancer

Our proof-of-principle manuscript shows that autophagy inhibitors can reduce cell viability in cisplatin-resistant cancer cells, and further sensitize resistant cancer cells towards cisplatin (publication 3.1.1) [119]. However, when dealing with common autophagy inhibitors, we have to be aware that most of these compounds do not only have multiple targets, but that these targets also have multiple functions of which autophagy is just one example. 3-MA is widely used as an autophagy inhibitor due to its inhibition of the class III PI3K activity, but researchers have shown that 3-MA can also enhance autophagic flux most likely via the inhibition of class I PI3K [179]. Treatment with 3-MA can also lead to mitosis-related apoptotic cell death independent of ATGs, which indicates a role for the PI3K pathway in mitosis regulation [204]. Therefore, all pan specific PI3K inhibitors could have dual roles in autophagy, but also autophagy-independent functions in cell death.

Similarly, some hydroxyanthraquinones seem to affect cell death independently of autophagy. While altersolanol A had a pronounced cytotoxic activity towards a panel of 34 different human tumor cell lines, also 1'-deoxyrhodoptilometrin and (S)-(-)-rhodoptilometrin induced cell death in glioma and colon carcinoma cells [205, 206]. Intriguingly, only altersolanol A and 1'-deoxyrhodoptilometrin but not (S)-(-)-rhodoptilometrin had an impact on autophagy in our screening. We therefore conclude that the anti-cancer effect of (S)-(-)-rhodoptilometrin is not correlated to autophagy modulation, which might also be the case for other derivatives of this family.

In the case of emodin, inhibition of autophagy by CQ reduced emodin-induced apoptosis in HCT116 and LOVO cells [207]. This finding suggests that the induction of autophagy contributes to anthraquinone-induced cancer cell death contingent on emodin. Further, emodin as the hydroxyanthraquinone derivative with most evidence to inhibit autophagy, sensitized platinum-resistant cancer cells to a second treatment with cisplatin [208]. Moreover, the combination of emodin and cisplatin was reported to selectively sensitize human prostate cancer cells (DU-145), but not human non-tumor dermal fibroblasts [209]. Huang et al. further show the inhibition of tumor growth by a combinational treatment of cisplatin and emodin in vivo, without detecting systemic toxicity of healthy tissue, making emodin a suitable candidate for further studies on cancer chemotherapy. Of note, sensitization towards

chemotherapeutics was also observed for aloe-emodin that induced cell death in combination therapy with cisplatin, doxorubicin, or 5-fluorouracil in Merkel carcinoma cells [210].

Like its biochemical congener emodin, phomoxanthone A was found to be cytotoxic against a range of cisplatin-resistant carcinoma cells [199]. While phomoxanthone A induced apoptotic cell death in apoptosis-incompetent cells, cisplatin-sensitive and cisplatin-resistant cancer cells in the same way, it was not as toxic to healthy human peripheral blood mononuclear cells or isolated lymphocytes [199, 211]. As spectacular as this finding is, there is so far no explanation for the supposed cancer-specificity of phomoxanthone A. The complex role of mitochondria in cancer cells might contribute to this phenomenon: Contrary to the early conception of the Warburg effect, stating that cancer cells only rely on glycolysis for their ATP production, it is now understood that especially proliferating cancer cells still depend on mitochondria to a great extent [212, 213]. Not only are many cancer cells able to switch from glycolysis to respiration as a source of energy, they also depend on intact mitochondria for the maintenance of ROS, the regulation of autophagy, and the inhibition of apoptosis. Cancer cells, more than non-malignant cells, rely on intact mitochondria for eluding apoptotic cell death [214]. Mitotoxins are therefore an important class of anti-cancer agents [215, 216]. Targeting mitochondria with phomoxanthone A could therefore serve as explanation for its cancer cell specificity.

Like phomoxanthone A, arzanol induced mitochondrial damage and reduced the cell viability in cisplatin-sensitive and cisplatin-resistant cancer cells (publication 3.1.4). Furthermore, arzanol sensitized RT-112 bladder carcinoma cells towards cisplatin, but was not able to sensitize resistant bladder cancer cells in our settings. Nevertheless, our data support findings of Rosa et al. who described anti-cancer properties of arzanol before [217]. How far the autophagy-related effects of arzanol play a role in the sensitization towards cisplatin remains to be examined. Autophagy is a dynamic pro-survival mechanism carefully interwoven with other cellular fate pathways. Although the inhibition of autophagy is not inevitably necessary to induce cancer cell death, autophagy is involved in the downstream response to mitochondrial toxicity as in the case of arzanol, and downstream of the AKT/PI3K/mTOR- or MAPK-pathway as in the case of hydroxyanthraquinones. As inhibition of autophagy can induce cell death in apoptosis-incompetent cells, these compounds could still be beneficial e.g. in p53- or BAX-negative carcinoma. However, one has to be aware that autophagy-accompanied cell death in apoptosis-incompetent cells can also be related to necrosis, which is unfavorable in a clinical setting [110].

So far, natural compounds can overcome therapy-resistance by acting cytotoxic in monotherapy such as some of the hydroxyanthraquinones, phomoxanthone A, or arzanol. They can also sensitize resistant cancer cells towards chemotherapy as in the case of emodin, 3-MA, SAR405, or CQ. Thereby, their biological efficacy can be either closely related to autophagy as in our proof-of-concept manuscript,

rather unrelated such as for (S)-(-)-rhodoptilometrin, or undesignedly related to autophagy as in the case of arzanol, where we so far could not reveal the complete pathway. Only when all pathways are fully revealed and autophagy-specific modulators are developed, the real role of autophagy in chemotherapy can be examined.

4.3 Outlook and a prospect of lead structures

Collectively, hydroxyanthraquinones, phomoxanthone A and arzanol share common pharmacodynamic features in targeting multiple cell death-related targets, but they also share structural similarities. All are cyclic natural compounds consisting of multiple rings that are substituted with hydroxyl-groups with oxygen being the only heteroatom, while they also share the α, β unsaturated ketone moiety. Regarding drug-likeliness, at least one aromatic ring can be found in 99% of a big pharma drug database, and molecules with more than three aromatic rings have proven undesirable pharmacokinetic properties [218, 219]. With one to two aromatic rings, our compounds seem ideal concerning drug development parameters such as solubility, lipophilicity, serum albumin binding, cytochrome P450 inhibition and cardiac potassium ion channel inhibition [220]. With three hydrogen donors each, less than ten total hydrogen acceptors and a log P value below 5, especially arzanol and emodin conform to Lipinski's rule of drug-likeliness [129, 221].

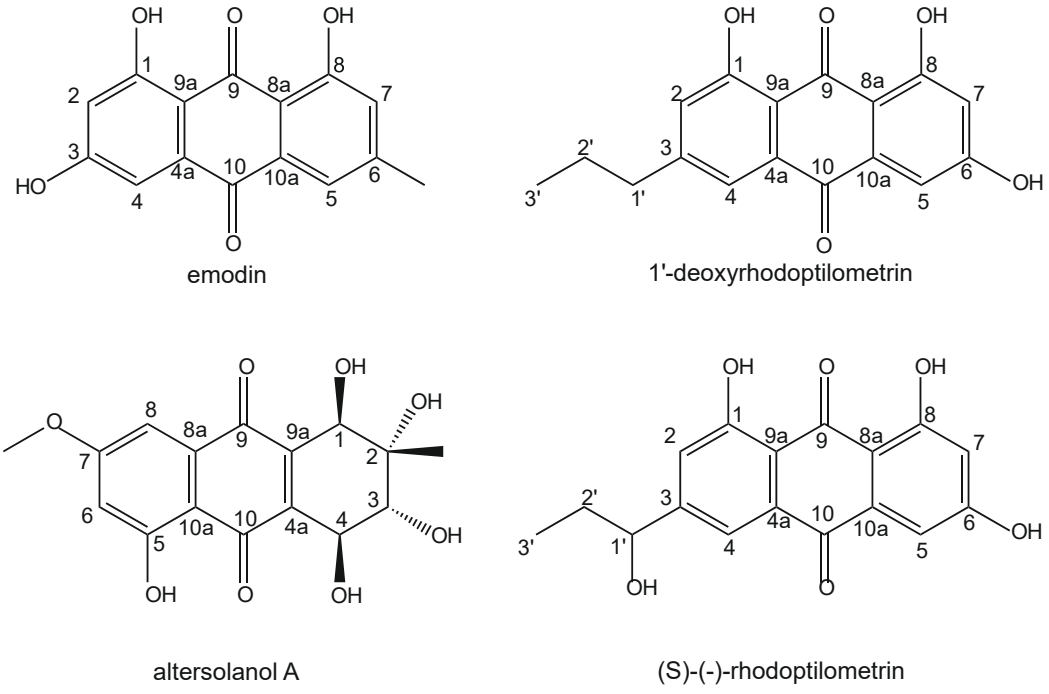

Figure 6. Structure of emodin, altersolanol A, 1'-deoxyrhodoptilometrin, and (s)-(-)-rhodoptilometrin.

For the development of anthraquinone derivatives, some moieties have to be maintained for biological activity. Acetylation of the hydroxyl-groups in altersolanol A result in tetraacetylaltersolanol A and improved the dynamic of induced cell death in human chronic leukemia cells, whereas reduction of the carbonyl groups of the quinone moiety in tetrahydroaltersolanol B and ampelanol abrogated cytotoxicity [222]. This quinone moiety is generally thought to contribute to hydroxyanthraquinone-dependent toxicity by either enzyme-catalyzed redox cycling or physicochemical production of radicals dependent on ring substitutions [223]. Also for the modulation of autophagy, a three-ring structure with two para-keto groups and hydroxylation of positions C1, C3 and C8 appear to be necessary for the bioactivity of anthraquinones [90]. Interestingly, several derivatives such as altersolanol A, 1'-deoxyrhodoptilometrin and (S)-(-)-rhodoptilometrin were found to be potent kinase inhibitors, with altersolanol A and 1'-deoxyrhodoptilometrin being the more active compounds [224, 205]. Combined, these data highlight the importance of hydroxyl-group substitutions directly at the ring, but not as secondary alcohol.

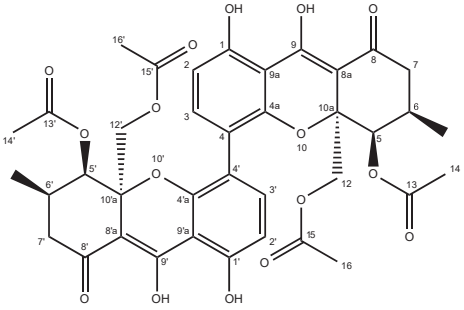

phomoxanthone A

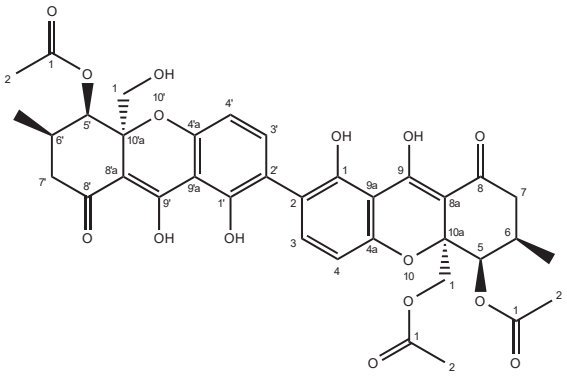

dicerandrol B

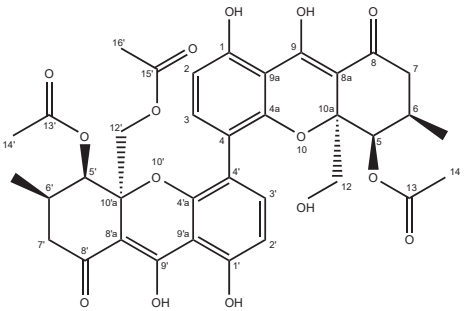

12-deacetylphomoxanthone A

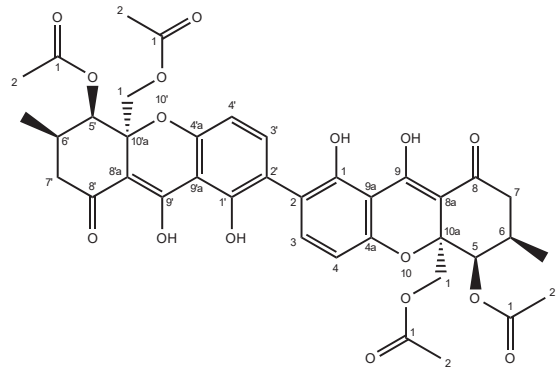

dicerandrol C

Figure 7. Structures of phomoxanthone A, 12-deacetylphomoxanthone A, dicerandrol B, and dicerandrol C.

Comparing bioactivities of phomoxanthone A, 12-deacetylphomoxanthone A, and the 2-2'-linked dicerandrol derivatives clearly shows that 4-4'-biaryl linkage of the two tetrahydroxanthones and C-12-acetylation are favorable in phomoxanthone A bioactivity [199]. Still, 2-2'-linked dimers such as dicerandrol C are highly potent cell death inducers, indicating an important role of the monomers in the anti-tumor activity [225]. The molecular docking analysis of the CPS1-phomoxanthone complex by our collaborator Matteo Mozzicafreddo (chapter 3.1.5), and the configurational free energy computations by Wang et al. could aid developing novel derivatives [203].

For arzanol, identified targets have to be further validated and their arzanol binding sites have to be revealed. So far, our data indicate a preference of arzanol to bind quinone-dependent oxidoreductases such as respiratory complexes I, II and III, but also NAD(P)H dehydrogenase [quinone] 1 (NQO1) and the mitochondrial superoxide dismutase (SOD2). Of note, the α-pyrone moiety of arzanol resembles the coumarin-group of dicoumarol, a published inhibitor of the quinone-dependent oxidoreductase NQO1 (formerly called DT diaphorase) [226, 227]. Similar to our findings from experiments with arzanol, dicoumarol was shown to bind serum albumins, and also uncoupled mitochondria as off-target effect by reducing activity of respiratory complexes II, III, and IV [228, 229]. In doing so, dicoumarol interferes with cell viability assays related to mitochondrial activity [230, 231]. As NQO1 could also be involved in the reduction of resazurin, one should be as careful with the interpretation of data from dicoumarol in the Alamar blue assay [232, 233]). Any derivatives of coumarin or arzanol have to be carefully assessed when testing for the induction of cancer cell death as standard viability test might result in false positive hits.

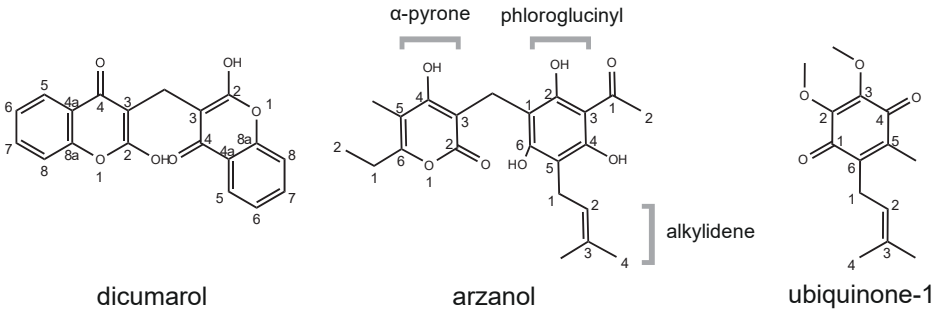

Figure 8. Structures of arzanol, dicoumarol, and ubiquinone-1.

Considering the preference of dicoumarol and arzanol to bind quinone-dependent enzymes, and the resemblance of the prenylated phloroglucinyl-group of arzanol with ubiquinone-1, antagonistic experiments, crystallization studies and in silico mapping should determine if arzanol is able to bind the quinone-binding site of proteins. In addition, del Gaudio et al. proposed that arzanol activates the brain glycogen phosphorylase (PYGB) by allosterically binding its ATP-binding site [234]. If this is true, it could explain binding of arzanol to other quinone-independent targets such as HSP90 or RAB1B1 in our assays. Moreover, other groups described arzanol to target the pro-inflammatory enzymes microsomal prostaglandin E2 synthase-1 (mPGES-1) and 5-lipo-oxygenase (5-LO) [235, 236]. In this,

methylation of the pyrone moiety was not essential for the inhibition of mPGES-1 activity, while methylation of the alkylidene linker decreased mPGES-1 activity [237]. Minassi et al. further proved that a benzylidene linker-dependent increase in lipophilicity also improved inhibition of mPGES-1, and that phloroglucinyl homodimers remained active, whereas pyrone dimers lost their activity against mPGES-1 and 5-LO. Loss of the α-pyrone moiety also reduces its ability to scavenge peroxyl radicals in lipid peroxidation [217]. Different substitutions at the pyrone and phloroglucinyl ring can possibly direct the target specificity in arzanol derivatives. If and how these derivatives modulate autophagy remains to be evaluated, however pharmacologically improved arzanol derivatives can be useful tools in studying both autophagosome maturation and cancer cell death.

Both for research and for clinical application, there is a great potential for these compounds. These compounds aid the induction of cancer cell death due to the modulation of various pathways at once, providing a lesser chance of cancer therapy resistance. Although natural compound research often struggles with the disadvantages of complex structures and the top-down drug discovery approach, synthetic approaches will always complement and never replace the ingenuity of nature.

5 References

1 E. Dolgin (2019). *Anticancer autophagy inhibitors attract 'resurgent' interest*. *Nat Rev Drug Discov* 18,408-410,doi:10.1038/d41573-019-00072-1.

2 M. Hochstrasser (2009). *Origin and function of ubiquitin-like proteins*. *Nature* 458,422-429,doi:10.1038/nature07958.

3 A. Hershko & A. Ciechanover (1998). *The ubiquitin system*. *Annu Rev Biochem* 67,425-479,doi:10.1146/annurev.biochem.67.1.425.

4 A. Hershko, A. Ciechanover & I. A. Rose (1981). *Identification of the active amino acid residue of the polypeptide of ATP-dependent protein breakdown*. *J Biol Chem* 256,1525-1528

5 A. Hershko, A. Ciechanover & I. A. Rose (1979). *Resolution of the ATP-dependent proteolytic system from reticulocytes: a component that interacts with ATP*. *Proc Natl Acad Sci U S A* 76,3107-3110,doi:10.1073/pnas.76.7.3107.

6 S. L. Clark, Jr. (1957). *Cellular differentiation in the kidneys of newborn mice studies with the electron microscope*. *J Biophys Biochem Cytol* 3,349-362,doi:10.1083/jcb.3.3.349.

7 A. B. Novikoff & E. Essner (1962). *Cytolysomes and mitochondrial degeneration*. *J Cell Biol* 15,140-146,doi:10.1083/jcb.15.1.140.

8 T. P. Ashford & K. R. Porter (1962). *Cytoplasmic components in hepatic cell lysosomes*. *J Cell Biol* 12,198-202,doi:10.1083/jcb.12.1.198.

9 Y. Kabeya, N. Mizushima, T. Ueno, A. Yamamoto, T. Kirisako, T. Noda, . . . T. Yoshimori (2000). *LC3, a mammalian homologue of yeast Apg8p, is localized in autophagosome membranes after processing*. *Embo j* 19,5720-5728,doi:10.1093/emboj/19.21.5720.

10 M. Komatsu, S. Waguri, M. Koike, Y. S. Sou, T. Ueno, T. Hara, . . . K. Tanaka (2007). *Homeostatic levels of p62 control cytoplasmic inclusion body formation in autophagy-deficient mice*. *Cell* 131,1149-1163,doi:10.1016/j.cell.2007.10.035.

11 G. Matsumoto, K. Wada, M. Okuno, M. Kurosawa & N. Nukina (2011). *Serine 403 phosphorylation of p62/SQSTM1 regulates selective autophagic clearance of ubiquitinated proteins*. *Mol Cell* 44,279-289,doi:10.1016/j.molcel.2011.07.039.

12 J. Dong & W. Chen (2013). *The role of autophagy in chloroplast degradation and chlorophagy in immune defenses during Pst DC3000 (AvrRps4) infection*. *PLoS One* 8,e73091,doi:10.1371/journal.pone.0073091.

13 S. Bernales, K. L. McDonald & P. Walter (2006). *Autophagy counterbalances endoplasmic reticulum expansion during the unfolded protein response*. *PLoS Biol* 4,e423,doi:10.1371/journal.pbio.0040423.

14 J. D. Mancias, X. Wang, S. P. Gygi, J. W. Harper & A. C. Kimmelman (2014). *Quantitative proteomics identifies NCOA4 as the cargo receptor mediating ferritinophagy*. *Nature* 509,105-109,doi:10.1038/nature13148.

15 O. B. Kotoulas, S. A. Kalamidas & D. J. Kondomerkos (2004). *Glycogen autophagy*. *Microsc Res Tech* 64,10-20,doi:10.1002/jemt.20046.

16 J. R. Buchan, R. M. Kolaitis, J. P. Taylor & R. Parker (2013). *Eukaryotic stress granules are cleared by autophagy and Cdc48/VCP function*. *Cell* 153,1461-1474,doi:10.1016/j.cell.2013.05.037.

17 R. Singh, S. Kaushik, Y. Wang, Y. Xiang, I. Novak, M. Komatsu, . . . M. J. Czaja (2009). *Autophagy regulates lipid metabolism*. *Nature* 458,1131-1135,doi:10.1038/nature07976.

18 S. P. Elmore, T. Qian, S. F. Grissom & J. J. Lemasters (2001). *The mitochondrial permeability transition initiates autophagy in rat hepatocytes*. *Faseb j* 15,2286-2287,doi:10.1096/fj.01-0206fje.

19 A. M. Tolkovsky, L. Xue, G. C. Fletcher & V. Borutaite (2002). *Mitochondrial disappearance from cells: a clue to the role of autophagy in programmed cell death and disease? Biochimie* 84,233-240,doi:10.1016/s0300-9084(02)01371-8.

20 J. A. Gomez-Sanchez, L. Carty, M. Iruarrizaga-Lejarreta, M. Palomo-Irigoyen, M. Varela-Rey, M. Griffith, . . . K. R. Jessen (2015). *Schwann cell autophagy, myelinophagy, initiates myelin clearance from injured nerves*. *J Cell Biol* 210,153-168,doi:10.1083/jcb.201503019.

21 P. Roberts, S. Moshitch-Moshkovitz, E. Kvam, E. O'Toole, M. Winey & D. S. Goldfarb (2003). *Piecemeal microautophagy of nucleus in Saccharomyces cerevisiae*. *Mol Biol Cell* 14,129-141,doi:10.1091/mbc.e02-08-0483.

22 Y. E. Park, Y. K. Hayashi, G. Bonne, T. Arimura, S. Noguchi, I. Nonaka & I. Nishino (2009). *Autophagic degradation of nuclear components in mammalian cells*. *Autophagy* 5,795-804,doi:10.4161/auto.8901.

23 K. M. Walter, M. J. Schonenberger, M. Trotzmuller, M. Horn, H. P. Elsasser, A. B. Moser, . . . W. J. Kovacs (2014). *Hif-2alpha promotes degradation of mammalian peroxisomes by selective autophagy*. *Cell Metab* 20,882-897,doi:10.1016/j.cmet.2014.09.017.

24 V. Cohen-Kaplan, I. Livneh, N. Avni, B. Fabre, T. Ziv, Y. T. Kwon & A. Ciechanover (2016). *p62- and ubiquitin-dependent stress-induced autophagy of the mammalian 26S proteasome*. *Proc Natl Acad Sci U S A* 113,E7490-e7499,doi:10.1073/pnas.1615455113.

25 C. Kraft, A. Deplazes, M. Sohrmann & M. Peter (2008). *Mature ribosomes are selectively degraded upon starvation by an autophagy pathway requiring the Ubp3p/Bre5p ubiquitin protease*. *Nat Cell Biol* 10,602-610,doi:10.1038/ncb1723.

26 B. Levine (2005). *Eating oneself and uninvited guests: autophagy-related pathways in cellular defense*. *Cell* 120,159-162,doi:10.1016/j.cell.2005.01.005.

27 S. B. Kudchodkar & B. Levine (2009). *Viruses and autophagy*. *Rev Med Virol* 19,359-378,doi:10.1002/rmv.630.

28 D. J. Klionsky (2007). *Autophagy: from phenomenology to molecular understanding in less than a decade*. *Nat Rev Mol Cell Biol* 8,931-937,doi:10.1038/nrm2245.

29 F. Reggiori, M. Komatsu, K. Finley & A. Simonsen (2012). *Autophagy: more than a nonselective pathway*. *Int J Cell Biol* 2012,219625,doi:10.1155/2012/219625.

30 J. F. Dice, H. L. Chiang, E. P. Spencer & J. M. Backer (1986). *Regulation of catabolism of microinjected ribonuclease A. Identification of residues 7-11 as the essential pentapeptide*. *J Biol Chem* 261,6853-6859

31 E. Y. Chan & S. A. Tooze (2009). *Evolution of Atg1 function and regulation*. *Autophagy* 5,758-765,doi:10.4161/auto.8709.

32 A. Matsuura, M. Tsukada, Y. Wada & Y. Ohsumi (1997). *Apg1p, a novel protein kinase required for the autophagic process in Saccharomyces cerevisiae*. *Gene* 192,245-250,doi:10.1016/s0378-1119(97)00084-x.

33 M. Tsukada & Y. Ohsumi (1993). *Isolation and characterization of autophagy-defective mutants of Saccharomyces cerevisiae*. *FEBS Lett* 333,169-174,doi:10.1016/0014-5793(93)80398-e.

34 H. Suzuki, T. Osawa, Y. Fujioka & N. N. Noda (2017). *Structural biology of the core autophagy machinery*. *Curr Opin Struct Biol* 43,10-17,doi:10.1016/j.sbi.2016.09.010.

35 G. Kroemer, G. Marino & B. Levine (2010). *Autophagy and the integrated stress response*. *Mol Cell* 40,280-293,doi:10.1016/j.molcel.2010.09.023.

36 D. H. Kim, D. D. Sarbassov, S. M. Ali, J. E. King, R. R. Latek, H. Erdjument-Bromage, . . . D. M. Sabatini (2002). *mTOR interacts with raptor to form a nutrient-sensitive complex that signals to the cell growth machinery*. *Cell* 110,163-175,doi:10.1016/s0092-8674(02)00808-5.

37 A. Saci, L. C. Cantley & C. L. Carpenter (2011). *Rac1 regulates the activity of mTORC1 and mTORC2 and controls cellular size*. *Mol Cell* 42,50-61,doi:10.1016/j.molcel.2011.03.017.

38 I. G. Ganley, H. Lam du, J. Wang, X. Ding, S. Chen & X. Jiang (2009). *ULK1.ATG13.FIP200 complex mediates mTOR signaling and is essential for autophagy*. *J Biol Chem* 284,12297-12305,doi:10.1074/jbc.M900573200.

39 N. Hosokawa, T. Hara, T. Kaizuka, C. Kishi, A. Takamura, Y. Miura, . . . N. Mizushima (2009). *Nutrient-dependent mTORC1 association with the ULK1-Atg13-FIP200 complex required for autophagy*. *Mol Biol Cell* 20,1981-1991,doi:10.1091/mbc.E08-12-1248.

40 C. H. Jung, C. B. Jun, S. H. Ro, Y. M. Kim, N. M. Otto, J. Cao, . . . D. H. Kim (2009). *ULK-Atg13-FIP200 complexes mediate mTOR signaling to the autophagy machinery*. *Mol Biol Cell* 20,1992-2003,doi:10.1091/mbc.E08-12-1249.

41 Y. Kamada, T. Funakoshi, T. Shintani, K. Nagano, M. Ohsumi & Y. Ohsumi (2000). *Tor-mediated induction of autophagy via an Apg1 protein kinase complex*. *J Cell Biol* 150,1507-1513,doi:10.1083/jcb.150.6.1507.

42 Y. Kamada, K. Yoshino, C. Kondo, T. Kawamata, N. Oshiro, K. Yonezawa & Y. Ohsumi (2010). *Tor directly controls the Atg1 kinase complex to regulate autophagy*. *Mol Cell Biol* 30,1049-1058,doi:10.1128/mcb.01344-09.

43 S. Alers, A. S. Loffler, S. Wesselborg & B. Stork (2012). *Role of AMPK-mTOR-Ulk1/2 in the regulation of autophagy: cross talk, shortcuts, and feedbacks*. *Mol Cell Biol* 32,2-11,doi:10.1128/mcb.06159-11.

44 E. Itakura & N. Mizushima (2010). *Characterization of autophagosome formation site by a hierarchical analysis of mammalian Atg proteins*. *Autophagy* 6,764-776,doi:10.4161/auto.6.6.12709.

45 K. Matsunaga, E. Morita, T. Saitoh, S. Akira, N. T. Ktistakis, T. Izumi, . . . T. Yoshimori (2010). *Autophagy requires endoplasmic reticulum targeting of the PI3-kinase complex via Atg14L*. *J Cell Biol* 190,511-521,doi:10.1083/jcb.200911141.

46 E. L. Axe, S. A. Walker, M. Manifava, P. Chandra, H. L. Roderick, A. Habermann, . . . N. T. Ktistakis (2008). *Autophagosome formation from membrane compartments enriched in phosphatidylinositol 3-phosphate and dynamically connected to the endoplasmic reticulum*. *J Cell Biol* 182,685-701,doi:10.1083/jcb.200803137.

47 M. Hayashi-Nishino, N. Fujita, T. Noda, A. Yamaguchi, T. Yoshimori & A. Yamamoto (2009). *A subdomain of the endoplasmic reticulum forms a cradle for autophagosome formation*. *Nat Cell Biol* 11,1433-1437,doi:10.1038/ncb1991.

48 P. Yla-Anttila, H. Vihinen, E. Jokitalo & E. L. Eskelinen (2009). *3D tomography reveals connections between the phagophore and endoplasmic reticulum*. *Autophagy* 5,1180-1185,doi:10.4161/auto.5.8.10274.

49 N. Mizushima, A. Yamamoto, M. Hatano, Y. Kobayashi, Y. Kabeya, K. Suzuki, . . . T. Yoshimori (2001). *Dissection of autophagosome formation using Apg5-deficient mouse embryonic stem cells*. *J Cell Biol* 152,657-668,doi:10.1083/jcb.152.4.657.

50 T. Shpilka, H. Weidberg, S. Pietrokovski & Z. Elazar (2011). *Atg8: an autophagy-related ubiquitin-like protein family*. *Genome Biol* 12,226,doi:10.1186/gb-2011-12-7-226.

51 I. Tanida, E. Tanida-Miyake, T. Ueno & E. Kominami (2001). *The human homolog of Saccharomyces cerevisiae Apg7p is a Protein-activating enzyme for multiple substrates including human Apg12p, GATE-16, GABARAP, and MAP-LC3*. *J Biol Chem* 276,1701-1706,doi:10.1074/jbc.C000752200.

52 I. Tanida, E. Tanida-Miyake, M. Komatsu, T. Ueno & E. Kominami (2002). *Human Apg3p/Aut1p homologue is an authentic E2 enzyme for multiple substrates, GATE-16, GABARAP, and MAP-LC3, and facilitates the conjugation of hApg12p to hApg5p*. *J Biol Chem* 277,13739-13744,doi:10.1074/jbc.M200385200.

53 Y. Kabeya, N. Mizushima, A. Yamamoto, S. Oshitani-Okamoto, Y. Ohsumi & T. Yoshimori (2004). *LC3, GABARAP and GATE16 localize to autophagosomal membrane depending on form-II formation*. *J Cell Sci* 117,2805-2812,doi:10.1242/jcs.01131.

54 A. B. Birgisdottir, T. Lamark & T. Johansen (2013). *The LIR motif - crucial for selective autophagy*. *J Cell Sci* 126,3237-3247,doi:10.1242/jcs.126128.

55 Yongyao Wang, Linsen Li, Chen Hou, Ying Lai, Jiangang Long, Jiankang Liu, . . . Jiajie Diao (2016). *SNARE-mediated membrane fusion in autophagy*. *Semin Cell Dev Biol* 60,97-104,doi:10.1016/j.semcdb.2016.07.009.

56 D. J. Klionsky, K. Abdelmohsen, A. Abe, M. J. Abedin, H. Abeliovich, A. Acevedo Arozena, . . . S. M. Zughaier (2016). *Guidelines for the use and interpretation of assays for monitoring autophagy (3rd edition)*. *Autophagy* 12,1-222,doi:10.1080/15548627.2015.1100356.

57 E. Shvets, E. Fass & Z. Elazar (2008). *Utilizing flow cytometry to monitor autophagy in living mammalian cells*. *Autophagy* 4,621-628,doi:10.4161/auto.5939.

58 S. Kimura, T. Noda & T. Yoshimori (2007). *Dissection of the autophagosome maturation process by a novel reporter protein, tandem fluorescent-tagged LC3*. *Autophagy* 3,452-460,doi:10.4161/auto.4451.

59 T. Kaizuka, H. Morishita, Y. Hama, S. Tsukamoto, T. Matsui, Y. Toyota, . . . N. Mizushima (2016). *An Autophagic Flux Probe that Releases an Internal Control*. *Mol Cell* 64,835-849,doi:10.1016/j.molcel.2016.09.037.

60 M. Priault, B. Salin, J. Schaeffer, F. M. Vallette, J. P. di Rago & J. C. Martinou (2005). *Impairing the bioenergetic status and the biogenesis of mitochondria triggers mitophagy in yeast*. *Cell Death Differ* 12,1613-1621,doi:10.1038/sj.cdd.4401697.

61 S. Honda, S. Arakawa, Y. Nishida, H. Yamaguchi, E. Ishii & S. Shimizu (2014). *Ulk1-mediated Atg5-independent macroautophagy mediates elimination of mitochondria from embryonic reticulocytes*. *Nat Commun* 5,4004,doi:10.1038/ncomms5004.

62 I. Novak, V. Kirkin, D. G. McEwan, J. Zhang, P. Wild, A. Rozenknop, . . . I. Dikic (2010). *Nix is a selective autophagy receptor for mitochondrial clearance*. *EMBO Rep* 11,45-51,doi:10.1038/embor.2009.256.

63 H. Sandoval, P. Thiagarajan, S. K. Dasgupta, A. Schumacher, J. T. Prchal, M. Chen & J. Wang (2008). *Essential role for Nix in autophagic maturation of erythroid cells*. *Nature* 454,232-235,doi:10.1038/nature07006.

64 R. L. Schweers, J. Zhang, M. S. Randall, M. R. Loyd, W. Li, F. C. Dorsey, . . . P. A. Ney (2007). *NIX is required for programmed mitochondrial clearance during reticulocyte maturation*. *Proc Natl Acad Sci U S A* 104,19500-19505,doi:10.1073/pnas.0708818104.

65 J. Bereiter-Hahn & M. Voth (1994). *Dynamics of mitochondria in living cells: shape changes, dislocations, fusion, and fission of mitochondria*. *Microsc Res Tech* 27,198-219,doi:10.1002/jemt.1070270303.

66 G. Twig, A. Elorza, A. J. Molina, H. Mohamed, J. D. Wikstrom, G. Walzer, . . . O. S. Shirihai (2008). *Fission and selective fusion govern mitochondrial segregation and elimination by autophagy*. *Embo j* 27,433-446,doi:10.1038/sj.emboj.7601963.

67 D. Narendra, A. Tanaka, D. F. Suen & R. J. Youle (2008). *Parkin is recruited selectively to impaired mitochondria and promotes their autophagy*. *J Cell Biol* 183,795-803,doi:10.1083/jcb.200809125.

68 S. Kimura, N. Fujita, T. Noda & T. Yoshimori (2009). *Monitoring autophagy in mammalian cultured cells through the dynamics of LC3*. *Methods Enzymol* 452,1-12,doi:10.1016/s0076-6879(08)03601-x.

69 S. Geisler, K. M. Holmstrom, D. Skujat, F. C. Fiesel, O. C. Rothfuss, P. J. Kahle & W. Springer (2010). *PINK1/Parkin-mediated mitophagy is dependent on VDAC1 and p62/SQSTM1*. *Nat Cell Biol* 12,119-131,doi:10.1038/ncb2012.

70 M. Lazarou, D. A. Sliter, L. A. Kane, S. A. Sarraf, C. Wang, J. L. Burman, . . . R. J. Youle (2015). *The ubiquitin kinase PINK1 recruits autophagy receptors to induce mitophagy*. *Nature* 524,309-314,doi:10.1038/nature14893.

71 K. Okamoto, N. Kondo-Okamoto & Y. Ohsumi (2009). *Mitochondria-anchored receptor Atg32 mediates degradation of mitochondria via selective autophagy*. *Dev Cell* 17,87-97,doi:10.1016/j.devcel.2009.06.013.

72 T. Kanki, K. Wang, Y. Cao, M. Baba & D. J. Klionsky (2009). *Atg32 is a mitochondrial protein that confers selectivity during mitophagy*. *Dev Cell* 17,98-109,doi:10.1016/j.devcel.2009.06.014.

73 T. Murakawa, O. Yamaguchi, A. Hashimoto, S. Hikoso, T. Takeda, T. Oka, . . . K. Otsu (2015). *Bcl-2-like protein 13 is a mammalian Atg32 homologue that mediates mitophagy and mitochondrial fragmentation*. *Nat Commun* 6,7527,doi:10.1038/ncomms8527.

74 T. Murakawa, K. Okamoto, S. Omiya, M. Taneike, O. Yamaguchi & K. Otsu (2019). *A Mammalian Mitophagy Receptor, Bcl2-L-13, Recruits the ULK1 Complex to Induce Mitophagy*. *Cell Rep* 26,338-345.e336,doi:10.1016/j.celrep.2018.12.050.

75 M. Lv, C. Wang, F. Li, J. Peng, B. Wen, Q. Gong, . . . Y. Tang (2017). *Structural insights into the recognition of phosphorylated FUNDC1 by LC3B in mitophagy*. *Protein Cell* 8,25-38,doi:10.1007/s13238-016-0328-8.

76 L. Liu, D. Feng, G. Chen, M. Chen, Q. Zheng, P. Song, . . . Q. Chen (2012). *Mitochondrial outer-membrane protein FUNDC1 mediates hypoxia-induced mitophagy in mammalian cells*. *Nat Cell Biol* 14,177-185,doi:10.1038/ncb2422.

77 M. J. Baker, P. A. Lampe, D. Stojanovski, A. Korwitz, R. Anand, T. Tatsuta & T. Langer (2014). *Stress-induced OMA1 activation and autocatalytic turnover regulate OPA1-dependent mitochondrial dynamics*. *Embo j* 33,578-593,doi:10.1002/embj.201386474.

78 M. V. Alavi & N. Fuhrmann (2013). *Dominant optic atrophy, OPA1, and mitochondrial quality control: understanding mitochondrial network dynamics*. *Mol Neurodegener* 8,32,doi:10.1186/1750-1326-8-32.

79 L. Griparic, N. N. van der Wel, I. J. Orozco, P. J. Peters & A. M. van der Bliek (2004). *Loss of the intermembrane space protein Mgm1/OPA1 induces swelling and localized constrictions along the lengths of mitochondria*. *J Biol Chem* 279,18792-18798,doi:10.1074/jbc.M400920200.

80 A. Olichon, L. Baricault, N. Gas, E. Guillou, A. Valette, P. Belenguer & G. Lenaers (2003). *Loss of OPA1 perturbates the mitochondrial inner membrane structure and integrity, leading to cytochrome c release and apoptosis*. *J Biol Chem* 278,7743-7746,doi:10.1074/jbc.C200677200.

81 C. Merkwirth, S. Dargazanli, T. Tatsuta, S. Geimer, B. Lower, F. T. Wunderlich, . . . T. Langer (2008). *Prohibitins control cell proliferation and apoptosis by regulating OPA1-dependent cristae morphogenesis in mitochondria*. *Genes Dev* 22,476-488,doi:10.1101/gad.460708.

82 B. C. Dickinson & C. J. Chang (2011). *Chemistry and biology of reactive oxygen species in signaling or stress responses*. *Nat Chem Biol* 7,504-511,doi:10.1038/nchembio.607.

83 P. Cejas, E. Casado, C. Belda-Iniesta, J. De Castro, E. Espinosa, A. Redondo, . . . M. Gonzalez-Baron (2004). *Implications of oxidative stress and cell membrane lipid peroxidation in human cancer (Spain)*. *Cancer Causes Control* 15,707-719,doi:10.1023/b:Caco.0000036189.61607.52.

84 T. Ozben (2007). *Oxidative stress and apoptosis: impact on cancer therapy*. *J Pharm Sci* 96,2181-2196,doi:10.1002/jps.20874.

85 Y. Chen, M. B. Azad & S. B. Gibson (2009). *Superoxide is the major reactive oxygen species regulating autophagy*. *Cell Death Differ* 16,1040-1052,doi:10.1038/cdd.2009.49.

86 A. L. Nieminen, A. K. Saylor, S. A. Tesfai, B. Herman & J. J. Lemasters (1995). *Contribution of the mitochondrial permeability transition to lethal injury after exposure of hepatocytes to t-butylhydroperoxide*. *Biochem J* 307 (Pt 1),99-106,doi:10.1042/bj3070099.

87 A. L. Nieminen, A. M. Byrne, B. Herman & J. J. Lemasters (1997). *Mitochondrial permeability transition in hepatocytes induced by t-BuOOH: NAD(P)H and reactive oxygen species*. *Am J Physiol* 272,C1286-1294,doi:10.1152/ajpcell.1997.272.4.C1286.

88 A. J. Kowaltowski, R. F. Castilho & A. E. Vercesi (1996). *Opening of the mitochondrial permeability transition pore by uncoupling or inorganic phosphate in the presence of Ca2+ is dependent on mitochondrial-generated reactive oxygen species*. *FEBS Lett* 378,150-152,doi:10.1016/0014-5793(95)01449-7.

89 B. Perillo, M. Di Donato, A. Pezone, E. Di Zazzo, P. Giovannelli, G. Galasso, . . . A. Migliaccio (2020). *ROS in cancer therapy: the bright side of the moon*. *Exp Mol Med* 52,192-203,doi:10.1038/s12276-020-0384-2.

90 J. Deitersen, D. H. El-Kashef, P. Proksch & B. Stork (2019). *Anthraquinones and autophagy - Three rings to rule them all? Bioorg Med Chem* 27,115042,doi:10.1016/j.bmc.2019.115042.

91 G. Liu, F. Pei, F. Yang, L. Li, A. D. Amin, S. Liu, . . . W. C. Cho (2017). *Role of Autophagy and Apoptosis in Non-Small-Cell Lung Cancer*. *Int J Mol Sci* 18,doi:10.3390/ijms18020367.

92 A. Qiao, K. Wang, Y. Yuan, Y. Guan, X. Ren, L. Li, . . . Y. Cheng (2016). *Sirt3-mediated mitophagy protects tumor cells against apoptosis under hypoxia*. *Oncotarget* 7,43390-43400,doi:10.18632/oncotarget.9717.

93 Y. Zhu, S. Massen, M. Terenzio, V. Lang, S. Chen-Lindner, R. Eils, . . . N. R. Brady (2013). *Modulation of serines 17 and 24 in the LC3-interacting region of Bnip3 determines pro-survival mitophagy versus apoptosis*. *J Biol Chem* 288,1099-1113,doi:10.1074/jbc.M112.399345.

94 W. Hou, J. Han, C. Lu, L. A. Goldstein & H. Rabinowich (2010). *Autophagic degradation of active caspase-8: a crosstalk mechanism between autophagy and apoptosis*. *Autophagy* 6,891-900,doi:10.4161/auto.6.7.13038.

95 S. Mukhopadhyay, P. K. Panda, N. Sinha, D. N. Das & S. K. Bhutia (2014). *Autophagy and apoptosis: where do they meet? Apoptosis* 19,555-566,doi:10.1007/s10495-014-0967-2.

96 L. Yu, A. Alva, H. Su, P. Dutt, E. Freundt, S. Welsh, . . . M. J. Lenardo (2004). *Regulation of an ATG7-beclin 1 program of autophagic cell death by caspase-8*. *Science* 304,1500-1502,doi:10.1126/science.1096645.

97 S. Shimizu, T. Kanaseki, N. Mizushima, T. Mizuta, S. Arakawa-Kobayashi, C. B. Thompson & Y. Tsujimoto (2004). *Role of Bcl-2 family proteins in a non-apoptotic programmed cell death dependent on autophagy genes*. *Nat Cell Biol* 6,1221-1228,doi:10.1038/ncb1192.

98 E. Ullman, Y. Fan, M. Stawowczyk, H. M. Chen, Z. Yue & W. X. Zong (2008). *Autophagy promotes necrosis in apoptosis-deficient cells in response to ER stress*. *Cell Death Differ* 15,422-425,doi:10.1038/sj.cdd.4402234.

99 E. Buytaert, G. Callewaert, J. R. Vandenheede & P. Agostinis (2006). *Deficiency in apoptotic effectors Bax and Bak reveals an autophagic cell death pathway initiated by photodamage to the endoplasmic reticulum*. *Autophagy* 2,238-240,doi:10.4161/auto.2730.

100 L. Galluzzi, I. Vitale, J. M. Abrams, E. S. Alnemri, E. H. Baehrecke, M. V. Blagosklonny, . . . G. Kroemer (2012). *Molecular definitions of cell death subroutines: recommendations of the Nomenclature Committee on Cell Death 2012*. *Cell Death Differ* 19,107-120,doi:10.1038/cdd.2011.96.

101 D. Hanahan & R. A. Weinberg (2011). *Hallmarks of cancer: the next generation*. *Cell* 144,646-674,doi:10.1016/j.cell.2011.02.013.

102 J. D. Rabinowitz & E. White (2010). *Autophagy and metabolism*. *Science* 330,1344-1348,doi:10.1126/science.1193497.

103 B. Levine, N. Mizushima & H. W. Virgin (2011). *Autophagy in immunity and inflammation*. *Nature* 469,323-335,doi:10.1038/nature09782.

104 Y. Matsuzawa-Ishimoto, S. Hwang & K. Cadwell (2018). *Autophagy and Inflammation*. *Annu Rev Immunol* 36,73-101,doi:10.1146/annurev-immunol-042617-053253.

105 S. S. Singh, S. Vats, A. Y. Chia, T. Z. Tan, S. Deng, M. S. Ong, . . . A. P. Kumar (2018). *Dual role of autophagy in hallmarks of cancer*. *Oncogene* 37,1142-1158,doi:10.1038/s41388-017-0046-6.

106 T. Huang, X. Song, Y. Yang, X. Wan, A. A. Alvarez, N. Sastry, . . . S. Y. Cheng (2018). *Autophagy and Hallmarks of Cancer*. *Crit Rev Oncog* 23,247-267,doi:10.1615/CritRevOncog.2018027913.

107 X. Qu, J. Yu, G. Bhagat, N. Furuya, H. Hibshoosh, A. Troxel, . . . B. Levine (2003). *Promotion of tumorigenesis by heterozygous disruption of the beclin 1 autophagy gene*. *J Clin Invest* 112,1809-1820,doi:10.1172/jci20039.

108 H. Tang, S. Sebti, R. Titone, Y. Zhou, C. Isidoro, T. S. Ross, . . . B. Levine (2015). *Decreased BECN1 mRNA Expression in Human Breast Cancer is Associated with Estrogen Receptor-Negative Subtypes and Poor Prognosis*. *EBioMedicine* 2,255-263,doi:10.1016/j.ebiom.2015.01.008.

109 X. H. Liang, S. Jackson, M. Seaman, K. Brown, B. Kempkes, H. Hibshoosh & B. Levine (1999). *Induction of autophagy and inhibition of tumorigenesis by beclin 1*. *Nature* 402,672-676,doi:10.1038/45257.

110 K. Degenhardt, R. Mathew, B. Beaudoin, K. Bray, D. Anderson, G. Chen, . . . E. White (2006). *Autophagy promotes tumor cell survival and restricts necrosis, inflammation, and tumorigenesis*. *Cancer Cell* 10,51-64,doi:10.1016/j.ccr.2006.06.001.

111 A. Vazquez-Martin, C. Oliveras-Ferraros & J. A. Menendez (2009). *Autophagy facilitates the development of breast cancer resistance to the anti-HER2 monoclonal antibody trastuzumab*. *PLoS One* 4,e6251,doi:10.1371/journal.pone.0006251.

112 N. Chen & V. Karantza (2011). *Autophagy as a therapeutic target in cancer*. *Cancer Biol Ther* 11,157-168,doi:10.4161/cbt.11.2.14622.

113 M. J. Abedin, D. Wang, M. A. McDonnell, U. Lehmann & A. Kelekar (2007). *Autophagy delays apoptotic death in breast cancer cells following DNA damage*. *Cell Death Differ* 14,500-510,doi:10.1038/sj.cdd.4402039.

114 J. S. Carew, S. T. Nawrocki, C. N. Kahue, H. Zhang, C. Yang, L. Chung, . . . J. L. Cleveland (2007). *Targeting autophagy augments the anticancer activity of the histone deacetylase inhibitor SAHA to overcome Bcr-Abl-mediated drug resistance*. *Blood* 110,313-322,doi:10.1182/blood-2006-10-050260.

115 R. K. Amaravadi, D. Yu, J. J. Lum, T. Bui, M. A. Christophorou, G. I. Evan, . . . C. B. Thompson (2007). *Autophagy inhibition enhances therapy-induced apoptosis in a Myc-induced model of lymphoma*. *J Clin Invest* 117,326-336,doi:10.1172/jci28833.

116 K. S. Choi (2012). *Autophagy and cancer*. *Exp Mol Med* 44,109-120,doi:10.3858/emm.2012.44.2.033.

117 S. Chen, S. K. Rehman, W. Zhang, A. Wen, L. Yao & J. Zhang (2010). *Autophagy is a therapeutic target in anticancer drug resistance*. *Biochim Biophys Acta* 1806,220-229,doi:10.1016/j.bbcan.2010.07.003.

118 Y. L. Hu, A. Jahangiri, M. Delay & M. K. Aghi (2012). *Tumor cell autophagy as an adaptive response mediating resistance to treatments such as antiangiogenic therapy*. *Cancer Res* 72,4294-4299,doi:10.1158/0008-5472.Can-12-1076.

119 D. Schlutermann, M. A. Skowron, N. Berleth, P. Bohler, J. Deitersen, F. Stuhldreier, . . . B. Stork (2018). *Targeting urothelial carcinoma cells by combining cisplatin with a specific inhibitor of the autophagy-inducing class III PtdIns3K complex*. *Urol Oncol* 36,160.e161-160.e113,doi:10.1016/j.urolonc.2017.11.021.

120 Y. Quan, H. Lei, W. Wahafu, Y. Liu, H. Ping & X. Zhang (2019). *Inhibition of autophagy enhances the anticancer effect of enzalutamide on bladder cancer*. *Biomed Pharmacother* 120,109490,doi:10.1016/j.biopha.2019.109490.

121 E. White & R. S. DiPaola (2009). *The double-edged sword of autophagy modulation in cancer*. *Clin Cancer Res* 15,5308-5316,doi:10.1158/1078-0432.Ccr-07-5023.

122 A. Ko, A. Kanehisa, I. Martins, L. Senovilla, C. Chargari, D. Dugue, . . . E. Deutsch (2014). *Autophagy inhibition radiosensitizes in vitro, yet reduces radioresponses in vivo due to deficient immunogenic signalling*. *Cell Death Differ* 21,92-99,doi:10.1038/cdd.2013.124.

123 S. Daido, T. Kanzawa, A. Yamamoto, H. Takeuchi, Y. Kondo & S. Kondo (2004). *Pivotal role of the cell death factor BNIP3 in ceramide-induced autophagic cell death in malignant glioma cells*. *Cancer Res* 64,4286-4293,doi:10.1158/0008-5472.Can-03-3084.

124 A. S. Arora, B. J. Jones, T. C. Patel, S. F. Bronk & G. J. Gores (1997). *Ceramide induces hepatocyte cell death through disruption of mitochondrial function in the rat*. *Hepatology* 25,958-963,doi:10.1002/hep.510250428.

125 N. Heidari, M. A. Hicks & H. Harada (2010). *GX15-070 (obatoclax) overcomes glucocorticoid resistance in acute lymphoblastic leukemia through induction of apoptosis and autophagy*. *Cell Death Dis* 1,e76,doi:10.1038/cddis.2010.53.

126 L. Bonapace, B. C. Bornhauser, M. Schmitz, G. Cario, U. Ziegler, F. K. Niggli, . . . J. P. Bourquin (2010). *Induction of autophagy-dependent necroptosis is required for childhood acute*

lymphoblastic leukemia cells to overcome glucocorticoid resistance. *J Clin Invest* 120,1310-1323,doi:10.1172/jci39987.

127 F. Basit, S. Cristofanon & S. Fulda (2013). *Obatoclax (GX15-070) triggers necroptosis by promoting the assembly of the necrosome on autophagosomal membranes*. *Cell Death Differ* 20,1161-1173,doi:10.1038/cdd.2013.45.

128 J. P. Hughes, S. Rees, S. B. Kalindjian & K. L. Philpott (2011). *Principles of early drug discovery*. *Br J Pharmacol* 162,1239-1249,doi:10.1111/j.1476-5381.2010.01127.x.

129 C. A. Lipinski (2004). *Lead- and drug-like compounds: the rule-of-five revolution*. *Drug Discov Today Technol* 1,337-341,doi:10.1016/j.ddtec.2004.11.007.

130 D. J. Newman & G. M. Cragg (2016). *Natural Products as Sources of New Drugs from 1981 to 2014*. *J Nat Prod* 79,629-661,doi:10.1021/acs.jnatprod.5b01055.

131 D. D. Baker, M. Chu, U. Oza & V. Rajgarhia (2007). *The value of natural products to future pharmaceutical discovery*. *Nat Prod Rep* 24,1225-1244,doi:10.1039/b602241n.

132 H. Choi, S. Y. Cho, H. J. Pak, Y. Kim, J. Y. Choi, Y. J. Lee, . . . H. Park (2017). *NPCARE: database of natural products and fractional extracts for cancer regulation*. *J Cheminform* 9,2,doi:10.1186/s13321-016-0188-5.

133 F. E. Koehn & G. T. Carter (2005). *The evolving role of natural products in drug discovery*. *Nat Rev Drug Discov* 4,206-220,doi:10.1038/nrd1657.

134 J. W. Li & J. C. Vederas (2009). *Drug discovery and natural products: end of an era or an endless frontier? Science* 325,161-165,doi:10.1126/science.1168243.

135 N. E. Thomford, D. A. Senthebane, A. Rowe, D. Munro, P. Seele, A. Maroyi & K. Dzobo (2018). *Natural Products for Drug Discovery in the 21st Century: Innovations for Novel Drug Discovery*. *Int J Mol Sci* 19,doi:10.3390/ijms19061578.

136 F. J. Dumont & Q. Su (1996). *Mechanism of action of the immunosuppressant rapamycin*. *Life Sci* 58,373-395,doi:10.1016/0024-3205(95)02233-3.

137 L. A. Banaszynski, C. W. Liu & T. J. Wandless (2005). *Characterization of the FKBP.rapamycin.FRB ternary complex*. *J Am Chem Soc* 127,4715-4721,doi:10.1021/ja043277y.

138 D. D. Sarbassov, S. M. Ali, D. H. Kim, D. A. Guertin, R. R. Latek, H. Erdjument-Bromage, . . . D. M. Sabatini (2004). *Rictor, a novel binding partner of mTOR, defines a rapamycin-insensitive and raptor-independent pathway that regulates the cytoskeleton*. *Curr Biol* 14,1296-1302,doi:10.1016/j.cub.2004.06.054.

139 E. Jacinto, R. Loewith, A. Schmidt, S. Lin, M. A. Ruegg, A. Hall & M. N. Hall (2004). *Mammalian TOR complex 2 controls the actin cytoskeleton and is rapamycin insensitive*. *Nat Cell Biol* 6,1122-1128,doi:10.1038/ncb1183.

140 D. D. Sarbassov, S. M. Ali, S. Sengupta, J. H. Sheen, P. P. Hsu, A. F. Bagley, . . . D. M. Sabatini (2006). *Prolonged rapamycin treatment inhibits mTORC2 assembly and Akt/PKB*. *Mol Cell* 22,159-168,doi:10.1016/j.molcel.2006.03.029.

141 J. D. Morrisett, G. Abdel-Fattah, R. Hoogeveen, E. Mitchell, C. M. Ballantyne, H. J. Pownall, . . . B. D. Kahan (2002). *Effects of sirolimus on plasma lipids, lipoprotein levels, and fatty acid metabolism in renal transplant patients*. *J Lipid Res* 43,1170-1180

142 Y. Y. Zaytseva, J. D. Valentino, P. Gulhati & B. M. Evers (2012). *mTOR inhibitors in cancer therapy*. *Cancer Lett* 319,1-7,doi:10.1016/j.canlet.2012.01.005.

143 Q. Liu, J. W. Chang, J. Wang, S. A. Kang, C. C. Thoreen, A. Markhard, . . . N. S. Gray (2010). *Discovery of 1-(4-(4-propionylpiperazin-1-yl)-3-(trifluoromethyl)phenyl)-9-(quinolin-3-yl)benzo[h][1,6]naphthyridin-2(1H)-one as a highly potent, selective mammalian target of rapamycin (mTOR) inhibitor for the treatment of cancer*. *J Med Chem* 53,7146-7155,doi:10.1021/jm101144f.

144 Q. Liu, J. Wang, S. A. Kang, C. C. Thoreen, W. Hur, T. Ahmed, . . . N. S. Gray (2011). *Discovery of 9-(6-aminopyridin-3-yl)-1-(3-(trifluoromethyl)phenyl)benzo[h][1,6]naphthyridin-2(1H)-one (Torin2) as a potent, selective, and orally available mammalian target of rapamycin (mTOR) inhibitor for treatment of cancer*. *J Med Chem* 54,1473-1480,doi:10.1021/jm101520v.

145 K. Yu, L. Toral-Barza, C. Shi, W. G. Zhang, J. Lucas, B. Shor, . . . A. Zask (2009). *Biochemical, cellular, and in vivo activity of novel ATP-competitive and selective inhibitors of the mammalian target of rapamycin*. *Cancer Res* 69,6232-6240,doi:10.1158/0008-5472.Can-09-0299.

146 Q. Liu, C. Xu, S. Kirubakaran, X. Zhang, W. Hur, Y. Liu, . . . N. S. Gray (2013). *Characterization of Torin2, an ATP-competitive inhibitor of mTOR, ATM, and ATR*. *Cancer Res* 73,2574-2586,doi:10.1158/0008-5472.Can-12-1702.

147 C. J. Vlahos, W. F. Matter, K. Y. Hui & R. F. Brown (1994). *A specific inhibitor of phosphatidylinositol 3-kinase, 2-(4-morpholinyl)-8-phenyl-4H-1-benzopyran-4-one (LY294002)*. *J Biol Chem* 269,5241-5248

148 R. Crazzolara, K. F. Bradstock & L. J. Bendall (2009). *RAD001 (Everolimus) induces autophagy in acute lymphoblastic leukemia*. *Autophagy* 5,727-728,doi:10.4161/auto.5.5.8507.

149 C. Wang, X. Wang, Z. Su, H. Fei, X. Liu & Q. Pan (2015). *The novel mTOR inhibitor Torin-2 induces autophagy and downregulates the expression of UHRF1 to suppress hepatocarcinoma cell growth*. *Oncol Rep* 34,1708-1716,doi:10.3892/or.2015.4146.

150 L. Li, Y. Chen & S. B. Gibson (2013). *Starvation-induced autophagy is regulated by mitochondrial reactive oxygen species leading to AMPK activation*. *Cell Signal* 25,50-65,doi:10.1016/j.cellsig.2012.09.020.

151 Y. Ji, W. Di, Q. Yang, Z. Lu, W. Cai & J. Wu (2015). *Inhibition of Autophagy Increases Proliferation Inhibition and Apoptosis Induced by the PI3K/mTOR Inhibitor NVP-BEZ235 in Breast Cancer Cells*. *Clin Lab* 61,1043-1051,doi:10.7754/clin.lab.2015.150144.

152 Z. Chang, G. Shi, J. Jin, H. Guo, X. Guo, F. Luo, . . . X. Jia (2013). *Dual PI3K/mTOR inhibitor NVP-BEZ235-induced apoptosis of hepatocellular carcinoma cell lines is enhanced by inhibitors of autophagy*. *Int J Mol Med* 31,1449-1456,doi:10.3892/ijmm.2013.1351.

153 H. R. Fei, H. Tian, X. L. Zhou, M. F. Yang, B. L. Sun, X. Y. Yang, . . . F. Z. Wang (2016). *Inhibition of autophagy enhances effects of PF-04691502 on apoptosis and DNA damage of lung cancer cells*. *Int J Biochem Cell Biol* 78,52-62,doi:10.1016/j.biocel.2016.06.023.

154 M. Buzzai, R. G. Jones, R. K. Amaravadi, J. J. Lum, R. J. DeBerardinis, F. Zhao, . . . C. B. Thompson (2007). *Systemic treatment with the antidiabetic drug metformin selectively impairs p53-deficient tumor cell growth*. *Cancer Res* 67,6745-6752,doi:10.1158/0008-5472.Can-06-4447.

155 J. L. Wright & J. L. Stanford (2009). *Metformin use and prostate cancer in Caucasian men: results from a population-based case-control study*. *Cancer Causes Control* 20,1617-1622,doi:10.1007/s10552-009-9407-y.

156 M. Bodmer, C. Meier, S. Krahenbuhl, S. S. Jick & C. R. Meier (2010). *Long-term metformin use is associated with decreased risk of breast cancer*. *Diabetes Care* 33,1304-1308,doi:10.2337/dc09-1791.

157 G. Zhou, R. Myers, Y. Li, Y. Chen, X. Shen, J. Fenyk-Melody, . . . D. E. Moller (2001). *Role of AMP-activated protein kinase in mechanism of metformin action*. *J Clin Invest* 108,1167-1174,doi:10.1172/jci13505.

158 W. Y. Shi, D. Xiao, L. Wang, L. H. Dong, Z. X. Yan, Z. X. Shen, . . . W. L. Zhao (2012). *Therapeutic metformin/AMPK activation blocked lymphoma cell growth via inhibition of mTOR pathway and induction of autophagy*. *Cell Death Dis* 3,e275,doi:10.1038/cddis.2012.13.

159 Z. Zhuo, A. Wang & H. Yu (2016). *Metformin targeting autophagy overcomes progesterone resistance in endometrial carcinoma*. *Arch Gynecol Obstet* 294,1055-1061,doi:10.1007/s00404-016-4148-0.

160 Y. Wang, W. Xu, Z. Yan, W. Zhao, J. Mi, J. Li & H. Yan (2018). *Metformin induces autophagy and G0/G1 phase cell cycle arrest in myeloma by targeting the AMPK/mTORC1 and mTORC2 pathways*. *J Exp Clin Cancer Res* 37,63,doi:10.1186/s13046-018-0731-5.

161 Y. Feng, C. Ke, Q. Tang, H. Dong, X. Zheng, W. Lin, . . . H. Zhang (2014). *Metformin promotes autophagy and apoptosis in esophageal squamous cell carcinoma by downregulating Stat3 signaling*. *Cell Death Dis* 5,e1088,doi:10.1038/cddis.2014.59.

162 Washington Soares Ferreira Júnior, Margarita Paloma Cruz, Lucilene Lima dos Santos & Maria Franco Trindade Medeiros (2012). *Use and importance of quina (Cinchona spp.) and ipeca (Carapichea ipecacuanha (Brot.) L. Andersson): Plants for medicinal use from the 16th century to the present*. *Journal of Herbal Medicine* 2,103-112,doi:https://doi.org/10.1016/j.hermed.2012.07.003.

163 C. A. Homewood, D. C. Warhurst, W. Peters & V. C. Baggaley (1972). *Lysosomes, pH and the anti-malarial action of chloroquine*. *Nature* 235,50-52,doi:10.1038/235050a0.

164 S. Ohkuma & B. Poole (1978). *Fluorescence probe measurement of the intralysosomal pH in living cells and the perturbation of pH by various agents*. *Proc Natl Acad Sci U S A* 75,3327-3331,doi:10.1073/pnas.75.7.3327.

165 M. Mauthe, I. Orhon, C. Rocchi, X. Zhou, M. Luhr, K. J. Hijlkema, . . . F. Reggiori (2018). *Chloroquine inhibits autophagic flux by decreasing autophagosome-lysosome fusion*. *Autophagy* 14,1435-1455,doi:10.1080/15548627.2018.1474314.

166 C. R. Loehberg, P. L. Strissel, R. Dittrich, R. Strick, J. Dittmer, A. Dittmer, . . . M. G. Schrauder (2012). *Akt and p53 are potential mediators of reduced mammary tumor growth by cloroquine and the mTOR inhibitor RAD001*. *Biochem Pharmacol* 83,480-488,doi:10.1016/j.bcp.2011.11.022.

167 L. Qin, T. Xu, L. Xia, X. Wang, X. Zhang, X. Zhang, . . . Z. Shen (2016). *Chloroquine enhances the efficacy of cisplatin by suppressing autophagy in human adrenocortical carcinoma treatment*. *Drug Des Devel Ther* 10,1035-1045,doi:10.2147/dddt.S101701.

168 Nagla Fawzy Abdel Karim, Imran Ahmad, Ola Gaber, Ihab Eldessouki, Olugbenga Olanrele Olowokure, Maria Farooq & John Charles Morris (2019). (American Society of Clinical Oncology).

169 A. Arnaout, S. J. Robertson, G. R. Pond, H. Lee, A. Jeong, L. Ianni, . . . M. Clemons (2019). *A randomized, double-blind, window of opportunity trial evaluating the effects of chloroquine in breast cancer patients*. *Breast Cancer Res Treat* 178,327-335,doi:10.1007/s10549-019-05381-y.

170 C. Verbaanderd, H. Maes, M. B. Schaaf, V. P. Sukhatme, P. Pantziarka, V. Sukhatme, . . . G. Bouche (2017). *Repurposing Drugs in Oncology (ReDO)-chloroquine and hydroxychloroquine as anti-cancer agents*. *Ecancermedicalscience* 11,781,doi:10.3332/ecancer.2017.781.

171 T. Manabe, T. Yoshimori, N. Henomatsu & Y. Tashiro (1993). *Inhibitors of vacuolar-type H(+)-ATPase suppresses proliferation of cultured cells*. *J Cell Physiol* 157,445-452,doi:10.1002/jcp.1041570303.

172 B. J. Bowman & E. J. Bowman (2002). *Mutations in subunit C of the vacuolar ATPase confer resistance to bafilomycin and identify a conserved antibiotic binding site*. *J Biol Chem* 277,3965-3972,doi:10.1074/jbc.M109756200.

173 A. Yamamoto, Y. Tagawa, T. Yoshimori, Y. Moriyama, R. Masaki & Y. Tashiro (1998). *Bafilomycin A1 prevents maturation of autophagic vacuoles by inhibiting fusion between autophagosomes and lysosomes in rat hepatoma cell line, H-4-II-E cells*. *Cell Struct Funct* 23,33-42,doi:10.1247/csf.23.33.

174 B. Whitton, H. Okamoto, G. Packham & S. J. Crabb (2018). *Vacuolar ATPase as a potential therapeutic target and mediator of treatment resistance in cancer*. *Cancer Med* 7,3800-3811,doi:10.1002/cam4.1594.

175 A. Arcaro & M. P. Wymann (1993). *Wortmannin is a potent phosphatidylinositol 3-kinase inhibitor: the role of phosphatidylinositol 3,4,5-trisphosphate in neutrophil responses*. *Biochem J* 296 (Pt 2),297-301,doi:10.1042/bj2960297.

176 E. F. Blommaart, U. Krause, J. P. Schellens, H. Vreeling-Sindelarova & A. J. Meijer (1997). *The phosphatidylinositol 3-kinase inhibitors wortmannin and LY294002 inhibit autophagy in isolated rat hepatocytes*. *Eur J Biochem* 243,240-246,doi:10.1111/j.1432-1033.1997.0240a.x.

177 A. Petiot, E. Ogier-Denis, E. F. Blommaart, A. J. Meijer & P. Codogno (2000). *Distinct classes of phosphatidylinositol 3'-kinases are involved in signaling pathways that control macroautophagy in HT-29 cells*. *J Biol Chem* 275,992-998,doi:10.1074/jbc.275.2.992.

178 P. O. Seglen & P. B. Gordon (1982). *3-Methyladenine: specific inhibitor of autophagic/lysosomal protein degradation in isolated rat hepatocytes*. *Proc Natl Acad Sci U S A* 79,1889-1892,doi:10.1073/pnas.79.6.1889.

179 Y. T. Wu, H. L. Tan, G. Shui, C. Bauvy, Q. Huang, M. R. Wenk, . . . H. M. Shen (2010). *Dual role of 3-methyladenine in modulation of autophagy via different temporal patterns of inhibition on class I and III phosphoinositide 3-kinase*. *J Biol Chem* 285,10850-10861,doi:10.1074/jbc.M109.080796.

180 J. V. Peppard, C. Rugg, M. Smicker, C. Dureuil, B. Ronan, O. Flamand, . . . B. Pasquier (2014). *Identifying Small Molecules which Inhibit Autophagy: a Phenotypic Screen Using Image-Based High-Content Cell Analysis*. *Curr Chem Genom Transl Med* 8,3-15,doi:10.2174/2213988501408010003.

181 B. Pasquier, Y. El-Ahmad, B. Filoche-Romme, C. Dureuil, F. Fassy, P. Y. Abecassis, . . . B. Ronan (2015). *Discovery of (2S)-8-[(3R)-3-methylmorpholin-4-yl]-1-(3-methyl-2-oxobutyl)-2-(trifluoromethyl)- 3,4-dihydro-2H-pyrimido[1,2-a]pyrimidin-6-one: a novel potent and selective inhibitor of Vps34 for the treatment of solid tumors*. *J Med Chem* 58,376-400,doi:10.1021/jm5013352.

182 B. Ronan, O. Flamand, L. Vescovi, C. Dureuil, L. Durand, F. Fassy, . . . B. Pasquier (2014). *A highly potent and selective Vps34 inhibitor alters vesicle trafficking and autophagy*. *Nat Chem Biol* 10,1013-1019,doi:10.1038/nchembio.1681.

183 J. New, L. Arnold, M. Ananth, S. Alvi, M. Thornton, L. Werner, . . . S. M. Thomas (2017). *Secretory Autophagy in Cancer-Associated Fibroblasts Promotes Head and Neck Cancer Progression and Offers a Novel Therapeutic Target*. *Cancer Res* 77,6679-6691,doi:10.1158/0008-5472.Can-17-1077.

184 J. Alfred Witjes, T. Lebret, E. M. Comperat, N. C. Cowan, M. De Santis, H. M. Bruins, . . . M. J. Ribal (2017). *Updated 2016 EAU Guidelines on Muscle-invasive and Metastatic Bladder Cancer*. *Eur Urol* 71,462-475,doi:10.1016/j.eururo.2016.06.020.

185 C. N. Sternberg, P. H. de Mulder, J. H. Schornagel, C. Theodore, S. D. Fossa, A. T. van Oosterom, . . . L. Collette (2001). *Randomized phase III trial of high-dose-intensity methotrexate, vinblastine, doxorubicin, and cisplatin (MVAC) chemotherapy and recombinant human granulocyte colony-stimulating factor versus classic MVAC in advanced urothelial tract tumors: European Organization for Research and Treatment of Cancer Protocol no. 30924*. *J Clin Oncol* 19,2638-2646,doi:10.1200/jco.2001.19.10.2638.

186 D. Raggi, R. Miceli, G. Sonpavde, P. Giannatempo, L. Mariani, M. D. Galsky, . . . A. Necchi (2016). *Second-line single-agent versus doublet chemotherapy as salvage therapy for metastatic urothelial cancer: a systematic review and meta-analysis*. *Ann Oncol* 27,49-61,doi:10.1093/annonc/mdv509.

187 D. Liu, Y. Yang, Q. Liu & J. Wang (2011). *Inhibition of autophagy by 3-MA potentiates cisplatin-induced apoptosis in esophageal squamous cell carcinoma cells*. *Med Oncol* 28,105-111,doi:10.1007/s12032-009-9397-3.

188 Y. Huang, Q. Xi, Y. Chen, J. Wang, P. Peng, S. Xia & S. Yu (2013). *A dual mTORC1 and mTORC2 inhibitor shows antitumor activity in esophageal squamous cell carcinoma cells and sensitizes them to cisplatin*. *Anticancer Drugs* 24,889-898,doi:10.1097/CAD.0b013e328363c64e.

189 B. B. Ma, V. W. Lui, E. P. Hui, C. P. Lau, K. Ho, M. H. Ng, . . . A. T. Chan (2010). *The activity of mTOR inhibitor RAD001 (everolimus) in nasopharyngeal carcinoma and cisplatin-resistant cell lines*. *Invest New Drugs* 28,413-420,doi:10.1007/s10637-009-9269-x.

190 S. Mabuchi, C. Kawase, D. A. Altomare, K. Morishige, K. Sawada, M. Hayashi, . . . T. Kimura (2009). *mTOR is a promising therapeutic target both in cisplatin-sensitive and cisplatin-resistant clear cell carcinoma of the ovary*. *Clin Cancer Res* 15,5404-5413,doi:10.1158/1078-0432.Ccr-09-0365.

191 K. H. Tam, Z. F. Yang, C. K. Lau, C. T. Lam, R. W. Pang & R. T. Poon (2009). *Inhibition of mTOR enhances chemosensitivity in hepatocellular carcinoma*. *Cancer Lett* 273,201-209,doi:10.1016/j.canlet.2008.08.018.

192 C. Wu, M. Wangpaichitr, L. Feun, M. T. Kuo, C. Robles, T. Lampidis & N. Savaraj (2005). *Overcoming cisplatin resistance by mTOR inhibitor in lung cancer*. *Mol Cancer* 4,25,doi:10.1186/1476-4598-4-25.

193 J. Garcia-Cano, G. Ambroise, R. Pascual-Serra, M. C. Carrion, L. Serrano-Oviedo, M. Ortega-Muelas, . . . R. Sanchez-Prieto (2015). *Exploiting the potential of autophagy in cisplatin therapy: A new strategy to overcome resistance*. *Oncotarget* 6,15551-15565,doi:10.18632/oncotarget.3902.

194 B. Ma, L. Z. Liang, G. Q. Liao, Y. J. Liang, H. C. Liu, G. S. Zheng & Y. X. Su (2013). *Inhibition of autophagy enhances cisplatin cytotoxicity in human adenoid cystic carcinoma cells of salivary glands*. *J Oral Pathol Med* 42,774-780,doi:10.1111/jop.12066.

195 Z. Zhao, L. Tao, C. Shen, B. Liu, Z. Yang & H. Tao (2014). *Silencing of Barkor/ATG14 sensitizes osteosarcoma cells to cisplatininduced apoptosis*. *Int J Mol Med* 33,271-276,doi:10.3892/ijmm.2013.1578.

196 T. Fukuda, K. Oda, O. Wada-Hiraike, K. Sone, K. Inaba, Y. Ikeda, . . . T. Fujii (2015). *The anti-malarial chloroquine suppresses proliferation and overcomes cisplatin resistance of endometrial cancer cells via autophagy inhibition*. *Gynecol Oncol* 137,538-545,doi:10.1016/j.ygyno.2015.03.053.

197 X. G. Zhao, R. J. Sun, X. Y. Yang, D. Y. Liu, D. P. Lei, T. Jin & X. L. Pan (2015). *Chloroquine-enhanced efficacy of cisplatin in the treatment of hypopharyngeal carcinoma in xenograft mice*. *PLoS One* 10,e0126147,doi:10.1371/journal.pone.0126147.

198 Guang-Chao Fu, Zhong-Duo Yang, Shuang-Yan Zhou, Xin-Ming Li, Hai-Tao Yu, Xiao-Jun Yao, . . . Yong-Gang Wang (2016). *Wortmannines A–C, three novel wortmannin derivatives with an unusual five-membered B ring from the endophytic fungus Talaromyces wortmannii LGT-4*. *Tetrahedron Letters* 57,4608-4611,doi:https://doi.org/10.1016/j.tetlet.2016.09.004.

199 D. Ronsberg, A. Debbab, A. Mandi, V. Vasylyeva, P. Bohler, B. Stork, . . . P. Proksch (2013). *Pro-apoptotic and immunostimulatory tetrahydroxanthone dimers from the endophytic fungus Phomopsis longicolla*. *J Org Chem* 78,12409-12425,doi:10.1021/jo402066b.

200 M. Brimmell, R. Mendiola, J. Mangion & G. Packham (1998). *BAX frameshift mutations in cell lines derived from human haemopoietic malignancies are associated with resistance to apoptosis and microsatellite instability*. *Oncogene* 16,1803-1812,doi:10.1038/sj.onc.1201704.

201 A. Muller, B. Gillissen, A. Richter, A. Richter, C. Chumduri, P. T. Daniel & C. W. Scholz (2018). *Pan-class I PI3-kinase inhibitor BKM120 induces MEK1/2-dependent mitotic catastrophe in non-Hodgkin lymphoma leading to apoptosis or polyploidy determined by Bax/Bak and p53*. *Cell Death Dis* 9,384,doi:10.1038/s41419-018-0413-4.

202 P. Bohler, F. Stuhldreier, R. Anand, A. K. Kondadi, D. Schlutermann, N. Berleth, . . . B. Stork (2018). *The mycotoxin phomoxanthone A disturbs the form and function of the inner mitochondrial membrane*. *Cell Death Dis* 9,286,doi:10.1038/s41419-018-0312-8.

203 C. Wang, L. Engelke, D. Bickel, A. Hamacher, M. Frank, P. Proksch, . . . M. U. Kassack (2019). *The tetrahydroxanthone-dimer phomoxanthone A is a strong inducer of apoptosis in cisplatin-resistant solid cancer cells*. *Bioorg Med Chem* 27,115044,doi:10.1016/j.bmc.2019.115044.

204 H. Hou, Y. Zhang, Y. Huang, Q. Yi, L. Lv, T. Zhang, . . . Q. Shi (2012). *Inhibitors of phosphatidylinositol 3'-kinases promote mitotic cell death in HeLa cells*. *PLoS One* 7,e35665,doi:10.1371/journal.pone.0035665.

205 W. Watjen, S. S. Ebada, A. Bergermann, Y. Chovolou, F. Totzke, M. H. G. Kubbutat, . . . P. Proksch (2017). *Cytotoxic effects of the anthraquinone derivatives 1'-deoxyrhodoptilometrin and (S)-(-)-rhodoptilometrin isolated from the marine echinoderm Comanthus sp*. *Arch Toxicol* 91,1485-1495,doi:10.1007/s00204-016-1787-7.

206 P. Mishra, V. Carelli, G. Manfredi & D. C. Chan (2014). *Proteolytic cleavage of Opa1 stimulates mitochondrial inner membrane fusion and couples fusion to oxidative phosphorylation*. *Cell Metab* 19,630-641,doi:10.1016/j.cmet.2014.03.011.

207 Y. Wang, Q. Luo, X. He, H. Wei, T. Wang, J. Shao & X. Jiang (2018). *Emodin Induces Apoptosis of Colon Cancer Cells via Induction of Autophagy in a ROS-Dependent Manner*. *Oncol Res* 26,889-899,doi:10.3727/096504017x15009419625178.

208 J. Ma, J. Yang, C. Wang, N. Zhang, Y. Dong, C. Wang, . . . X. Lin (2014). *Emodin augments cisplatin cytotoxicity in platinum-resistant ovarian cancer cells via ROS-dependent MRP1 downregulation*. *Biomed Res Int* 2014,107671,doi:10.1155/2014/107671.

209 X. Z. Huang, J. Wang, C. Huang, Y. Y. Chen, G. Y. Shi, Q. S. Hu & J. Yi (2008). *Emodin enhances cytotoxicity of chemotherapeutic drugs in prostate cancer cells: the mechanisms involve ROS-mediated suppression of multidrug resistance and hypoxia inducible factor-1*. *Cancer Biol Ther* 7,468-475,doi:10.4161/cbt.7.3.5457.

210 E. Fenig, J. Nordenberg, E. Beery, J. Sulkes & L. Wasserman (2004). *Combined effect of aloe-emodin and chemotherapeutic agents on the proliferation of an adherent variant cell line of Merkel cell carcinoma*. *Oncol Rep* 11,213-217

211 G. B. Pavao, V. P. Venancio, A. L. de Oliveira, L. C. Hernandes, M. R. Almeida, L. M. Antunes & H. M. Debonsi (2016). *Differential genotoxicity and cytotoxicity of phomoxanthone A isolated from the fungus Phomopsis longicolla in HL60 cells and peripheral blood lymphocytes*. *Toxicol In Vitro* 37,211-217,doi:10.1016/j.tiv.2016.08.010.

212 O. Warburg, F. Wind & E. Negelein (1927). *THE METABOLISM OF TUMORS IN THE BODY*. *J Gen Physiol* 8,519-530,doi:10.1085/jgp.8.6.519.

213 E. A. Mandujano-Tinoco, J. C. Gallardo-Perez, A. Marin-Hernandez, R. Moreno-Sanchez & S. Rodriguez-Enriquez (2013). *Anti-mitochondrial therapy in human breast cancer multi-cellular spheroids*. *Biochim Biophys Acta* 1833,541-551,doi:10.1016/j.bbamcr.2012.11.013.

214 V. Gogvadze, S. Orrenius & B. Zhivotovsky (2008). *Mitochondria in cancer cells: what is so special about them? Trends Cell Biol* 18,165-173,doi:10.1016/j.tcb.2008.01.006.

215 S. Fulda, L. Galluzzi & G. Kroemer (2010). *Targeting mitochondria for cancer therapy*. *Nat Rev Drug Discov* 9,447-464,doi:10.1038/nrd3137.

216 T. M. Ashton, W. G. McKenna, L. A. Kunz-Schughart & G. S. Higgins (2018). *Oxidative Phosphorylation as an Emerging Target in Cancer Therapy*. *Clin Cancer Res* 24,2482-2490,doi:10.1158/1078-0432.Ccr-17-3070.

217 A. Rosa, A. Atzeri, M. Nieddu & G. Appendino (2017). *New insights into the antioxidant activity and cytotoxicity of arzanol and effect of methylation on its biological properties*. *Chem Phys Lipids* 205,55-64,doi:10.1016/j.chemphyslip.2017.05.001.

218 S. D. Roughley & A. M. Jordan (2011). *The medicinal chemist's toolbox: an analysis of reactions used in the pursuit of drug candidates*. *J Med Chem* 54,3451-3479,doi:10.1021/jm200187y.

219 S. E. Ward & P. Beswick (2014). *What does the aromatic ring number mean for drug design? Expert Opin Drug Discov* 9,995-1003,doi:10.1517/17460441.2014.932346.

220 T. J. Ritchie & S. J. Macdonald (2009). *The impact of aromatic ring count on compound developability--are too many aromatic rings a liability in drug design? Drug Discov Today* 14,1011-1020,doi:10.1016/j.drudis.2009.07.014.

221 B. Jayaram, T. Singh, G. Mukherjee, A. Mathur, S. Shekhar & V. Shekhar (2012). *Sanjeevini: a freely accessible web-server for target directed lead molecule discovery*. *BMC Bioinformatics* 13 Suppl 17,S7,doi:10.1186/1471-2105-13-s17-s7.

222 M. H. Teiten, F. Mack, A. Debbab, A. H. Aly, M. Dicato, P. Proksch & M. Diederich (2013). *Anticancer effect of altersolanol A, a metabolite produced by the endophytic fungus Stemphylium globuliferum, mediated by its pro-apoptotic and anti-invasive potential via the inhibition of NF-kappaB activity*. *Bioorg Med Chem* 21,3850-3858,doi:10.1016/j.bmc.2013.04.024.

223 E. M. Malik & C. E. Muller (2016). *Anthraquinones As Pharmacological Tools and Drugs*. *Med Res Rev* 36,705-748,doi:10.1002/med.21391.

224 A. Debbab, A. H. Aly, R. Edrada-Ebel, V. Wray, W. E. Muller, F. Totzke, . . . R. Ebel (2009). *Bioactive metabolites from the endophytic fungus Stemphylium globuliferum isolated from Mentha pulegium*. *J Nat Prod* 72,626-631,doi:10.1021/np8004997.

225 M. Frank, H. Niemann, P. Bohler, B. Stork, S. Wesselborg, W. Lin & P. Proksch (2015). *Phomoxanthone A--From Mangrove Forests to Anticancer Therapy*. *Curr Med Chem* 22,3523-3532,doi:10.2174/0929867322666150716115300.

226 N. Robertson, A. Haigh, G. E. Adams & I. J. Stratford (1994). *Factors affecting sensitivity to EO9 in rodent and human tumour cells in vitro: DT-diaphorase activity and hypoxia*. *Eur J Cancer* 30a,1013-1019,doi:10.1016/0959-8049(94)90134-1.

227 J. A. Plumb, M. Gerritsen & P. Workman (1994). *DT-diaphorase protects cells from the hypoxic cytotoxicity of indoloquinone EO9*. *Br J Cancer* 70,1136-1143,doi:10.1038/bjc.1994.461.

228 S. Garten & W. D. Wosilait (1971). *Comparative study of the binding of coumarin anticoagulants and serum albumins*. *Biochem Pharmacol* 20,1661-1668,doi:10.1016/0006-2952(71)90294-2.

229 D. Gonzalez-Aragon, J. Ariza & J. M. Villalba (2007). *Dicoumarol impairs mitochondrial electron transport and pyrimidine biosynthesis in human myeloid leukemia HL-60 cells*. *Biochem Pharmacol* 73,427-439,doi:10.1016/j.bcp.2006.10.016.

230 A. C. Collier & C. A. Pritsos (2003). *The mitochondrial uncoupler dicumarol disrupts the MTT assay*. *Biochem Pharmacol* 66,281-287,doi:10.1016/s0006-2952(03)00240-5.

231 R. Hamid, Y. Rotshteyn, L. Rabadi, R. Parikh & P. Bullock (2004). *Comparison of alamar blue and MTT assays for high through-put screening*. *Toxicol In Vitro* 18,703-710,doi:10.1016/j.tiv.2004.03.012.

232 A. A. Zalata, N. Lammertijn, A. Christophe & F. H. Comhaire (1998). *The correlates and alleged biochemical background of the resazurin reduction test in semen*. *Int J Androl* 21,289-294,doi:10.1046/j.1365-2605.1998.00126.x.

233 J. O'Brien, I. Wilson, T. Orton & F. Pognan (2000). *Investigation of the Alamar Blue (resazurin) fluorescent dye for the assessment of mammalian cell cytotoxicity*. *Eur J Biochem* 267,5421-5426,doi:10.1046/j.1432-1327.2000.01606.x.

234 F. Del Gaudio, F. Pollastro, M. Mozzicafreddo, R. Riccio, A. Minassi & M. C. Monti (2018). *Chemoproteomic fishing identifies arzanol as a positive modulator of brain glycogen phosphorylase*. *Chem Commun (Camb)* 54,12863-12866,doi:10.1039/c8cc07692h.

235 G. Appendino, M. Ottino, N. Marquez, F. Bianchi, A. Giana, M. Ballero, . . . E. Munoz (2007). *Arzanol, an anti-inflammatory and anti-HIV-1 phloroglucinol alpha-Pyrone from Helichrysum italicum ssp. microphyllum*. *J Nat Prod* 70,608-612,doi:10.1021/np060581r.

236 J. Bauer, A. Koeberle, F. Dehm, F. Pollastro, G. Appendino, H. Northoff, . . . O. Werz (2011). *Arzanol, a prenylated heterodimeric phloroglucinyl pyrone, inhibits eicosanoid biosynthesis and exhibits anti-inflammatory efficacy in vivo*. *Biochem Pharmacol* 81,259-268,doi:10.1016/j.bcp.2010.09.025.

237 Alberto Minassi, Lavinia Cicione, Andreas Koeberle, Julia Bauer, Stefan Laufer, Oliver Werz & Giovanni Appendino (2012). *A Multicomponent Carba-Betti Strategy to Alkylidene Heterodimers – Total Synthesis and Structure–Activity Relationships of Arzanol*. 2012,772-779,doi:10.1002/ejoc.201101193.

6 Curriculum Vitae

CONTACT INFORMATION

Name	Jana Deitersen
Address	[redacted]
	[redacted]
Telephone	[redacted]
Email	Jana.Deitersen@hhu.de

ACADEMIC EDUCATION

12/2016 to 06/2020	**Doctorate at Institute of Molecular Medicine I** Heinrich Heine University, Düsseldorf, Germany Supervisor: Prof. Dr. rer. nat. Björn Stork Research Training Group 2158: 'Natural products and natural product analogs against therapy-resistant tumors and microorganisms: new lead structures and modes of action'
10/2014 to 09/2016	**Master's degree Biology** Heinrich Heine University, Düsseldorf, Germany Certificate: Master of Science (Grade 1.3) Master thesis at Institute of Molecular Medicine I Supervisor: Prof. Dr. rer. nat. Björn Stork
10/2011 to 08/2014	**Bachelor's degree Biochemistry** Heinrich Heine University, Düsseldorf, Germany Certificate: Bachelor of Science (Grade 2.25) Bachelor thesis at Cécile und Oskar Vogt Institute of Brain Research Supervisor: Dr. rer. nat. Christina Herold

EMPLOYMENT HISTORY

12/2016 to 06/2020	Scientific Employee at University Hospital Düsseldorf
07/2015 to 12/2016	Scientific Assistant at University Hospital Düsseldorf
07/2013 to 12/2015	Student Assistant at University Hospital Düsseldorf

Licensing & Copyright

- Publication “The mycotoxin phomoxanthone A disturbs the form and function of the inner mitochondrial membrane”
  Copyright Böhler et al. 2018.
  DOI: 10.1038/s41419-018-0312-8

Reprinted under the Creative Commons CC-BY-NC-ND 4.0 license (as indicated by Nature).

- Publication “Carbamoyl-phosphate synthase 1 as a novel target of phomoxanthone A, a bioactive fungal metabolite”
  Copyright Ceccacci et al. 2020.

Reprinted with the copyright as author. Any reproduction of any parts of this manuscript in any form is not permitted without the explicit consent of the authors.

Appendix

Publication 1

Targeting urothelial carcinoma cells by combining cisplatin with a specific inhibitor of the autophagy-inducing class III PtdIns3K complex

David Schlütermann, Margaretha A. Skowron, Niklas Berleth, Philip Böhler, Jana Deitersen, Fabian Stuhldreier, Nora Wallot-Hieke, Wenxian Wu, Christoph Peter, Michèle J. Hoffmann, Günter Niegisch, Björn Stork

Urologic Oncology: Seminars and Original Investigations, volume 36, issue 4, pages 160.e1-160.e13, April 2018

DOI: 10.1016/j.urolonc.2017.11.021

ELSEVIER

CrossMark

Urologic Oncology: Seminars and Original Investigations 36 (2018) 160.e1–160.e13

UROLOGIC ONCOLOGY

Original article

Targeting urothelial carcinoma cells by combining cisplatin with a specific inhibitor of the autophagy-inducing class III PtdIns3K complex

David Schlütermann, M.Sc.[a], Margaretha A. Skowron, M.Sc.[b], Niklas Berleth, M.Sc.[a], Philip Böhler, M.Sc.[a], Jana Deitersen, M.Sc.[a], Fabian Stuhldreier, M.Sc.[a], Nora Wallot-Hieke, Ph.D.[a], Wenxian Wu, M.Sc.[a], Christoph Peter, Ph.D.[a], Michèle J. Hoffmann, Ph.D.[b], Günter Niegisch, M.D.[b], Björn Stork, Ph.D.[a,*]

[a] *Institute of Molecular Medicine I, Medical Faculty, Heinrich Heine University Düsseldorf, Düsseldorf, Germany*
[b] *Department of Urology, Medical Faculty, Heinrich Heine University Düsseldorf, Düsseldorf, Germany*

Received 7 June 2017; received in revised form 31 October 2017; accepted 30 November 2017

Abstract

Background: Cisplatin-based regimens are routinely employed for the treatment of urothelial carcinoma. However, therapeutic success is hampered by the primary presence of or the development of cisplatin resistance. This chemoresistance is executed by multiple cellular pathways. In recent years, the cellular process of autophagy has been identified as a prosurvival pathway of cancer cells. On the one hand, autophagy enables cancer cells to survive conditions of low oxygen or nutrient supply, frequently found in tumors. On the other hand, autophagy supports chemoresistance of cancer cells. Here, we aimed at investigating the involvement of autophagy for cisplatin resistance in different urothelial carcinoma cell lines.

Materials & Methods: We analyzed the expression levels of different autophagy-related proteins in cisplatin-sensitive and cisplatin-resistant urothelial carcinoma cell lines. Furthermore, we performed cell viability assays and caspase activity assays with cells treated with cisplatin, non-specific or specific autophagy inhibitors (chloroquine, 3-methyladenine, SAR405) or combinations thereof.

Results: We found that autophagy-related proteins are up-regulated in different cisplatin-resistant urothelial carcinoma cells compared to the sensitive parental cell lines. Furthermore, inhibition of autophagy, in general, or of the autophagy-inducing class III PtdIns3K complex, in particular, sensitized both sensitive and resistant urothelial carcinoma cells to cisplatin-induced cytotoxic effects.

Conclusion: We propose that targeting the autophagic machinery might represent a suitable approach to complement or even increase cisplatin efficacy in order to overcome cisplatin resistance in urothelial carcinoma.

Keywords: Autophagy; Cisplatin; Urothelial carcinoma; VPS34; Chemoresistance

1. Introduction

Bladder cancer (BC) is the fifth most common cancer in the developed world, with approximately 400,000 new cases diagnosed per year and 150,000 deaths worldwide [1]. In industrial countries, about 90% of BCs are urothelial carcinomas (UC) which may be further classified into muscle-invasive and non–muscle-invasive cancers. These UC subtypes are distinct in clinical behavior and molecular alterations [2]. Comprising up to one-third of UC, muscle-invasive tumors often progress to metastatic disease and patients face a poor prognosis with only 50% to 60% survival after 5 years [3]. Although platinum-based chemotherapy is the standard first-line treatment for advanced UC, its impact on cancer-specific survival is limited [4]. Despite frequent initial treatment responses, overall survival does not exceed 12 to 16 months in metastatic patients [5]. Its anticancer efficacy mainly originates from the formation of bivalent DNA intrastrand crosslinks blocking transcription and replication [6,7]. Subsequently generated DNA double-strand breaks stimulate DNA damage response and initiate the intrinsic mitochondrial apoptosis pathway [8–10]. However, cisplatin treatment frequently leads to the development of chemoresistance, and the molecular mechanisms of resistance are multifaceted [8]. Several factors have been

*Corresponding author. Tel.: +49 211 81 11954; fax: +49 211 81 14103.
E-mail address: bjoern.stork@uni-duesseldorf.de (B. Stork).

https://doi.org/10.1016/j.urolonc.2017.11.021

suggested to determine the response to cisplatin treatment, including factors regulating mechanisms of apoptosis, DNA repair and transport, as well as phenotype plasticity [8,11,12]. However, the mechanisms underlying cisplatin resistance of UC cells have not been clearly identified yet, and current preclinical research aims at increasing efficacy of cisplatin treatment or re-sensitizing cisplatin-resistant cells for cytotoxic effects.

In recent years, autophagy has emerged as an attractive target for cancer therapy [13–15]. During autophagy, intracellular cargo becomes engulfed by double-membraned vesicles termed autophagosomes. Autophagosomes fuse with lysosomes, and within the resulting autolysosomes, the engulfed cargo becomes degraded [16]. Autophagy occurs at basal levels in most cell types, but can also be actively induced upon stress conditions like nutrient deprivation or treatment with anticancer drugs. The induction of autophagy is centrally regulated by 2 kinase complexes: (1) the ULK1 protein kinase complex consisting of the Ser/Thr protein kinase unc51-like kinase 1 (ULK1) and the interacting proteins autophagy-related (ATG) protein 13 (ATG13), ATG101, and RB1-inducible coiled-coil 1 (RB1CC1; alternatively termed FAK family kinase-interacting protein of 200 kDa, FIP200) and (2) the class III phosphatidylinositol 3-kinase (PtdIns3K) lipid kinase complex consisting of the catalytic subunit vacuolar protein sorting 34 (VPS34; alternatively termed phosphatidylinositol 3-kinase catalytic subunit type 3, PIK3C3) and the interacting proteins VPS15/PIK3R4, Beclin 1, ATG14, and nuclear receptor-binding factor 2 (NRBF2) [16,17]. The activation of these 2 complexes initiates autophagosome biogenesis, most likely at specific subdomains of the endoplasmic reticulum (ER) [18]. Several additional ATG proteins are involved in the formation of autophagosomes; among them the ubiquitin-like protein microtubule-associated proteins 1A/1B light chain 3 (MAP1LC3 or briefly LC3), which can be conjugated to phosphatidylethanolamine and thus be recruited to the autophagosomal membrane [19]. Anticancer therapies frequently induce autophagy as a prosurvival response that contributes to chemoresistance [14,20]. Consequently, drugs that inhibit autophagy are tested in clinical trials in combination with different anticancer drugs to increase their cytotoxic potential. Several of these trials make use of chloroquine/hydroxychloroquine, which raise the lysosomal pH and thus block fusion of autophagosomes and lysosomes [14]. So far, more specific inhibitors targeting the kinase activities of ULK1 or VPS34 have only been assessed in preclinical studies. These inhibitors include the ULK1 inhibitor MRT68921 or the VPS34 inhibitor SAR405 [21,22].

In this study, we made use of the urothelial carcinoma cell line (UCC) RT-112 and its respective cisplatin-resistant subline RT-112$^{CisPt\text{-}R}$ [12]. We observed that the expression levels of several autophagy-related proteins are increased in RT-112$^{CisPt\text{-}R}$ cells compared to the parental line. Furthermore, it appears that basal autophagy is increased in the resistant cells, but they still remain responsive to autophagy-inducing stimuli. The inhibition of autophagy either by chloroquine or the VPS34-Beclin 1 complex-targeting inhibitors 3-MA or SAR405 complemented or even increased the cytotoxic effects of cisplatin in both parental and RT-112$^{CisPt\text{-}R}$ cells. Furthermore, we obtained similar results with other UCCs representing the heterogeneity of this disease. Accordingly, we hypothesize that the inhibition of the autophagy-inducing VPS34-Beclin 1 complex represents a promising approach to increase the efficacy of cisplatin or to overcome cisplatin resistance in UC.

2. Material and methods

2.1. Antibodies and reagents

Antibodies against β-actin (clone AC-74, Sigma-Aldrich, #A5316), ATG13 (Sigma-Aldrich, #SAB4200100), ATG14 (MBL, #PD026), Beclin 1 (Santa Cruz, #sc-11427 or Sigma-Aldrich, #B6186), Caspase-3 (R&D Systems, #AF-605-NA), GAPDH (Abcam, #ab8245), LC3B (Cell Signaling Technology, #2775), PARP (Enzo, #BML-SA250), RB1CC1 (Bethyl Laboratories, #A301–574A), α-Tubulin (Sigma-Aldrich, #T5168), ULK1 (clone D8H5, Cell Signaling Technology, #8054), and VPS34 (Thermo Fisher Scientific, #PA1–46456) were used. IRDye 800- or IRDye 680-conjugated secondary antibodies were purchased from LI-COR Biosciences (926–68070, 926–68071 and 926–32211). Other reagents used were 3-MA (Sigma-Aldrich, #M9281), Bafilomycin A_1 (Sigma-Aldrich, #B1793), Chloroquine (Sigma-Aldrich, #C6628), Cisplatin (Accord Healthcare GmbH, PZN: 00370955), DMSO (Sigma-Aldrich, #D4540), Q-VD-OPh (MP Biomedicals, #03OPH109), and SAR405 (Selleck Chemicals, #7682).

2.2. Cell lines and cell culture

All cell lines were cultured in Dulbecco's Modified Eagle Medium (DMEM) containing 10% FCS and 4.5 g/l D-glucose in a humidified atmosphere at 37°C and 5% CO_2. The Cisplatin-resistant sublines were generated over several months by increasing dosages of cisplatin added with every passage up to concentrations of 12, 1, 2, 7, 3.5, or 1.5 µg/ml to RT-112, J82, 253J, T24, 5637, and SW-1710 cells, respectively. Accordingly, the respective concentration of cisplatin was added to the media of the cisplatin-resistant sublines with every passage. For amino acid starvation, RT-112 cells were washed once with PBS and incubated for 2 hours in EBSS (Gibco, #24010–043).

2.3. Microscopy

RT-112 and RT-112$^{CisPt\text{-}R}$ cells were cultured in regular medium or medium containing 12 µg/ml cisplatin, respectively. Phase contrast images were captured using an Axio Observer A1 microscope (Carl Zeiss) with a magnification of 200× (Objective: ZEISS, LD A-Plan 20×/0.30 Ph1).

2.4. Cell viability assay

RT-112, J82, 253J or T24 cells were seeded in 96-well plates with a density of 1×10^4 cells/well. For combination analysis, the cell density of J82, 253J, and T24 cells was reduced to 0.5×10^4. The following day, the cells were treated with cisplatin and autophagy inhibitors for 72 hours. Cell viability was determined by using an MTT assay. Briefly, MTT (Calbiochem, #475989) was added to the cells and incubated at 37°C for 1 hour. Afterwards, the plates were centrifuged at 600 rcf and 4°C for 5 minutes, and cells were lysed in DMSO for 20 minutes in the dark. Finally, the absorbance was measured at 570 nm and 650 nm for reference, using a microplate reader (BioTek, Synergy Mx). The mean of the absorbance of the control samples was set as 100%.

2.5. Caspase activity assay

1×10^4 RT-112 or RT-112$^{CisPt\text{-}R}$ cells were seeded in 96-well plates, and the following day, the cells were treated with cisplatin and autophagy inhibitors for 48 hours. After treatment, plates were centrifuged at 600 rcf and 4°C for 5 minutes, quickly frozen at −80°C, and cells were lysed in lysis buffer (20 mM HEPES, 84 mM KCl, 10 mM $MgCl_2$, 200 µM EDTA, 200 µM EGTA, 0.5% NP-40, 1 µg/ml Leupeptin, 1 µg/ml Pepstatin, and 5 µg/ml Aprotinin) for 10 minutes on ice. Subsequently, reaction buffer (50 mM HEPES, 100 mM NaCl, 10% Sucrose, 0.1% CHAPS [Carl Roth GmbH & Co., #1479.3], 2 mM $CaCl_2$, 13.35 mM DTT, and 70 µM Ac-DEVD-AMC [Biomol, #ABD-13402]) was added to the lysates and fluorescence (with an excitation of 360 nm, and an emission of 450 nm) was measured every 2 minutes over a period of 2.5 hours at 37°C, using a microplate reader (BioTek, Synergy Mx). Caspase-3 activity was measured by the cleavage of the substrate Ac-DEVD-AMC and the following release of the fluorophore AMC (7-amido-4-methylcoumarin). For evaluation, the rise of the linear sector of the resulting curve was determined and the mean of the control samples was set as "1."

2.6. Immunoblotting

Cells were harvested by scraping, pelletized at 600 rcf and 4°C for 5 minutes, quickly frozen in liquid nitrogen and lysed in lysis buffer (50 mM Tris-HCl, pH 7.5, 150 mM NaCl, 1 mM EDTA, 1 mM EGTA, 10 µM Na_2MoO_4, 1 mM Na_3VO_4, 50 mM NaF, 5 mM $Na_4P_2O_7$, 1% [v/v] Triton X-100 [Carl Roth GmbH & Co., #3051.2], and protease inhibitor cocktail [Sigma-Aldrich, #P2714]) for 30 minutes on ice. Lysates were cleared by centrifugation at 18,000 rcf and 4°C for 15 minutes. Equal protein amounts were determined by Bradford assay, prepared by addition of sample buffer (125 mM Tris-HCl, pH 6.8, 17.2% [v/v] glycerol, 4.1% [w/v] SDS [AppliChem GmbH, #A7249], 200 µg/ml bromophenol blue, and 2% [v/v] β-mercaptoethanol) and heated at 95°C for 5 minutes. Proteins were separated on SDS-PAGE, transferred to PVDF membranes (Merck, Millipore, IPFL00010), and analyzed using the indicated primary antibodies and appropriate IRDye 800- or IRDye 680-conjugated secondary antibodies (LI-COR Biosciences). Signals were detected by using an Odyssey Infrared Imaging system (LI-COR Biosciences). Quantifications were performed with Image Studio (LI-COR Biosciences).

2.7. Statistical analysis

IC_{50} values were calculated using GraphPad Prism 7.01. For isobologram analysis, CompuSyn 1.0 was used, which also allows a computerized simulation of synergism, additivism, and antagonism at any effect level [23]. The resulting Combination Index (CI) values represent synergism ($CI < 1$), additivism ($CI = 1$), and antagonism ($CI > 1$). For immunoblotting, the density of each protein band was divided by the average of the density of all bands from the same protein on the membrane. The ratios of the proteins of interest were normalized to the loading control, and fold changes were calculated by dividing each normalized density ratio by the average of the density ratios of the wild type control lane (control lane: fold change = 1.00, $n \geq 3$). For all analyses, results are shown as mean ± standard deviation, and P values were determined by two-way ANOVA and are given in the bar diagrams.

3. Results

In order to analyze the effect of autophagy modulation on the efficacy of cisplatin treatment, we first generated a cisplatin-resistant subline of the UCC RT-112. Cisplatin resistance was confirmed by a cell viability assay (Fig. 1). Notably, cisplatin-resistant RT-112 cells (RT-112$^{CisPt\text{-}R}$) revealed morphologic alterations, including increased cell size and number of protrusions (Fig. S1), which is in accordance with previous observations [11,12].

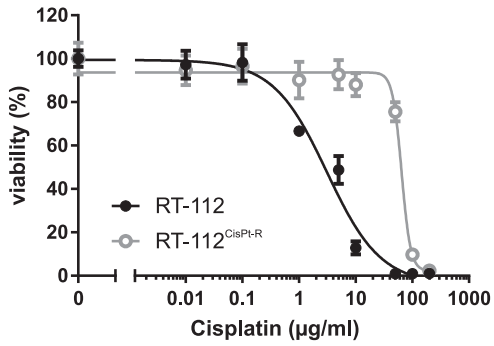

Fig. 1. Characterization of RT-112 and RT-112$^{CisPt\text{-}R}$ cells. RT-112 and RT-112$^{CisPt\text{-}R}$ cells were treated with different concentrations of cisplatin (0.01–200 µg/ml) for 72 hours. After treatment, cell viability was measured using an MTT assay. The results are shown as means ± standard deviation of 3 independent experiments which were performed in triplicates.

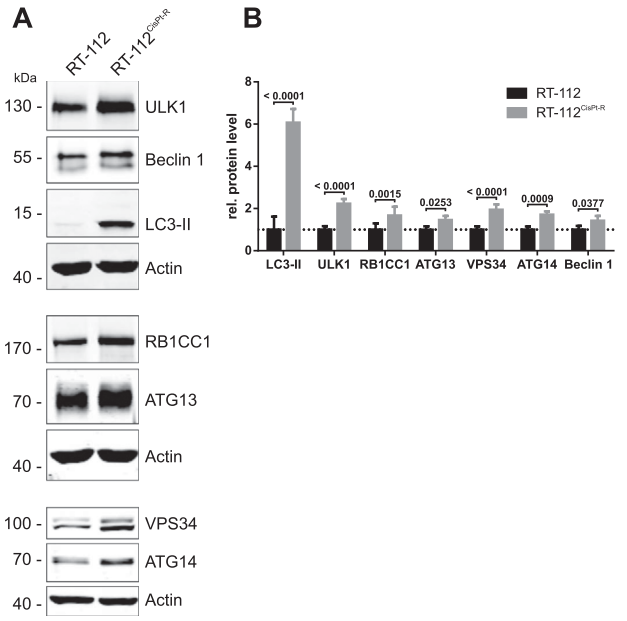

Fig. 2. ATG proteins are differentially expressed in RT-112 and RT-112$^{CisPt-R}$ cells. (A) RT-112 and RT-112$^{CisPt-R}$ cells were lysed and cleared cellular lysates were subjected to SDS-PAGE and immunoblotting for ULK1, Beclin 1, LC3, RB1CC1, ATG13, VPS34, ATG14, and Actin. One representative immunoblot is shown. (B) The densities of bands on immunoblots of at least 3 independent experiments were quantified using Image Studio (LI-COR Biosciences) and normalized to Actin. The mean of the resulting values for RT-112 cells were set as "1" for each protein. Then, the values of RT-112$^{CisPt-R}$ cells were normalized to the values of RT-112 cells. The bars represent the means + standard deviation. A two-way ANOVA was used to compare the differences in protein expression between RT-112 and RT-112$^{CisPt-R}$ cells. The respective *P* values are depicted in the diagram.

3.1. Autophagy-related (ATG) proteins are up-regulated in RT-112$^{CisPt-R}$ cells

Next we aimed at investigating whether cisplatin resistance affects expression levels of different autophagy-related (ATG) proteins. As determined by immunoblotting, several subunits of the autophagy-inducing ULK1 and VPS34-Beclin 1 complexes were significantly up-regulated, including the catalytic subunits ULK1 and VPS34 as well as the associated proteins RB1CC1, ATG13, Beclin 1, and ATG14 (Fig. 2). Additionally, expression of the ubiquitin-like autophagy marker protein LC3-II was strongly increased in RT-112$^{CisPt-R}$ cells (Fig. 2, $P < 0.0001$). Although the up-regulation of ATG proteins might indicate an increased potential to execute autophagy, this upregulation is not sufficient evidence of increased autophagy [24]. This is best exemplified by LC3-II, which is increasingly generated during autophagy induction and at the same time accumulates during autophagy inhibition [24]. In order to investigate whether autophagy is functional in RT-112$^{CisPt-R}$ cells, we performed an LC3 turnover assay using starvation as proautophagic stimulus. In this assay, lysosomal degradation is blocked by the V-ATPase inhibitor bafilomycin A_1, which ultimately blocks the fusion of autophagosomes with lysosomes [24]. We detected LC3 turnover by immunoblotting and observed increased LC3-II levels in RT-112$^{CisPt-R}$ cells under all conditions (Fig. S2). Nevertheless, the RT-112$^{CisPt-R}$ remained responsive to starvation by incubation in Earle's Balanced Salt Solution (EBSS). Collectively, these data suggest that RT-112$^{CisPt-R}$ cells possess an enhanced capacity for basal autophagy but can still respond to proautophagic stimuli.

3.2. Inhibition of autophagy complements or increases cisplatin-mediated cytotoxicity in both RT-112$^{CisPt-R}$ and parental cells

The increased protein expression of several ATG proteins in RT-112$^{CisPt-R}$ cells and the possibly increased potential to execute autophagy led us to hypothesize that targeting the autophagy machinery might be a reasonable approach to increase the efficacy of cisplatin treatment. To date, most clinical studies investigating the effects of autophagy inhibition rely on the usage of chloroquine, a lysosomotropic compound that raises the lysosomal pH and thus inhibits the fusion between autophagosomes and lysosomes [24]. First, we confirmed the autophagy-inhibiting properties of chloroquine in RT-112 and RT-112$^{CisPt-R}$ cells by an LC3 turnover assay. We observed that LC3-II accumulated in EBSS-treated cells upon co-incubation with chloroquine (Figure S3A). In order to investigate whether cisplatin and chloroquine exhibit a combined effect on cell viability in these two cell lines, the effect of chloroquine treatment alone (Fig. 3A) or in combination with cisplatin was analyzed, and isobologram analysis was performed (Fig. 3B and C; the corresponding isobologram is shown in Fig. S4A). For this analysis, concentrations of 0.25×, 0.5× or 1× of the IC_{50} values of the individual compounds (cisplatin or chloroquine) were applied. As can be deduced from the combination index plot, in RT-112 cells, the combination of cisplatin and chloroquine was synergistic ($CI < 1$) if used at concentrations of 1× IC_{50}. In RT-112$^{CisPt-R}$ cells, the effect was rather additive at high effect levels. These results indicate that inhibition of autophagy might indeed represent a suitable tool to increase cisplatin efficacy in responsive UCCs or to target resistant UCCs, respectively.

3.3. Inhibition of the VPS34-Beclin 1 complex sensitizes RT-112$^{CisPt-R}$ and parental cells to cisplatin treatment

We observed that general inhibition of autophagy supports cisplatin-mediated cytotoxicity in UCCs. However, chloroquine is not a specific autophagy inhibitor. Additionally, it has recently been suggested that the enhanced drug efficacy of anticancer therapeutics in combination with chloroquine might be due to lysosomal cell death rather than to regulation of autophagy [25]. Taken these drawbacks of chloroquine together, we analyzed whether the direct and specific inhibition of the autophagy-inducing

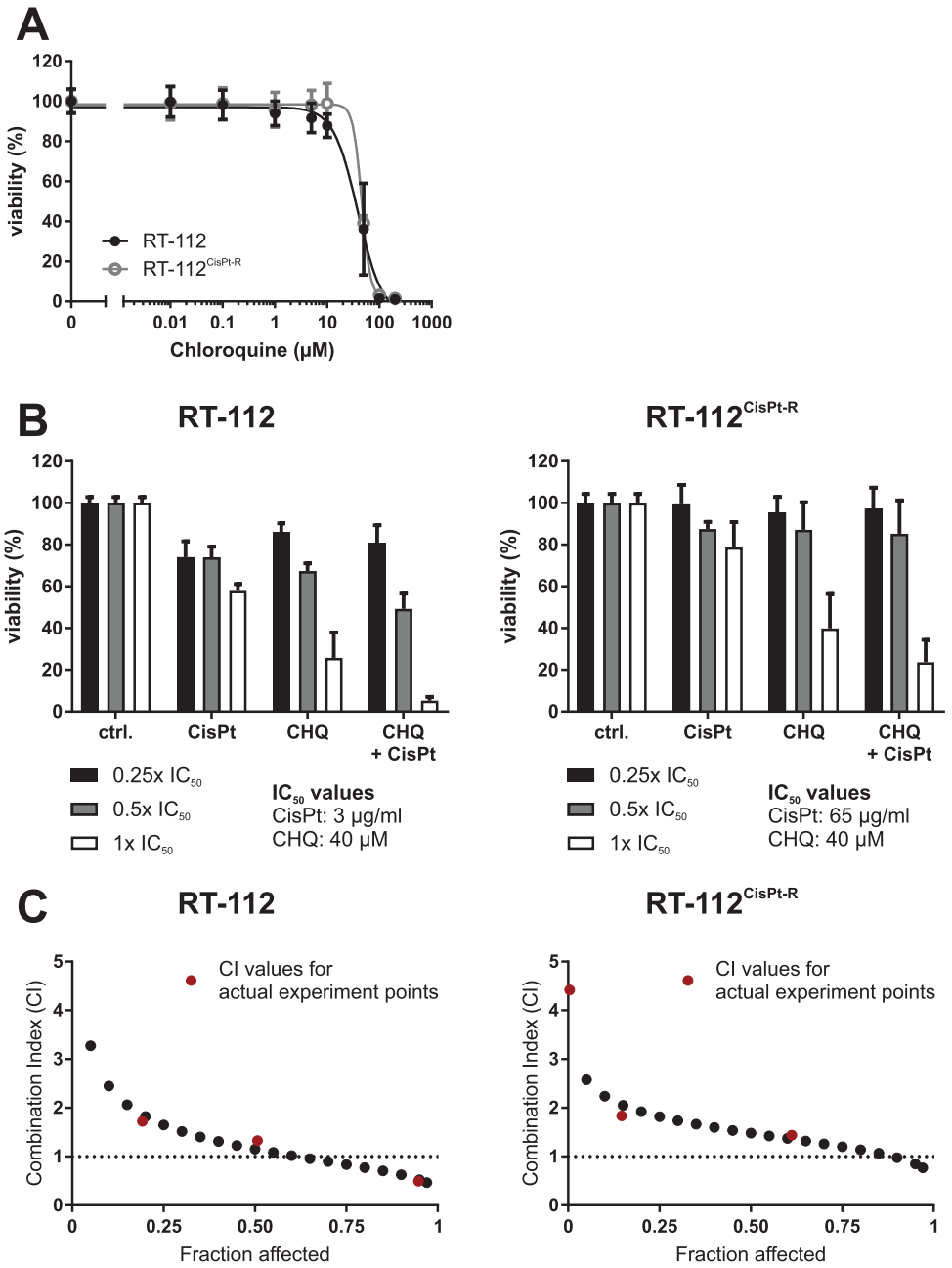

Fig. 3. Chloroquine complements or increases cisplatin-mediated cytotoxicity in both RT-112$^{CisPt-R}$ and parental cells. (A and B) RT-112 and RT-112$^{CisPt-R}$ cells were treated with different concentrations of chloroquine (CHQ; 0.01–200 µM) (A) or with cisplatin, chloroquine, or a combination of both (B) for 72 hours. For combination analysis (B), IC_{50} values of 3 µg/ml (RT-112) or 65 µg/ml (RT-112$^{CisPt-R}$) cisplatin and 40 µM chloroquine (RT-112 and RT-112$^{CisPt-R}$) were used. After treatment, cell viability was measured using an MTT assay. At least 3 independent experiments were performed in triplicates. The results are shown as means ± or + standard deviations of the independent experiments. For all experiments, 0.1% DMSO was used as control. For 1× IC_{50}, 0.5× IC_{50}, and 0.25× IC_{50} in Figs. 3B, 4B, and 5B, the same controls are shown for each cell line. (C) Combination Index (CI) values were calculated using the software CompuSyn in order to determine synergistic (CI < 1), additive (CI = 1), or antagonistic (CI > 1) effects for the combination of cisplatin and chloroquine. CompuSyn uses algorithms for a computerized simulation to show synergism, additivism, and antagonism at any effect level.

VPS34-Beclin 1 complex can phenocopy the effect of chloroquine. We interfered with the VPS34-Beclin 1 complex using the class III PtdIns3K inhibitor 3-methyladenine (3-MA). Again, we confirmed the autophagy-inhibitory potential of 3-MA in our cellular model systems. Cells treated with 3-MA did not accumulate LC3-II upon bafilomycin A_1 treatment, verifying that 3-MA blocks an early step of the autophagic pathway (Fig. S3B). Next, we performed cell viability assays using individual (Fig. 4A) and combined treatments (Fig. 4B and C). As shown in the CI plots, we found that 3-MA synergistically sensitizes both parental and RT-112$^{CisPt-R}$ cells to cisplatin-induced cell death. In RT-112 cells, this was the case for all applied concentrations; for the RT-112$^{CisPt-R}$ cells, the synergistic effect could be observed for concentrations in the range of the IC_{50} (Fig. 4B and C; the corresponding isobologram is

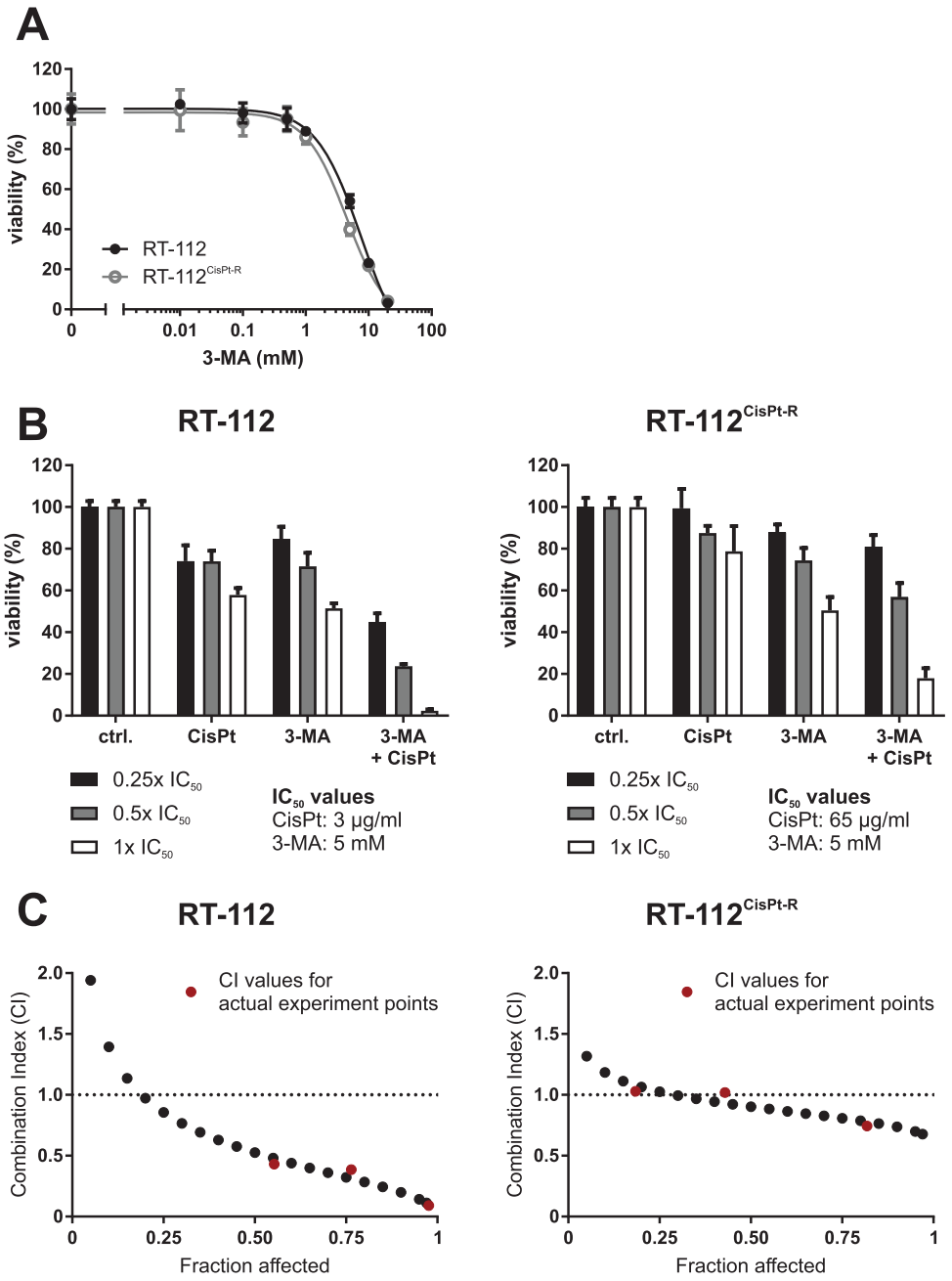

Fig. 4. The PtdIns3K inhibitor 3-MA sensitizes both RT-112 and RT-112$^{CisPt-R}$ cells to cisplatin-induced cell death. (A and B) RT-112 and RT-112$^{CisPt-R}$ cells were treated with different concentrations of 3-methyladenine (3-MA; 0.01–20 mM) (A) or with cisplatin, 3-MA or a combination of both (B) for 72 hours. For combination analyses (B), IC_{50} values of 3 µg/ml (RT-112) or 65 µg/ml (RT-112$^{CisPt-R}$) cisplatin and 5 mM 3-MA (RT-112 and RT-112$^{CisPt-R}$) were used. After treatment, cell viability was measured using an MTT assay. At least 3 independent experiments were performed in triplicates. The results are shown as means ± or + standard deviations of the independent experiments. For all experiments, 0.1% DMSO was used as control. For 1× IC_{50}, 0.5× IC_{50}, and 0.25× IC_{50} in Figs. 3B, 4B, and 5B, the same controls are shown for each cell line. (C) Combination Index (CI) values were calculated using the software CompuSyn in order to determine synergistic (CI $<$ 1), additive (CI $=$ 1), or antagonistic (CI $>$ 1) effects for the combination of cisplatin and 3-MA. CompuSyn uses algorithms for a computerized simulation to show synergism, additivism, and antagonism at any effect level.

shown in Fig. S4B). It has been reported that 3-MA inhibits both class I and class III PtdIns3Ks with different kinetics, and that 3-MA can indeed promote autophagy in long-term experiments [26]. Accordingly, we also tested the recently described VPS34-specific inhibitor SAR405 [22]. Of note, the IC_{50} of SAR405 alone was 5 to 7 times lower in RT-112$^{CisPt-R}$ cells compared to the parental RT-112 cell line, indicating a clearly increased sensitivity toward VPS34 inhibition in the cisplatin-resistant cell line (Fig. 5A). This observation is in line with our analysis of autophagy inhibition using SAR405 in both cell lines. In RT-112$^{CisPt-R}$ cells, SAR405 efficiently inhibited autophagy at concentrations of 0.5 µM, whereas 5 µM were necessary in parental RT-112 cells (Fig. S3C). Again, we performed

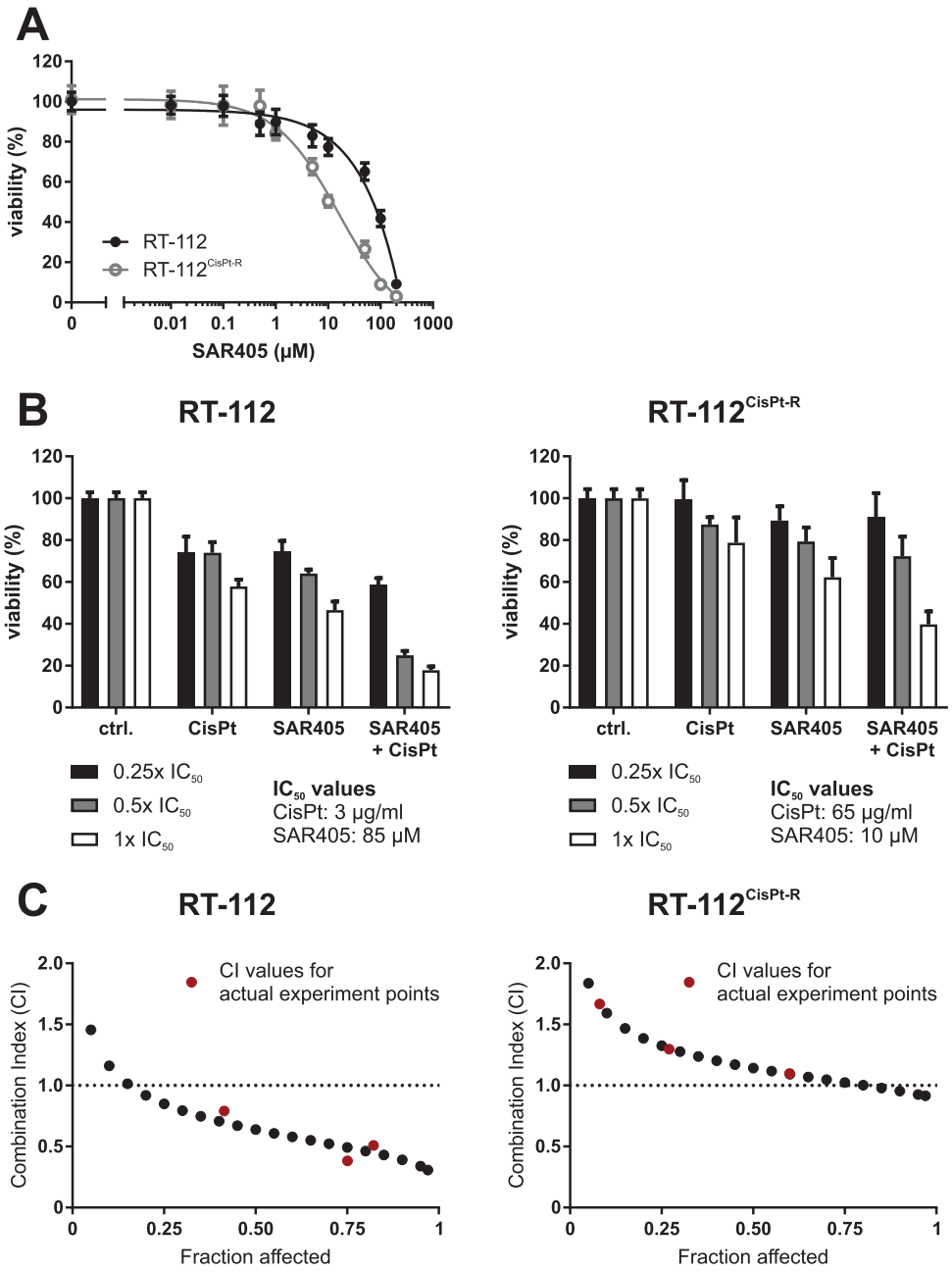

Fig. 5. The VPS34-specific inhibitor SAR405 supports cisplatin-induced cell death in both RT-112 and RT-112$^{CisPt-R}$ cells. (A and B) RT-112 and RT-112$^{CisPt-R}$ cells were treated with different concentrations of SAR405 (0.01–200 µM) (A) or with cisplatin, SAR405 or a combination of both (B) for 72 hours. For combination analyses (B), IC_{50} values of 3 µg/ml (RT-112) or 65 µg/ml (RT-112$^{CisPt-R}$) cisplatin and 85 µM (RT-112) or 10 µM (RT-112$^{CisPt-R}$) SAR405 were used. After treatment, cell viability was measured using an MTT assay. At least 3 independent experiments were performed in triplicates. The results are shown as means ± or + standard deviations of the independent experiments. For all experiments, 0.1% DMSO was used as control. For 1× IC_{50}, 0.5× IC_{50}, and 0.25× IC_{50} in Figs. 3B, 4B, and 5B, the same controls are shown for each cell line. (C) Combination Index (CI) values were calculated using the software CompuSyn in order to determine synergistic (CI < 1), additive (CI = 1), or antagonistic (CI > 1) effects for the combination of cisplatin and SAR405. CompuSyn uses algorithms for a computerized simulation to show synergism, additivism, and antagonism at any effect level.

combination treatments with subsequent isobologram analyses. In RT-112 cells, SAR405 and cisplatin exhibit a synergistic interaction for all concentrations analyzed. In RT-112$^{CisPt-R}$ cells, the effect was additive if concentrations were used in the range of the IC_{50} of the individual compounds (Fig. 5B and C; the corresponding isobologram is shown in Fig. S4C). The presence of an additive effect instead of synergism might be partly caused by the increased cytotoxicity of SAR405 alone in RT-112$^{CisPt-R}$ cells. Accordingly, the combination of cisplatin with SAR405 concentrations of approximately 10 µM might open a valuable therapeutic window. In a next step, we wanted to confirm the results of the cell viability assay by an assay detecting caspase activity. For that, 0.5× IC_{50} or

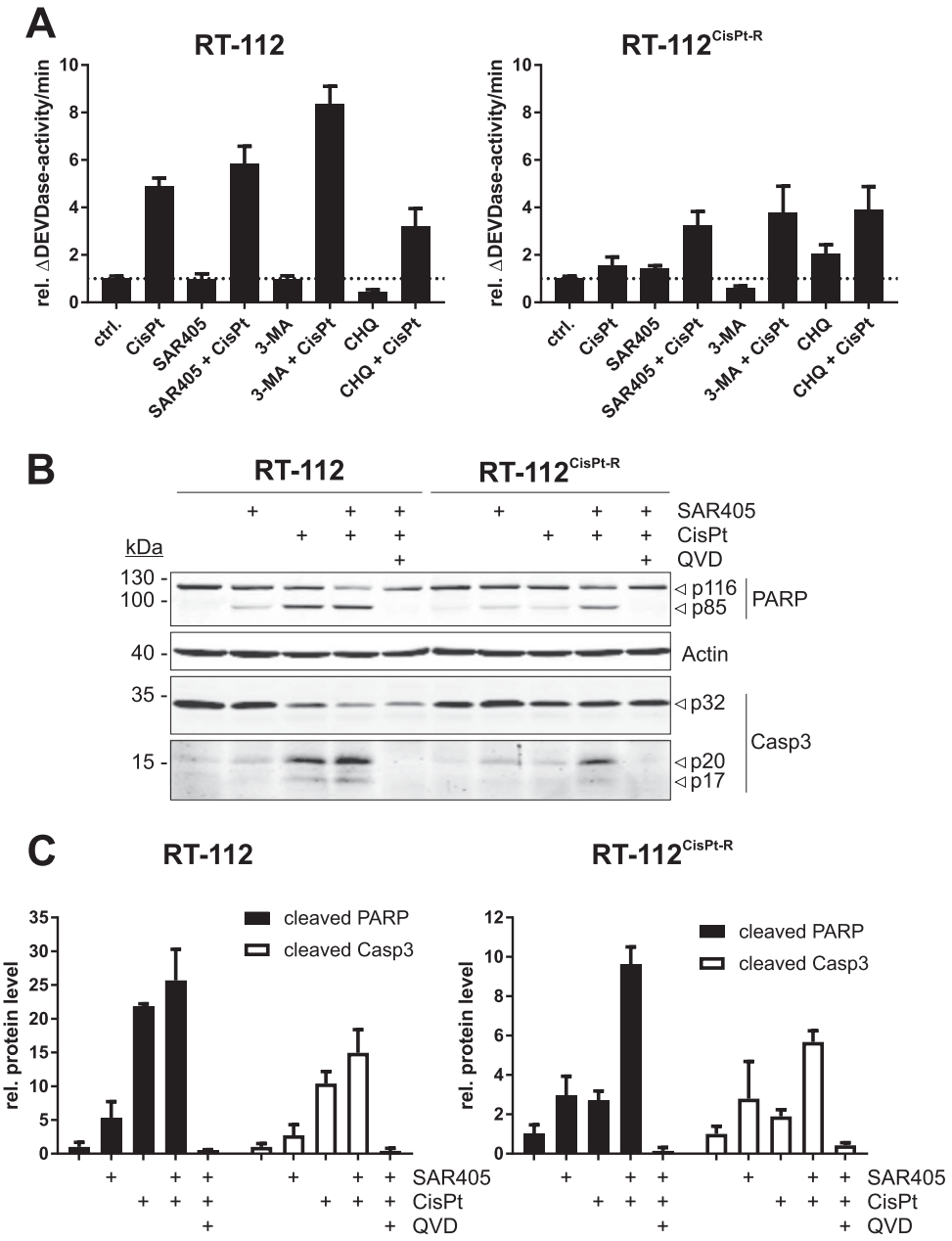

Fig. 6. The combination of cisplatin and SAR405 induces apoptosis in RT-112 and RT-112$^{CisPt-R}$ cells. (A) RT-112 and RT-112$^{CisPt-R}$ cells were treated with cisplatin, SAR405, 3-MA, or chloroquine (CHQ) alone or in combination. The concentrations used are the IC_{50} or half IC_{50} values for RT-112$^{CisPt-R}$ and RT-112, respectively (Figs. 3–5). Caspase-3 activity was measured after 48 hours using a DEVD assay. The obtained values were normalized to the mean of the control values of each cell line. The results are shown as means + standard deviation of 3 independent experiments which were performed in triplicates. For all experiments, 0.1% DMSO was used as control. (B) RT-112 and RT-112$^{CisPt-R}$ cells were treated with cisplatin, SAR405, and a combination of both in absence and presence of QVD (10 μM). Again, the concentrations used were the IC_{50} or half IC_{50} values for RT-112$^{CisPt-R}$ and RT-112, respectively (Figs. 3–5). After 48 hours, the cells were lysed, and cleared cellular lysates were subjected to SDS-PAGE and immunoblotting for PARP, caspase-3 (Casp3), and Actin. One representative immunoblot is shown. (C) The densities of bands on immunoblots of at least 3 independent experiments were quantified using Image Studio (LI-COR Biosciences) and normalized to Actin. The mean of the resulting control values for each cell line were set as "1" for each protein. The bars represent the means + standard deviation.

1× IC_{50} of each compound were used in RT-112 or RT-112$^{CisPt-R}$ cells, respectively. Of note, caspase activity was increased in parental and resistant cells if cisplatin was combined with either 3-MA or SAR405 compared to cisplatin alone (Fig. 6A). We also investigated caspase activation by immunoblot analysis detecting the cleavage of either the caspase-3 substrate poly (ADP-ribose) polymerase (PARP) or caspase-3 itself, respectively (Fig. 6B and C). Increased PARP and caspase-3 cleavage was especially evident in RT-112$^{CisPt-R}$ cells using SAR405 in combination with cisplatin compared to the individual treatments. Both PARP cleavage and caspase-3 activation could be inhibited using the caspase-inhibitor QVD, confirming that these treatments induce apoptosis. Collectively,

it appears that inhibition of the VPS34-Beclin 1 complex can sensitize both cisplatin-responsive and -resistant cells to cisplatin-induced cell death. Additionally, treatment with a VPS34-specific inhibitor such as SAR405 in a monotherapy might be a reasonable therapeutic approach in a setting with acquired cisplatin resistance.

3.4. VPS34 inhibition supports cisplatin-induced cell death in various UCC lines

RT-112 cells represent a UC with the histological grade G2. In order to investigate the general validity of our observations, we included several additional cell lines representing the heterogeneity of UC in our analyses, including epithelial-like 5637 and mesenchymal-like J82, 253J, T24, and SW-1710. Similar to RT-112 cells, we analyzed the expression levels of several ATG proteins in cisplatin-sensitive and -resistant cell pairs. Again, we observed the up-regulation of different ATG proteins in cisplatin-resistant derivatives (Fig. 7). Subsequently, we determined the IC_{50} values for cisplatin and SAR405 within the cell lines J82, 253J, and T24 (Fig. S5A, S5B and S5C), and repeated the above described combination experiments for the cisplatin-sensitive and -resistant variants. In all cell lines except for $T24^{CisPt\text{-}R}$, the combination of cisplatin and SAR405 resulted in the highest reduction of cell viability (Fig. 8). For $J82^{CisPt\text{-}R}$ and $253J^{CisPt\text{-}R}$ cells, isobologram analysis allowed the generation of CI plots. Whereas the combination was synergistic in $J82^{CisPt\text{-}R}$ cells for concentrations in the range of the IC_{50}, it was rather additive for $253J^{CisPt\text{-}R}$ cells (Fig. 8D). Clearly, in $J82^{CisPt\text{-}R}$ cells, the synergistic effect was most prominent. Like in $RT\text{-}112^{CisPt\text{-}R}$ cells, $J82^{CisPt\text{-}R}$ cells reveal an increased expression of ULK1 (Figs 2 and 7), which is a central regulator of the VPS34-Beclin 1 complex [17]. Accordingly, we hypothesize that the combination of cisplatin with a VPS34-specific inhibitor might be especially effective in UCCs with increased expression of components of both the VPS34 and the ULK1 complex.

4. Discussion

The European Association of Urology recommends cisplatin-based chemotherapy as upfront treatment in advanced and metastatic urothelial carcinoma, whenever not precluded by comorbidities. For perioperative systemic therapy, cisplatin-based chemotherapy is likewise the treatment of choice in eligible patients [27]. However, both the primary presence of or the development of chemoresistance are major obstacles for successful therapies. In this study, we characterized the autophagy signaling pathway as an appropriate target to increase cisplatin efficacy or to resensitize resistant cells. We found that several ATG proteins are up-regulated in various cisplatin-resistant UCC lines, suggesting that basal autophagy is increased in these cells. Nevertheless, they still respond to proautophagic conditions. Furthermore, we inhibited the autophagic pathway by different pharmacological inhibitors and found synergistic or additive cytotoxic effects when combined with cisplatin compared to control conditions. Therefore, we propose that the efficacy of cisplatin-based therapy might be enhanced by combination with autophagy-inhibiting compounds. Under certain circumstances, the approach of autophagy inhibition might also be effective as monotherapy.

Current translational research aims at identifying and characterizing specific autophagy-modulating compounds. To date, chloroquine and hydroxychloroquine are still the substances of choice in the clinic if inhibition of autophagy is desired. However, there is an urgent need for more specific inhibitors of the autophagic pathway. The autophagy-inducing protein and lipid kinase complexes based on ULK1 and VPS34 are druggable targets, and recently some specific inhibitors targeting these kinases have been reported [21,22,28–30]. Interestingly, we observed that VPS34 inhibition was especially effective in cells with high ULK1 expression, i.e., $RT\text{-}112^{CisPt\text{-}R}$ and $J82^{CisPt\text{-}R}$ cells. There exists a strong crosstalk between these 2 complexes, but future studies have to assess whether an effective application of SAR405 requires high ULK1 expression.

We observed that both cisplatin-responsive and -resistant cells were sensitized for cisplatin-mediated effects by autophagy inhibition. This indicates that autophagy plays a central role for cytoprotection during de novo cisplatin treatment and during acquired cisplatin resistance. The dependency of cisplatin-resistant cells on autophagy is especially evident from the SAR405 experiments where mono-treatment with SAR405 was sufficient to significantly reduce cell viability of resistant cells. Hence, basal and constitutive autophagy is essential for supporting survival of resistant cells and/or for maintaining their resistant phenotype. However, these observations were not made for chloroquine or 3-MA as mono-treatment. Accordingly, we speculate that—next to autophagy—additional VPS34- or PtdIns3P-dependent processes might contribute to the establishment of cisplatin resistance, which are not efficiently targeted by chloroquine or 3-MA, respectively.

Among several molecular mechanisms of cisplatin resistance, autophagy has been suggested as one mode of off-target resistance [8]. Off-target resistance mechanisms describe cellular processes which are not directly engaged by cisplatin, but interfere with its lethal outcome [8]. The involvement of autophagy in cisplatin resistance has been shown for several cancer entities, and accordingly inhibition of autophagy sensitized resistant cells to cisplatin-induced cytotoxic effects [31–37]. However, it should be noted that also mTOR inhibition, which induces rather than inhibits autophagy, has been shown to be effective for overcoming cisplatin resistance [38–43]. Of note, Garcia-Cano et al. [44] reported that monoplatin, which promotes autophagy, is able to promote cell death of both cisplatin-sensitive and -resistant cells. In an analogous manner, conflicting results of autophagy modulation have been proposed with regard to

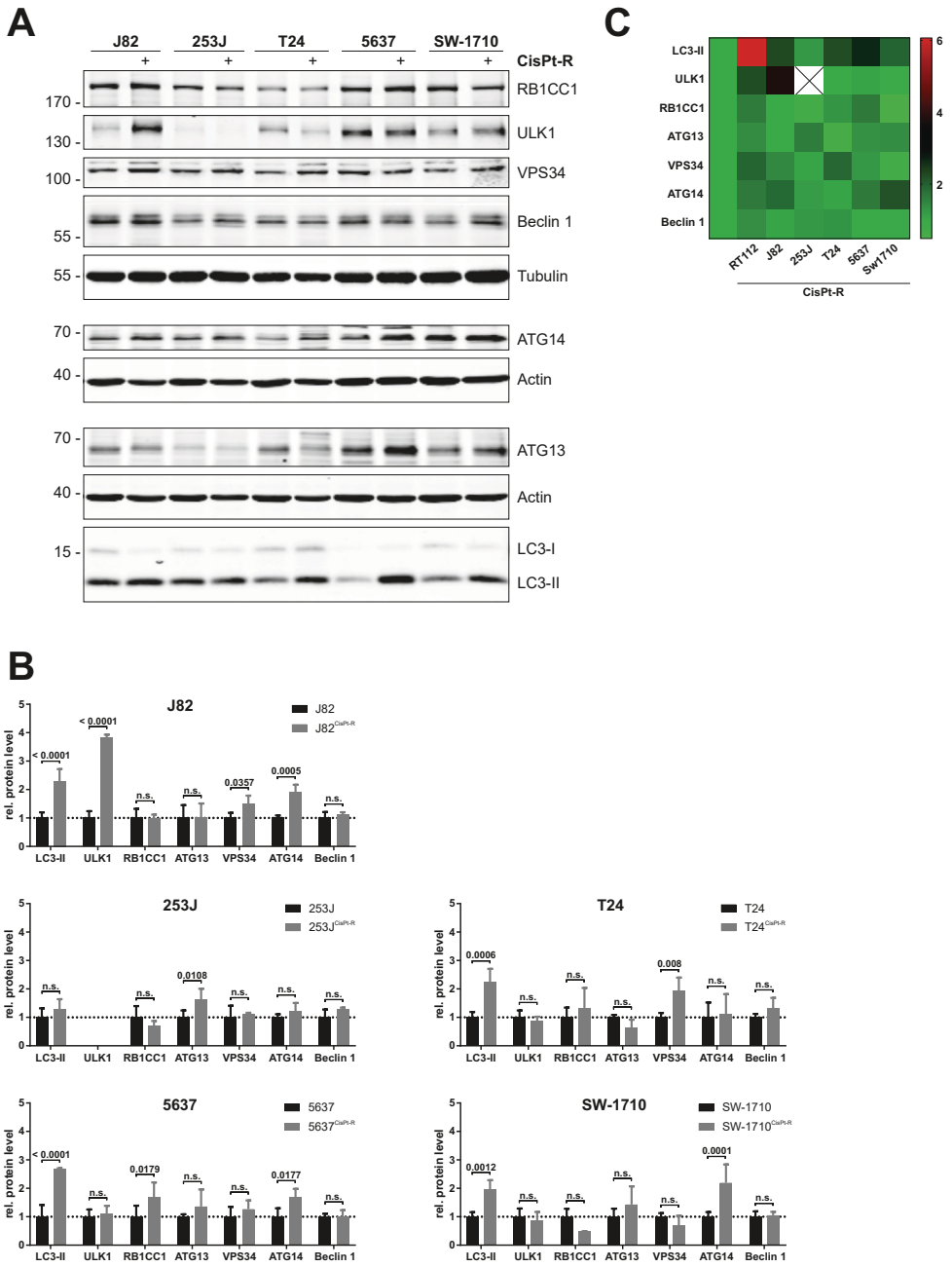

Fig. 7. ATG proteins are differentially expressed in various cisplatin-sensitive and -resistant UCCs. (A) Cells from various cisplatin-sensitive and -resistant UCCs (J82, 253J, T24, 5637, and SW-1710) were lysed and cleared cellular lysates were subjected to SDS-PAGE and immunoblotting for ULK1, Beclin 1, LC3, RB1CC1, ATG13, VPS34, ATG14, Actin, and Tubulin. One representative immunoblot is shown. (B) The densities of bands on immunoblots of at least 3 independent experiments were quantified using Image Studio (LI-COR Biosciences) and normalized to Actin or Tubulin. The mean of the resulting values for each cisplatin-sensitive cell line was set as "1" for each protein. Then, the values of the cisplatin-resistant cell lines were normalized to the values of their parental cells. The bars represent the means + standard deviation. A two-way ANOVA was used to compare the differences in protein expression between cisplatin-sensitive and -resistant cells. The respective *P* values are depicted in the diagram. (C) The expression of ATG proteins in cisplatin-resistant UCCs normalized to the expression in their parental cells (Figs. 2B and 7B) are summarized in a Heat Map. Please note, 253J cells lack quantifiable levels of ULK1 expression.

UC (reviewed in Ref. [45]). Ojiha et al. [46] observed that inhibition of autophagy by chloroquine potentiates the cytotoxicity of cisplatin. Along these lines, Mani et al. suggested that enhanced autophagy might play an important role for the chemoresistant phenotype of bladder cancer. They observed a significant increase in apoptosis in cisplatin-resistant UCCs treated with the BH3-mimetic (−)-gossypol upon knockdown of ATG5 or 3-MA treatment [47]. In contrast to these findings, Li et al. [48] reported that inhibition of the autophagic flux by chloroquine appears to be a survival mechanism of UCCs. Additionally, Pinto-Leite et al. [49] suggested using a combination of the mTOR

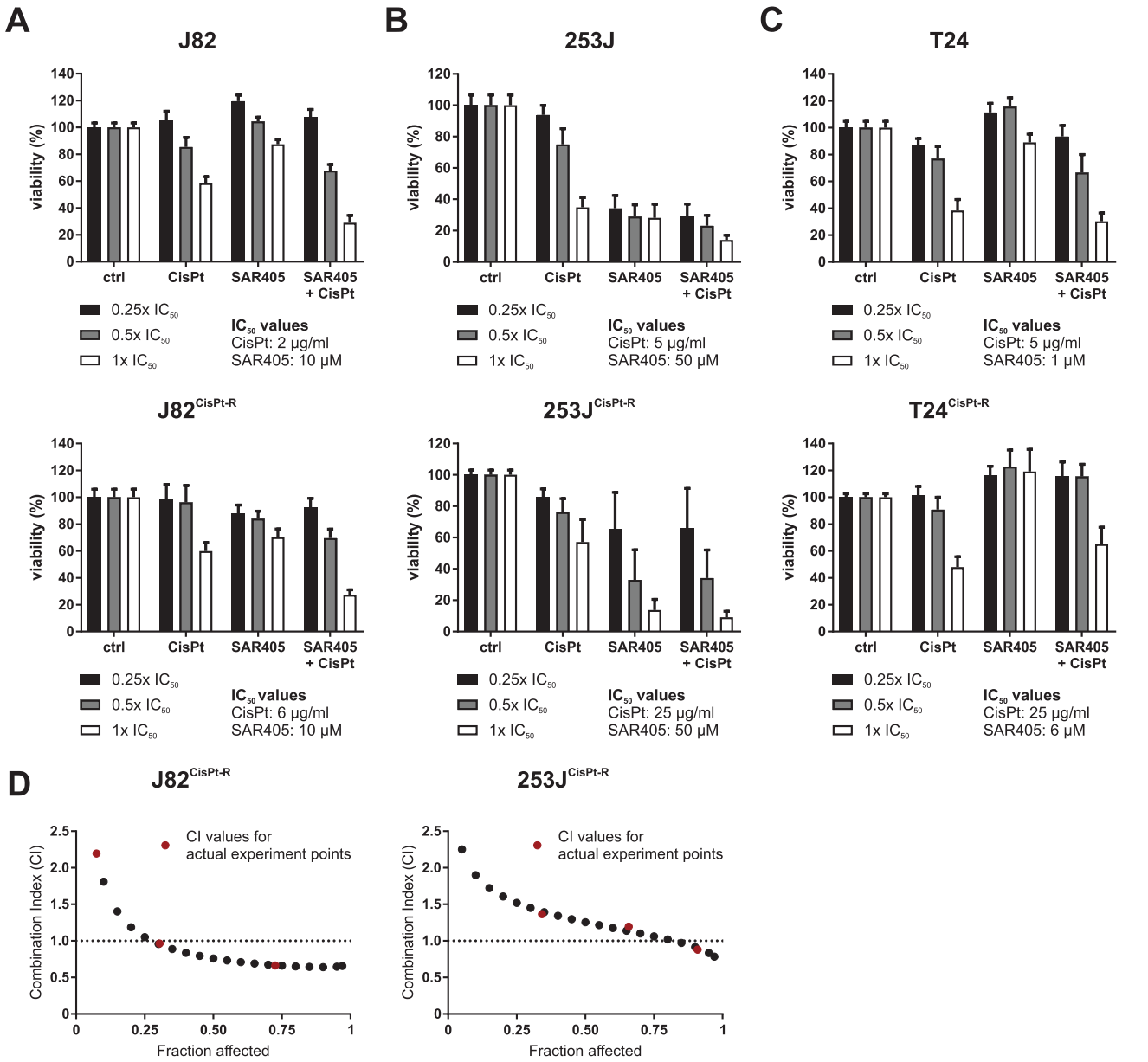

Fig. 8. Combination of cisplatin and SAR405 in various UCCs. (A-C) Cisplatin-sensitive and -resistant J82 (A), 253J (B), and T24 (C) cells were treated with cisplatin, SAR405, or a combination of both for 72 hours. The IC_{50} values used for the combination treatment are shown in the figure. After treatment, cell viability was measured using an MTT assay. At least 3 independent experiments were performed in triplicates. The results are shown as means + standard deviations of the independent experiments. For all experiments, 0.1% DMSO was used as control. For 1× IC_{50}, 0.5× IC_{50}, and 0.25× IC_{50}, the same controls are shown for each cell line. (D) Combination Index (CI) values for $J82^{CisPt\text{-}R}$ and $253J^{CisPt\text{-}R}$ were calculated using the software CompuSyn in order to determine synergistic (CI $<$ 1), additive (CI $=$ 1), or antagonistic (CI $>$ 1) effects for the combination of cisplatin and SAR405. CompuSyn uses algorithms for a computerized simulation to show synergism, additivism, and antagonism at any effect level.

inhibitor Everolimus and cisplatin for UC. These discrepancies suggest that therapeutic approaches employing autophagy modulation might depend on the individual stage and grade of UC. In addition, the modes of action of chloroquine or mTOR inhibitors might include autophagy-independent effects. To our knowledge, specific inhibitors targeting the autophagy signaling pathway in general or the autophagy-inducing VPS34-Beclin 1 complex have not been evaluated for UCCs so far and would be worthwhile to be assessed in future preclinical or clinical studies.

Conflict of interest statement

The authors declare that there are no competing financial interests in relation to the work described.

Author contribution statement

DS designed the experiments, performed cell viability and caspase-3 activity assays, and performed immunoblot

analyses. MAS generated the cell lines and supported immunoblot analyses. NB, PB, JD, FS, NWH, WW, and CP gave technical support. DS, MAS, MJH, GN and BS analyzed and interpreted the data and wrote the manuscript. MJH, GN, and BS supervised the project. All authors discussed the results and commented on the manuscript.

Acknowledgments

We thank Wolfgang A. Schulz for helpful discussions and critical reading of the manuscript. This work was supported by the Deutsche Forschungsgemeinschaft STO 864/3-1, STO 864/4-1, STO 864/5-1, and GRK 2158 (to BS), the Research Committee of the Medical Faculty of the Heinrich Heine University Düsseldorf (22/2015 to BS), and the Düsseldorf School of Oncology (to GN and BS; funded by the Comprehensive Cancer Center Düsseldorf/Deutsche Krebshilfe and the Medical Faculty of the Heinrich Heine-University Düsseldorf).

Appendix A. Supporting information

Supplementary data associated with this article can be found in the online version at https://doi.org/10.1016/j.urolonc.2017.11.021.

References

[1] Jemal A, Bray F, Center MM, Ferlay J, Ward E, Forman D. Global cancer statistics. CA Cancer J Clin 2011;61:69–90.
[2] Knowles MA. Molecular subtypes of bladder cancer: jekyll and Hyde or chalk and cheese? Carcinogenesis 2006;27:361–73.
[3] Stenzl A, Cowan NC, De Santis M, Kuczyk MA, Merseburger AS, Ribal MJ, et al. Treatment of muscle-invasive and metastatic bladder cancer: update of the EAU guidelines. Eur Urol 2011;59:1009–18.
[4] Abida W, Bajorin DF, Rosenberg JE. First-line treatment and prognostic factors of metastatic bladder cancer for platinum-eligible patients. Hematol Oncol Clin North Am 2015;29:319–28:ix-x.
[5] von der Maase H, Sengelov L, Roberts JT, Ricci S, Dogliotti L, Oliver T, et al. Long-term survival results of a randomized trial comparing gemcitabine plus cisplatin, with methotrexate, vinblastine, doxorubicin, plus cisplatin in patients with bladder cancer. J Clin Oncol 2005;23:4602–8.
[6] Cohen SM, Lippard SJ. Cisplatin: from DNA damage to cancer chemotherapy. Prog Nucleic Acid Res Mol Biol 2001;67:93–130.
[7] Ljungman M. The transcription stress response. Cell Cycle 2007;6:2252–7.
[8] Galluzzi L, Senovilla L, Vitale I, Michels J, Martins I, Kepp O, et al. Molecular mechanisms of cisplatin resistance. Oncogene 2012;31:1869–83.
[9] Olive PL, Banath JP. Kinetics of H2AX phosphorylation after exposure to cisplatin. Cytometry B Clin Cytom 2009;76:79–90.
[10] Roos WP, Kaina B. DNA damage-induced cell death: from specific DNA lesions to the DNA damage response and apoptosis. Cancer Lett 2013;332:237–48.
[11] Hohn A, Kruger K, Skowron MA, Bormann S, Schumacher L, Schulz WA, et al. Distinct mechanisms contribute to acquired cisplatin resistance of urothelial carcinoma cells. Oncotarget 2016;7:41320–35.
[12] Skowron MA, Niegisch G, Fritz G, Arent T, van Roermund JG, Romano A, et al. Phenotype plasticity rather than repopulation from CD90/CK14+ cancer stem cells leads to cisplatin resistance of urothelial carcinoma cell lines. J Exp Clin Cancer Res 2015;34:144.
[13] Chude CI, Amaravadi RK. Targeting autophagy in cancer: update on clinical trials and novel inhibitors. Int J Mol Sci 2017;18.
[14] Rebecca VW, Amaravadi RK. Emerging strategies to effectively target autophagy in cancer. Oncogene 2016;35:1–11.
[15] White E. The role for autophagy in cancer. J Clin Invest 2015;125:42–6.
[16] Mizushima N, Yoshimori T, Ohsumi Y. The role of Atg proteins in autophagosome formation. Annu Rev Cell Dev Biol 2011;27:107–32.
[17] Wesselborg S, Stork B. Autophagy signal transduction by ATG proteins: from hierarchies to networks. Cell Mol Life Sci 2015;72:4721–57.
[18] Axe EL, Walker SA, Manifava M, Chandra P, Roderick HL, Habermann A, et al. Autophagosome formation from membrane compartments enriched in phosphatidylinositol 3-phosphate and dynamically connected to the endoplasmic reticulum. J Cell Biol 2008;182:685–701.
[19] Geng J, Klionsky DJ. The Atg8 and Atg12 ubiquitin-like conjugation systems in macroautophagy. 'Protein modifications: beyond the usual suspects' review series. EMBO Rep 2008;9:859–64.
[20] Amaravadi RK, Thompson CB. The roles of therapy-induced autophagy and necrosis in cancer treatment. Clin Cancer Res 2007;13:7271–9.
[21] Petherick KJ, Conway OJ, Mpamhanga C, Osborne SA, Kamal A, Saxty B, et al. Pharmacological inhibition of ULK1 kinase blocks mammalian target of rapamycin (mTOR)-dependent Autophagy. J Biol Chem 2015;290:11376–83.
[22] Ronan B, Flamand O, Vescovi L, Dureuil C, Durand L, Fassy F, et al. A highly potent and selective Vps34 inhibitor alters vesicle trafficking and autophagy. Nat Chem Biol 2014;10:1013–9.
[23] Chou TC. Drug combination studies and their synergy quantification using the Chou-Talalay method. Cancer Res 2010;70:440–6.
[24] Klionsky DJ, Abdelmohsen K, Abe A, Abedin MJ, Abeliovich H, Acevedo Arozena A, et al. Guidelines for the use and interpretation of assays for monitoring autophagy (3rd edition). Autophagy 2016;12:1-222.
[25] King MA, Ganley IG, Flemington V. Inhibition of cholesterol metabolism underlies synergy between mTOR pathway inhibition and chloroquine in bladder cancer cells. Oncogene 2016;35:4518–28.
[26] Wu YT, Tan HL, Shui G, Bauvy C, Huang Q, Wenk MR, et al. Dual role of 3-methyladenine in modulation of autophagy via different temporal patterns of inhibition on class I and III phosphoinositide 3-kinase. J Biol Chem 2010;285:10850–61.
[27] Witjes JA, Comperat E, Cowan NC, De Santis M, Gakis G, Lebret T, et al. EAU guidelines on muscle-invasive and metastatic bladder cancer: summary of the 2013 guidelines. Eur Urol 2014;65:778–92.
[28] Bago R, Malik N, Munson MJ, Prescott AR, Davies P, Sommer E, et al. Characterization of VPS34-IN1, a selective inhibitor of Vps34, reveals that the phosphatidylinositol 3-phosphate-binding SGK3 protein kinase is a downstream target of class III phosphoinositide 3-kinase. Biochem J 2014;463:413–27.
[29] Dowdle WE, Nyfeler B, Nagel J, Elling RA, Liu S, Triantafellow E, et al. Selective VPS34 inhibitor blocks autophagy and uncovers a role for NCOA4 in ferritin degradation and iron homeostasis in vivo. Nat Cell Biol 2014;16:1069–79.
[30] Egan DF, Chun MG, Vamos M, Zou H, Rong J, Miller CJ, et al. Small molecule inhibition of the autophagy kinase ULK1 and identification of ULK1 substrates. Mol Cell 2015;59:285–97.
[31] Ma B, Liang LZ, Liao GQ, Liang YJ, Liu HC, Zheng GS, et al. Inhibition of autophagy enhances cisplatin cytotoxicity in human adenoid cystic carcinoma cells of salivary glands. J Oral Pathol Med 2013;42:774–80.

[32] Liu D, Yang Y, Liu Q, Wang J. Inhibition of autophagy by 3-MA potentiates cisplatin-induced apoptosis in esophageal squamous cell carcinoma cells. Med Oncol 2011;28:105–11.
[33] Zhao Z, Tao L, Shen C, Liu B, Yang Z, Tao H. Silencing of Barkor/ATG14 sensitizes osteosarcoma cells to cisplatininduced apoptosis. Int J Mol Med 2014;33:271–6.
[34] Fukuda T, Oda K, Wada-Hiraike O, Sone K, Inaba K, Ikeda Y, et al. The anti-malarial chloroquine suppresses proliferation and overcomes cisplatin resistance of endometrial cancer cells via autophagy inhibition. Gynecol Oncol 2015;137:538–45.
[35] Zhao XG, Sun RJ, Yang XY, Liu DY, Lei DP, Jin T, et al. Chloroquine-enhanced efficacy of cisplatin in the treatment of hypopharyngeal carcinoma in xenograft mice. PLoS One 2015;10:e0126147.
[36] Zhao J, Nie Y, Wang H, Lin Y. MiR-181a suppresses autophagy and sensitizes gastric cancer cells to cisplatin. Gene 2016;576:828–33.
[37] Liu X, Sun K, Wang H, Dai Y. Knockdown of retinoblastoma protein may sensitize glioma cells to cisplatin through inhibition of autophagy. Neurosci Lett 2016;620:137–42.
[38] Gaur S, Chen L, Yang L, Wu X, Un F, Yen Y. Inhibitors of mTOR overcome drug resistance from topoisomerase II inhibitors in solid tumors. Cancer Lett 2011;311:20–8.
[39] Huang Y, Xi Q, Chen Y, Wang J, Peng P, Xia S, et al. A dual mTORC1 and mTORC2 inhibitor shows antitumor activity in esophageal squamous cell carcinoma cells and sensitizes them to cisplatin. Anticancer Drugs 2013;24:889–98.
[40] Ma BB, Lui VW, Hui EP, Lau CP, Ho K, Ng MH, et al. The activity of mTOR inhibitor RAD001 (everolimus) in nasopharyngeal carcinoma and cisplatin-resistant cell lines. Invest New Drugs 2010;28:413–20.
[41] Mabuchi S, Kawase C, Altomare DA, Morishige K, Sawada K, Hayashi M, et al. mTOR is a promising therapeutic target both in cisplatin-sensitive and cisplatin-resistant clear cell carcinoma of the ovary. Clin Cancer Res 2009;15:5404–13.
[42] Tam KH, Yang ZF, Lau CK, Lam CT, Pang RW, Poon RT. Inhibition of mTOR enhances chemosensitivity in hepatocellular carcinoma. Cancer Lett 2009;273:201–9.
[43] Wu C, Wangpaichitr M, Feun L, Kuo MT, Robles C, Lampidis T, et al. Overcoming cisplatin resistance by mTOR inhibitor in lung cancer. Mol Cancer 2005;4:25.
[44] Garcia-Cano J, Ambroise G, Pascual-Serra R, Carrion MC, Serrano-Oviedo L, Ortega-Muelas M, et al. Exploiting the potential of autophagy in cisplatin therapy: a new strategy to overcome resistance. Oncotarget 2015;6:15551–65.
[45] Chandrasekar T, Evans CP. Autophagy and urothelial carcinoma of the bladder: a review. Investig Clin Urol 2016;57(Suppl 1):S89–97.
[46] Ojha R, Singh SK, Bhattacharyya S, Dhanda RS, Rakha A, Mandal AK, et al. Inhibition of grade dependent autophagy in urothelial carcinoma increases cell death under nutritional limiting condition and potentiates the cytotoxicity of chemotherapeutic agent. J Urol 2014;191:1889–98.
[47] Mani J, Vallo S, Rakel S, Antonietti P, Gessler F, Blaheta R, et al. Chemoresistance is associated with increased cytoprotective autophagy and diminished apoptosis in bladder cancer cells treated with the BH3 mimetic (-)-Gossypol (AT-101). BMC Cancer 2015;15:224.
[48] Li JR, Cheng CL, Yang CR, Ou YC, Wu MJ, Ko JL. Dual inhibitor of phosphoinositide 3-kinase/mammalian target of rapamycin NVP-BEZ235 effectively inhibits cisplatin-resistant urothelial cancer cell growth through autophagic flux. Toxicol Lett 2013;220:267–76.
[49] Pinto-Leite R, Arantes-Rodrigues R, Palmeira C, Colaco B, Lopes C, Colaco A, et al. Everolimus combined with cisplatin has a potential role in treatment of urothelial bladder cancer. Biomed Pharmacother 2013;67:116–21.

Publication 2

Anthraquinones and autophagy–Three rings to rule them all?

Jana Deitersen, Dina H. El-Kashef, Peter Proksch, Björn Stork

Bioorganic and Medicinal Chemistry, Volume 27, Issue 20, 115042, October 2019.

DOI: 10.1016/j.bmc.2019.115042

Bioorganic & Medicinal Chemistry 27 (2019) 115042

Contents lists available at ScienceDirect

Bioorganic & Medicinal Chemistry

journal homepage: www.elsevier.com/locate/bmc

Review article

Anthraquinones and autophagy – Three rings to rule them all?

Jana Deitersen[a,*], Dina H. El-Kashef[b], Peter Proksch[b], Björn Stork[a,*]

[a] Institute for Molecular Medicine I, Medical Faculty, Heinrich Heine University, Universitätsstraße 1, 40225 Düsseldorf, Germany
[b] Institute of Pharmaceutical Biology and Biotechnology, Faculty of Mathematics and Natural Sciences, Heinrich Heine University, Universitätsstraße 1, 40225 Düsseldorf, Germany

ARTICLE INFO

Keywords:
Anthraquinones
Autophagy
AKT pathway
Emodin
Chemotherapy-resistance

ABSTRACT

In order to overcome therapy resistance in cancer, scientists search in nature for novel lead structures for the development of improved chemotherapeutics. Anthraquinones belong to a class of tricyclic organic natural compounds with promising anti-cancer effects. Anthraquinone derivatives are rich in structural diversity, and exhibit pleiotropic properties, among which the modulation of autophagy seems promising in the context of overcoming cancer-therapy resistance. Among the most promising derivatives in this regard are emodin, aloe emodin, rhein, physcion, chrysophanol and altersolanol A. On the molecular level, these compounds target autophagy via different upstream pathways including the AKT/mTOR-axis and transcription of autophagy-related proteins. The role of autophagy is pro-survival as well as cell death-promoting, depending on derivatives and their cell type specificity. This review summarizes observed effects of anthraquinone derivatives on autophagy and discusses targeted pathways and crosstalks. A cumulative knowledge about this topic paves the way for further research on modes of action, and aids to find a therapeutic window of anthraquinones in cancer-therapy.

1. Introduction

Autophagy is a process of intracellular sequestration of cytoplasmic material like misfolded proteins, aggregated molecules or damaged organelles and its subsequent lysosomal degradation. By providing macronutrients from the degradation of bulk or targeted cargo, autophagy contributes to intracellular homeostasis and serves as energy source. Because of this catabolic function, the modulation of autophagy is often termed as 'double-edged sword' in cancer therapy. A high autophagic flux has been observed in hypoxic regions of tumors where it contributed to the metabolism and survival of malignant cells.[1] In addition, autophagy can act as pro-survival mechanism in response to various chemotherapeutics, supposedly via clearance of the drug.[2] On the contrary, there are cases where elevated autophagic flux led to autophagic cell death highlighting its tumor-suppressive role.[3,4] Both pro-survival and death-promoting effects of autophagy make it a promising pathway to target in cancer treatment.

Nature is a nearly inexhaustible source of novel therapeutic compounds targeting various cancer-related pathways. Structurally similar to anthracyclins, a class of applied broad-spectrum chemotherapeutics, anthraquinones are a group of polycyclic organic natural compounds consisting of three rings with two keto groups located at the central ring. They comprise a class of colorful, biologically abundant secondary metabolites in plants, bacteria and fungi including emodin, aloe emodin, rhein, physcion, chrysophanol and the modified anthraquinone derivative altersolanol A (Fig. 1).

Historical evidence for the research of anthraquinones can be found in the *Compendium of Materia Medica*, a Chinese collection of herbs for traditional Chinese medicine written by Li Shizen in 1578, which is based on the ancient texts *Shennong Bencaojing* (translated by Yang, 1998).[5] Li described the laxative effect of rhubarb roots, which are rich in emodin, aloe emodin, chrysophanol, rhein and their corresponding glucopyranosides.[6] As of today, anthraquinones still play a major role in ethnopharmacological medicine around the globe from Da Huang/Qingchangligan formula of traditional Chinese medicine to the Indian ayurvedic system as well as in the phytotherapy of the western world.[7,8] Pharmacological effects of anthraquinones include among others a range of antiviral,[9] antibacterial,[10] pro-apoptotic,[11–13] anti-oxidant,[14] pro-oxidative,[15] phototoxic,[16,17] anti-proliferative,[18] and anti-cancer effects.[19,20]

In a number of studies anthraquinone derivatives were suggested to be promising therapeutic agents against a variety of diseases.[21–24] Years of research confirmed that the study of anthraquinones in cancer related topics is an auspicious endeavor and that especially their role in apoptosis and autophagy could lead to a better understanding of their cytotoxic effects. However, anthraquinones have rarely been

* Corresponding authors.
E-mail addresses: jana.deitersen@hhu.de (J. Deitersen), bjoern.stork@hhu.de (B. Stork).

https://doi.org/10.1016/j.bmc.2019.115042
Received 31 March 2019; Received in revised form 27 June 2019; Accepted 6 August 2019
Available online 08 August 2019

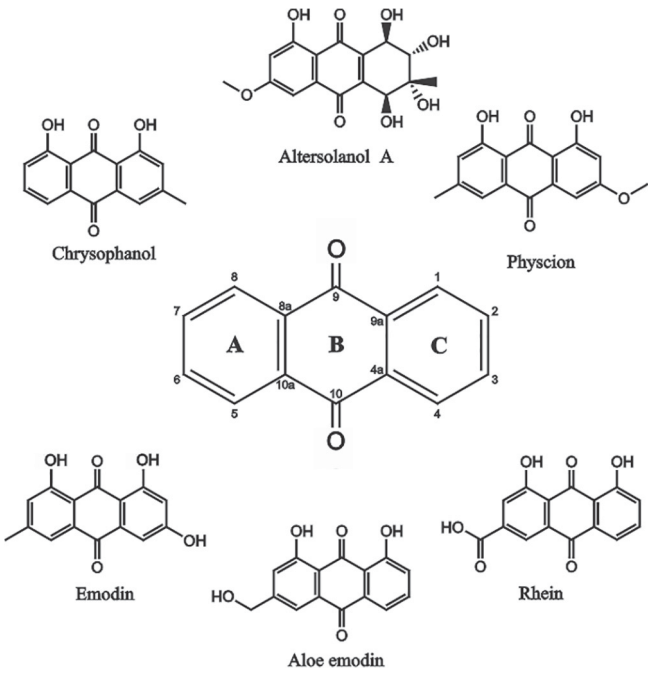

Fig. 1. General chemical structure of anthraquinone including three characteristic rings (A, B, and C) and derivatives.

systematically tested in autophagic assays. The objective of this article is therefore to recapitulate achievements in anthraquinone research in the context of autophagy and to serve as a basis for future research of anthraquinones in this regard. Moreover, this review pinpoints the importance of derivate-specific modes of action.

2. (Macro-)autophagy core machinery

Among different subtypes of autophagy, macroautophagy is the most extensive researched subtype and is referred to as autophagy hereafter. It is characterized by the sequestration of cytoplasmic content by the double-membraned autophagosome in contrast to chaperone-mediated autophagy or microautophagy, where cargo is either guided to the lysosome by chaperones or directly engulfed by the lysosome.[25]

In mammals, different steps of autophagy are coordinated by a multitude of autophagy-related (ATG) proteins and protein complexes (Fig. 2). Autophagy requires a coordinated sequence of events starting with its initiation. Autophagy initiation is regulated by energy or stress sensing upstream kinases such as mammalian/mechanistic target of rapamycin (mTOR) and 5′ adenosine monophosphate-activated protein kinase (AMPK). These kinases are in turn finely controlled by extracellular stimuli such as growth factors and intracellular stimuli such as oxygen level, DNA damage, amino acids, or ATP levels. Involved pathways include the axis from human epidermal growth factor receptor 2 (Her2/neu) or insulin-like growth factor 1 receptor (IGF1-R) via protein kinase B (AKT) and extracellular signal-regulated kinases 1/2 (ERK), or the axis from tumor necrosis factor (TNF) receptors via nuclear factor kappa-light-chain-enhancer of activated B cells (NF-κB). All pro-survival and stress factors and their respective pathways influence the rate of autophagic flux in a highly complex manner. However, AMPK and mTOR serve as rheostats in this regulation of autophagy. Both, inhibition by mTOR and activation by AMPK, regulate a key complex for autophagy termed the ULK1 complex. Eponymous and central for this complex is the serine/threonine protein kinase unc-51 like autophagy activating kinase 1 (ULK1) that interacts with autophagy-related protein 13 (ATG13), retinoblastoma 1-inducible coiled-coil 1 (RB1CC1; alternatively named focal adhesion kinase family

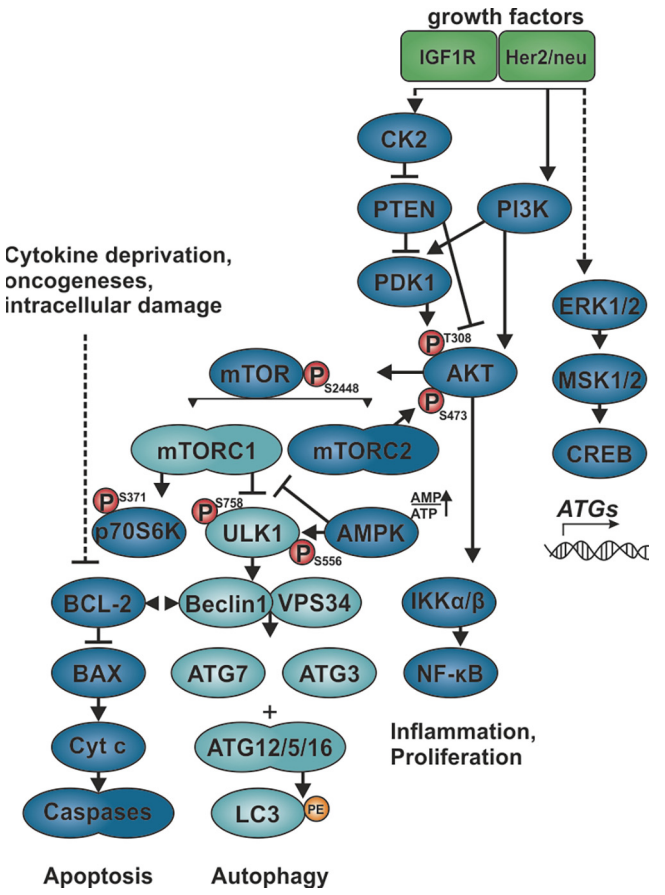

Fig. 2. Schematic pathway of the (macro-)autophagic core machinery and autophagy-related crosstalks. Growth factors bind to their corresponding receptors initiating signaling cascades via the phosphoinositide 3-kinase (PI3K)-, ERK1/2/mitogen-activated protein kinase (MAPK)-, casein kinase II (CK2)/phosphatase and tensin homolog (PTEN)- or NF-κB-axes maintaining cell survival and proliferation. Within multiple pathways, AKT is activated and serves as a bottleneck protein kinase responsible for signal transduction to downstream pathways and coordinating crosstalk between them. Upon growth factor and nutrient supply, AKT is phosphorylated at Thr308. Activated AKT can in turn phosphorylate mTOR causing its activation. mTOR itself is present in two multisubunit kinase complexes, i.e. mTOR complex 1 (mTORC1) and mTORC2. Whereas active mTORC1 phosphorylates p70/p85 S6 kinases and mediates proliferation and the downstream inhibition of autophagy, mTORC2 phosphorylates AKT at Ser473 for its maximum activation. Upon energy depletion, AMPK inhibits mTORC1, resulting in the dissociation of mTORC1 from the ULK1 complex, which then initiates autophagy. The ULK1 complex further recruits and activates ATGs such as the VPS34-Beclin 1-ATG14 complex and the ubiquitin-like conjugation systems of ATG12–ATG5-ATG16L and Atg8/LC3, allowing phagophore nucleation and autophagosome elongation. LC3 is conjugated in an E1/2/3-like enzymatic cascade to phosphatidylethanolamine (PE) enabling its integration into the autophagosomal membrane and facilitating its function as anchoring adapter protein. Depending on the subcellular localization, BCL-2 either binds Beclin 1 and thus inhibits autophagy or promotes apoptosis via activation of BAX, cytochrome *c* release from mitochondria and formation of the caspase-activating apoptosome. In addition, activation of the ERK1/2/MAPK or NF-κB pathway can activate the transcription of *ATG genes* like *BECN1* (the gene encoding Beclin 1).

interacting protein of 200 kDa, FIP200) and ATG101. Upstream activation of AMPK due to amino acid starvation, hypoxia or growth factor withdrawal, leads to AMPK-dependent direct phosphorylation and activation of ULK1.[26–30] In addition, AMPK furthermore inactivates mTOR and promotes autophagy initiation.[31] Following the initiation of autophagy, a phagophore (alternatively termed isolation membrane, IM) is nucleated presumably at specific subdomains of the ER.[32]

The active ULK1 complex then initiates the subsequent activation of the class III PI3K complex involving the core components vacuolar protein sorting 34 (VPS34), Beclin 1 and VPS15 (also termed p150). In mammals, the PI3K complex is regulated via Beclin 1 and its association with activating proteins such as Atg14-like (Atg14L; also termed Beclin 1-associated autophagy-related key regulator, Barkor), UV radiation resistance-associated gene protein (UVRAG) or activating molecule in Beclin 1-regulated autophagy protein 1 (AMBRA1). Furthermore, the complex is negatively regulated by run domain Beclin 1 interacting and cysteine-rich containing protein (RUBICON) and the apoptosis regulator B cell lymphoma 2 (BCL2).[33] Within the activated PI3K complex, VPS34 phosphorylates inositol lipids to phosphatidylinositol 3-phosphate (PI3P), which recruits downstream effector proteins like WD-repeat protein interacting with phosphoinositide 1/2 (WIPI1/2) to the phagophore.[34] WIPI1/2 further recruits two ubiquitin-like conjugation systems, ATG12–ATG5-ATG16L and microtubule-associated proteins 1A/1B light chain 3B (LC3), to the phagophore. The ATG12–ATG5-ATG16L complex, whose assembly is supported by ATG7 and ATG10, determines the site of LC3 lipidation and contributes to autophagosome elongation.[34]

During starvation-induced autophagy, a C-terminal peptide of cytosolic pro-LC3 is cleaved off by the protease ATG4 generating LC3-I. Then, ATG7, ATG3 and presumably ATG12–ATG5-ATG16L conjugate the truncated LC3-I to phosphatidylethanolamine (PE) in an E1/E2/E3-cascade mechanism forming lipidated LC3-II.[35] On the outer autophagosomal membrane, LC3-II recruits members of the autophagy machinery and is involved in lipid assembly for autophagosome elongation. In the inner autophagosomal membrane, it serves as an anchor to target proteins for degradation. After fusion of autophagosome and lysosome, ATG4 cleaves LC3-II off the outer autophagosomal membrane. LC3-II on the inner membrane is degraded along with the cargo inside the autolysosome.[36] One of the receptor proteins recruited by LC3-II during autophagy is p62/sequestosome 1 (SQSTM1). Directly associated with LC3-II via its LC3-interacting region (LIR) motif, p62 binds ubiquitinated cargo via its C-terminal ubiquitin-associated (UBA) domain and thus links the cargo to the autophagosomal membrane where it is sequestered for autolysosomal degradation. In the late stage of autophagy, lysosomal hydrolases degrade the autophagy receptor p62 along with LC3-II.

Activation of the autophagic machinery induced by mildly toxic agents is understood to serve pro-survival functions in order to remove sources of damage. Examples are mitotoxins in mitophagic clearance, DNA-damaging agents in nucleophagy or viral/bacterial components in xenophagy.[37] A prolonged activation or disrupted completion of autophagy can result in an elevation of the intracellular stress level above a threshold, ultimately leading to the induction of apoptosis. Via several molecular cross-regulatory events—including the caspase-dependent cleavage of ATGs—apoptosis then inhibits autophagy. The mode of action of numerous cytotoxic natural compounds involves the initiation of apoptosis being accompanied with either pro- or anti-autophagic effects depending on cell lines, concentrations and especially time points investigated. Generally, one should consider kinetic aspects of autophagy and apoptosis assays following treatment with different stimuli. Usually natural compounds induce the intrinsic apoptosis signaling pathway, characterized by the release of cytochrome *c* from mitochondria, the formation of an apoptosome and a cascade of caspases. Assays monitoring such apoptosis induction often rely on the detection of cleaved caspases, an event relatively late in the pathway. On the other hand, both formation and lysosomal degradation of autophagosomes happen within minutes. The accumulation of autophagy markers such as LC3 is a rapid dynamic process within the first minutes to hours after autophagy induction.[38,39] Furthermore, this LC3 accumulation can be indicative of contrasting events: an induction of canonical autophagy including LC3 lipidation, an acceleration of the lipidation process independent from canonical autophagy, or a late-stage inhibition of autolysosome formation or lysosomal degradation. Increasing levels of total LC3 can also be indicative for increased *LC3* transcription. Therefore, conclusions about pro- or anti-autophagic effects of stimuli require thorough examination of multiple autophagic markers and time points. Additionally, assays should be performed in combination with known autophagy initiators or inhibitors.

3. Emodin

One of the best-studied anthraquinones is emodin, which got its name from the Himalayan rhubarb (*Rheum emodi*). It passes the cell membrane and can be detected in the cytoplasm of macrophages by its autofluorescence.[40] Within the cell, emodin exerts a range of pharmacological actions, such as anti-inflammatory,[41] anti-fibrotic,[42] anti-proliferative,[19] anti-angiogenic,[43] and pro-apoptotic effects.[11–13,15] The anti-cancer activity of emodin was observed in a wide range of different cancer types and through the involvement of various molecular pathways including the PI3K/AKT pathway in cervical cancer, breast cancer and pancreatic cancer.[44] Emodin displays over 25-fold differential cytotoxicity against *ras*-transformed bronchial epithelial cells in comparison to non-transformed human bronchial epithelial cells and is therefore often designated the 'new lead anticancer agent'.[45] It also appears to have a high specificity on human neuroectodermal tumors both *in vitro* and *in vivo* due to its pro-apoptotic effects.[20]

Apart from cancer, emodin has been proposed to be beneficial in a wide range of chronic diseases as it downregulates transcription factors such as nuclear factor (erythroid-derived 2)-like 2 (Nrf-2) in a model of chronic lung disease, NF-κB in models of rheumatoid arthritis, cardiovascular, lung and kidney diseases or peroxisome proliferator-activated receptor gamma (PPARγ) in diabetes and cardiovascular diseases.[46] Following an inhibition of NF-κB, emodin led to downregulation of inflammatory-related proteins such as vascular endothelial growth factor (VEGF), hypoxia-inducible factor 1-alpha (HIF-1α), cyclooxygenase-2 (COX-2), interleukin 1 beta (IL-1β), matrix metalloproteinases MMP-1, MMP-13 and pro-inflammatory cytokines such as prostaglandin E2, tumor necrosis factor (TNF-α), interleukins 6 and 8 (IL-6, IL-8). The inhibition of the NF-κB pathway is associated with an induction of autophagy in the case of natural compounds such as resveratrol or cucurmin.[47] Activation of the NF-κB pathway on the other hand is associated with an inhibitor of kappa B kinase (IKK)-dependent activation of mTOR resulting in the inhibition of the autophagic flux.[48–50] In contrast, activation of the NF-κB pathway can result in nuclear translocation of the NF-κB family member p65, inducing transcription of the *BECN1* gene (encoding Beclin 1) and thus facilitating autophagy.[51] As a transcription factor, NF-κB rather contributes to the long-term regulation of autophagy. Accordingly, additional pathways are likely to account for short-term autophagy-modulating effects of natural compounds.

Co-treatment of emodin and TNF-α attenuated pro-apoptotic and pro-autophagic effects, such as the upregulation of Beclin 1, ATG7 and LC3-II as well as cleaved caspase 3 and cleaved poly (ADP-ribose) polymerase (PARP), in mouse C2C12 myoblasts probably via inhibition of the NF-κB pathway and increased AKT phosphorylation.[52] On the opposite, treatment with emodin alone was shown to decrease mTOR- and CK2-dependent phosphorylation of AKT in HeLa cells.[53] A decrease in AKT phosphorylation was also observed after treatment with emodin loaded liposomes in Her2/neu over-expressing breast cancer cell line MDA-MB-453.[54] Furthermore, it was reported that emodin inhibits casein kinase II (CK2).[55,56] The inhibition of CK2 was recently linked to the induction of autophagy. It was found that both CK2-targeting siRNA and the specific CK2 inhibitor CX-4945 led to an induction of autophagy in the three different human pancreatic cancer cell lines BxPC3, 8902 and MIA PaCa-2, and to an autophagy-accelerated apoptotic cell death, since suppression of ATG7 reduced CX-4945-induced apoptosis.[57] Structurally, it appears that the hydroxy group at C3 of emodin is essential for binding to and inhibition of CK2.[58–60] In addition to CK2, emodin inhibits serum- and glucocorticoid induced kinase (SGK).[61]

Inhibition of SGK either by the specific inhibitor GSK650394 or SGK1 shRNA has been shown to induce autophagy in the human prostate cancer cell line PC3 via a reduction of mTOR phosphorylation and a phospho-FOXO3a-LC3 interaction, which ultimately resulted in both autophagy and apoptotic cell death.[62] In the case of NRK-52E cells, emodin also induced the activation of AMPK, which resulted in LC3 lipidation and was reversed by the AMPK inhibitor dorsomorphin (compound C). A second stage activation of AMPK after 6 h was coincident with decreased autophosphorylation of mTOR at Ser2481 and transphosphorylation of p70 S6 kinase (p70 S6K) at Ser371.[63] In addition, emodin treatment resulted in an early decrease of mTOR Ser2448 phosphorylation in HL-60 cells and was responsible for decreased mTOR-dependent AKT Ser473 phosphorylation.[53,64] Downstream of mTOR, it was shown that emodin prevents phosphorylation of p70 S6K at Ser371 and its IGF-1 induced phosphorylation at T389, as well as phosphorylation of p85 S6K at T412.[53,63] By downregulating both the AKT-mTOR-axis and the p38 pathway, emodin also inhibited cell proliferation of HBZY-1 rat mesangial cells.[65] Supporting the scenario of mTOR inhibition, plenty of evidence has been found for the induction of autophagy by emodin. ATG12–ATG5 is increased in HO-8910, HeLa and Jar cells upon prolonged emodin treatment, and emodin-dependent autophagosome accumulation was observed in human vascular smooth muscle and HeLa cells as investigated by electron microscopy.[42,66,67] Reinforcing the modulation of autophagy by emodin, the accumulation of autophagy markers LC3, especially lipidated LC3-II, and Beclin 1 has been observed in a range of different cell lines (see Table 1). The decrease of these markers can be indicative for the degradation by either autolysosomal hydrolases or apoptosis-related caspases, or for the negative transcriptional regulation in response to other upstream pathways.[68,69] Finally, also opposite observations have been made. Hu et al. reported that emodin prevents the lipidation of LC3 during starvation-induced autophagy by specifically activating mTOR in a rat kidney cell line.[70] The balance of mTOR inhibition and activation might therefore be cell type-specific, while the data hints to an mTOR-inhibitory effect of emodin in cancer cells. In these cells, emodin was shown to have additive or synergistic effects with chemotherapeutic drugs, such as arsenic trioxide, TRAIL, or cisplatin, sensitizing those cells to cell death. Non-tumor cells were not responsive to the combination treatments.[71–75] Most importantly, combination treatment with cisplatin and emodin induced cell death in platinum-resistant cancer cells by decreasing AKT phosphorylation and inducing caspase-mediated apoptosis.[76]

4. Aloe emodin

Aloe emodin had a pronounced anti-proliferative effect in Merkel carcinoma cells, a highly aggressive and resistant cell line, and it potentiated the anti-proliferative effect of chemotherapeutic agents such as cisplatin, doxorubicin, and 5–fluoroucil.[80]

Similar to emodin, aloe emodin exhibited a higher cytotoxicity against oral squamous cell carcinoma and salivary gland tumor cells than against normal human gingival fibroblasts (HGF).[81] It has further been suggested to be a 'new lead anticancer agent' due to its cancer specific cytotoxicity both *in vitro* and *in vivo*.[20] Aloe emodin seems to induce apoptosis, and this effect is even more pronounced in human neuroectodermal tumors in comparison to normal fibroblasts or hematopoietic progenitor cells. The uptake of aloe emodin was extremely pronounced in these cells and involved an energy-dependent drug import.

The drug specifically inhibited TNF-α induced but not UV radiation- or hydrogen peroxide-induced apoptosis and necrosis in L929 mouse fibrosarcoma and U251 human glioma cell lines.[82] Under these treatments as well as under basal conditions, aloe emodin inhibited the activation of the ERK1/2 pathway. Along these lines, a selective ERK

Table 1
Effect of emodin treatment on components of the autophagic pathway.

Experimental model	Dosage and duration of treatment	Autophagy-related response	Reference
NRK-52E cells	10–100 μM; 1 h 50 μM; 30 min-6 h	LC3-I, -II↑ phospho-p70 S6K Ser371↓ phospho-mTOR Ser2481↓ phospho-AMPK Thr172↑	Liu et al., 2016 (Ref.[63])
HeLa cells	40 μM; 4 h 30 μM; 12 h	mTOR activity↓ IGF-1 induced phospho-p70 S6K Thr389↓ IGF-1 induced phospho-p85 S6K Thr412↓	Olsen et al., 2007 (Ref.[53])
HeLa cells	1–100 μM; 48 h	autophagosomes in electron microscopy↑ lysosomal permeability↑	Trybus et al., 2017 (Ref.[66])
hVSMC	25 μg/mL = 92.5 μM; 24 h	autophagosomes in EM↑	Wang et al., 2007 (Ref.[42])
HO-8910, HeLa & Jar cells	0–15 μM; 72 h	LC3 (via microscopy)↑ Beclin 1↑ Atg12–Atg5↑	Wang et al., 2015 (Ref.[67])
HCT116 & LOVO cells	5–40 μM; 6–36 h	p62↓ LC3-I↑ LC3-II↑ Beclin 1↑ + chloroquine: LC3-II↑	Wang et al., 2018 (Ref.[13])
HL-60 cells	10–80 μM; 12–48 h	mTOR↓ phospho-mTOR Ser2448 (12 h; 80 μM)↓	Zheng et al., 2007 (Ref.[64])
Model of acute pancreatitis in Wistar rats	40 mg/kg per day, intragastrically	LC3 mRNA, LC3-II↓ p62 mRNA, p62↓ Beclin 1 mRNA, Beclin 1↓	Yu et al., 2018 (Ref.[69])
IEC-6 cells	6–24 h; in hypoxia	Beclin 1 mRNA↑ LC3 mRNA↑	Zheng et al., 2015 (Ref.[77])
NRK-52E cells	10 μM	starvation-induced LC3 lipidation↓ via mTOR pathway	Hu et al., 2015 (Ref.[70])
HK-2 cells	40 μM; 24.5 h + 24 h FCS-free pre-treatment + 10 μg/L TGF-β1	LC3↑ LC3 mRNA↑ Beclin 1↑ Beclin 1 mRNA↑	Dou et al., 2018 (Ref.[78])
SW480 cells	10–20 μM; 24 h	LC3-II↑ Beclin 1↑ p62↓	Li et al., 2017 (Ref.[79])

inhibitor mimicked the cytoprotective action of the anthraquinone derivative. Similar to the effect of rhein in the murine glioma cell line F98 (described below), aloe emodin also markedly inhibited the activation of ERK1/2 in the murine glioma cell line C6, while it did not affect p38, c-Jun *N*-terminal kinases (JNK) or NF-κB pathways.[83]

During the cytoprotective bioactivity of aloe emodin in TNF-α induced apoptosis, intracellular acidified autophagic vesicles accumulated. Additional inhibition of autophagy with bafilomycin A_1 or 3-methyladenine (3-MA) efficiently prevented the cytoprotective effect of aloe emodin.[82] On its own, aloe emodin treatment resulted in increased autophagy whereas inhibition of autophagy enhanced aloe emodin cytotoxicity.

Furthermore, aloe emodin has been assessed in the development of photodynamic therapy (PDT), a new promising approach for anticancer therapy of solid tumors. Aloe emodin serves as photosensitizer to produce reactive oxygen species (ROS) and triggers autophagy and apoptosis of MG-63 cells. Inhibition of autophagy enhanced apoptosis and sensitized the cells to aloe emodin-PDT treatment. The formation of ROS was responsible for a subsequent phosphorylation of JNK.[17] Even though the effect on autophagy and apoptosis are congruent with non-PDT aloe emodin treatment, it can be speculated that they can be coordinated via different pathways (JNK or ERK) depending on the PDT-triggered induction of ROS.

5. Rhein

Rhein is one of the bioactive dihydroxy-anthraquinone compounds in Chinese rhubarb and is involved in its effects in improving renal dysfunction in patients with chronic kidney diseases.[84] Studies have proven that rhein inhibits the expression of transforming growth factor (TGF)-β1, fibronectin and actin in unilateral ureteral obstruction (UUO) kidneys ameliorating renal fibrosis *in vivo*.[85]

Studies using both rhubarb decoction and isolated rhein revealed a decrease in fibrotic protein levels in rat kidney cells accompanied by an anti-autophagic mode of action of rhein.[86] Similar to the findings of Hu et al. who detected an mTOR-dependent inhibition of LC3 lipidation by emodin, Tu et al. show that rhein prevented the starvation-induced lipidation of LC3 by inhibiting AMPK and thereby increasing mTOR activity in rat renal tubular cells.[70,86] In the same study, treatment with rhein decreased AKT phosphorylation but this event does not appear to be involved in the inhibition of LC3 lipidation.

Consistent with a malfunction of the autophagic flux, rhein induced the accumulation of acidic compartments indicative of either an induction of autolysosome formation or a failure in autolysosomal degradation in both human and murine glioma cells.[87] Matching the accumulation of autolysosomes, Tang et al. observed increased protein levels of autophagy-related Beclin 1 and LC3. They also observed increased apoptosis-related levels of BCL-2, BAX, and caspase 3 in the glioma model, which might point toward the induction of apoptosis after a prolonged disruption of the autophagic flux. Although the increase of apoptotic and autophagic proteins was accompanied by an inhibition of ERK1/2 activity, specific ERK inhibitors failed to mimic the rhein-induced autophagic vesicle accumulation. Similar to AKT, rhein-dependent modulation of autophagy seems to be independent of ERK1/2. In contrast to the inhibition of the ERK1/2 pathway, rhein did not affect p38 or JNK in rat F98 glioma cells but inhibited the p38 pathway in rat kidney cells and JNK in mouse epidermal cells indicating that the modulation of rhein-dependent pathways is tissue specific and not necessarily connected to its effect on autophagy.[86–89]

Previous studies also suggested that rhein suppresses the PI3K/AKT pathway and phosphorylation of ERK while it also inhibited the activity of heat shock protein 90 alpha (HSP90α), an event that induced the degradation of HSP90 client proteins like NF-κB, COX-2, and HER-2.[90] Hsp90 also serves as chaperone for ATGs like Beclin 1 and Ulk1.[57,91,92] The degradation of ATGs, which are required for autophagy, via a rhein-dependent inactivation of HSP90 might be a cause of incomplete autophagic flux and the induction of cell death pathways such as apoptosis.

6. Chrysophanol

Chrysophanol (also chrysophanic acid), another dihydroxy-anthraquinone, can be found as component of rhubarb plants.[19] In a number of cytotoxicity studies, chrysophanol inhibits cell growth in cancer cells.[93,94] The inhibition of cell growth was accompanied by an induction of cell death in J5 human liver cancer cells, which is reported to be independent of apoptosis.[95] Although chrysophanol increased ROS and promoted Ca^{2+} release from mitochondria in the human lung cancer cell line A549, apoptosis was not triggered in this cell line.[96] The generation of ROS might be one explanation for an additionally observed induction of DNA damage. Also in response to ROS production, treatment with chrysophanol further disrupted the mitochondrial membrane potential, which increased the intracellular AMP:ATP ratio. Following the disruption of mitochondria, cytochrome *c* was released which interestingly did not trigger apoptosis but necrosis.[96] In the same cell line, chrysophanol upregulated p53 while inhibiting its translocation into the nucleus, which in turn increased mTOR expression and inhibited autophagy.[97] Supporting an anti-autophagic role of chrysophanol, a screening of compound libraries on GFP-LC3-positive cells revealed that chrysophanol is a very potent inhibitor of autophagolysosomal degradation.[98]

Additionally, a screening with different cancer cell lines revealed that chrysophanol preferably exhibits anticancer activity in EGF-R-overexpressing cells.[99] In these cells, chrysophanol treatment inhibited the EGF-mediated activation of its receptor (EGF-R) and thereby suppressed downstream activation of AKT, ERK, and mTOR. This effect contrasts with the situation in EGF-R non-overexpressing A549 cells, where chrysophanol exhibited anti-autophagic activity via increasing protein levels of mTOR.[96]

Both events, the induction of a mitochondrial catastrophe via increased ROS and the indirect suppression of the AKT/mTOR-axis can be triggers for the induction of autophagy. However, the extensive damage on the mitochondrial network triggering necrosis might eventually prevent autophagic completion and cause LC3 accumulation. The exact sequence of events including the activation or inhibition of the mTOR pathway and modulation of the autophagic flux might be dependent on the EGF-R-status of the tumor cell line and the modulation of pro-necrotic pathways.

7. Physcion

Physcion, also named parietin, resembles chrysophanol except for an additional methoxy-group at the C6 position. It is postulated to be a promising anti-cancer agent as two groups individually showed that physcion induced caspase-dependent apoptosis and dose-dependently suppressed the tumor growth in a murine xenograft model.[100,101] Similar to chrysophanol, physcion was able to enhance ROS levels, which was responsible for both pro-autophagic and pro-apoptotic signals in cancer cells.[101] More precisely, ROS production resulted in a decrease in specificity protein 1 (Sp1) and microRNA 27a (miR27-a) expression, which was responsible for physcion-induced increase in acidic vesicular organelles, LC3 lipidation and degradation of p62. Physcion-induced reduction of cell viability could partially be abolished by the autophagy inhibitor 3-MA.

In turn, the inhibition of apoptosis enhanced physcion-induced autophagy while still inducing a form of cell death, supporting two possible scenarios: The inhibition of apoptosis prevents apoptotic cell death, but a prolonged incubation with physcion drives the cell into an autophagic cell death. Alternatively, the inhibition of apoptosis initially keeps the intracellular stress signal below a certain threshold, activating the autophagic pathway as a pro-survival mechanism, which ultimately fails and induces non-autophagic, non-apoptotic cell death.

Supporting a pro-survival role of autophagy in physcion-induced cell death, inhibition of autophagy using ATG5-targeting siRNA elevated apoptotic cell death even further in human hepatocellular carcinoma and endocervical adenocarcinoma cell lines.[100]

Both autophagy and apoptosis markers were increased in these cells upon physcion treatment: the cells exhibited an increase in LC3 lipidation, Beclin 1 and ATG5 protein levels and degradation of p62, synchronously to an accumulation of cleaved caspases. Both effects seem to be mediated via the JAK2/STAT3 pathway in the two cell lines. This pathway is known to have multiple inhibitory connections with the autophagy pathway; e.g. cytosolic STAT3 constitutively inhibits autophagy by regulating microRNAs and interacting with the autophagy-relevant transcription factors FOXO1 and FOXO3.[102] Additionally, nuclear STAT3 dimers transcriptionally repress pro-autophagic target genes such as *BECN1* or *PIK3C3*, the gene encoding for VPS34, while activating the transcription of anti-autophagic factors such as *BCL2*.[103–105]

8. Altersolanol A

Altersolanol A is a pentahydroxy-anthraquinone derivative exhibiting four hydroxy groups at ring C, forming a highly substituted cyclohexane moiety in comparison to all other anthraquinone derivatives discussed in this manuscript. Its investigated effects include a high cytotoxicity especially towards cancer cell lines.[106,107] Altersolanol A induced apoptosis in human chronic myeloid K562 leukemia and A549 lung cancer cells with markedly lower cytotoxicity in non-cancerous isolated peripheral blood mononuclear cells.[107] Furthermore, it inhibited TNF-α induced activity of NF-κB in the human leukemia cell line K562 in a dose dependent manner. In addition to inactivation of the NF-κB pathway, altersolanol A is an effective inhibitor of various kinases including AKT1, EGF-R and IGF-R.[108–110]

Both the potentially wide therapeutic window and its cytotoxicity towards a range of cancer cells highlight altersolanol A as a promising new chemotherapeutic agent. So far, it revealed a potent cytotoxic activity towards a panel of 34 different human tumor cell lines after 4 days of treatment with IC50 values between 0.001 and 0.412 μg/ml (resp. 0.003 and 1.225 μM).[106] The cytotoxic effect was mediated by an induction of apoptotic cell death accompanied by common markers such as an induction of caspases-3/-9 cleavage and a decrease in the expression of anti-apoptotic proteins. These pro-apoptotic effects were also observed by our group: We detected common apoptosis-related events such as caspase-3 activity, PARP cleavage, and DNA fragmentation in human T cell leukemia, acute myeloid leukemia, and Burkitt's lymphoma cell lines (unpublished data). Additionally, we detected an accumulation of fluorophore-tagged LC3 in human embryonic kidney (HEK) and mouse embryonic fibroblast (MEF) cells after starvation-induced autophagy, indicating an anti-autophagic effect of altersolanol A.

Two groups emphasized the importance of the paraquinone moiety of altersolanol A for its bioactivity: Teiten et al. showed that the ablation of the paraquinone moiety with or without substitution with hydroxy groups as in the case of tetrahydroaltersolanol B or ampelanol prevents the cytotoxicity of the respective altersolanol A derivatives.[107] Acetylation of altersolanol A into tetraacetylaltersolanol A does not prevent altersolanol A bioactivity. Although the lipophilicity is an important factor in pharmacokinetics—e.g. affecting membrane passage or tissue distribution—an increased lipophilic character of altersolanol A derivatives does not appear to have a huge impact on the examined pathways. Similarly, Aly et al. detected a high cytotoxic activity of altersolanol A toward L5178Y mouse lymphoma cells while altersolanol J, harboring a hydroxy group instead of the second keto group at the central ring, showed only weak activities.[111]

9. The two towers–autophagy and apoptosis

Most researchers agree on the role of autophagy being predominantly pro-survival, whereas apoptosis is a form of programmed cell death. These two mechanisms have very distinct characteristics; while autophagy is characterized by the activity of ATGs and the formation of autophagosomes/autophagic vesicles, apoptosis involves the activation of a cascade of caspases and the formation of apoptotic bodies. The characteristics include that autophagy is a basal mechanism in almost all cells, which can be dimmed or elevated, while apoptosis is an escalating event without reversibility if a certain threshold has been passed. Often however, these two pathways are induced by the same stimuli, although it is thought that they pursue very different intentions. Natural compounds inducing damage might trigger initial autophagy to eradicate the source of damage and afflicted organelles. This can co-occur with an autophagy-dependent inhibition of apoptosis e.g. by autophagic clearance of mitochondria prior to cytochrome *c* release (mitophagy), by autophagic degradation of pro-apoptotic proteins, or directly by proteins that are both pro-autophagic and anti-apoptotic, such as BCL-2 and proteins of the Bcl-2 associated athanogene (BAG) family.[112] Upon reaching lethal concentrations of cytotoxins, a certain threshold will be passed and irreversible cell death will be initialized. The nature of this cell death depends on a finely regulated array of pathways and additional triggers and can show features of necrosis, autosis, apoptosis, necroptosis, anoikis or autophagic cell death. For the latter, the Nomenclature Committee on Cell Death (NCCD) defined autophagic cell death as a process involving ATGs, which can be suppressed by pharmaceutic or genetic inhibition of the autophagic pathway and proven by knockdowns of at least two essential autophagic genes.[113] Due to the considerable methodical and theoretical expenditure of this definition, most reports usually describe the co-existence of autophagic and apoptotic effects and lack an in-depth characterization of the relationship between the two pathways. Still, three possible modes have been proposed: (I) autophagy and apoptosis occur simultaneously but unconnected, (II) autophagy acts cytoprotective against apoptosis, (III) autophagy precedes apoptosis in a time- or concentration-dependent manner.[114] In the case of anthraquinones, evidence on emodin and physcion hint towards two possible relations. First, autophagy appears to promote apoptosis in the case of physcion treatment in CNE2 cells and emodin treatment in HCT116 and LOVO colon carcinoma cells, since in both cases inhibition of autophagy by 3-MA or chloroquine mitigates apoptotic cell death.[13,101] However, the inhibition of autophagy does not completely rescue the cells from apoptotic events or cell death, indicating an additional autophagy-independent induction of apoptosis by the examined anthraquinones. Second, autophagy can also prevent apoptosis induced by anthraquinones. In rat renal epithelial cells, the induction of autophagy by emodin lessened cisplatin-induced apoptotic cell death.[63] Similarly, aloe emodin induced autophagy, which prevented TNFα-induced cell death of the mouse fibrosarcoma cell line L929 and a TNF-sensitive subclone of the human glioma cell line U251.[82] In the case of physcion treatment in Hep3B and SMMC7721 hepatic carcinoma cells, inhibition of autophagy by 3-MA or ATG5 siRNA exacerbated the apoptotic phenotype.[100] It is important to note that not only apoptosis was attenuated by physcion-induced autophagy, but also cancer cell migration and invasion. Due to cell type specific differences and other contributing factors, it is not trivial to determine the order of events that finally lead to cell death, but the modulation of autophagy seems to contribute to a large part to cancer cell fate during anthraquinone treatment and is most effective at early time points and sublethal concentrations.

One contributing factor is the balance of ROS, which serve as signaling molecules within redox signaling. They increase upon starvation, hypoxia, TNFα treatment, and nerve growth factor (NGF) deprivation and trigger autophagy in order to reduce intracellular oxidative stress.[115] Increased ROS directly oxidize a cysteine residue of ATG4, the protease that also mediates the deconjugation of LC3 from phosphatidylethanolamine on the outer autophagosomal membrane, and thus further increase autophagy.[116] ROS induction was also found to be involved in the modulation of autophagic core components by emodin.

Table 2
ROS-dependent effects of anthraquinones on the autophagic and apoptotic pathway.

Experimental model	Dosage and duration of treatment	Response	Reference
DU-145 & HDF cells	50 μM emodin	ROS↑ + As_2O_3/DDP/Taxol/DOX: viability↓, apoptosis↑ + NAC: viability↑, apoptosis↓	Huang et al., 2008 (Ref.[71])
A549 cells	50 μM emodin; 0.5–6 h	ROS↑ + Asc: apoptosis↓ + NAC: apoptosis↓	Huang et al., 2013 (Ref. [119])
COC1 & COC1/DPP cells	50 μM emodin; 24 h	+ DDP: ROS↑, apoptosis↑ + NAC: ROS↓, apoptosis↓	Ma et al., 2014 (Ref.[76])
hVSMC	0–25 μg/mL (92.5 μM) emodin; 0–72 h	ROS↑ + DPI: ROS↓, apoptosis↓	Wang et al., 2007 (Ref.[42])
HCT116 & LOVO cells	40 μM emodin	ROS↑ + NAC: apoptosis↓, autophagy↓	Wang et al., 2018 (Ref.[13])
CNE2 cells	0–20 μM physcion; 48 h	ROS↑ + NAC: apoptosis↓, autophagy↓	Pang et al., 2016 (Ref.[101])
SW480 cells	emodin	ROS↑ + NAC: apoptosis↓, autophagy↓	Li et al., 2017 (Ref.[79])
EC/CUHK1 cells	10 μM emodin; 72 h	+ As_2O_3: ROS↑, ΔΨm↓, apoptosis↑ + NAC: apoptosis↓	Yang et al., 2004 (Ref.[75])
EC/CUHK1 cells	25 μM aloe emodin; 72 h	+ As_2O_3: ROS↑, apoptosis↑ + NAC: apoptosis↓	Yang et al., 2004 (Ref.[75])

As_2O_3: arsenic trioxide; Asc: ascorbic acid; DDP: *cis*-diamminedichloroplatinum(II)/cisplatin; DOX: doxorubicin; DPI: diphenylene iodonium; NAC: *N*-acetylcysteine; ΔΨm: mitochondrial membrane potential.

One of the most rapid effects is the dynamic phosphorylation of AMPK.[63,117] AMPKα phosphorylation at Thr172 occurred in rat kidney epithelial NRK-52E cells after 30 min of 50 μM emodin treatment and in L6 myotubes after 1 min of 3 μM emodin treatment.[63] This phosphorylation is catalyzed by LKB1 in response to an increased AMP:ATP ratio.[118] Song et al. showed that emodin-mediated activation of AMPK is ROS- and CaMKK-dependent and included the inhibition of mitochondrial complex I within the first 10 min of emodin treatment causing an increase in the AMP:ATP ratio.[117]

There are several additional indications that the increase in ROS caused by anthraquinones contributes to the modulation of autophagy and cell viability (Table 2). It has been shown that emodin and physcion increase intracellular ROS, while co-treatment with antioxidants such as *N*-acetyl cysteine (NAC), ascorbic acid (vitamin C, Asc) or diphenylene iodonium (DPI) counteracted anthraquinone-induced autophagy, apoptosis, and cell death. The importance of ROS induction for cell death is especially true for combination treatments with emodin and other chemotherapeutics.[71,76] Yang et al. also noted that cell death induced by combination treatment of emodin and arsenic trioxide was facilitated by increased ROS levels, which induced a collapse of the mitochondrial transmembrane potential, the release of cytochrome *c*, and the activation of caspases-3 and -9, while it suppressed the activation of NF-κB and downregulated the anti-apoptotic protein survivin.[75] Using a cDNA microarray-based global transcription profiling, Wang et al. postulated that an increase in ROS modulates the expression of a number of genes involved in signal transduction, cell-cycle regulation, and organelle functions, which in turn contribute to the sensitization towards cell death.[74] Anthraquinone-induced increase in ROS levels as well as ROS-mediated autophagic modulation might therefore be involved in the shaping of cancer cells' fate in multiple ways.

10. Structure activity relationships

Structurally, anthraquinones discussed in this manuscript share two main characteristics: the paraquinone moiety and substitution with hydroxy groups. Kamei et al. therefore tested mono-, bi- and tricyclic quinones with several hydroxy substitution patterns on cell growth inhibition of human colon carcinoma cells.[120] They found that bi- and tricyclic compounds were more effective than the monocyclic quinones and that substitution with at least two or more hydroxy groups was essential for their cytostatic effects. Of course not only the number of hydroxy groups is important, but also their position. Cai et al. confirmed that hydroxy groups were essential for the bioactivity of anthraquinones, and proposed a necessity of the *ortho*-dihydroxy structure to enhance radical scavenging effects.[6,121]

There are also multiple indications highlighting the importance of a hydroxy group at C3 position of ring C (Fig. 1) of anthraquinones for bioactivity. For once, computational investigations of the theoretical bond dissociation enthalpy (BDE) and density functional theory (DFT) predicted that the 3-OH group of emodin is important for its anti-oxidant role as radical scavenger.[122] They also confirm the preferred enol over the keto conformation of emodin due to stabilization of the π-conjugation. For protein binding it has been shown that the 3-OH is essential for the interaction with the amino acid residues Asp175 and Lys68 within the binding pocket of CK2 facilitating the inactivation of various downstream pathways (Fig. 4).[59]

Furthermore, the substitution of the anthraquinone rings eventually influences pharmacokinetic parameters such as hydrophilicity but also drug metabolization. Pharmacokinetic screenings of anthraquinones revealed several drug modifications *in vitro* and *in vivo*.[123,124] Especially emodin gets rapidly glucuronidated in intestinal and liver microsomes of humans and rats at C3 position, fitting to the scheme of glucuronidation of anthraquinones containing β-oriented hydroxy groups by UDP-glucuronosyltransferases of the 2B2 subfamily.[124] In contrast to the aglycone parent emodin, glucuronidated emodin is the main bioactive compound in ROS scavenging.[125] On the other hand, glycosylation of the rings abolished bioactive effects like radical scavenging, inhibition of cell proliferation, inflammatory cytokine production and Ca^{2+} mobilization.[126] It remains to be determined if the parent anthraquinones or their respective glucuronidated derivatives mediate the modulation of autophagy.

In our screening for anthraquinones with modulating effect on autophagy, we identified 1′-deoxyrhodoptilometrin, 1′-deoxyrhodoptilometrin-6-O-sulfate, emodin, altersolanol A, skyrin and biemodin as anti-autophagic in amino acid starvation-induced autophagy (Fig. 3). SAR studies revealed an importance of the *ortho*-hydroxylation of C1 and C8, and the presence of an oxygen atom at C3 (even if sulfated as in the case of 1′-deoxyrhodoptilometrin-6-O-sulfate). Furthermore, an additional hydroxy-containing moiety at C6 completely abolished the effect as in the case of (S)–(–)–rhodoptilometrin. The positions C1, C3 and C8 seem to be involved in the target-binding ability of hydroxy-anthraquinones, scavenging effects and their effect

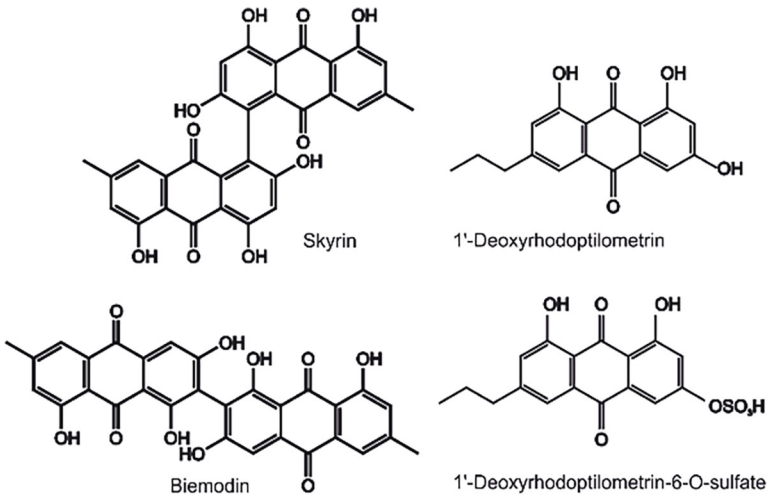

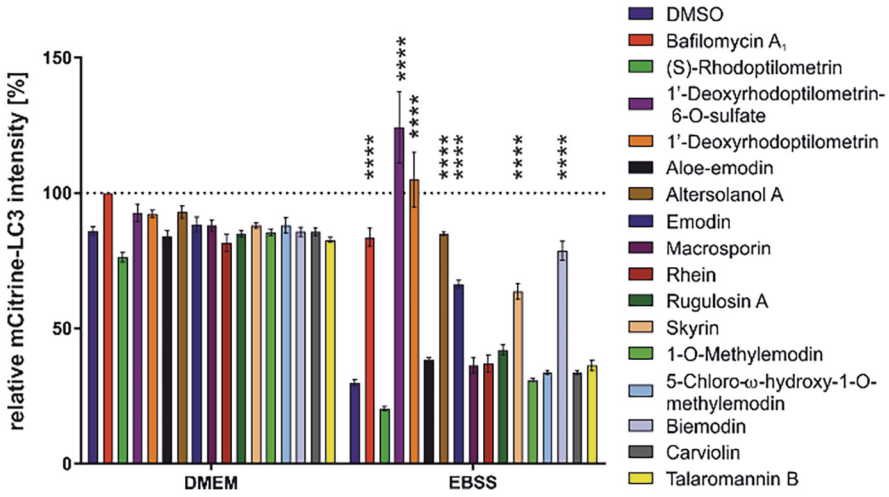

Fig. 3. Inhibitory effect of the anthraquinone derivatives 1′-deoxyrhodoptilometrin-6-O-sulfate, 1′-deoxyrhodoptilometrin, altersolanol A, emodin, skyrin and biemodin on starvation-induced autophagy. Mouse embryonic fibroblasts expressing mCitrine-LC3 were treated with 10 μM of indicated anthraquinone derivatives in either full medium (DMEM) or starvation medium (EBSS) for 6 h in biological triplicates. Fluorescence intensity of mCitrine-LC3 was measured via flow cytometry and normalized to complete inhibition of basal autophagy in full medium (DMEM + bafilomycin A_1). Low mCitrine-LC3B fluorescence intensity correlates to increased autophagy and vice versa. Statistical analysis was performed by a two-way ANOVA plus Dunnett's multiple comparisons post-hoc analysis of $n = 3$ with $\alpha = 0.05$. ****P value < 0.0001 treatment versus DMSO control. Error bars represent SEM.

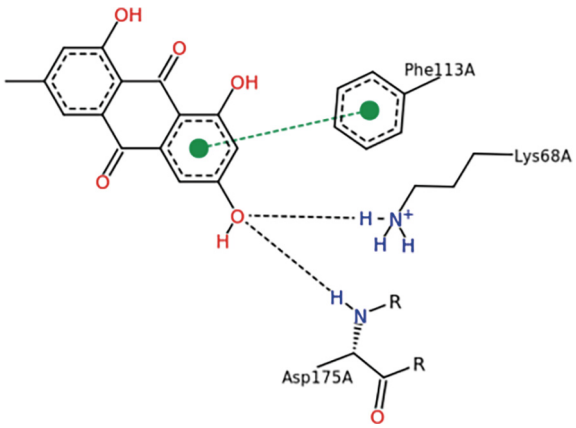

Fig. 4. 2D diagram of amino acid residues facilitating binding of emodin within CK2 binding pocket. PDB ID: 3BQC.[59]

on autophagy modulation. Therefore the modulation of autophagy by anthraquinone treatment might depend on their radical scavenging or ROS producing function in addition to specifically targeted pathways.

11. Conclusion

There is a great potential of pleiotropic cytotoxic compounds in the treatment of cancer as their advantages are usually a rapid induction of cell death due to the modulation of various pathways at once, and a lesser chance of cancer therapy resistance. As in the case of altersolanol A, a high specificity towards cancer cells indicates that these compounds target pathways that are upregulated in cancer. With further research on the structure activity relationships of anthraquinone derivatives it might be possible not only to use natural anthraquinones but also to synthesize custom-designed compounds based on the three rings, two keto-groups core structure of anthraquinones to specifically target relevant pathways.

Pro-/anti-apoptotic and pro-/anti-autophagic effects of all anthraquinones seem to be dependent on various factors such as cellular model system, parallel stimulation of pathways, concentration of compounds, administration form and incubation times. Each compound seems to have its own fingerprint-like mode of action in different cell types. A possible scenario for the observed pleiotropic effects on autophagy might be an early induction of autophagy via the inhibition of the PI3K/AKT/mTOR pathway or the formation of ROS. Further toxic exposition to the anthraquinone stimulus might push the intracellular homeostasis over a tipping point inducing apoptosis and simultaneously inhibiting autophagy.

The core characteristics—three rings, two *para*-keto groups, and hydroxylation of positions C1, C3 and C8—appear to be necessary for the bioactivity of anthraquinones and their "ruling" of various pathways. Keeping in mind a possible importance for glucuronidated metabolites of anthraquinones, a fourth ring might be necessary to rule at least some involved pathways.

Acknowledgments

We thank Michelle Klein for the technical support in the analysis of cell death mediated by altersolanol A. We thank the Deutsche Forschungsgemeinschaft (DFG, German Research Foundation) for financial support of the projects 315775584/STO 864/5-1 (to BS) and 270650915/GRK 2158 (subproject 1c to PP and subproject 3b to BS).

Dedication

JD and BS would like to dedicate this review article to our co-author and colleague Peter Proksch. Peter introduced us to natural compounds and wholeheartedly supports our interdisciplinary approaches in order to understand the cell biological effects of natural compounds.

References

1. Mathew R, Karantza-Wadsworth V, White E. *Chapter 4 assessing metabolic stress and autophagy status in epithelial tumors, autophagy*. Amsterdam: Elsevier Acad. Press; 2009:53–81.
2. Sui X, Chen R, Wang Z, et al. Autophagy and chemotherapy resistance: a promising therapeutic target for cancer treatment. *Cell Death Dis.* 2013;4:e838.
3. Scarlatti F, Maffei R, Beau I, Codogno P, Ghidoni R. Role of non-canonical Beclin 1-independent autophagy in cell death induced by resveratrol in human breast cancer cells. *Cell Death Differ.* 2008;15:1318–1329.
4. Shimizu S, Kanaseki T, Mizushima N, et al. Role of Bcl-2 family proteins in a non-apoptotic programmed cell death dependent on autophagy genes. *Nat Cell Biol.* 2004;6:1221–1228.
5. Yang S. *The divine farmer's materia medica: a translation of the Shen Nong Ben Cao Jing*. Blue Poppy Enterprises, Inc; 1998.
6. Cai Y, Sun M, Xing J, Corke H. Antioxidant phenolic constituents in roots of Rheum officinale and Rubia cordifolia: structure-radical scavenging activity relationships. *J Agric Food Chem.* 2004;52:7884–7890.
7. Dave H, Ledwani L. A review on anthraquinones isolated from Cassia species and their applications. 0976-0512. 2012.
8. Zhang X, Ding J, Gou C, et al. Qingchangligan formula attenuates the inflammatory response to protect the liver from acute failure induced by d-galactosamine/lipopolysaccharide in mice. *J Ethnopharmacol.* 2017;201:108–116.
9. Barnard DL, Huffman JH, Morris JLB, Wood SG, Hughes BG, Sidwell RW. Evaluation of the antiviral activity of anthraquinones, anthrones and anthraquinone derivatives against human cytomegalovirus. *Antiviral Res.* 1992;17:63–77.
10. Chukwujekwu JC, Coombes PH, Mulholland DA, van Staden J. Emodin, an antibacterial anthraquinone from the roots of Cassia occidentalis. *S Afr J Bot.* 2006;72:295–297.
11. Chen Y-C, Shen S-C, Lee W-R, et al. Emodin induces apoptosis in human promyeloleukemic HL-60 cells accompanied by activation of caspase 3 cascade but independent of reactive oxygen species production. *Biochem Pharmacol.* 2002;64:1713–1724.
12. Shieh D-E, Chen Y-Y, Yen M-H, Chiang L-C, Lin C-C. Emodin-induced apoptosis through p53-dependent pathway in human hepatoma cells. *Life Sci.* 2004;74:2279–2290.
13. Wang Y, Luo Q, He X, et al. Emodin induces apoptosis of colon cancer cells via induction of autophagy in a ROS-dependent manner. *Oncol Res.* 2018;26:889–899.
14. Yen G. Antioxidant activity of anthraquinones and anthrone. *Food Chem.* 2000;70:437–441.
15. Su Y-T, Chang H-L, Shyue S-K, Hsu S-L. Emodin induces apoptosis in human lung adenocarcinoma cells through a reactive oxygen species-dependent mitochondrial signaling pathway. *Biochem Pharmacol.* 2005;70:229–241.
16. Lin H-D, Li K-T, Duan Q-Q, et al. The effect of aloe-emodin-induced photodynamic activity on the apoptosis of human gastric cancer cells: a pilot study. *Oncology Letters.* 2017;13:3431–3436.
17. Tu P, Huang Q, Ou Y, et al. Aloe-emodin-mediated photodynamic therapy induces autophagy and apoptosis in human osteosarcoma cell line MG-63 through the ROS/JNK signaling pathway. *Oncol Rep.* 2016;35:3209–3215.
18. Aviello G, Rowland I, Gill CI, et al. Anti-proliferative effect of rhein, an anthraquinone isolated from Cassia species, on Caco-2 human adenocarcinoma cells. *J Cell Mol Med.* 2010;14:2006–2014.
19. Huang Q, Lu G, Shen H-M, Chung MCM, Ong CN. Anti-cancer properties of anthraquinones from rhubarb. *Med Res Rev.* 2007;27:609–630.
20. Pecere T, Gazzola MV, Mucignat C, et al. Aloe-emodin is a new type of anticancer agent with selective activity against neuroectodermal tumors. *Cancer Res.* 2000;60:2800–2804.
21. Convertino M, Pellarin R, Catto M, Carotti A, Caflisch A. 9,10-Anthraquinone hinders beta-aggregation: how does a small molecule interfere with Abeta-peptide amyloid fibrillation? *Protein Sci: A Publ Protein Soc.* 2009;18:792–800.
22. Savarino L, Fioravanti A, Leo G, Aloisi R, Mian M. Anthraquinone-2,6-Disulfonic Acid as a Disease-modifying Osteoarthritis Drug. *Clin Orthop Relat Res.* 2007;PAP..
23. Souza Alves CCD, Collison A, Hatchwell L, et al. Inhibiting AKT phosphorylation employing non-cytotoxic anthraquinones ameliorates TH2 mediated allergic airways disease and rhinovirus exacerbation. *PloS One.* 2013;8:e79565.
24. Xiong H-R, Luo J, Hou W, Xiao H, Yang Z-Q. The effect of emodin, an anthraquinone derivative extracted from the roots of Rheum tanguticum, against herpes simplex virus in vitro and in vivo. *J Ethnopharmacol.* 2011;133:718–723.
25. Tekirdag K, Cuervo AM. Chaperone-mediated autophagy and endosomal microautophagy: Joint by a chaperone. *J Biol Chem.* 2018;293:5414–5424.
26. Bach M, Larance M, James DE, Ramm G. The serine/threonine kinase ULK1 is a target of multiple phosphorylation events. *Biochem J.* 2011;440:283–291.
27. Egan DF, Shackelford DB, Mihaylova MM, et al. Phosphorylation of ULK1 (hATG1) by AMP-activated protein kinase connects energy sensing to mitophagy. *Science (New York, N.Y.).* 2010;331:456–461.
28. Kim J, Kundu M, Viollet B, Guan K-L. AMPK and mTOR regulate autophagy through direct phosphorylation of Ulk1. *Nat Cell Biol.* 2011;13:132–141.
29. Mack HID, Zheng B, Asara JM, Thomas SM. AMPK-dependent phosphorylation of ULK1 regulates ATG9 localization. *Autophagy.* 2012;8:1197–1214.
30. Shang L, Chen S, Du F, Li S, Zhao L, Wang X. Nutrient starvation elicits an acute autophagic response mediated by Ulk1 dephosphorylation and its subsequent dissociation from AMPK. *PNAS.* 2011;108:4788–4793.
31. Hindupur SK, González A, Hall MN. The Opposing Actions of Target of Rapamycin and AMP-Activated Protein Kinase in Cell Growth Control. *Cold Spring Harbor Perspect Biol.* 2015;7.
32. Mercer TJ, Gubas A, Tooze SA. A molecular perspective of mammalian autophagosome biogenesis. *J Biol Chem.* 2018;293:5386–5395.
33. Funderburk SF, Wang QJ, Yue Z. The Beclin 1-VPS34 complex–at the crossroads of autophagy and beyond. *Trends Cell Biol.* 2010;20:355–362.
34. Itakura E, Mizushima N. Characterization of autophagosome formation site by a hierarchical analysis of mammalian Atg proteins. *Autophagy.* 2010;6:764–776.
35. Tanida I, Ueno T, Kominami E. LC3 conjugation system in mammalian autophagy. *Int J Biochem Cell Biol.* 2004;36:2503–2518.
36. He C, Klionsky DJ. Regulation mechanisms and signaling pathways of autophagy. *Annu Rev Genet.* 2009;43:67–93.
37. Sharma V, Verma S, Seranova E, Sarkar S, Kumar D. Selective autophagy and xenophagy in infection and disease. *Front Cell Dev Biol.* 2018;6:147.
38. Klionsky DJ, Abdelmohsen K, Abe A, et al. Guidelines for the use and interpretation of assays for monitoring autophagy (3rd edition). *Autophagy.* 2016;12:1–222.
39. Mizushima N, Yoshimori T. How to Interpret LC3 Immunoblotting. *Autophagy.* 2007;3:542–545.
40. Gao Q, Wang F, Guo S, et al. Sonodynamic effect of an anti-inflammatory agent–emodin on macrophages. *Ultrasound Med Biol.* 2011;37:1478–1485.
41. Chang CH, Lin CC, Yang JJ, Namba T, Hattori M. Anti-inflammatory effects of emodin from ventilago leiocarpa. *Am J Chin Med.* 1996;24:139–142.
42. Wang X, Zou Y, Sun A, et al. Emodin induces growth arrest and death of human vascular smooth muscle cells through reactive oxygen species and p53. *J Cardiovasc Pharmacol.* 2007;49:253–260.
43. Kwak H-J, Park M-J, Park C-M, et al. Emodin inhibits vascular endothelial growth factor-A-induced angiogenesis by blocking receptor-2 (KDR/Flk-1) phosphorylation. *Int J Cancer.* 2006;118:2711–2720.
44. Wei W-T, Lin S-Z, Liu D-L, Wang Z-H. The distinct mechanisms of the antitumor activity of emodin in different types of cancer (Review). *Oncol Rep.* 2013;30:2555–2562.
45. Chan TC, Chang CJ, Koonchanok NM, Geahlen RL. Selective inhibition of the growth of ras-transformed human bronchial epithelial cells by emodin, a protein-tyrosine kinase inhibitor. *Biochem Biophys Res Commun.* 1993;193:1152–1158.
46. Monisha BA, Kumar N, Tiku AB. Emodin and its role in chronic diseases. *Adv Exp Med Biol.* 2016;928:47–73.
47. Trocoli A, Djavaheri-Mergny M. The complex interplay between autophagy and NF-κB signaling pathways in cancer cells. *Am J Cancer Res.* 2011;1:629–649.
48. Dan HC, Baldwin AS. Differential involvement of I B kinases and in cytokine- and insulin-induced mammalian target of rapamycin activation determined by Akt. *J Immunol.* 2008;180:7582–7589.
49. Dan HC, Cooper MJ, Cogswell PC, Duncan JA, Ting JP-Y, Baldwin AS. Akt-dependent regulation of NF-κB is controlled by mTOR and Raptor in association with IKK. *Genes Dev.* 2008;22:1490–1500.
50. Lee D-F, Kuo H-P, Chen C-T, et al. IKK beta suppression of TSC1 links inflammation and tumor angiogenesis via the mTOR pathway. *Cell.* 2007;130:440–455.
51. Copetti T, Bertoli C, Dalla E, Demarchi F, Schneider C. p65/RelA modulates BECN1 transcription and autophagy. *Mol Cell Biol.* 2009;29:2594–2608.
52. Chen D, Liu J, Lu L, et al. Emodin attenuates TNF-α-induced apoptosis and autophagy in mouse C2C12 myoblasts though the phosphorylation of Akt. *Int Immunopharmacol.* 2016;34:107–113.
53. Olsen BB, Bjørling-Poulsen M, Guerra B. Emodin negatively affects the phosphoinositide 3-kinase/AKT signalling pathway: a study on its mechanism of action. *Int J Biochem Cell Biol.* 2007;39:227–237.
54. Cheema SK, Gobin AS, Rhea R, Lopez-Berestein G, Newman RA, Mathur AB. Silk fibroin mediated delivery of liposomal emodin to breast cancer cells. *Int J Pharm.* 2007;341:221–229.
55. Janeczko M, Masłyk M, Kubiński K, Golczyk H. Emodin, a natural inhibitor of protein kinase CK2, suppresses growth, hyphal development, and biofilm formation of Candida albicans. *Yeast (Chichester, England).* 2017;34:253–265.
56. Yim H, Lee YH, Lee CH, Lee SK. Emodin, an anthraquinone derivative isolated from the rhizomes of Rheum palmatum, selectively inhibits the activity of casein kinase II as a competitive inhibitor. *Planta Med.* 1999;65:9–13.
57. Hwang DW, So KS, Kim SC, et al. Autophagy Induced by CX-4945, a Casein Kinase 2 Inhibitor, Enhances Apoptosis in Pancreatic Cancer Cell Lines. *Pancreas.* 2017;46:575–581.
58. Mazzorana M, Pinna LA, Battistutta R. A structural insight into CK2 inhibition. *Mol Cell Biochem.* 2008;316:57–62.
59. Raaf J, Klopffleisch K, Issinger O-G, Niefind K, High pH-value crystal structure of emodin in complex with the catalytic subunit of protein kinase CK2, 2008.
60. Sarno S, Moro S, Meggio F, et al. Toward the rational design of protein kinase casein

kinase-2 inhibitors. *Pharmacol Ther.* 2002;93:159–168.
61. Sarno S, Moliner ED, Ruzzene M, et al. Biochemical and three-dimensional-structural study of the specific inhibition of protein kinase CK2 by 5-oxo-5,6-dihydroindolo-(1,2-a)quinazolin-7-ylacetic acid (IQA). *Biochem J.* 2003;374:639–646.
62. Liu W, Wang X, Liu Z, et al. SGK1 inhibition induces autophagy-dependent apoptosis via the mTOR-Foxo3a pathway. *Br J Cancer.* 2017;117:1139–1153.
63. Liu H, Gu L-b, Tu Y, Hu H. Huang Y-r, Sun W. Emodin ameliorates cisplatin-induced apoptosis of rat renal tubular cells in vitro by activating autophagy. *Acta Pharmacol Sin.* 2016;37:235–245.
64. Zheng H-y, Hu J-d, Zheng Z-h, et al. Emodin induces leukemic HL-60 cells apoptosis probably by inhibiting Akt signal pathway. *Yao xue xue bao = Acta pharmaceutica Sinica.* 2007;42:1142–1146.
65. Li X, Liu W, Wang Q, et al. Emodin suppresses cell proliferation and fibronectin expression via p38MAPK pathway in rat mesangial cells cultured under high glucose. *Mol Cell Endocrinol.* 2009;307:157–162.
66. Trybus W, Król T, Trybus E, Kopacz-Bednarska A, Król G, Karpowicz E. Changes in the Lysosomal System of Cervical Cancer Cells Induced by Emodin Action. *Anticancer Res.* 2017;37:6087–6096.
67. Wang Y, Yu H, Zhang J, et al. Anti-tumor effect of emodin on gynecological cancer cells. *Cell Oncol (Dordrecht).* 2015;38:353–363.
68. Wirawan E, Vande Walle L, Kersse K, et al. Caspase-mediated cleavage of Beclin-1 inactivates Beclin-1-induced autophagy and enhances apoptosis by promoting the release of proapoptotic factors from mitochondria. *Cell Death Dis.* 2010;1:e18-.
69. Yu X, Li C, Song H, et al. Emodin attenuates autophagy response to protect the pancreas from acute pancreatitis failure. *Pancreas.* 2018;47:892–897.
70. Hu H, Sun W, Gu L-b, Tu Y, Liu H. Molecular mechanism of emodin on inhibiting autophagy induced by HBSS in renal tubular cells. *China J Chin Mater Med.* 2015;40:1965–1970.
71. Huang X-z, Wang J, Huang C, et al. Emodin enhances cytotoxicity of chemotherapeutic drugs in prostate cancer cells: The mechanisms involve ROS-mediated suppression of multidrug resistance and hypoxia inducible factor-1. *Cancer Biol Ther.* 2008;7:468–475.
72. Ravi R, Bedi A. Sensitization of tumor cells to Apo2 ligand/TRAIL-induced apoptosis by inhibition of casein kinase II. *Cancer Res.* 2002;62:4180–4185.
73. Subramaniam A, Loo SY, Rajendran P, et al. An anthraquinone derivative, emodin sensitizes hepatocellular carcinoma cells to TRAIL induced apoptosis through the induction of death receptors and downregulation of cell survival proteins. *Apoptosis: An Int J Programmed Cell Death.* 2013;18:1175–1187.
74. Wang XJ, Yang J, Cang H, Zou YQ, Yi J. Gene expression alteration during redox-dependent enhancement of arsenic cytotoxicity by emodin in HeLa cells. *Cell Res.* 2005;15:511–522.
75. Yang J, Li H, Chen Y-y, et al. Anthraquinones sensitize tumor cells to arsenic cytotoxicity in vitro and in vivo via reactive oxygen species-mediated dual regulation of apoptosis. *Free Radical Biol Med.* 2004;37:2027–2041.
76. Ma J, Yang J, Wang C, et al. Emodin augments cisplatin cytotoxicity in platinum-resistant ovarian cancer cells via ROS-dependent MRP1 downregulation. *Biomed Res Int.* 2014;2014:107671.
77. Zheng Y, Ha X, Wang Y, Wang J, Gao C. Emodin in hypoxic intestinal stress damage and the protection of autophagy. *J Shaanxi Univ Sci Technol (Nat Sci Ed).* 2015:134–138.
78. Dou F, Ding Y, Yao M-n, et al. Effect of emodin on fibrosis factor of HK-2 cells stimulated by TGF-β1 through activation of autophagy. *Chin Pharmacol Bull.* 2018;34:1555–1559.
79. Li L, Puji.. Effect of emodin on autophagic apoptosis of colon cancer cells and its mechanism. *Huaxi Pharm J.* 2017:15.
80. Fenig E, Nordenberg J, Beery E, Sulkes J, Wasserman L. Combined effect of aloe-emodin and chemotherapeutic agents on the proliferation of an adherent variant cell line of Merkel cell carcinoma. *Oncol Rep.* 2004.
81. Shi YQ, Fukai T, Sakagami H, et al. Cytotoxic and DNA damage-inducing activities of low molecular weight phenols from rhubarb. *Anticancer Res.* 2001;21:2847–2853.
82. Harhaji L, Mijatovic S, Maksimovic-Ivanic D, et al. Aloe emodin inhibits the cytotoxic action of tumor necrosis factor. *Eur J Pharmacol.* 2007;568:248–259.
83. Mijatovic S, Maksimovic-Ivanic D, Radovic J, et al. Aloe-emodin prevents cytokine-induced tumor cell death: the inhibition of auto-toxic nitric oxide release as a potential mechanism. *Cell Mol Life Sci: CMLS.* 2004;61:1805–1815.
84. Khan IA, Nasiruddin M, Haque SF, Khan RA. Evaluation of rhubarb supplementation in stages 3 and 4 of chronic kidney disease: a randomized clinical trial. *Int J Chron Dis.* 2014;2014:789340.
85. He D, Lee L, Yang J, Wang X. Preventive effects and mechanisms of rhein on renal interstitial fibrosis in obstructive nephropathy. *Biol Pharm Bull.* 2011;34:1219–1226.
86. Tu Y, Gu L, Chen D, et al. Rhein Inhibits Autophagy in Rat Renal Tubular Cells by Regulation of AMPK/mTOR Signaling. *Sci Rep.* 2017;7:43790.
87. Tang N, Chang J, Lu H-C, et al. Rhein induces apoptosis and autophagy in human and rat glioma cells and mediates cell differentiation by ERK inhibition. *Microb Pathog.* 2017;113:168–175.
88. Lin S, Li J-J, Fujii M, Hou D-X. Rhein inhibits TPA-induced activator protein-1 activation and cell transformation by blocking the JNK-dependent pathway. *Int J Oncol.* 2003.
89. Tu Y, Sun W, Gu L-b, Wan Y-G, Hu H, Liu H. Molecular mechanism of rhein on inhibiting autophagic protein expression in renal tubular epithelial cells via regulating mTOR signaling pathway activation. *Zhongguo zhongyao zazhi = China J Chin Mater Med.* 2014;39:4090–4095.
90. Fernand VE, Losso JN, Truax RE, et al. Rhein inhibits angiogenesis and the viability of hormone-dependent and -independent cancer cells under normoxic or hypoxic conditions in vitro. *Chem Biol Interact.* 2011;192:220–232.
91. Joo JH, Dorsey FC, Joshi A, et al. Hsp90-Cdc37 chaperone complex regulates Ulk1- and Atg13-mediated mitophagy. *Mol Cell.* 2011;43:572–585.
92. Xu C, Liu J, Hsu L-C, Luo Y, Xiang R, Chuang T-H. Functional interaction of heat shock protein 90 and Beclin 1 modulates Toll-like receptor-mediated autophagy. *FASEB J: Official Publ Fed Am Soc Exp Biol.* 2011;25:2700–2710.
93. Kang SC, Lee CM, Choung ES, et al. Anti-proliferative effects of estrogen receptor-modulating compounds isolated from Rheum palmatum. *Arch Pharmacal Res.* 2008;31:722–726.
94. Ueno Y, Umemori K, Niimi E-C, et al. Induction of apoptosis by T-2 toxin and other natural toxins in HL-60 human promyelotic leukemia cells. *Nat Toxins.* 1995;3:129–137.
95. Lu C-C, Yang J-S, Huang A-C, et al. Chrysophanol induces necrosis through the production of ROS and alteration of ATP levels in J5 human liver cancer cells. *Mol Nutr Food Res.* 2010;54:967–976.
96. Ni C-H, Yu C-S, Lu H-F, et al. Chrysophanol-induced cell death (necrosis) in human lung cancer A549 cells is mediated through increasing reactive oxygen species and decreasing the level of mitochondrial membrane potential. *Environ Toxicol.* 2014;29:740–749.
97. Kamil M, Haque E, Mir SS, et al. Hydroxyl group difference between anthraquinone derivatives regulate different cell death pathways via nucleo-cytoplasmic shuttling of p53. *Anti-Cancer Agents Med Chem.* 2018.
98. Chauhan S, Ahmed Z, Bradfute SB, et al. Pharmaceutical screen identifies novel target processes for activation of autophagy with a broad translational potential. *Nat Commun.* 2015;6:8620.
99. Lee MS, Cha EY, Sul JY, Song IS, Kim JY. Chrysophanic acid blocks proliferation of colon cancer cells by inhibiting EGFR/mTOR pathway. *Phytotherapy Res: PTR.* 2011;25:833–837.
100. Pan X, Wang C, Li Y, Zhu L, Zhang T. Protective autophagy induced by physcion suppresses hepatocellular carcinoma cell metastasis by inactivating the JAK2/STAT3 Axis. *Life Sci.* 2018;214:124–135.
101. Pang M-J, Yang Z, Zhang X-L, Liu Z-F, Fan J, Zhang H-Y. Physcion, a naturally occurring anthraquinone derivative, induces apoptosis and autophagy in human nasopharyngeal carcinoma. *Acta Pharmacol Sin.* 2016;37:1623–1640.
102. You L, Wang Z, Li H, et al. The role of STAT3 in autophagy. *Autophagy.* 2015;11:729–739.
103. Feng Y, Ke C, Tang Q, et al. Metformin promotes autophagy and apoptosis in esophageal squamous cell carcinoma by downregulating Stat3 signaling. *Cell Death Dis.* 2014;5:e1088.
104. Miao L-J, Huang F-X, Sun Z-T, Zhang R-X, Huang S-F, Wang J. Stat3 inhibits Beclin 1 expression through recruitment of HDAC3 in nonsmall cell lung cancer cells. *Tumour Biol: J Int Soc Oncodevelopmental Biol Med.* 2014;35:7097–7103.
105. Yamada E, Bastie CC, Koga H, Wang Y, Cuervo AM, Pessin JE. Mouse skeletal muscle fiber-type-specific macroautophagy and muscle wasting are regulated by a Fyn/STAT3/Vps34 signaling pathway. *Cell Reports.* 2012;1:557–569.
106. Mishra PD, Verekar SA, Deshmukh SK, Joshi KS, Fiebig HH, Kelter G. Altersolanol A: a selective cytotoxic anthraquinone from a Phomopsis sp. *Lett Appl Microbiol.* 2015;60:387–391.
107. Teiten M-H, Mack F, Debbab A, et al. Anticancer effect of altersolanol A, a metabolite produced by the endophytic fungus Stemphylium globuliferum, mediated by its pro-apoptotic and anti-invasive potential via the inhibition of NF-κB activity. *Bioorg Med Chem.* 2013;21:3850–3858.
108. Aly AH, Debbab A, Kjer J, Proksch P. Fungal endophytes from higher plants: a prolific source of phytochemicals and other bioactive natural products. *Fungal Diversity.* 2010;41:1–16.
109. Debbab A, Aly AH, Edrada-Ebel R, et al. Bioactive metabolites from the endophytic fungus Stemphylium globuliferum isolated from Mentha pulegium. *J Nat Prod.* 2009;72:626–631.
110. Debbab A, Ebel R, Edrada R, Wray V, Kubbutat MHG, Proksch P. Protein kinase inhibitors from the endophytic fungus Stemphylium globuliferum. *Planta Med.* 2009;75.
111. Aly AH, Edrada-Ebel R, Wray V, et al. Bioactive metabolites from the endophytic fungus Ampelomyces sp. isolated from the medicinal plant Urospermum picroides. *Phytochemistry.* 2008;69:1716–1725.
112. Gurusamy N, Lekli I, Gherghiceanu M, Popescu LM, Das DK. BAG-1 induces autophagy for cardiac cell survival. *Autophagy.* 2009;5:120–121.
113. Galluzzi L, Bravo-San Pedro JM, Vitale I, et al. Essential versus accessory aspects of cell death: recommendations of the NCCD 2015. *Cell Death Differ.* 2015;22:58–73.
114. Marino G, Niso-Santano M, Baehrecke EH, Kroemer G. Self-consumption: the interplay of autophagy and apoptosis. *Nat Rev Mol Cell Biol.* 2014;15:81–94.
115. Cooper KF. Till Death Do Us Part: The Marriage of Autophagy and Apoptosis. *Oxid Med Cell Longev.* 2018;2018:4701275.
116. Scherz-Shouval R, Shvets E, Fass E, Shorer H, Gil L, Elazar Z. Reactive oxygen species are essential for autophagy and specifically regulate the activity of Atg4. *EMBO J.* 2007;26:1749–1760.
117. Song P, Kim JH, Ghim J, et al. Emodin regulates glucose utilization by activating AMP-activated protein kinase. *J Biol Chem.* 2013;288:5732–5742.
118. Zhou X, Cao Y, Ao G, et al. CaMKKβ-dependent activation of AMP-activated protein kinase is critical to suppressive effects of hydrogen sulfide on neuroinflammation. *Antioxid Redox Signal.* 2014;21:1741–1758.
119. Huang X, Wu Z, Mei Y, Wu M. XIAP inhibits autophagy via XIAP-Mdm2-p53 signalling. *The EMBO journal.* 2013;32:2204–2216.
120. Kamei H, Koide T, Kojima T, Hashimoto Y, Hasegawa M. Inhibition of cell growth in culture by quinones. *Cancer Biother Radiopharm.* 1998;13:185–188.
121. Cai Y-Z, Mei S, Jie X, Luo Q, Corke H. Structure-radical scavenging activity relationships of phenolic compounds from traditional Chinese medicinal plants. *Life Sci.* 2006;78:2872–2888.

122. Marković ZS, Manojlović NT. DFT study on the reactivity of OH groups in emodin: structural and electronic features of emodin radicals. *Monatshefte für Chemie - Chemical Monthly*. 2009;140:1311–1318.
123. Teng Z-H, Zhou S-Y, Yang R-T, et al. Quantitation assay for absorption and first-pass metabolism of emodin in isolated rat small intestine using liquid chromatography-tandem mass spectrometry. *Biol Pharm Bull*. 2007;30:1628–1633.
124. Wu W, Hu N, Zhang Q, et al. In vitro glucuronidation of five rhubarb anthraquinones by intestinal and liver microsomes from humans and rats. *Chem Biol Interact*. 2014;219:18–27.
125. Shia C-S, Hou Y-C, Tsai S-Y, Huieh P-H, Leu Y-L, Chao P-DL. Differences in pharmacokinetics and ex vivo antioxidant activity following intravenous and oral administrations of emodin to rats. *J Pharm Sci*. 2010;99:2185–2195.
126. Kuo YC, Meng HC, Tsai WJ. Regulation of cell proliferation, inflammatory cytokine production and calcium mobilization in primary human T lymphocytes by emodin from Polygonum hypoleucum Ohwi. *Inflammation Research*. 2001;50:73–82.

Publication 3

High-throughput screening for natural compound-based autophagy modulators reveals novel chemotherapeutic mode of action for arzanol

Jana Deitersen, Fabian Stuhldreier, Sara Ceccacci, David Schlütermann, Lena Berning, Wenxian Wu, Yadong Sun, Niklas Berleth, Maria José Mendiburo, Sabine Seggewiß, Maria Chiara Monti, Peter Proksch, Björn Stork

Manuscript in preparation.

High-throughput screening for natural compound-based autophagy modulators reveals novel chemotherapeutic mode of action for arzanol

Jana Deitersen[1], Fabian Stuhldreier[1], Sara Ceccacci[2], David Schlütermann[1], Lena Berning[1], Wenxian Wu[1], Yadong Sun[1], Niklas Berleth[1], Maria José Mendiburo[1], Sabine Seggewiß[1], Maria Chiara Monti[2], Peter Proksch[3], Björn Stork[1,*]

[1]Institute of Molecular Medicine I, Medical Faculty, Heinrich Heine University, Universitätsstraße 1, 40225 Düsseldorf, Germany

[2]Department of Pharmacy, University of Salerno, Via Giovanni Paolo II 132, Salerno, Italy

[3]Institute of Pharmaceutical Biology and Biotechnology, Faculty of Mathematics and Natural Sciences, Heinrich Heine University, Universitätsstraße 1, 40225 Düsseldorf, Germany

*Correspondence: bjoern.stork@hhu.de

RUNNING TITLE: Mode of action of arzanol

KEYWORDS: arzanol, autophagy, natural compounds, chemotherapy, mitochondria

Abstract

Autophagy is an intracellular recycling pathway with implications for intracellular homeostasis and cell survival. Its pharmacological modulation can aid chemotherapy by sensitizing cancer cells towards approved drugs and overcoming chemoresistance. Recent translational data on autophagy modulators show promising results in reducing tumor growth and metastasis, but also reveal a need for more specific compounds and novel lead structures. Here, we searched for such autophagy-modulating compounds in a microtubule-associated proteins 1A/1B light chain 3B (LC3)-based high-throughput screening of an in-house natural compound library. We successfully identified novel inducers and inhibitors of the autophagic pathway. Among these, we identified arzanol as autophagy-modulating drug that is able to sensitize RT-112 bladder cancer cells towards cisplatin (CDDP). Its anticancer activity was further confirmed in monotherapy against both CDDP-sensitive and -resistant bladder cancer cells. We determine arzanol as novel mitotoxin, inducing the fragmentation of mitochondrial membranes, and identified a series of new targets for arzanol that involve proteins of the class of mitochondria-associated quinone-binding oxidoreductases. Using fluorescence microscopy, we show that arzanol further causes the accumulation of ATG16L1-positive structures, while it also induces the accumulation of lipidated LC3. Surprisingly, we observed a reduction of the size of autophagosomes compared to the bafilomycin control and a pronounced accumulation of p62/SQSTM1 in response to arzanol treatment in HeLa cells. We therefore speculate that arzanol acts both as inducer of early autophagosome biogenesis and as inhibitor of later autophagy events. Collectively, our results suggest arzanol as valuable tool for autophagy research and cancer therapy.

Introduction

As of today, the discovery of approved anticancer drugs falls behind the rapid increase in cancer-related mortality. Cancer drug discovery therefore focusses on repurposing approved and identifying novel bioactive compounds that can serve as lead compounds or clinical drug candidates. Most drugs over the last decades are based on natural compounds[1, 2]. Their advantages lie in the inexhaustible quantity of compounds available in nature, their often non-synthesizable complexity, and a high degree of stereochemistry[3]. They often target evolutionary conserved pathways that play central roles in cell fate-regulating pathways such as apoptosis, necrosis, senescence, or autophagy.

Autophagy is a lysosomal pathway with mainly cytoprotective purpose that plays a role in different human pathologies such as neurodegeneration or cancer[4, 5, 6, 7]. The main characteristic of macroautophagy (henceforth referred to as autophagy) is the sequestration of aggregates, long-lived proteins, or damaged organelles by an autophagosomal membrane and its subsequent fusion with the lysosome for the degradation of bulk or selected cargo. Autophagy is a conserved pathway that is basally active in most cell types, but can also be induced by stimuli like withdrawal of growth factors, nutrient deficiency, hypoxia, aggregates or mitochondrial damage[8, 9, 10]. Dependent on the inducing stimulus, specific autophagy receptors can target and help to eliminate sources of damage such as aggregates in aggrephagy, parts of the ER in ERphagy, bacterial or viral components in xenophagy, isolated damaged mitochondria in mitophagy and many more.

In canonical autophagy, 5' AMP-activated protein kinase (AMPK)-dependent activation and mechanistic/mammalian target of rapamycin (mTOR)-dependent inhibition regulate the autophagy-initiating unc-51-like kinase 1 (ULK1) complex, which consists of ULK1, autophagy-related protein (ATG) 13, ATG101, and RB1-inducible coiled-coil protein 1 (RB1CC1/FIP200). Upon induction of autophagy, the ULK1 complex activates the class III phosphatidylinositol 3-kinase (PIK3C3/VPS34) lipid kinase complex that produces phosphatidylinositol 3-phosphate (PI3P) at subregions of the ER forming so called omegasomes[11]. ATG9A as well as the PI3P-binding proteins DCFP1 and WIPI1/2 are involved in membrane elongation and recruit the ubiquitin-like ATG12—ATG5-ATG16L1 complex, which conjugates phosphatidylethanolamine to LC3[12]. Lipidated LC3 decorates autophagosomal membranes and serves as “anchor” for the recruitment of autophagosomal cargo or downstream autophagy regulators. For instance, LC3 binds p62 (also known as sequestosome 1, SQSTM1), which is an autophagic receptor for ubiquitinated proteins and organelle surfaces[13]. After fusion of autophagosome

and lysosome, lysosomal hydrolases degrade both autophagic cargo and LC3-bound autophagic receptors such as p62/SQSTM1. Accordingly, both proteins serve as markers for autophagic flux.

As intracellular quality control, autophagy ensures cell survival and prevents the accumulation of carcinogenic stimuli in healthy cells. Knockdown or deletion of Beclin 1 and ATG7 promoted tumor development[14, 15]. In line with this, biomarkers for poor prognosis in leukemia are degraded by chaperone-mediated autophagy, suggesting a protective role of autophagy against tumorigenesis[16, 17, 18, 19]. In late stage cancer, on the other hand, autophagy can act tumor-promoting due to its catabolic function, supporting solid tumors in hypoxic regions and enabling the tumor microenvironment to contribute nutrients and growth factors[20, 21, 22, 23, 24]. In these solid tumors, autophagy has been found to contribute to cancer cell survival and poor outcome[25, 26]. Recent attempts in translational cancer research therefore investigate the inhibition of autophagy in both monotherapy and combinational treatment in order to sensitize cancer to chemotherapy[27, 28, 29, 30]. In contrast, inducers of autophagy are also discussed as potential chemotherapeutics, driving cancer cells into the so-called autophagy-associated or autophagic cell death[31, 32, 33, 34, 35].

This work investigates an in-house library of natural compounds in order to find modulators of autophagy, which can be applied as novel chemotherapeutics for monotherapy or combinational therapy. We found that arzanol impairs the viability of bladder cancer cells and investigated its molecular mode of action. We identify arzanol as dual modulator of autophagy, and expand the list of arzanol targets by mitochondria-related oxidoreductases and autophagy-related proteins. Taken together, we propose arzanol as new tool to study autophagic mechanisms and as potential lead structure for combinational chemotherapy with CDDP in urothelial bladder carcinoma cells.

Results

High-throughput Screening Reveals Novel Modulators of Autophagy

To identify novel modulators of autophagy among natural compounds, we screened an in-house library of 300 natural compounds derived from marine sponges and endophytic fungi, using a flow cytometric high-throughput screening (Figure 1). The autophagic flux was measured in live mouse embryonic fibroblasts (MEFs) stably expressing mCitrine-tagged LC3 as a marker. During serum- and amino acid starvation, autophagosome-bound mCitrine-LC3 is quenched by the low lysosomal pH and degraded by lysosomal hydrolases, causing a reduction of the mCitrine-LC3 signal (Figure 1A). Upon treatment with the lysosomal inhibitor bafilomycin A_1 (baf A_1), both basal and starvation-induced autophagic flux is inhibited and the mCitrine-LC3 signal increases (Figure 1A). These data confirm the sensitivity of this assay to identify both inducers and inhibitors of autophagy.

For the classification of inducers and inhibitors, we set the threshold at 15% decrease or increase of the mCitrine-LC3 signal upon treatment with the compounds, in addition to a statistically fairly moderate and higher effect ($|\text{SSMD score}| \geq 1$) (Figure 1; Table 1 and 2; Supplementary Table 1)[36]. In doing so, the screening of MEFs treated with natural compounds in full medium revealed eight potential novel inducers of autophagy (Figure 1B, Table 1) and five potential inhibitors of basal autophagy (Figure 1B). Thereof, we classified the cyclopeptide enniatin A1, the lignans (-)-arctigenin and (-)-matairesinol, and 4,6-dibromo-2-(2',4'-dibromophenoxy)phenol as inducers of autophagy. Beauvericin J, enniatin B1, pergularinin and viriditoxin caused LC3 degradation upon full medium but acted inhibitory during starvation. Aaptamine, stemphyltoxin I, manzamine J N-oxid, secalonic acid F and kuanoniamin D on the other hand inhibit both basal and starvation-induced autophagy.

The screening upon starvation conditions revealed in total 64 potential inhibitors of autophagic flux (Figure 1C, Table 2). In addition to the aforementioned five inhibitors, and four dual modulators (i.e. activating in full medium but inhibitory under starvation), 55 compounds were classified as potential autophagy inhibitors. However, we issue a caveat with two of the potential autophagy inhibitors, stemphyltoxin I and g114, as they display an increased autofluorescence upon excitation with 488 nm (data not shown). Interestingly, (-)-ageloxime D and catechin further enhanced starvation-induced autophagy. Of the 300 tested natural compounds, two thirds did not have a considerate effect on autophagy in our screening (Figure 1D).

Arzanol Intereferes with Late Stage Autophagy

Among the novel modulators of autophagy, we identified the phloroglucinol α-pyrone arzanol (marked as red dots in Figures 1B and 1C), which was isolated from the aerial parts of *Helichrysum italicum*[37]. Arzanol is known for its anti-inflammatory, anti-viral[38], anti-oxidative and cytotoxic effects[39], however no effect on autophagy was reported before. We first validated the accumulation of LC3 in human HeLa cells expressing the GFP-LC3-RFP-LC3ΔG reporter construct by flow cytometry[40] (Figure 2A). To identify the pathway affected by arzanol, we performed immunoblotting analyses of key components of the canonical autophagy pathway along the protein kinase B (AKT)/mTOR/ULK1-axis (Figures 2B and 2C).

Upon growth stimulating signals, such as full medium including serum, AKT phosphorylates tuberous sclerosis complex 2 (TSC2) at Ser939, which destabilizes and inactivates TSC2[41]. Withdrawal of growth factors on the other hand leads to a stabilization of TSC2, which inactivates Ras homolog enriched in brain (RHEB) and thereby inhibits mTOR[42]. Reduced mTOR activity leads to a reduction in phosphorylation of the mTOR target proteins ribosomal protein S6 kinase beta-1 (p70 S6K) at Ser371[43] and ULK1 at Ser758[44]. Hypo-phosphorylation of ULK1 is associated with the dissociation of mTOR from the ULK1 complex, allowing its activation and the initiation of autophagosome formation[45]. During the early biogenesis of autophagosomes, cytosolic LC3-I gets lipidated to autophagosomal membrane-bound LC3-II, which is—along with the autophagy receptor protein p62/SQSTM1—later degraded by lysosomal hydrolases[46].

Checking for these parameters, we observed that arzanol does not inhibit starvation-induced inactivation of mTOR; however, it causes the accumulation of LC3-II and p62 during starvation-induced autophagy (Figures 2C). We also validated these effects using commercially available arzanol and subcloned HeLa cells stably expressing the above-mentioned GFP-LC3-RFP-LC3ΔG construct (Figure 2D). As determined by immunoblotting of HeLa cell lysates, similar to self-isolated arzanol, commercially available arzanol had a minimum effective dose below 3 μM and a maximal effective dose of 5 μM (Figure 2E). Its effect on autophagy is consistent within all our assays (i.e. murine vs. human cells, immunoblotting vs. flow cytometric assays, and self-isolated vs. commercial arzanol). Interestingly, arzanol caused accumulation of LC3-II upon both amino acid and serum starvation as well as serum starvation alone, whereas its effect on p62/SQSTM1 accumulation was more prominent upon amino acid starvation (Figure 2F).

Arzanol Changes ATG16L1 Localization

An increase in LC3 can be indicative of disrupted autophagic degradation or increased protein expression, while an increase in LC3-II can additionally hint to its enhanced lipidation. To determine the circumstances that led to the accumulation of the late stage autophagic markers LC3 and p62/SQSTM1 (Figure 2), we located both overexpressed GFP-LC3 (Figure 3A) and endogenous LC3 (Figure 3B) using fluorescence microscopy and quantified both size and amount of LC3-positive dots that commonly correlate to autophagosomes[47]. A clear trend towards increasing numbers of LC3 dots upon arzanol treatment was observed (Figures 3A and 3B). However, to our surprise, the size of these LC3 dots appeared rather small, making them partly indistinguishable for the quantification software. Nevertheless, we think one can appreciate the increase in number of both overexpressed and endogenous LC3 dots and their significantly smaller size compared to bafilomycin A_1-treated cells (Figures 3A and 3B, i. and ii.). Further, we examined the location, size and amount of ATG16L1, which is a core component of the LC3 lipidation machinery. Arzanol treatment caused a significant increase in ATG16L1-positive structures (Figure 3C, i.), while the total protein level of ATG16L1 remained unaltered (data not shown). These data are in line with increased LC3-II in response to arzanol treatment we described above (Figure 2).

Next, we aimed at investigating, which other components of the autophagic machinery are involved in the response to the treatment with arzanol. Since the PI3P-binding WIPI2b recruits ATG16L1 to PE-containing phagophores during membrane expansion and cargo sequestration[48, 49], which in turn depends on the interaction between ATG13 and ATG101 (components of the ULK1 complex)[50], colocalization studies were used to determine mutual recruitment of these proteins upon arzanol exposure. We observed colocalization of ATG16L1 dots with both WIPI2 (Figure 4A) and ATG13 (Figure 4B) by immunofluorescence microscopy.

Arzanol as anti-Cancer Drug in Mono- and CDDP-Combination Therapy

In addition to monotherapy, combinational therapies of approved drugs with autophagy modulators have been proposed to overcome tumor survival[51, 52, 53].

In order to test the cytotoxic effect of arzanol on cancer cells, we performed MTT assays for 24 h for both arzanol monotherapy and combinational therapy with cisplatin (CDDP) in starved RT-112 urothelial bladder carcinoma cells. The results of the cell viability assay reveal that arzanol is a moderate

chemotherapeutic alone in both normal RT-112 cells and CDDP-resistant cells (IC50: 13.2 µM and 22.6 µM, respectively; Figures 5A and 5B), but also sensitizes bladder cancer cells towards CDDP-treatment (IC50 shift from 20.7 µM to 6.3 µM; Figure 5C). The amount of arzanol used for combinational therapy exacerbated CDDP-induced cytotoxicity and combinational treatment was more successful in reducing cell viability compared to single treatments in CDDP-sensitive bladder carcinoma cells (Figure 5D).

Surprisingly, for CDDP-resistant cells the treatment with low amounts of arzanol resulted in an increased reduction of MTT, but a decreased reduction of resazurin in the Alamar blue assay (Figure 5E), suggesting an effect of arzanol on the involved oxidoreductases. Similarly, Hamid et al. observed the same phenomenon for the NAD(P)H dehydrogenase [quinone] 1 (NQO1) inhibitor dicoumarol[54], which shares structural similarity with arzanol. In contrast to their observations on dicoumarol, we still witnessed that the cells die at higher concentrations of arzanol. Nevertheless, we tested arzanol in a NQO1 enzyme activity assay and identified arzanol as potential new inhibitor of NQO1 (Figure 5F).

Arzanol Targets Mitochondria

On our search for upstream causes of ATG16L1 accumulation, we next investigated mitochondrial integrity. Different mitotoxins can stimulate mitophagy as means of cell survival. They induce the fragmentation of damaged mitochondria as well as the recruitment of mitophagy-associated proteins PTEN-induced putative kinase protein 1 (PINK) and the E3 ubiquitin ligase Parkin[55, 56, 57].

In microscopy assays, arzanol induced the fragmentation of the inner and outer mitochondrial membrane determined with mito-DsRed localizing to the mitochondrial matrix and staining of translocase of outer membrane 20 kDa subunit (TOM20) (Figure 6A). In line with this, we observed the mitochondrial stress-induced cleavage of optic atrophy protein 1 (OPA1), presumable ubiquitination of Parkin, and stabilization of PINK (Figure 6B).

Consistent with mitochondrial damage, arzanol treatment reduced the activity of mitochondrial respiratory chain complexes, especially complexes II and III (Figure 7A). To confirm proteins of these complexes as potential targets, we followed two approaches: We performed affinity purification with arzanol covalently immobilized on beads and fished for binding-partners in both cellular lysates and lysates from isolated mitochondria. We also performed Drug Affinity Responsive Target Stability (DARTS) assays in mitochondrial lysates followed by immunoblots monitoring the stability of arzanol-binding targets upon enzymatic proteolysis. Both approaches were followed by mass spectrometry to identify the protein targets of arzanol. Collectively, we identified mitochondrial respiratory chain complex

III proteins mitochondrial cytochrome b-c1 complex subunit 6 (UQCRH) and cytochrome c (CYC), and complex I-related NADH dehydrogenase [ubiquinone] iron-sulfur protein 4 (NDUS4) bound to immobilized arzanol in affinity purification in mitochondrial lysates (Figure 7B). Among the potential novel target proteins of arzanol (Supplementary table 2), we identified autophagy-relevant proteins Ras-related protein Rab-1B (RAB1B), heat shock protein HSP 90-alpha (HS90A) and ubiquitin-40S ribosomal protein S27a (RS27A), mitochondria-related proteins heat shock protein 75 kDa (TRAP1), carbamoyl-phosphate synthase [ammonia] (CPS1), mitochondrial stress-70 protein (GRP75) and superoxide dismutase [Mn] (SOD2). We further found tubulin beta-4A chain (TBB5) and heterogeneous nuclear ribonucleoprotein H (HNRH1) bound to arzanol-beads in affinity purification. Using DARTS, we verified the iron-sulfur subunit of the succinate dehydrogenase (respiratory chain complex II) and the Rieske subunit of cytochrome b-c1 complex (respiratory chain complex III) as molecular targets of arzanol (Figure 7C).

Taken together our results show that arzanol is a promising new anti-cancer drug and modulator of autophagy. It sensitizes RT-112 bladder carcinoma cells towards CDDP, and reduces cell viability of both normal and CDDP-resistant RT-112 in monotherapy. Arzanol is able to target different quinone-dependent reductases such as NQO1 and oxidoreductases of the mitochondrial respiratory chain that maintain mitochondrial integrity. Arzanol reduces mitochondrial respiration, targeting complex II and III, and induces fission of the mitochondrial membranes independent from reactive oxygen species. We observed the accumulation of ATG16L1 and lipidated LC3, but also smaller autophagosomal membranes and the accumulation of p62/SQSTM1 upon arzanol treatment during starvation. We therefore suggest a dual mode of action of arzanol within the autophagy pathway.

Discussion

The modulation of autophagy is used as anti-cancer treatment in more than seventy clinical trials treating more than eighteen different cancer types (https://clinicaltrials.gov/, accessed on 20th April, 2020). We used the top-down drug discovery approach to identify eight potential inducers and sixty-four potential inhibitors of autophagy in our high-throughput autophagy screening. Among these compounds, we identified arzanol as a novel modulator of autophagy.

In our assays, arzanol was initially identified as inhibitor of starvation-induced autophagy by causing accumulation of overexpressed mCitrine-LC3 in murine fibroblasts. Consistently, it also caused accumulation of overexpressed GFP-LC3 and endogenous total LC3 as well as lipidated LC3 in human cancer cells as determined by flow cytometry, fluorescence microscopy, and immunoblot analyses. Lipidation of LC3 is facilitated by the activation of the ubiquitin-like LC3 processing cascade involving ATG16L1, which is essential for LC3 lipidation[58]. Dudley et al. showed that ATG16L1 homodimerizes to bind to phosphatidylinositol 3-phosphate (PI3P)-covered pre-autophagosomal sites, and that modulating the PI3P-binding capacity of ATG16L1 impairs lipidation of LC3[12]. It is therefore likely that the accumulation of ATG16L1 dots upon arzanol treatment in starvation is the cause of the increase in LC3-II that we observed in immunoblot analysis, which in turn contributes to the observed increase in total LC3 measured by flow cytometry. As platforms for autophagosome biogenesis, ATG16L1-positive dots are also likely to account for the number of small LC3-positive dots detected by microscopy. However, also the inhibition of the autophagic flux can account for these phenomena by preventing autophagosome maturation and lysosomal LC3 degradation.

It was shown that accumulation of ATG16L1 increases during autophagy to ensure autophagosome maturation and autophagic activity[12]. During starvation-induced autophagy, ATG16L1 dots colocalize with proteins of the autophagic machinery such as ULK1, ATG14, and WIPI1[59]. The colocalization of ATG16L1 and ATG13, resp. ATG16L1 and WIPI2, upon arzanol treatment matches these data. In addition, Bansal et al. observed that ATG16L1 is able to colocalize with LC3-binding mitophagy receptors such as ubiquitin-binding optic neuropathy inducing protein (optineurin/OPTN)[60, 61, 62, 63]. Mitophagy is the selective autophagy of damaged mitochondria and aims to deplete damaged organelles and their associated triggers such as mitotoxins[55, 56, 57]. To induce mitophagy, PINK accumulates at the outer membrane of damaged mitochondria where it recruits and activates the E3 ubiquitin ligase Parkin, which then ubiquitinates the mitochondrial surface proteins. This allows the recruitment of autophagic receptors such as LC3 and OPTN, but also ULK1, FIP200, ATG9A, WIPI

proteins and ATG16L1 to form a de novo autophagosome around the damaged organelle[64, 65, 66]. When we checked for mitochondrial damage induced by arzanol, we observed the fragmentation of the inner and outer mitochondrial membranes. We further found accumulation of PINK in immunoblot analysis, and observed GFP-Parkin to run at a higher molecular mass, which we interpret as ubiquitinated Parkin. Along with the markers for mitochondrial damage, we detected cleaved OPA1, a protein involved in mitochondrial fusion[67, 68, 69, 70]. In line with these data, we found arzanol to reduce the activity of mitochondrial respiratory complexes, mainly complexes II and III. Interestingly, among protein targets from affinity purification, we also identified NDUS4, a protein of respiratory complex I. As novel targets for arzanol, we identified not only the respiratory complexes I, II and III, but also NQO1 and SOD2, which all function as quinone-dependent reductases required for mitochondrial integrity[71, 72, 73, 74, 75]. Combined with structural data on arzanol, we hypothesize that arzanol binds to the quinone-binding pockets of these proteins and accounts for the observed mitochondrial damage. TRAP1, another potential target of arzanol, regulates a metabolic switch between mitochondrial oxidative phosphorylation and glycolysis in cancer cells[76]. It is reported to maintain mitochondrial integrity downstream of respiratory complex I and PINK1[77]. We speculate that arzanol-induced mitochondrial damage provokes in situ autophagosome formation and explains ATG16L1 accumulation. Additionally, we identified autophagy-relevant proteins, such as RAB1B as potential binding-partner of arzanol. RAB1B colocalizes with ATGs and is involved in autophagosome biogenesis[78, 79, 80, 81], and knockdown of RAB1B induced the accumulation of LC3-II[82]. Inhibition of RAB1B could support increased lipidation of LC3 upon arzanol treatment.

In addition, arzanol caused accumulation of p62, while we observed smaller autophagosomes upon arzanol treatment. We interpret the pronounced accumulation of p62 upon arzanol during additional starvation as indicator of an inhibited autophagic flux. It remains unclear whether the dysregulation in LC3 lipidation itself is ultimately sufficient to inhibit autophagy or if additional targets are involved. In support of the latter, we found HS90A bound to arzanol in affinity purification. HS90A acts as chaperone for many client proteins, some of which are involved in autophagy e.g. AKT, Beclin 1, ULK1 or lysosome-associated membrane protein 2 (LAMP2)[83]. Dissociation of chaperones can destabilize their client proteins, preventing them from fulfilling their tasks. HS90A inhibition by arzanol could result in subsequent destabilization of LAMP2A, a protein, which is essential for maintaining the integrity of the lysosome and autolysosome[84, 85, 86]. Non-functional lysosomes are prevented from fusing with autophagosomes and cause the accumulation of different autophagic markers such as LC3 and p62[87,

[88]. Therefore, HS90A could be a target of arzanol accounting for a disturbed autophagosome maturation and autolysosomal degradation of p62. Admittedly, we could not validate all identified targets of arzanol, due to methodical blind spots of each assay, i.e. sterical problems in affinity purification, or detectability issues of small proteins in DARTS. Accordingly, further validation experiments are required.

We tested the novel modulator of autophagy in monotherapy and combinational therapy with CDDP against sensitive and CDDP-resistant bladder cancer cells. CDDP-based chemotherapy is the first-line treatment in many cases of advanced or metastatic urothelial carcinoma according to The European Association of Urology[89]. However, innate and acquired chemoresistance remain a main reason for cancer-related lethality in patients. Similar to other autophagy inhibitors that reduced tumor growth rate and prolonged patient survival[90, 91, 92, 93, 94], we found arzanol to reduce cell viability in both bladder carcinoma cells in monotherapy, while it also sensitized RT-112 cells to CDDP treatment.

Conclusively, from our data we characterize arzanol as an inducer of mitochondrial damage and autophagosome formation and as inhibitor of autophagy. Its different targets might account for the multifaceted mode of action that leads to cytotoxic effects in bladder cancer cells. Taking in consideration its pharmacological activities, we propose arzanol as new lead structure for the treatment of bladder cancer and suggest further investigations on its target- and cancer-specificity.

Acknowledgements

This study was supported by the Deutsche Forschungsgemeinschaft GRK 2158 (to P.P. and to B.S.), STO 864/4-1 (to B.S.) and STO 864/5-1 (to B.S.), and the Düsseldorf School of Oncology (to B.S.; funded by the Comprehensive Cancer Center Düsseldorf/Deutsche Krebshilfe and the Medical Faculty of the Heinrich Heine University Düsseldorf). We thank Andreas Reichert (Institute of Biochemistry and molecular Biology I, Heinrich Heine University Düsseldorf, Germany) for providing HeLa cells expressing mito-DsRed, and the OPA1 antibody. We thank Philip Böhler for providing the mito-DsRed HeLa cells tranfected with EGFP-Parkin. We thank Julia Werner for isolating arzanol used in Figures 1 and 2. We thank Tullia Lindsten (Memorial Sloan Kettering Cancer Center, New York City, USA) for providing wild type mouse embryonic fibroblasts. We thank Toshio Kitamura (Institute of Medical Science, University of Tokyo, Japan) for providing Plat-E cells.

Author contributions

JD designed the experiments, performed flow cytometry analyses, microscopy and cell viability assays, performed the NQO1 activity assay and immunoblot analyses, and prepared samples for AP-MS and DARTS. JD analyzed and interpreted the data and wrote the manuscript. FS performed the Mito Check experiments. SC and MCM performed DARTS and AP-MS. DS provided expertise on microscopy and quantifications. LB performed cell viability assays. MJM, WW, YS, NB, and SS gave technical support. PP provided an in-house natural compound library. PP and BS supervised the project. All authors discussed the results and commented on the manuscript.

Conflict of Interest

The authors declare no conflict of interest.

Materials and Methods

Reagents

Natural compounds isolated from endophytic fungi, lichens, marine sponges or plants were provided by Peter Proksch (Institute of Pharmaceutical Biology and Biotechnology of the Heinrich Heine University (Düsseldorf, Germany). Bafilomycin A_1 (Sigma-Aldrich, #B1793) and arzanol (Sigma-Aldrich, #SBR00002) were dissolved in dimethyl sulfoxide (DMSO; AppliChem GmbH, #A3672). We purchased respiratory chain complex inhibitors antimycin A from Sigma (#A8674) and oligomycin A from Toronto Research Chemicals (#O532970). For transfection of cells, we used FuGENE®6 (Promega, #E2692) and polybrene (hexadimethrine bromide; Sigma-Aldrich, #H9268-106). Western blots were performed using Immobilon™-FL PVDF membrane (Merck-Millipore, #IPFL00010), milk powder (Carl Roth, #T145.2), and Protease Inhibitor Cocktail powder (Sigma-Aldrich, #P2714-1BTL). Cells were cultivated using full medium DMEM (Gibco® by Life Technologies, #41965-039), starvation medium EBSS (Gibco® by Life Technologies, #24010-043), PBS (Gibco® by Life Technologies, #14190-094), fetal bovine serum (GE Healthcare, #A15-101), 0.05% trypsin/EDTA solution (Gibco® by Life Technologies, #25300-062), penicillin/streptomycin (10000 U/ml, Biochrom GmbH, #A2213), puromycin (InvivoGen, ant-pr), or blasticidin (InvivoGen, ant-bl).

For immunoblotting, antibodies against ACTB/β-actin (Sigma-Aldrich, #A5316), LC3 (Cell Signaling Technology, #2775), SQSTM1/p62 (PROGEN Biotechnik, GP62-C), ULK1 (clone D8H5, Cell Signaling Technology, #8054), phospho ULK1 Ser758 (Cell Signaling Technology, #6888), phospho TSC2 Ser939 (Cell Signaling Technology, #3615), phospho p70S6K Ser371 (Cell Signaling Technology, #9208), OPA1 (described previously[95]; kindly provided by Andreas Reichert), PINK (Cell Signaling Technology, #6946), (GFP-)Parkin (Abcam, #ab15954), SDHB (Thermo Fisher, #459230), UQCRFS1 (Invitrogen, #MA5-27471), CPS1, and GAPDH were used. IRDye 800- or IRDye 680-conjugated secondary antibodies were purchased from LI-COR Biosciences (#926-32210/11, #926–68070/71, #926–68024, #926-68077, #926–32214).

For immunofluorescence, antibodies against ATG16L (MBL #PM040), LC3B (MBL #PM036 and #M152-3), WIPI2 (AbD Serotec/BIORAD, #MCA5780GA), ATG13 (MBL, #M183-3), TOM20 (Santa Cruz Biotechnology, #17764) were used. Alexa Fluor® 488-conjugated and Alexa Fluor® 647-conjugated antibodies were purchased from Jackson ImmunoResearch Laboratories.

NQO1 activity of HeLa cells was measured using the NQO1 Activity Assay Kit (Abcam, #184867) according to the manufacturer. Respiratory chain complex activities were measured from isolated mitochondria using the MitoCheck Complex Activity Assay Kits (Cayman Chemicals, #700930, #700940, #700950, #700990, #701000). Both assays were measured using a microplate reader (BioTek, Synergy Mx).

Generation and culture of cell lines

Mouse embryonic fibroblasts (MEFs) (kindly provided by Tullia Lindsten, Memorial Sloan Kettering Cancer Center, New York City, USA) were retrovirally transfected with pMSCVblast/mCitrine-LC3B. Generation of pMSCVblast/mCitrine-LC3B was described previously[96]. For transfection, Plat-E cells (kindly provided by Toshio Kitamura, Institute of Medical Science, University of Tokyo, Japan) were transfected with 1.9 µg pMSCV-based retroviral vectors using FuGENE® 6 (Promega) transfection reagent according to the manufacturer's manual. The cells were incubated for three days before selection with 35 µg/ml blasticidin.

HeLa cells (kindly provided by Richard Youle, John Edward Porter Neuroscience Research Center, Bethesda, USA) were retrovirally transfected with pMRX-IP/GFP-LC3-RFP-LC3ΔG (kindly provided by Noboru Mizushima, Department of Biochemistry and Molecular Biology, University of Tokyo, Tokyo, Japan). Therefore, Plat-E cells were transfected with 1.9 µg pMRX-based retroviral vectors and 1.0 µg pVSV-G vector DNA using FuGENE® 6 (Promega) transfection reagent according to the manufacturer's manual. The cells were incubated for three days before selection with 2.5 µg/ml puromycin. For Figure 2D, cells were subcloned in order to prevent homologous recombination.

Cells were cultured in high glucose (4.5 g/l) DMEM supplemented with 10% FCS at 37°C in a 5% CO_2 humidified atmosphere. For amino acid starvation, cells were washed once with PBS and incubated for the indicated time points in EBSS.

High-throughput autophagy screening

Mouse embryonic fibroblasts stably expressing mCitrine-LC3 were incubated with 10 µM of each natural compound solved in DMSO in serum-containing full medium or starvation medium for 6 h. During screening, compound samples were blinded by labelling with a randomized code and unblinded post-experiments. Cells were harvested by trypsination, washed using PBS and centrifugation at 300 g, and measured via flow cytometry of 10,000 events in the FITC channel of an LSRFortessa (Becton Dickinson,

Heidelberg, Germany). Median fluorescence intensities were measured in biological triplicates and normalized to the DMSO control.

GFP-LC3-RFP-LC3ΔG assay

HeLa cells stably expressing GFP-LC3-RFP-LC3ΔG were incubated with the indicated concentrations of self-isolated or commercial arzanol solved in DMSO in starvation medium for 6 h. Cells were harvested and analyzed using flow cytometry as described above.

Immunoblotting

Cleared cell lysates were prepared and suspected to immunoblotting as described before[96]. Signal intensities of protein bands were quantified using Image Studio lite 4.0 (LI-COR) and each band was normalized to the average protein signal to correct for technical variance. The signals were then normalized to the corresponding loading control (ACTB). Panels for at least three biological replicates were prepared using GraphPad Prism 7.0.

Fluorescence microscopy

On the day before treatment, cells were grown on glass cover slips (Marienfeld). After treatment, cells were fixed with 4% formaldehyde-PBS for 30 min on ice, and quenched with 50 mM NH_4Cl for 15 min. For immunofluorescence labelling, cells were then permeabilized with 0.2% Triton X-100-PBS for 15 min, or 50 µg/ml digitonin (Roth, #4005) for 5 min according to the antibody manufacturers. Samples were blocked with 3% BSA (Roth, #8076)-PBS for 30 min and incubated with primary antibodies for 1-2 h. After washing and 30 min of secondary antibody incubation, samples were again washed three times with PBS. Cells were embedded in ProLong Glass Antifade Mountant (Thermo Fisher Scientific, #P36980) including DAPI. Imaging was performed with a Zeiss Axio Observer 7 fluorescence microscope (Zeiss, Köln, Germany) with a Plan Apochromat 40x/1.4 oil objective (Zeiss, Köln, Germany). Quantification of images was performed with ImageJ. For that, signals and nuclei were counted per image and a signal-to-nuclei ratio was calculated. Macros for the quantifications are provided in supplementary Methods.

Cell viability assays

Cell viability was determined using the colorimetric Alamar Blue and MTT assays, which measure the reduction of non-fluorescent dyes to the fluorescent metabolites resorufin and formazan. For both assays, cells were cultivated in 96 well plates. The following day, the cells were treated with cisplatin and/or arzanol for 24 h. For the MTT assay, MTT (Roth #4022) was added to the cells at 0.5 mg/ml concentration and incubated at 37°C for 1 h. Afterwards, the plates were centrifuged at 600 rcf and 4°C for 5 minutes, and cells were lysed in DMSO for 20 min in the dark. Finally, the absorbance was measured at 570 nm and 650 nm for reference, using a microplate reader (BioTek, Synergy Mx). For the Alamar blue assay, 40 µM resazurin sodium salt (Cayman Chemicals, #14322) was added to the cells and incubated at 37°C for 3 h. Afterwards, the absorbance was measured at 590 nm, using a microplate reader (BioTek, Synergy Mx). The mean of the absorbance of untreated control samples was set as 100%.

Isolation of Mitochondria

For isolation of mitochondria, HeLa wild type cells were cultivated on 150 mm diameter tissue culture treated dishes (Sarstedt) and ~3.6 x 10^8 cells were harvested the next day via scraping. Cells were pelleted at 500 g for 5 min and washed twice with PBS (Gibco). The pellet was resuspended in 10 ml mitochondria isolation buffer (210 mM mannitol, 70 mM sucrose, 1 mM EDTA, 20 mM HEPES and protease inhibitor cocktail [Sigma-Aldrich, #P2714]) for 5 min on ice before rupturing by seven strokes through a 26 G canule. The cell lysate was then centrifuged at 1000 g and 4°C for 5 min and the supernatant was collected. The remaining pellet of non-lysed cells was resuspended in 2 ml mitochondria isolation buffer and ruptured again before centrifugation, and the two fractions were pooled. The pooled lysate was centrifuged again at 1000 g and 4°C for 5 min and the pellet was discarded. The remaining lysate was centrifuged at 8000 g and 4°C for 10 min. The supernatant (cytosolic fraction) was collected and centrifuged again before transferring into a new tube and freezing in liquid nitrogen. The pellet (mitochondrial fraction) was washed three times at 8000 g for 10 min in 250 µl mito isolation buffer. The pellet was finally centrifuged at 10,000 g and 4°C for 10 min. The supernatant was discarded and the pellet containing isolated mitochondria was frozen in liquid nitrogen and stored at -80°C.

Statistics

Sample sizes were chosen with reference to pragmatic considerations and the principle of saturation due to previously published work in this field and preliminary experiments. For high-throughput analysis of the flow cytometric mCitrine-LC3-based autophagy screening we used uniformly minimal variance unbiased estimate (UMVUE) of strictly standardized mean difference (SSMD)[36]. For immunoblotting quantifications of Figure 2C, statistical analysis was performed using a 2way ANOVA with Dunnett's multiple comparison test comparing treated to untreated control samples. For comparing size and number of dots in Figure 3, statistical analysis was performed using an ordinary 1way ANOVA with Tukey's multiple comparison test comparing all treatments with each other. For NQO1 activity data, statistical analysis was performed using a 1way ANOVA with Dunnett's multiple comparison test comparing treated to untreated control samples. All IC_{50} values in Figure 5 were calculated using GraphPad Prism 7.01 (function log[inhibitor] vs. response - variable slope [four parameters]). Representative data or means of biological replicates are shown for every experiment with error bars that indicate standard error. All statistical analyses were performed using Prism v7.01 (GraphPad Software, La Jolla, CA, USA).

Table 1. List of potential autophagy inducers. Data show mean difference ±SD (% of control) of mCitrine-LC3 decrease upon full medium monitored by flow cytometry. In total, 8 compounds causing equal to or greater than 15% LC3 degradation at a fairly moderate and higher effect (|SSMD score| ≥1) at 10 μM after 6 h of treatment were classified as potential inducers of autophagy.

Compound	Mean difference of mCit-LC3 (%)	SD	SSMD
Beauvericin J	-34.4	±6.0	-3.25
Enniatin A1	-28.8	±1.3	-12.58
Enniatin B1	-27.4	±5.6	-2.75
4,6-dibromo-2-(2',4'- dibromophenoxy)phenol	-22.0	±11.2	-1.11
Pergularinine	-19.9	±4.6	-2.43
(-)-Matairesinol	-18.1	±8.1	-1.26
Viriditoxin	-17.7	±3.3	-3.04
(-)-Arctigenin	-17.3	±6.0	-1.62

SD: standard deviation; SSMD: strictly standardized mean difference

Table 2. List of potential autophagy inhibitors. Data show mean difference ±SD (% of control) of mCitrine-LC3 increase upon starvation medium monitored by flow cytometry. In total, 64 compounds causing equal to or greater than 15% LC3 protection at a fairly moderate and higher effect (|SSMD score| ≥1) at 10 µM after 6 h of treatment were classified as potential inhibitors of autophagy.

Compound	Mean difference of mCit-LC3 (%)	SD	SSMD
g114	+2590.4*	±765.1	1.91
Daldinone I	+536.3	±294.2	1.03
Kuanoniamin D	+336.7	±182.2	1.04
Deoxyfunicone	+335.7	±85.5	2.21
Manzamine J N-Oxid	+256.2	±45.0	3.21
Helenalin	+249.9	±38.4	3.67
Wortmannin C	+243.9	±45.4	3.03
Wortmannin A	+240.8	±49.9	2.72
8-0-manzamine A	+235.2	±32.0	4.14
Stemphyltoxin I	+234.4*	±44.8	2.95
(+)-Aeroplysinin-1	+224.6	±19.1	6.65
2-(1'E-styryl)-5-geranyl-resorcin-1-carboxylic acid	+221.8	±21.1	5.92
Manzamine A	+220.6	±37.8	3.29
Dienon (3,5-dibromo-1-hydroxy-4-oxo-2,5-cyclohexadiene-1-acetamide)	+209.4	±55.6	2.13
Sekikaic acid	+174.5	±21.1	4.67
Isospongiaquinone	+174.3	±30.7	3.21
Isofistularin 3	+170.9	±67.0	1.44
5-epi-Ilimaquinone	+166.1	±48.5	1.93
Arzanol	+164.6	±63.9	1.45
3,4,6-tribromo-2-(2',4'-dibromophenoxy)phenol	+159.6	±45.8	1.97
Monomethyl-mitorubrin	+158.8	±53.8	1.67
Homosekikaic Acid	+158.7	±52.9	1.69
Pyrenocine A	+158.2	±19.3	4.63
4'-hydroxy-3'-methoxy-mitorubrin	+153.1	±69.7	1.24
Broussochalcone B	+149.6	±47.0	1.80
Diaporthins B	+149.0	±32.9	2.55
Luffariellolid	+138.3	±37.5	2.08
Aranorosin	+122.0	±63.9	1.08
Ilimaquinone	+105.1	±55.0	1.08
Xanthoangelol	+98.3	±29.4	1.88
Avaron	+93.7	±44.5	1.19
Pyrrocidine D	+93.4	±34.7	1.52
Beauvericin	+87.2	±39.5	1.24
Secalonic acid F	+78.1	±19.0	2.32
Beauvericin J	+67.4	±19.5	1.95
Aaptamine	+67.1	±15.6	2.43
Amorphastilbol	+66.9	±30.5	1.24
Neobavaisoflavone	+60.7	±25.1	1.36
11-hydroxyamorphispironone	+59.4	±12.7	2.64
Viriditoxin	+53.3	±13.2	2.28
Amorphispironone B	+46.0	±14.1	1.84
Berberin hemisulfate	+41.8	±16.6	1.42
Enniatin B1	+40.0	±16.0	1.41
Anomalin A	+38.7	±3.4	6.44
Ochratoxin A	+36.9	±15.9	1.31
Norlichexanthone	+35.4	±17.2	1.16

*could be caused by autofluorescence; SD: standard deviation; SSMD: strictly standardized mean difference

Continued table 2. List of potential autophagy inhibitors. Data show mean difference ±SD (% of control) of mCitrine-LC3 increase upon starvation medium monitored by flow cytometry. In total, 64 compounds causing equal to or greater than 15% LC3 protection at a fairly moderate and higher effect (|SSMD score| ≥1) at 10 μM after 6 h of treatment were classified as potential inhibitors of autophagy.

Compound	Mean difference of mCit-LC3 (%)	SD	SSMD
Pergularinine	+34.8	±5.1	3.85
Citreodrimene B	+33.6	±17.6	1.08
15-dehydroxy-integracin B	+33.2	±12.4	1.51
Aplysamine-2	+33.2	±2.4	7.93
Br2Hexylamide	+32.1	±17.3	1.05
Chrysin 6-C-(2″-O-α-L-rhamnopyranosyl)-ß-D-glucopyranoside	+31.3	±6.8	2.59
Sclerotiorin	+29.8	±14.2	1.18
Manzamine F	+27.6	±5.6	2.76
Aerothionin	+25.1	±6.8	2.10
Flavomannin D	+23.8	±7.2	1.86
4,5-Dibromo-1H-pyrrol-2-carboxylic acid	+23.1	±8.3	1.57
Pretrichodermamide A	+22.9	±5.5	2.36
Midpacamide	+22.0	±9.0	1.39
Penicillic Acid	+21.1	±4.0	3.01
Dammarenolic acid	+18.2	±9.2	1.12
Bitalin A	+17.2	±8.0	1.21
Solanapyrone C	+17.2	±7.5	1.30
6-Methoxycomaparvin-5-methyl ether	+15.9	±3.5	2.56

SD: standard deviation; SSMD: strictly standardized mean difference

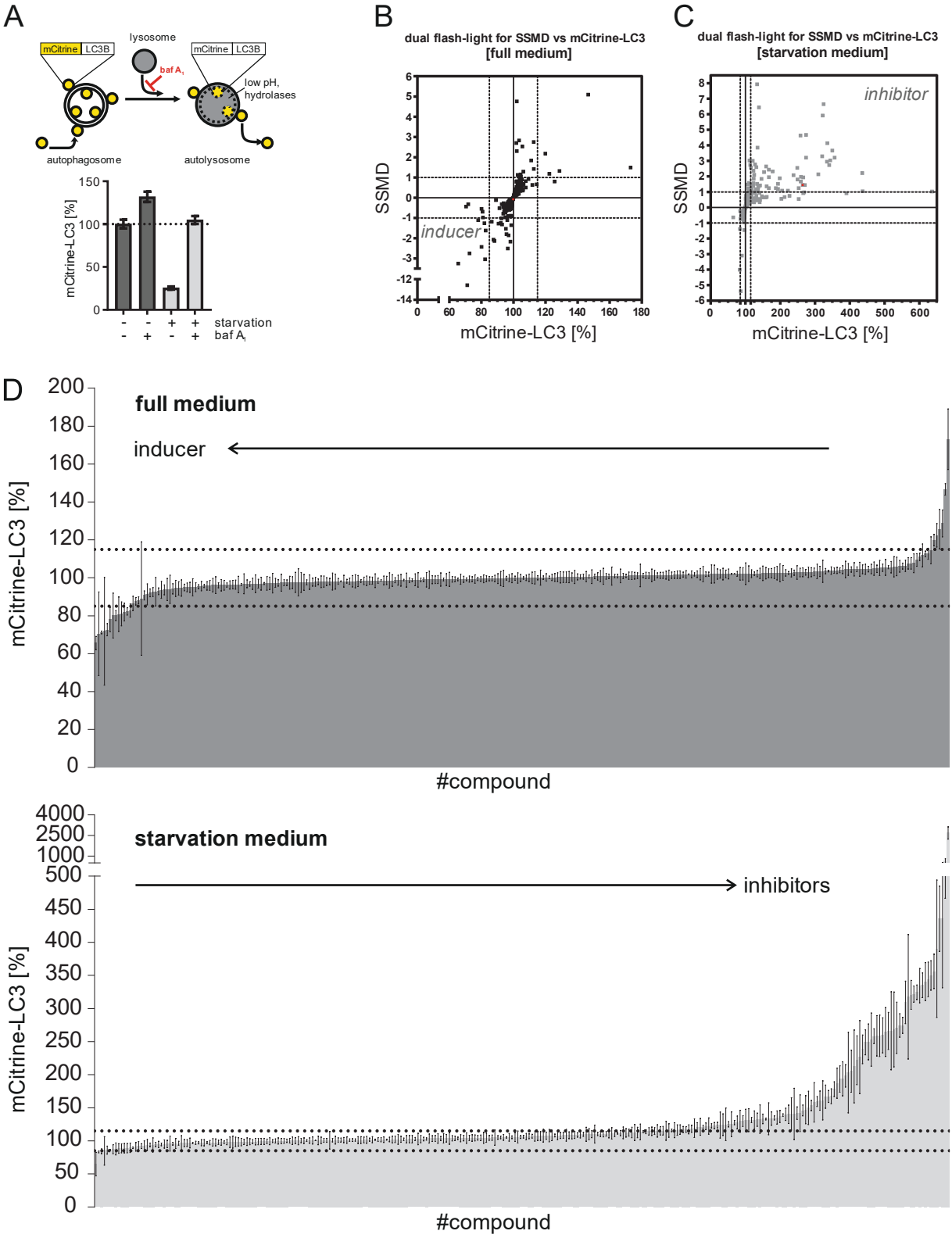

Figure 1. High-throughput screening natural compound-based autophagy modulators.

(A) Detection of starvation-induced and bafilomycin A_1-inhibited autophagy in a flow cytometric screening. MEF cells stably expressing mCitrine-LC3 were cultured in either full medium plus serum, or starvation medium and treated with 10 nM bafilomycin A_1 for 6 h ($n \geq 19$). The mCitrine fluorescence is shown as a percentage relative to that of mock-treated (DMSO) cells. Data represent means ± SEM.

(B, C) High-throughput autophagy screening of 300 natural compounds. The diagram shows dual-flashlight plots for strictly standardized mean difference (SSMD) versus average percentage of mCitrine-LC3. Dotted lines define potential inducer and inhibitors of autophagy. Cells were treated with 10 μM of each compound for 6 h (n = 3). Arzanol is highlighted in red.

(D) The diagram shows individual levels of mCitrine-LC3 fluorescence from (B, C) for each of the 300 compounds in full or starvation medium. Dotted lines mark the ±15% difference in mCitrine-LC3 levels. Data represent means ± SEM.

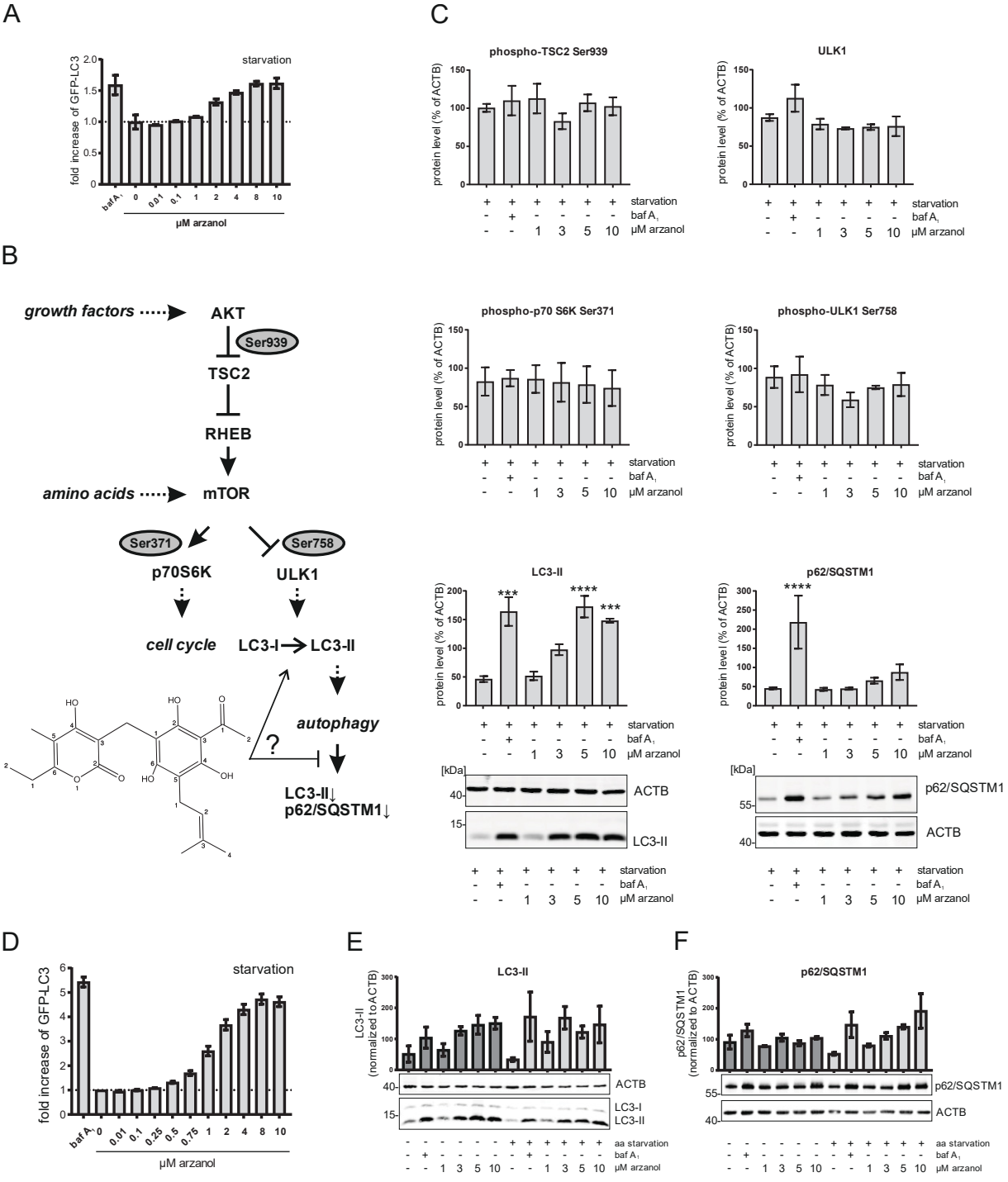

Figure 2. Arzanol drives LC3-II accumulation independent of the AKT/mTOR-pathway.

(A) Nonclonal HeLa cells stably expressing GFP-LC3-RFP-LC3ΔG were starved in serum- and amino acid-free medium for 6 h while incubated with different concentrations of self-isolated arzanol. Data show fold increase of GFP-LC3 fluorescence relative to mock treated control as means ± SEM of three biological replicates.

(B) Simplified pathway of key proteins of the AKT/mTOR/ULK1-axis in starvation-induced autophagy. Arzanol is a modulator of starvation-induced autophagy.

(C) Western blot analysis of AKT/mTOR/ULK1-pathway proteins during serum- and amino acid-starvation. HeLa wild type cells were starved in serum- and amino acid-free medium for 6 h while being incubated with baf A_1 or different concentrations of self-

isolated arzanol. Data show quantified means of biological triplicates normalized to ACTB ± SEM. Statistical analysis was performed using 2way ANOVA with Dunnett's multiple comparison test comparing treated to untreated samples, ***p<0.001, ****p<0.0001.

(D) Subcloned HeLa cells stably expressing GFP-LC3-RFP-LC3ΔG were starved in serum- and amino acid-free medium for 6 h while incubated with different concentrations of commercially available arzanol. Data show fold increase of GFP-LC3 fluorescence relative to mock treated control as means ± SEM of three biological replicates.

(E) Western blot analysis of LC3-II and p62/SQSTM1 during serum-starvation. HeLa wild type cells were starved in serum-free (dark bars) or serum- and amino acid-free (light bars) medium for 6 h while being incubated with baf A_1 or different concentrations of commercially available arzanol. Data show quantified means of biological triplicates normalized to ACTB ± SEM.

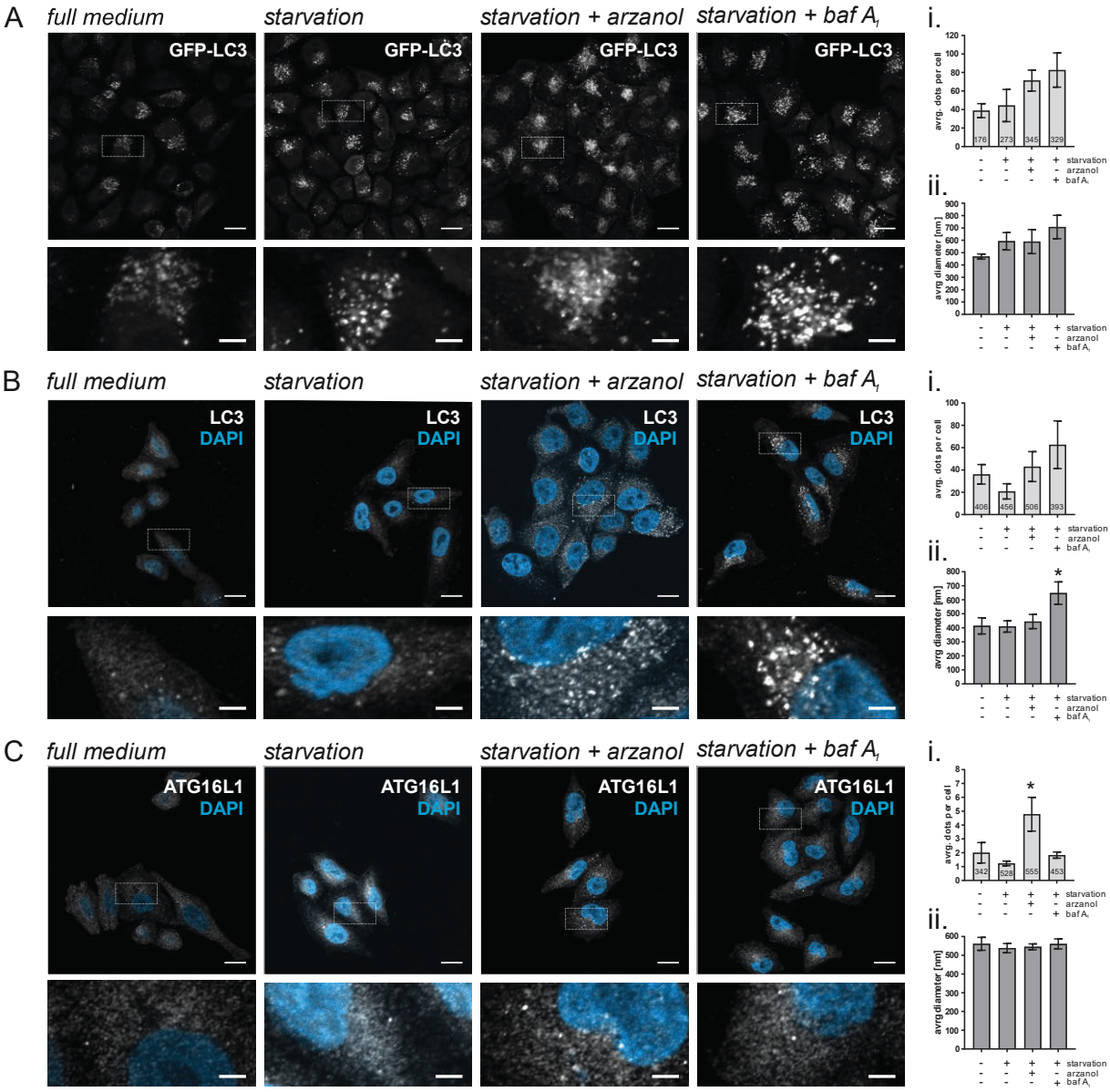

Figure 3. Arzanol interferes with autophagosome biogenesis.

Shown are representative microscopy images of HeLa cells stably expressing GFP-LC3-RFP-LC3ΔG (A), HeLa wild type cells immunofluorescence-labelled for endogenous LC3 (B), ATG16L1 (C), or WIPI2 (D). All cells were starved in serum- and amino acid-free medium for 2 h while incubated with 3 µM arzanol or 10 nM bafilomycin A_1. Scale bars in upper panels are 15.5 µm, scale bars in magnifications are 3.875 µm. (i.) Data show average number of dots per cell from biological triplicates for GFP-LC3, n=6 for LC3 and ATG16L1, nd n=5 for WIPI2 as mean ± SEM. Digits in bars show total number of cells quantified using ImageJ software. (ii.) Data show average diameter of dots in nm as mean ± SEM. Statistical analysis was performed using ordinary 1way ANOVA with Tukey's multiple comparison test, *p<0.1.

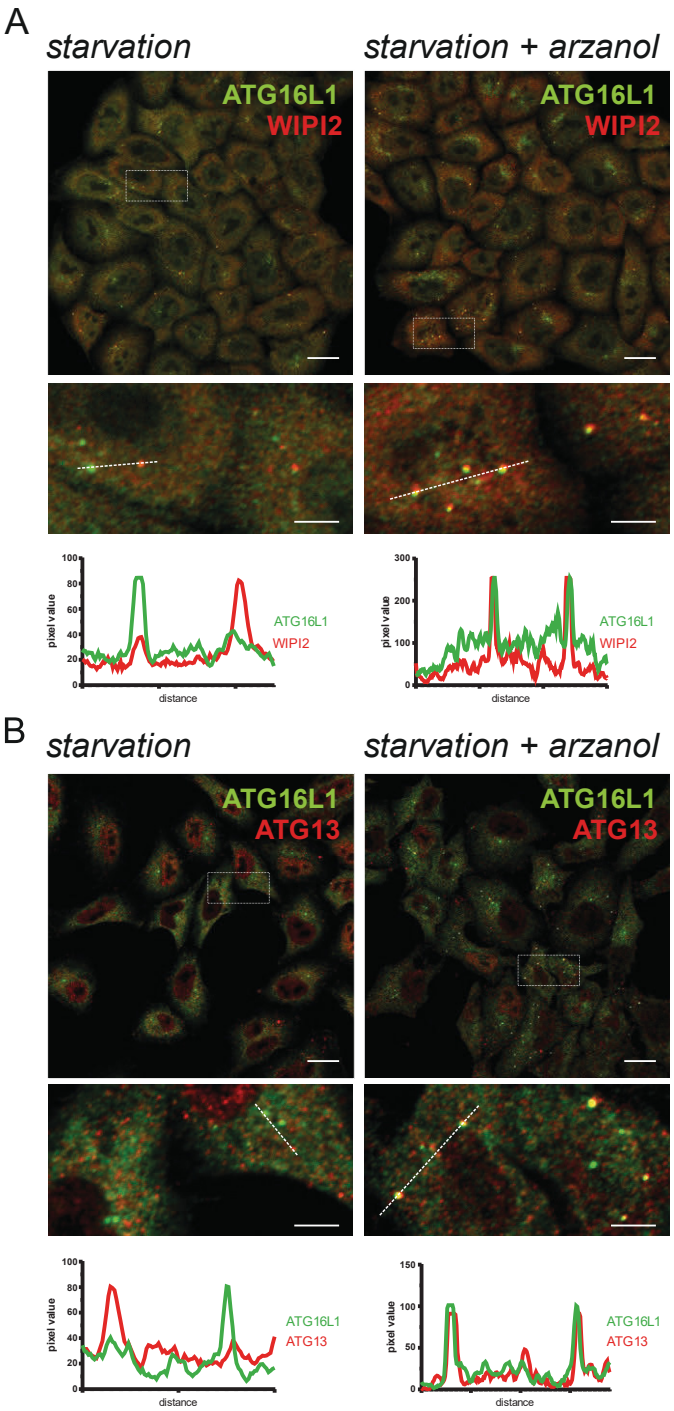

Figure 4. Arzanol-induced ATG16L1 accumulations at perinuclear regions colocalize with ATG13 and WIPI2.

Shown are representative microscopy images of HeLa wild type cells immunofluorescence-labelled for endogenous ATGs. Upon starvation, arzanol-induced ATG16L1 dots colocalize with WIPI2 (A), and ATG13 (B). These ATG16L1 dots accumulate at perinuclear regions that are also surrounded by LC3 dots (C). Cells were starved in serum- and amino acid-free medium for 2 h while incubated with 3 µM arzanol. Scale bar in panels are 15.5 µm, scale bars in magnifications are 3.875 µm. Diagrams show immunofluorescence intensities for the indicated proteins measured using ImageJ software for the cross sections marked as white dotted lines.

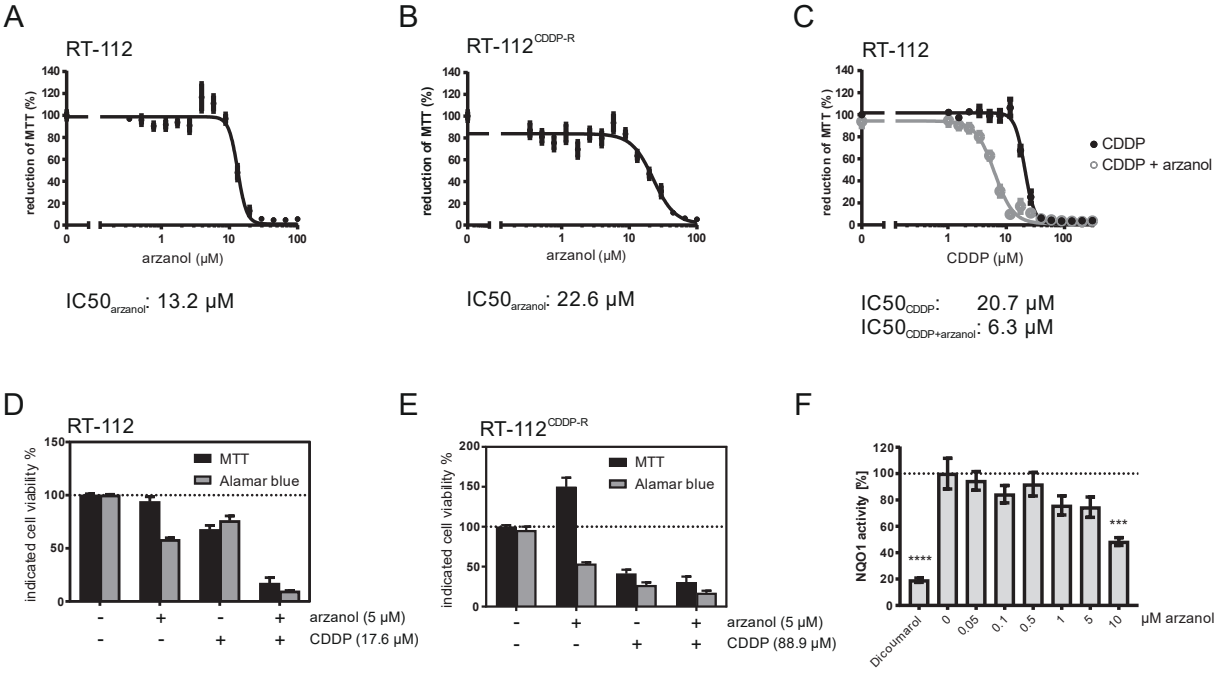

Figure 5. Arzanol is cytotoxic for bladder carcinoma cells in mono- and CDDP-combination therapy.

Arzanol reduces cell viability in bladder cancer cells. RT-112 bladder carcinoma cells were incubated with indicted concentrations of arzanol (A) or indicted concentrations of CDDP ± 5 µM arzanol (B) during starvation for 24 h. Cell viability was measured using an MTT assay.

(C) Arzanol sensitizes bladder cancer cells towards cisplatin. The diagram shows a depiction of the synergistic effect of 5 µM arzanol and 17.6 µM CDDP from (B) compared to the same treatments analyzed by Alamar blue assay.

The results are shown as mean ± SEM of at four individual experiments performed in triplicates for treatments with arzanol alone, and six biological replicates performed in technical triplicates for combination of arzanol and CDDP.

(D) CDDP-resistant RT-112 bladder carcinoma cells were incubated with indicted concentrations of arzanol during starvation for 24 h. Cell viability was measured using an MTT assay. (E) The diagram compares Alamar blue and MTT assay for the combination of 5 µM arzanol and 88.9 µM CDDP in starved CDDP-resistant RT-112. (F) Arzanol reduces the enzyme activity in an NQO1 Activity Assay Kit similar to the positive control 20 µM dicoumarol (n=3). ***p<0.001, ****p<0.0001.

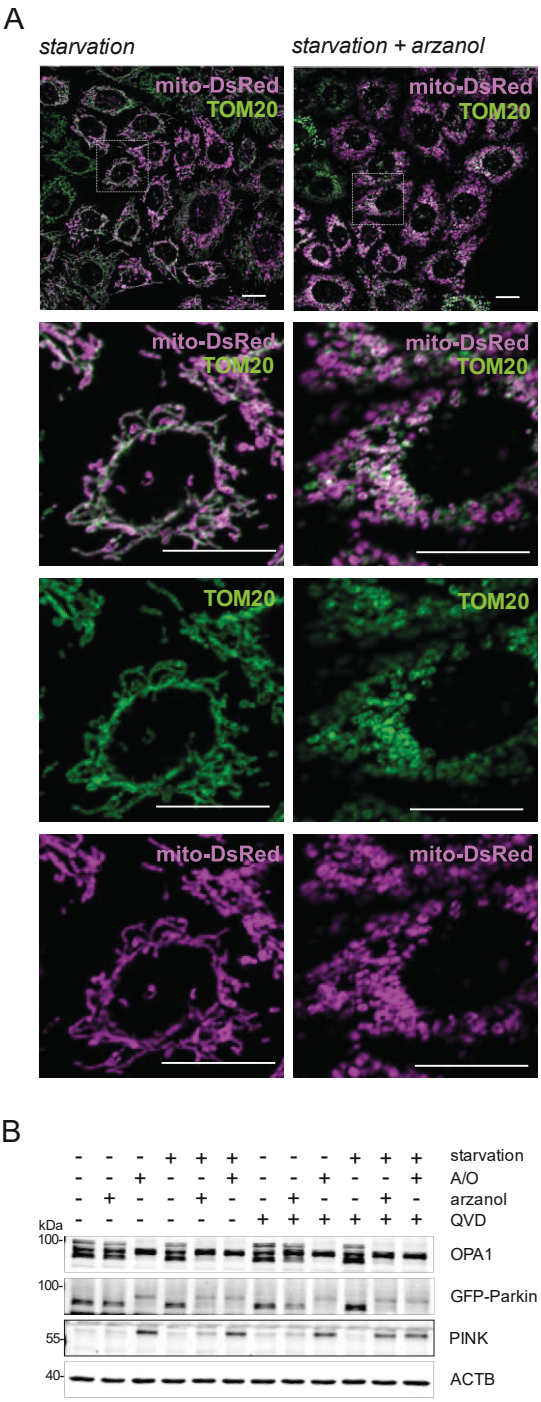

Figure 6. Arzanol causes damage-induced fragmentation of mitochondrial membranes.

(A) Shown are microscopy images of mito-DsRed-expressing HeLa cells immunofluorescence-labelled for endogenous TOM20. Upon starvation, arzanol induces a fragmentation of both inner (mito-DsRed) and outer (TOM20) mitochondrial membranes. Cells were starved in serum- and amino acid-free medium for 2 h while incubated with 5 μM arzanol. Scale bars in all panels are 20 μm.

(B) Immunoblot for markers of mitochondrial damage (OPA1 fragmentation, Parkin ubiquitination, PINK accumulation) reveals that arzanol induced mitochondrial fragmentation independent of apoptosis induction. HeLa cells stably expressing mito-DsRed GFP-Parkin were incubated with serum-free full medium or starvation medium and treated with 5 μM arzanol or a combination of 4 μM antimycin and 10 μM oligomycin (A/O) with/without 1 μM QVD for 6 h. Shown blot is representative of three independent experiments.

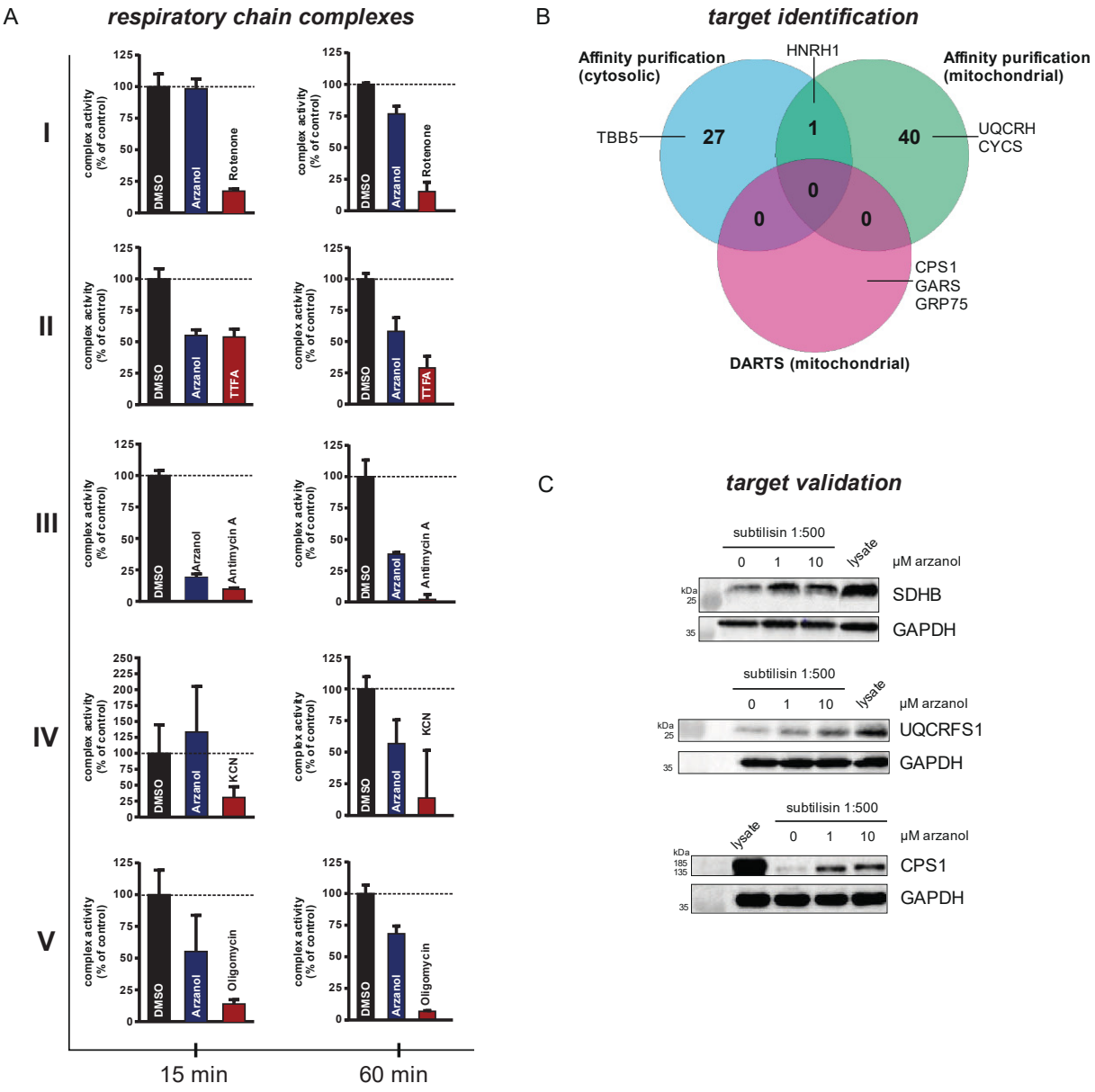

Figure 7. Target identification for arzanol reveals respiratory chain complexes II and III as targets for arzanol.

(A) Arzanol inhibits complexes II and III in a respiratory chain activity assay of isolated mitochondria after incubation for 15 min and 60 min. (B) Target identification by affinity purification from whole lysates and isolated mitochondria, and DARTS experiments reveal potential targets of arzanol. (C) Targets of arzanol are validated by DARTS via protection of arzanol-bound proteins from subtilisin proteolysis.

References

1. Choi H, Cho SY, Pak HJ, Kim Y, Choi JY, Lee YJ*, et al.* NPCARE: database of natural products and fractional extracts for cancer regulation. *Journal of cheminformatics* 2017, **9:** 2.
2. Newman DJ, Cragg GM. Natural Products as Sources of New Drugs from 1981 to 2014. *Journal of natural products* 2016, **79**(3)**:** 629-661.
3. Baker DD, Chu M, Oza U, Rajgarhia V. The value of natural products to future pharmaceutical discovery. *Natural product reports* 2007, **24**(6)**:** 1225-1244.
4. Frake RA, Ricketts T, Menzies FM, Rubinsztein DC. Autophagy and neurodegeneration. *The Journal of clinical investigation* 2015, **125**(1)**:** 65-74.
5. Harris H, Rubinsztein DC. Control of autophagy as a therapy for neurodegenerative disease. *Nature reviews Neurology* 2011, **8**(2)**:** 108-117.
6. Levine B, Kroemer G. Biological Functions of Autophagy Genes: A Disease Perspective. *Cell* 2019, **176**(1-2)**:** 11-42.
7. Mizushima N, Levine B, Cuervo AM, Klionsky DJ. Autophagy fights disease through cellular self-digestion. *Nature* 2008, **451**(7182)**:** 1069-1075.
8. Graef M, Nunnari J. Mitochondria regulate autophagy by conserved signalling pathways. *The EMBO journal* 2011, **30**(11)**:** 2101-2114.
9. Li L, Chen Y, Gibson SB. Starvation-induced autophagy is regulated by mitochondrial reactive oxygen species leading to AMPK activation. *Cellular signalling* 2013, **25**(1)**:** 50-65.
10. Papandreou I, Lim AL, Laderoute K, Denko NC. Hypoxia signals autophagy in tumor cells via AMPK activity, independent of HIF-1, BNIP3, and BNIP3L. *Cell death and differentiation* 2008, **15**(10)**:** 1572-1581.
11. Axe EL, Walker SA, Manifava M, Chandra P, Roderick HL, Habermann A*, et al.* Autophagosome formation from membrane compartments enriched in phosphatidylinositol 3-phosphate and dynamically connected to the endoplasmic reticulum. *The Journal of cell biology* 2008, **182**(4)**:** 685-701.
12. Dudley LJ, Cabodevilla AG, Makar AN, Sztacho M, Michelberger T, Marsh JA*, et al.* Intrinsic lipid binding activity of ATG16L1 supports efficient membrane anchoring and autophagy. *The EMBO journal* 2019, **38**(9).
13. Lee Y, Weihl CC. Regulation of SQSTM1/p62 via UBA domain ubiquitination and its role in disease. *Autophagy* 2017, **13**(9)**:** 1615-1616.
14. Takamura A, Komatsu M, Hara T, Sakamoto A, Kishi C, Waguri S*, et al.* Autophagy-deficient mice develop multiple liver tumors. *Genes & development* 2011, **25**(8)**:** 795-800.
15. Yue Z, Jin S, Yang C, Levine AJ, Heintz N. Beclin 1, an autophagy gene essential for early embryonic development, is a haploinsufficient tumor suppressor. *Proceedings of the National Academy of Sciences of the United States of America* 2003, **100**(25)**:** 15077-15082.
16. Goussetis DJ, Gounaris E, Wu EJ, Vakana E, Sharma B, Bogyo M*, et al.* Autophagic degradation of the BCR-ABL oncoprotein and generation of antileukemic responses by arsenic trioxide. *Blood* 2012, **120**(17)**:** 3555-3562.
17. Isakson P, Bjoras M, Boe SO, Simonsen A. Autophagy contributes to therapy-induced degradation of the PML/RARA oncoprotein. *Blood* 2010, **116**(13)**:** 2324-2331.
18. Larrue C, Saland E, Boutzen H, Vergez F, David M, Joffre C*, et al.* Proteasome inhibitors induce FLT3-ITD degradation through autophagy in AML cells. *Blood* 2016, **127**(7)**:** 882-892.
19. Li P, Ji M, Lu F, Zhang J, Li H, Cui T*, et al.* Degradation of AF1Q by chaperone-mediated autophagy. *Experimental cell research* 2014, **327**(1)**:** 48-56.
20. Degenhardt K, Mathew R, Beaudoin B, Bray K, Anderson D, Chen G*, et al.* Autophagy promotes tumor cell survival and restricts necrosis, inflammation, and tumorigenesis. *Cancer cell* 2006, **10**(1)**:** 51-64.
21. Martinez-Outschoorn UE, Balliet RM, Rivadeneira DB, Chiavarina B, Pavlides S, Wang C*, et al.* Oxidative stress in cancer associated fibroblasts drives tumor-stroma co-evolution: A new paradigm for understanding tumor metabolism, the field effect and genomic instability in cancer cells. *Cell cycle (Georgetown, Tex)* 2010, **9**(16)**:** 3256-3276.

22. Mathew R, Karantza-Wadsworth V, White E. Assessing metabolic stress and autophagy status in epithelial tumors. *Methods in enzymology* 2009, **453:** 53-81.
23. New J, Arnold L, Ananth M, Alvi S, Thornton M, Werner L*, et al.* Secretory Autophagy in Cancer-Associated Fibroblasts Promotes Head and Neck Cancer Progression and Offers a Novel Therapeutic Target. *Cancer research* 2017, **77**(23)**:** 6679-6691.
24. Rouschop KM, van den Beucken T, Dubois L, Niessen H, Bussink J, Savelkouls K*, et al.* The unfolded protein response protects human tumor cells during hypoxia through regulation of the autophagy genes MAP1LC3B and ATG5. *The Journal of clinical investigation* 2010, **120**(1)**:** 127-141.
25. Karantza-Wadsworth V, Patel S, Kravchuk O, Chen G, Mathew R, Jin S*, et al.* Autophagy mitigates metabolic stress and genome damage in mammary tumorigenesis. *Genes & development* 2007, **21**(13)**:** 1621-1635.
26. Lazova R, Camp RL, Klump V, Siddiqui SF, Amaravadi RK, Pawelek JM. Punctate LC3B expression is a common feature of solid tumors and associated with proliferation, metastasis, and poor outcome. *Clinical cancer research : an official journal of the American Association for Cancer Research* 2012, **18**(2)**:** 370-379.
27. Wiedmer T, Blank A, Pantasis S, Normand L, Bill R, Krebs P*, et al.* Autophagy Inhibition Improves Sunitinib Efficacy in Pancreatic Neuroendocrine Tumors via a Lysosome-dependent Mechanism. *Molecular cancer therapeutics* 2017, **16**(11)**:** 2502-2515.
28. Cook KL, Warri A, Soto-Pantoja DR, Clarke PA, Cruz MI, Zwart A*, et al.* Hydroxychloroquine inhibits autophagy to potentiate antiestrogen responsiveness in ER+ breast cancer. *Clinical cancer research : an official journal of the American Association for Cancer Research* 2014, **20**(12)**:** 3222-3232.
29. Degtyarev M, De Maziere A, Orr C, Lin J, Lee BB, Tien JY*, et al.* Akt inhibition promotes autophagy and sensitizes PTEN-null tumors to lysosomotropic agents. *The Journal of cell biology* 2008, **183**(1)**:** 101-116.
30. Ratikan JA, Sayre JW, Schaue D. Chloroquine engages the immune system to eradicate irradiated breast tumors in mice. *International journal of radiation oncology, biology, physics* 2013, **87**(4)**:** 761-768.
31. Chen JL, David J, Cook-Spaeth D, Casey S, Cohen D, Selvendiran K*, et al.* Autophagy Induction Results in Enhanced Anoikis Resistance in Models of Peritoneal Disease. *Molecular cancer research : MCR* 2017, **15**(1)**:** 26-34.
32. Cui L, Song Z, Liang B, Jia L, Ma S, Liu X. Radiation induces autophagic cell death via the p53/DRAM signaling pathway in breast cancer cells. *Oncology reports* 2016, **35**(6)**:** 3639-3647.
33. Kim DE, Kim Y, Cho DH, Jeong SY, Kim SB, Suh N*, et al.* Raloxifene induces autophagy-dependent cell death in breast cancer cells via the activation of AMP-activated protein kinase. *Molecules and cells* 2015, **38**(2)**:** 138-144.
34. Peng PL, Kuo WH, Tseng HC, Chou FP. Synergistic tumor-killing effect of radiation and berberine combined treatment in lung cancer: the contribution of autophagic cell death. *International journal of radiation oncology, biology, physics* 2008, **70**(2)**:** 529-542.
35. Yu P, Zhang C, Gao CY, Ma T, Zhang H, Zhou MM*, et al.* Anti-proliferation of triple-negative breast cancer cells with physagulide P: ROS/JNK signaling pathway induces apoptosis and autophagic cell death. *Oncotarget* 2017, **8**(38)**:** 64032-64049.
36. Zhang XD. Illustration of SSMD, z score, SSMD*, z* score, and t statistic for hit selection in RNAi high-throughput screens. *Journal of biomolecular screening* 2011, **16**(7)**:** 775-785.
37. Werner J, Ebrahim W, Ozkaya FC, Mandi A, Kurtan T, El-Neketi M*, et al.* Pyrone derivatives from Helichrysum italicum. *Fitoterapia* 2019, **133:** 80-84.
38. Appendino G, Ottino M, Marquez N, Bianchi F, Giana A, Ballero M*, et al.* Arzanol, an anti-inflammatory and anti-HIV-1 phloroglucinol alpha-Pyrone from Helichrysum italicum ssp. microphyllum. *Journal of natural products* 2007, **70**(4)**:** 608-612.

39. Rosa A, Atzeri A, Nieddu M, Appendino G. New insights into the antioxidant activity and cytotoxicity of arzanol and effect of methylation on its biological properties. *Chemistry and physics of lipids* 2017, **205:** 55-64.
40. Kaizuka T, Morishita H, Hama Y, Tsukamoto S, Matsui T, Toyota Y*, et al.* An Autophagic Flux Probe that Releases an Internal Control. *Molecular cell* 2016, **64**(4)**:** 835-849.
41. Inoki K, Li Y, Zhu T, Wu J, Guan KL. TSC2 is phosphorylated and inhibited by Akt and suppresses mTOR signalling. *Nature cell biology* 2002, **4**(9)**:** 648-657.
42. Inoki K, Li Y, Xu T, Guan KL. Rheb GTPase is a direct target of TSC2 GAP activity and regulates mTOR signaling. *Genes & development* 2003, **17**(15)**:** 1829-1834.
43. Saitoh M, Pullen N, Brennan P, Cantrell D, Dennis PB, Thomas G. Regulation of an activated S6 kinase 1 variant reveals a novel mammalian target of rapamycin phosphorylation site. *The Journal of biological chemistry* 2002, **277**(22)**:** 20104-20112.
44. Shang L, Chen S, Du F, Li S, Zhao L, Wang X. Nutrient starvation elicits an acute autophagic response mediated by Ulk1 dephosphorylation and its subsequent dissociation from AMPK. *Proceedings of the National Academy of Sciences of the United States of America* 2011, **108**(12)**:** 4788-4793.
45. Alers S, Loffler AS, Wesselborg S, Stork B. Role of AMPK-mTOR-Ulk1/2 in the regulation of autophagy: cross talk, shortcuts, and feedbacks. *Molecular and cellular biology* 2012, **32**(1)**:** 2-11.
46. Mizushima N, Yoshimori T. How to interpret LC3 immunoblotting. *Autophagy* 2007, **3**(6)**:** 542-545.
47. Klionsky DJ, Abdelmohsen K, Abe A, Abedin MJ, Abeliovich H, Acevedo Arozena A*, et al.* Guidelines for the use and interpretation of assays for monitoring autophagy (3rd edition). *Autophagy* 2016, **12**(1)**:** 1-222.
48. Dooley HC, Razi M, Polson HE, Girardin SE, Wilson MI, Tooze SA. WIPI2 links LC3 conjugation with PI3P, autophagosome formation, and pathogen clearance by recruiting Atg12-5-16L1. *Molecular cell* 2014, **55**(2)**:** 238-252.
49. Polson HE, de Lartigue J, Rigden DJ, Reedijk M, Urbe S, Clague MJ*, et al.* Mammalian Atg18 (WIPI2) localizes to omegasome-anchored phagophores and positively regulates LC3 lipidation. *Autophagy* 2010, **6**(4)**:** 506-522.
50. Wallot-Hieke N, Verma N, Schlutermann D, Berleth N, Deitersen J, Bohler P*, et al.* Systematic analysis of ATG13 domain requirements for autophagy induction. *Autophagy* 2018, **14**(5)**:** 743-763.
51. Quan Y, Lei H, Wahafu W, Liu Y, Ping H, Zhang X. Inhibition of autophagy enhances the anticancer effect of enzalutamide on bladder cancer. *Biomedicine & pharmacotherapy = Biomedecine & pharmacotherapie* 2019, **120:** 109490.
52. Schlütermann D, Skowron MA, Berleth N, Böhler P, Deitersen J, Stuhldreier F*, et al.* Targeting urothelial carcinoma cells by combining cisplatin with a specific inhibitor of the autophagy-inducing class III PtdIns3K complex. *Urologic oncology* 2018, **36**(4)**:** 160.e161-160.e113.
53. White E, DiPaola RS. The double-edged sword of autophagy modulation in cancer. *Clinical cancer research : an official journal of the American Association for Cancer Research* 2009, **15**(17)**:** 5308-5316.
54. Hamid R, Rotshteyn Y, Rabadi L, Parikh R, Bullock P. Comparison of alamar blue and MTT assays for high through-put screening. *Toxicology in vitro : an international journal published in association with BIBRA* 2004, **18**(5)**:** 703-710.
55. Vives-Bauza C, Zhou C, Huang Y, Cui M, de Vries RL, Kim J*, et al.* PINK1-dependent recruitment of Parkin to mitochondria in mitophagy. *Proceedings of the National Academy of Sciences of the United States of America* 2010, **107**(1)**:** 378-383.
56. Tanaka A, Cleland MM, Xu S, Narendra DP, Suen DF, Karbowski M*, et al.* Proteasome and p97 mediate mitophagy and degradation of mitofusins induced by Parkin. *The Journal of cell biology* 2010, **191**(7)**:** 1367-1380.
57. Twig G, Shirihai OS. The interplay between mitochondrial dynamics and mitophagy. *Antioxidants & redox signaling* 2011, **14**(10)**:** 1939-1951.

58. Fujita N, Itoh T, Omori H, Fukuda M, Noda T, Yoshimori T. The Atg16L complex specifies the site of LC3 lipidation for membrane biogenesis in autophagy. *Molecular biology of the cell* 2008, **19**(5)**:** 2092-2100.
59. Itakura E, Mizushima N. Characterization of autophagosome formation site by a hierarchical analysis of mammalian Atg proteins. *Autophagy* 2010, **6**(6)**:** 764-776.
60. Wong YC, Holzbaur EL. Temporal dynamics of PARK2/parkin and OPTN/optineurin recruitment during the mitophagy of damaged mitochondria. *Autophagy* 2015, **11**(2)**:** 422-424.
61. Bansal M, Moharir SC, Sailasree SP, Sirohi K, Sudhakar C, Sarathi DP*, et al.* Optineurin promotes autophagosome formation by recruiting the autophagy-related Atg12-5-16L1 complex to phagophores containing the Wipi2 protein. *The Journal of biological chemistry* 2018, **293**(1)**:** 132-147.
62. Moore AS, Holzbaur EL. Dynamic recruitment and activation of ALS-associated TBK1 with its target optineurin are required for efficient mitophagy. *Proceedings of the National Academy of Sciences of the United States of America* 2016, **113**(24)**:** E3349-3358.
63. Wild P, Farhan H, McEwan DG, Wagner S, Rogov VV, Brady NR*, et al.* Phosphorylation of the autophagy receptor optineurin restricts Salmonella growth. *Science (New York, NY)* 2011, **333**(6039)**:** 228-233.
64. Itakura E, Kishi-Itakura C, Koyama-Honda I, Mizushima N. Structures containing Atg9A and the ULK1 complex independently target depolarized mitochondria at initial stages of Parkin-mediated mitophagy. *Journal of cell science* 2012, **125**(Pt 6)**:** 1488-1499.
65. Heo JM, Ordureau A, Paulo JA, Rinehart J, Harper JW. The PINK1-PARKIN Mitochondrial Ubiquitylation Pathway Drives a Program of OPTN/NDP52 Recruitment and TBK1 Activation to Promote Mitophagy. *Molecular cell* 2015, **60**(1)**:** 7-20.
66. Lazarou M, Sliter DA, Kane LA, Sarraf SA, Wang C, Burman JL*, et al.* The ubiquitin kinase PINK1 recruits autophagy receptors to induce mitophagy. *Nature* 2015, **524**(7565)**:** 309-314.
67. Duvezin-Caubet S, Jagasia R, Wagener J, Hofmann S, Trifunovic A, Hansson A*, et al.* Proteolytic processing of OPA1 links mitochondrial dysfunction to alterations in mitochondrial morphology. *The Journal of biological chemistry* 2006, **281**(49)**:** 37972-37979.
68. Baricault L, Segui B, Guegand L, Olichon A, Valette A, Larminat F*, et al.* OPA1 cleavage depends on decreased mitochondrial ATP level and bivalent metals. *Experimental cell research* 2007, **313**(17)**:** 3800-3808.
69. Guillery O, Malka F, Landes T, Guillou E, Blackstone C, Lombes A*, et al.* Metalloprotease-mediated OPA1 processing is modulated by the mitochondrial membrane potential. *Biology of the cell* 2008, **100**(5)**:** 315-325.
70. Ishihara N, Fujita Y, Oka T, Mihara K. Regulation of mitochondrial morphology through proteolytic cleavage of OPA1. *The EMBO journal* 2006, **25**(13)**:** 2966-2977.
71. Benit P, Lebon S, Rustin P. Respiratory-chain diseases related to complex III deficiency. *Biochimica et biophysica acta* 2009, **1793**(1)**:** 181-185.
72. Byun HO, Kim HY, Lim JJ, Seo YH, Yoon G. Mitochondrial dysfunction by complex II inhibition delays overall cell cycle progression via reactive oxygen species production. *Journal of cellular biochemistry* 2008, **104**(5)**:** 1747-1759.
73. Kwon J, Han E, Bui CB, Shin W, Lee J, Lee S*, et al.* Assurance of mitochondrial integrity and mammalian longevity by the p62-Keap1-Nrf2-Nqo1 cascade. *EMBO reports* 2012, **13**(2)**:** 150-156.
74. Li Y, Huang TT, Carlson EJ, Melov S, Ursell PC, Olson JL*, et al.* Dilated cardiomyopathy and neonatal lethality in mutant mice lacking manganese superoxide dismutase. *Nature genetics* 1995, **11**(4)**:** 376-381.
75. Voets AM, Huigsloot M, Lindsey PJ, Leenders AM, Koopman WJ, Willems PH*, et al.* Transcriptional changes in OXPHOS complex I deficiency are related to anti-oxidant pathways and could explain the disturbed calcium homeostasis. *Biochimica et biophysica acta* 2012, **1822**(7)**:** 1161-1168.

76. Yoshida S, Tsutsumi S, Muhlebach G, Sourbier C, Lee MJ, Lee S*, et al.* Molecular chaperone TRAP1 regulates a metabolic switch between mitochondrial respiration and aerobic glycolysis. *Proceedings of the National Academy of Sciences of the United States of America* 2013, **110**(17)**:** E1604-1612.
77. Zhang L, Karsten P, Hamm S, Pogson JH, Muller-Rischart AK, Exner N*, et al.* TRAP1 rescues PINK1 loss-of-function phenotypes. *Human molecular genetics* 2013, **22**(14)**:** 2829-2841.
78. Mochizuki Y, Ohashi R, Kawamura T, Iwanari H, Kodama T, Naito M*, et al.* Phosphatidylinositol 3-phosphatase myotubularin-related protein 6 (MTMR6) is regulated by small GTPase Rab1B in the early secretory and autophagic pathways. *The Journal of biological chemistry* 2013, **288**(2)**:** 1009-1021.
79. Ao X, Zou L, Wu Y. Regulation of autophagy by the Rab GTPase network. *Cell death and differentiation* 2014, **21**(3)**:** 348-358.
80. Kakuta S, Yamaguchi J, Suzuki C, Sasaki M, Kazuno S, Uchiyama Y. Small GTPase Rab1B is associated with ATG9A vesicles and regulates autophagosome formation. *FASEB journal : official publication of the Federation of American Societies for Experimental Biology* 2017, **31**(9)**:** 3757-3773.
81. Zoppino FC, Militello RD, Slavin I, Alvarez C, Colombo MI. Autophagosome formation depends on the small GTPase Rab1 and functional ER exit sites. *Traffic (Copenhagen, Denmark)* 2010, **11**(9)**:** 1246-1261.
82. Winslow AR, Chen CW, Corrochano S, Acevedo-Arozena A, Gordon DE, Peden AA*, et al.* alpha-Synuclein impairs macroautophagy: implications for Parkinson's disease. *The Journal of cell biology* 2010, **190**(6)**:** 1023-1037.
83. Wang B, Chen Z, Yu F, Chen Q, Tian Y, Ma S*, et al.* Hsp90 regulates autophagy and plays a role in cancer therapy. *Tumour biology : the journal of the International Society for Oncodevelopmental Biology and Medicine* 2016, **37**(1)**:** 1-6.
84. Bandyopadhyay U, Kaushik S, Varticovski L, Cuervo AM. The chaperone-mediated autophagy receptor organizes in dynamic protein complexes at the lysosomal membrane. *Molecular and cellular biology* 2008, **28**(18)**:** 5747-5763.
85. Eskelinen EL, Illert AL, Tanaka Y, Schwarzmann G, Blanz J, Von Figura K*, et al.* Role of LAMP-2 in lysosome biogenesis and autophagy. *Molecular biology of the cell* 2002, **13**(9)**:** 3355-3368.
86. Huynh KK, Eskelinen EL, Scott CC, Malevanets A, Saftig P, Grinstein S. LAMP proteins are required for fusion of lysosomes with phagosomes. *The EMBO journal* 2007, **26**(2)**:** 313-324.
87. Tanida I, Minematsu-Ikeguchi N, Ueno T, Kominami E. Lysosomal turnover, but not a cellular level, of endogenous LC3 is a marker for autophagy. *Autophagy* 2005, **1**(2)**:** 84-91.
88. Zhang X, Garbett K, Veeraraghavalu K, Wilburn B, Gilmore R, Mirnics K*, et al.* A role for presenilins in autophagy revisited: normal acidification of lysosomes in cells lacking PSEN1 and PSEN2. *The Journal of neuroscience : the official journal of the Society for Neuroscience* 2012, **32**(25)**:** 8633-8648.
89. Alfred Witjes J, Lebret T, Comperat EM, Cowan NC, De Santis M, Bruins HM*, et al.* Updated 2016 EAU Guidelines on Muscle-invasive and Metastatic Bladder Cancer. *European urology* 2017, **71**(3)**:** 462-475.
90. Abdel Karim NF, Ahmad I, Gaber O, Eldessouki I, Olowokure OO, Farooq M*, et al.* Phase I trial of chloroquine (CQ)/hydroxychloroquine (HCQ) in combination with carboplatin-gemcitabine (CG) in patients with advanced solid tumors. American Society of Clinical Oncology; 2019.
91. Qin L, Xu T, Xia L, Wang X, Zhang X, Zhang X*, et al.* Chloroquine enhances the efficacy of cisplatin by suppressing autophagy in human adrenocortical carcinoma treatment. *Drug design, development and therapy* 2016, **10:** 1035-1045.
92. Yu L, Gu C, Zhong D, Shi L, Kong Y, Zhou Z*, et al.* Induction of autophagy counteracts the anticancer effect of cisplatin in human esophageal cancer cells with acquired drug resistance. *Cancer letters* 2014, **355**(1)**:** 34-45.
93. Zhang HQ, Fang N, Liu XM, Xiong SP, Liao YQ, Jin WJ*, et al.* Antitumor activity of chloroquine in combination with Cisplatin in human gastric cancer xenografts. *Asian Pacific journal of cancer prevention : APJCP* 2015, **16**(9)**:** 3907-3912.

94. Zhao XG, Sun RJ, Yang XY, Liu DY, Lei DP, Jin T*, et al.* Chloroquine-enhanced efficacy of cisplatin in the treatment of hypopharyngeal carcinoma in xenograft mice. *PloS one* 2015, **10**(4)**:** e0126147.
95. Barrera M, Koob S, Dikov D, Vogel F, Reichert AS. OPA1 functionally interacts with MIC60 but is dispensable for crista junction formation. *FEBS Lett* 2016, **590**(19)**:** 3309-3322.
96. Hieke N, Loffler AS, Kaizuka T, Berleth N, Bohler P, Driessen S*, et al.* Expression of a ULK1/2 binding-deficient ATG13 variant can partially restore autophagic activity in ATG13-deficient cells. *Autophagy* 2015, **11**(9)**:** 1471-1483.

Supplementary Methods

Image J Macro for quantification of DAPI-positive nuclei

```
dir1 = getDirectory("INPUT");
dir2 = getDirectory("OUTPUT");
setBatchMode(true);
list = getFileList(dir1);
for (i=0; i<list.length; i++)
  {
    open(dir1+list[i]);
    title = File.nameWithoutExtension ;
          run("Split Channels");
           saveAs("Tiff", dir2+title+"_DAPI.tif");
                                        close();
                                        close();

                          open(dir2+title+"_DAPI.tif");
                           run("Unsharp Mask...", "radius=500 mask=0.90");
                           run("Median...", "radius=10");
                           run("Make Binary");
                           run("Fill Holes");
                           run("Adjustable Watershed", "tolerance=9");
                           run("Analyze Particles...", "size=6-Infinity summarize");
                           saveAs("Tiff", dir2+title+"_DAPI_counts.tif");
                                close();

}
setBatchMode(false);
selectWindow("Results");
saveAs("Results", output + filename + ".csv");
showMessage("You're awesome!");
exit();
```

Image J Macro for quantification of LC3-positive dots

```
dir1 = getDirectory("INPUT");
dir2 = getDirectory("OUTPUT");
setBatchMode(true);
list = getFileList(dir1);
for (i=0; i<list.length; i++)
  {
    open(dir1+list[i]);
    title = File.nameWithoutExtension ;
          run("Split Channels");
           saveAs("Tiff", dir2+title+"_LC3L.tif");
                                    close();
                                    close();



                                                  run("Subtract Background...",
"rolling=60");
                                                  setThreshold(75, 255);
                                  run("Convert to Mask");
                                  run("Watershed");
                                  run("Analyze Particles...", "  summarize");
                                          saveAs("Tiff", dir2+title+"_LC3_binary.tif");
                                                  close();



}
setBatchMode(false);
selectWindow("Results");
saveAs("Results", output + filename + ".csv");
showMessage("You're awesome!");
exit();
```

Image J Macro for quantification of ATG16L1-positive dots

```
dir1 = getDirectory("INPUT");
dir2 = getDirectory("OUTPUT");
setBatchMode(true);
list = getFileList(dir1);
for (i=0; i<list.length; i++)
  {
    open(dir1+list[i]);
    title = File.nameWithoutExtension ;
        run("Split Channels");
         saveAs("Tiff", dir2+title+"_ATG16L.tif");
                                    close();
                                    close();

                                                run("Gaussian Blur...", "sigma=3");
                                                run("Subtract Background...", "rolling=8");

                                                setThreshold(50, 255);
                                    run("Convert to Mask");
                                    run("Watershed");
                                    run("Analyze Particles...", "  summarize");
                                            saveAs("Tiff", dir2+title+"_ATG16L_binary.tif");
                                                close();

}
setBatchMode(false);
selectWindow("Summary");
saveAs("Text", dir2+"Summary2.txt");
showMessage("You're awesome!");
exit();
```

Image J Macro for quantification of WIPI2-positive dots

```
dir1 = getDirectory("INPUT");
dir2 = getDirectory("OUTPUT");
setBatchMode(true);
list = getFileList(dir1);
for (i=0; i<list.length; i++)
   {
     open(dir1+list[i]);
     title = File.nameWithoutExtension ;
          run("Split Channels");
           saveAs("Tiff", dir2+title+"_WIPI2.tif");
                                    close();
                                    close();
                                    run("Gaussian Blur...", "sigma=3");
                                                run("Subtract Background...", "rolling=6");
                                                setThreshold(40, 255);
                                        run("Convert to Mask");
                                        run("Analyze Particles...", "  summarize");
                                                saveAs("Tiff", dir2+title+"_WIPI2_binary.tif");
                                                close();

}
setBatchMode(false);
selectWindow("Summary");
saveAs("Text", dir2+"Summary2.txt");
showMessage("You're awesome!");
exit();
```

Publication 4

The mycotoxin phomoxanthone A disturbs the form and function of the inner mitochondrial membrane

Philip Böhler, Fabian Stuhldreier, Ruchika Anand, Arun Kumar Kondadi, David Schlütermann, Niklas Berleth, Jana Deitersen, Nora Wallot-Hieke, Wenxian Wu, Marian Frank, Hendrik Niemann, Elisabeth Wesbuer, Andreas Barbian, Tomas Luyten, Jan B. Parys, Stefanie Weidtkamp-Peters, Andrea Borchardt, Andreas S. Reichert, Aida Peña-Blanco, Ana J. García-Sáez, Samuel Itskanov, Alexander M. van der Bliek, Peter Proksch, Sebastian Wesselborg, Björn Stork

Cell Death and Disease, 19;9(3):286, February 2018.

DOI: 10.1038/s41419-018-0312-8

Böhler et al. *Cell Death and Disease* (2018)9:286
DOI 10.1038/s41419-018-0312-8

Cell Death & Disease

ARTICLE Open Access

The mycotoxin phomoxanthone A disturbs the form and function of the inner mitochondrial membrane

Philip Böhler[1], Fabian Stuhldreier[1], Ruchika Anand[2], Arun Kumar Kondadi[2], David Schlütermann[1], Niklas Berleth[1], Jana Deitersen[1], Nora Wallot-Hieke[1], Wenxian Wu[1], Marian Frank[3], Hendrik Niemann[3], Elisabeth Wesbuer[4], Andreas Barbian[4], Tomas Luyten[5], Jan B. Parys[5], Stefanie Weidtkamp-Peters[6], Andrea Borchardt[2], Andreas S. Reichert[2], Aida Peña-Blanco[7], Ana J. García-Sáez[7], Samuel Itskanov[8], Alexander M. van der Bliek[8], Peter Proksch[3], Sebastian Wesselborg[1] and Björn Stork[1]

Abstract

Mitochondria are cellular organelles with crucial functions in the generation and distribution of ATP, the buffering of cytosolic Ca^{2+} and the initiation of apoptosis. Compounds that interfere with these functions are termed mitochondrial toxins, many of which are derived from microbes, such as antimycin A, oligomycin A, and ionomycin. Here, we identify the mycotoxin phomoxanthone A (PXA), derived from the endophytic fungus *Phomopsis longicolla*, as a mitochondrial toxin. We show that PXA elicits a strong release of Ca^{2+} from the mitochondria but not from the ER. In addition, PXA depolarises the mitochondria similarly to protonophoric uncouplers such as CCCP, yet unlike these, it does not increase but rather inhibits cellular respiration and electron transport chain activity. The respiration-dependent mitochondrial network structure rapidly collapses into fragments upon PXA treatment. Surprisingly, this fragmentation is independent from the canonical mitochondrial fission and fusion mediators DRP1 and OPA1, and exclusively affects the inner mitochondrial membrane, leading to cristae disruption, release of pro-apoptotic proteins, and apoptosis. Taken together, our results suggest that PXA is a mitochondrial toxin with a novel mode of action that might prove a useful tool for the study of mitochondrial ion homoeostasis and membrane dynamics.

Introduction

Mitochondria are cellular organelles that are crucial to almost all eukaryotic organisms. Among their most important functions are generation and distribution of ATP, buffering of cytosolic Ca^{2+} and, in animal cells, initiation of apoptosis. Disturbance of these or other functions by mitochondrial toxins can lead to cellular stress and cell death[1,2].

Mitochondria produce ATP through oxidative phosphorylation (OXPHOS), which depends on the electron transport chain (ETC) embedded in the inner mitochondrial membrane (IMM). The ETC pumps protons out of the mitochondrial matrix and into the mitochondrial intermembrane space. This generates a proton gradient (ΔpH_m) and, consequently, a membrane potential ($\Delta\Psi_m$) across the IMM. The $\Delta\Psi_m$ is then used to drive the mitochondrial ATP synthase[3].

To provide all regions within the cell with sufficient ATP, mitochondria often form a network that constantly undergoes balanced fission and fusion. This allows

Correspondence: Sebastian Wesselborg (sebastian.wesselborg@uni-duesseldorf.de) or Björn Stork (bjoern.stork@uni-duesseldorf.de)
[1]Institute of Molecular Medicine I, Medical Faculty, Heinrich Heine University Düsseldorf, 40225 Düsseldorf, Germany
[2]Institute of Biochemistry and Molecular Biology I, Medical Faculty, Heinrich Heine University Düsseldorf, 40225 Düsseldorf, Germany
Full list of author information is available at the end of the article
Philip Böhler, Fabian Stuhldreier, Sebastian Wesselborg, Björn Stork contributed equally to this work.
Edited by G. Raschellà

SPRINGER NATURE CDDpress

remodelling of the network as well as removal and recycling of damaged mitochondria through mitophagy[1,4,5]. Excessive fission can be triggered by mitochondrial toxins that cause loss of $\Delta\Psi_m$, such as the protonophore carbonyl cyanide *m*-chlorophenyl hydrazone (CCCP)[6].

The $\Delta\Psi_m$ also plays a role in the mitochondrial buffering of cytosolic Ca^{2+}. Normally, the cytosol of a typical animal cell contains only a very low Ca^{2+} concentration ($[Ca^{2+}]_{cyt}$, ~0.1 μM), whereas the concentration of Ca^{2+} within the endoplasmic reticulum ($[Ca^{2+}]_{ER}$, > 100 μM) or outside the cell ($[Ca^{2+}]_{ext}$, > 1000 μM) is up to 10,000-fold higher[2]. In response to certain stimuli, Ca^{2+} channels in the ER and/or the plasma membrane open to release Ca^{2+} into the cytosol as a second messenger. Mitochondria contribute to removal of cytosolic Ca^{2+} by uptake into their matrix via $\Delta\Psi_m$-driven Ca^{2+} transporters. After that, a slow, regulated efflux moves the Ca^{2+} out of the matrix and into the cristae, which are folds in the IMM, from where it is slowly released and shuttled back to the ER[2,7–9]. A separate mechanism through which Ca^{2+} can cross the IMM is the mitochondrial permeability transition pore (mPTP), which can open irreversibly in response to severe mitochondrial stress. The mPTP directly connects the mitochondrial matrix with the cytosol to allow the free exchange of molecules up to 1.5 kDa in size, including Ca^{2+}. Irreversible mPTP opening leads to release of mitochondrial Ca^{2+}, loss of $\Delta\Psi_m$, swelling of the matrix and eventually mitochondrial outer membrane permeabilisation (MOMP)[10,11].

In animal cells, MOMP initiates apoptosis. Several proteins normally contained in the cristae attain a pro-apoptotic function if they pass the outer mitochondrial membrane (OMM) and are released into the cytosol. Among these proteins are cytochrome c (CYCS), SMAC (DIABLO) and OMI (HTRA2). Cytosolic CYCS becomes part of the caspase-activating apoptosome complex, while DIABLO and HTRA2 bind and inhibit the inhibitor of apoptosis proteins (IAPs), thus attenuating their inhibition of caspases[1]. MOMP can be caused either passively through rupture of the OMM, such as triggered by the mPTP, or actively through the formation of pores in the OMM by the pro-apoptotic proteins BAK and BAX, which can be induced in response to severe cellular stress[12].

A variety of mitochondrial toxins with different effects and molecular targets is known today[13]. Several of these toxins are natural products, such as the *Streptomyces*-derived ETC inhibitor antimycin A and the ATP synthase inhibitor oligomycin A.

Phomoxanthone A and B (PXA and PXB) are natural products named after the fungus *Phomopsis*, from which they were first isolated, and after their xanthonoid structure (Fig. S1). PXA is a homodimer of two acetylated tetrahydroxanthones symmetrically linked at C-4,4', whereas PXB is structurally almost identical but asymmetrically linked at C-2,4'. Both possess antibiotic activity against diverse organisms from all biological kingdoms. Originally described in 2001, PXA and PXB were tested against the protozoan *Plasmodium falciparum*, the Gram-positive *Mycobacterium tuberculosis*, and three animal cell lines. In all of these organisms, both PXA and PXB showed significant cytotoxic activity, with PXA being more toxic in every case[14]. A later study in different organisms produced similar results, showing that PXA inhibits the growth of the Gram-positive *Bacillus megaterium*, the alga *Chlorella fusca*, and the fungus *Ustilago violacea*[15].

We previously showed that PXA induces apoptosis in human cancer cell lines. Signs of apoptosis were observed as early as after 4 h of treatment with low micromolar doses of PXA[16,17]. However, the mechanism by which PXA causes apoptosis or cytotoxicity in general has never before been investigated.

The aim of this study was to elucidate the mechanism through which PXA exerts its toxicity. Following our initial results, we hypothesised that PXA directly affects the mitochondria and thus investigated its effects on the ETC, $\Delta\Psi_m$, ATP production, Ca^{2+} buffering, and mitochondrial morphology. It appears that PXA is a mitochondrial toxin that specifically affects the IMM, leading to loss of $\Delta\Psi_m$, ETC inhibition, Ca^{2+} efflux, mitochondrial fragmentation, cristae disruption, and finally to the release of mitochondrial pro-apoptotic factors.

Results

PXA induces Ca^{2+} release from an intracellular store

To determine how PXA induces apoptosis, we analysed its effect on cellular Ca^{2+} levels since ionic imbalance can be an apoptotic trigger. Treatment of Ramos cells with PXA resulted in a strong, steady increase of $[Ca^{2+}]_{cyt}$ (Fig. 1a). Interestingly, there was a delay of about 2–5 min between addition of PXA and increase in $[Ca^{2+}]_{cyt}$. Since this pattern of Ca^{2+} release is similar to that caused by the tyrosine phosphatase inhibitor pervanadate (VO_4^{3-}) (Fig. S2a), and since tyrosine phosphatase inhibition can induce apoptosis, we tested the effect of PXA on tyrosine phosphorylation. However, in contrast to pervanadate, we could not detect any effect (Fig. S2b). In a broader picture, PXA had no inhibitory effect on any of 141 protein kinases against which we tested it (Table S1).

We next tried to determine the origin of the released Ca^{2+}. Since PXA increases $[Ca^{2+}]_{cyt}$ even in the absence of extracellular Ca^{2+}, we tested if it releases Ca^{2+} from the ER. Using thapsigargin, which causes a net efflux of Ca^{2+} from the ER, we could induce an increase in $[Ca^{2+}]_{cyt}$ even after PXA-inducible Ca^{2+} stores were depleted

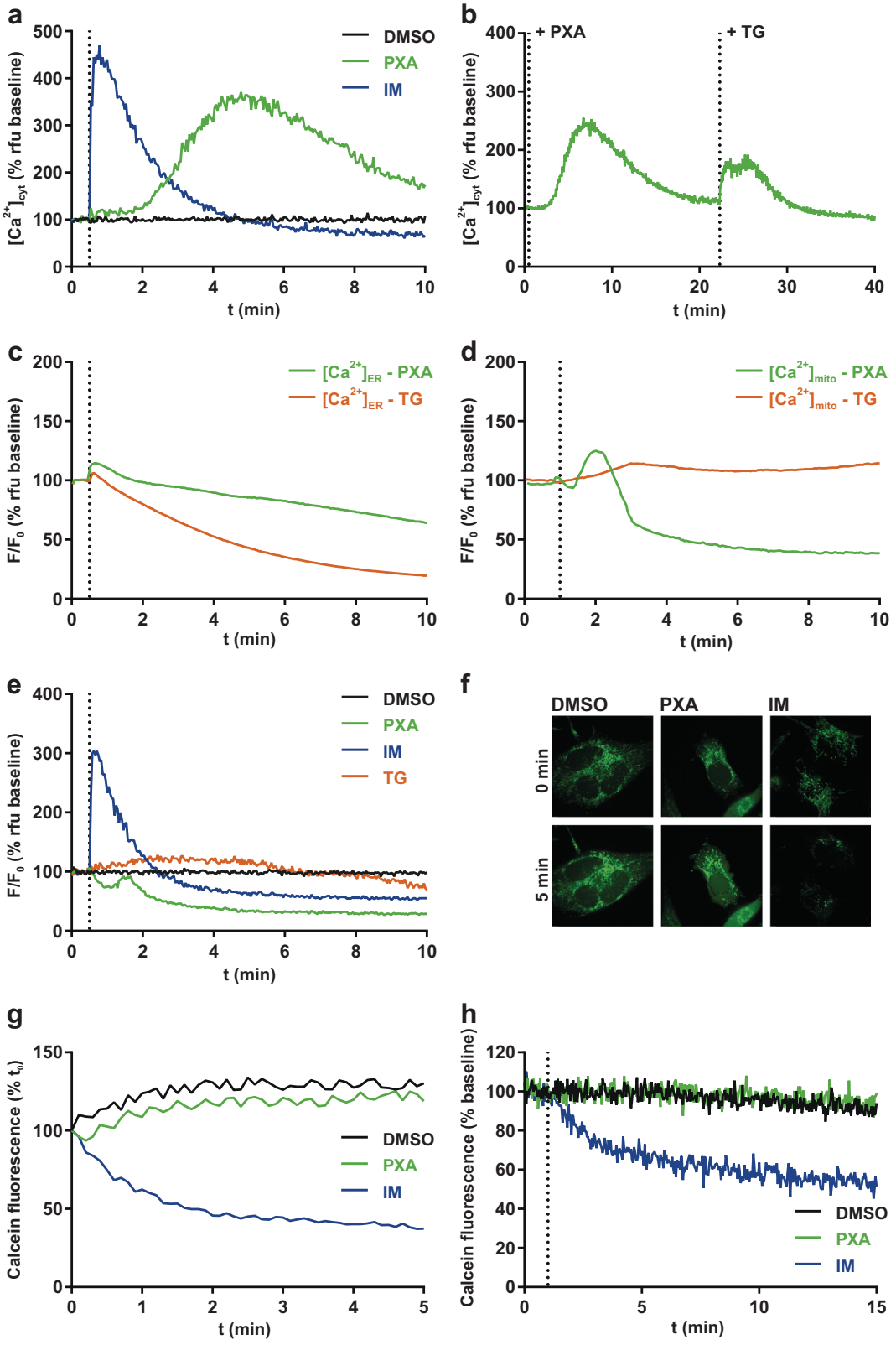

Fig. 1 (See legend on next page.)

Fig. 1 PXA causes an increase of $[Ca^{2+}]_{cyt}$ and a release of $[Ca^{2+}]_{mito}$ but not $[Ca^{2+}]_{ER}$. a Live measurement of the effect of PXA (10 μM) on $[Ca^{2+}]_{cyt}$ in Ramos cells, where DMSO (0.1% v/v) was used as vehicle control and ionomycin (IM; 2 μM) was used as positive control, and **b** live measurement of $[Ca^{2+}]_{cyt}$ after PXA followed by thapsigargin (TG; 10 μM). Measurements were performed by flow cytometry using the Ca^{2+}-sensitive fluorescent probe Fluo-4-AM (Ex 488 nm, Em 530 ± 30 nm) in the absence of extracellular Ca^{2+} by maintaining the cells in Krebs-Ringer buffer containing 0.5 mM EGTA during measurement. **c**, **d** Comparison of the effect of PXA (10 μM) and thapsigargin (TG; 1 μM) on either $[Ca^{2+}]_{ER}$ or $[Ca^{2+}]_{mito}$ as measured by the Ca^{2+}-sensitive fluorescent protein CEPIA targeted to the respective organelle in HeLa cells. All traces were normalised (F/F_0) where F_0 is the starting fluorescence of each trace. **e** Comparison of the effect of PXA (10 μM), ionomycin (IM; 2 μM), and thapsigargin (TG; 1 μM) on $[Ca^{2+}]_{mito}$ in Ramos cells stably transfected with the Ca^{2+}-sensitive ratiometric fluorescent protein mito-Pericam. DMSO (0.1% v/v) was used as vehicle control. F/F_0 is the ratio of fluorescence with excitation at 488 nm (high $[Ca^{2+}]$) to 405 nm (low Ca^{2+}]). **f**, **g** Live imaging and quantification of the effect of PXA (10 μM) on mPTP opening in HeLa cells as measured by mitochondrial calcein fluorescence using the calcein/cobalt quenching method. DMSO (0.1% v/v) was used as vehicle control and ionomycin (IM; 2 μM) was used as positive control. Mitochondrial calcein fluorescence was quantified. **h** Additional live measurement of the effect of PXA on mPTP opening in Ramos cells by the calcein/cobalt quenching method using flow cytometry

(Fig. 1b), suggesting that the Ca^{2+} released by PXA at least partially originates from a source other than the ER.

PXA induces Ca^{2+} release mainly from the mitochondria

To quantify the effect of PXA on Ca^{2+} stores, we used HeLa cells expressing CEPIA Ca^{2+} probes targeted to either the ER or the mitochondria. Although PXA provoked some Ca^{2+} release from the ER, it was much slower and weaker than that evoked by thapsigargin (Fig. 1c). Mitochondria, however, were quickly and severely depleted (Fig. 1d). This effect of PXA on mitochondrial Ca^{2+} was confirmed in Ramos cells, making use of the Ca^{2+} probe Pericam (Fig. 1e).

Mitochondrial Ca^{2+} release caused by PXA is independent from the mPTP

Large-scale Ca^{2+} efflux from the mitochondria can result from persistent opening of the mPTP. We thus tested whether PXA induces mPTP opening by using the cobalt/calcein method, comparing PXA to the mPTP inducer ionomycin (IM). While IM caused a strong decrease in mitochondrial calcein fluorescence as expected, PXA had no observable effect (Fig. 1f, g; Supplementary Movies S1–S3). Similar results were obtained by further live measurement using flow cytometry (Fig. 1h). In addition, we tested whether the mPTP inhibitor cyclosporin A (CsA) can prevent the mitochondrial Ca^{2+} release caused by PXA. We measured mitochondrial Ca^{2+} retention capacity in isolated mitochondria, comparing PXA to IM and CCCP. This was done in either normal isolated mitochondria or mitochondria loaded with Ca^{2+}, and in the presence of either CsA or its derivative cyclosporin H (CsH), which does not affect the mPTP (Fig. 2)[18]. While PXA caused a decrease in calcium green fluorescence, indicating Ca^{2+} release, under every condition, i.e., regardless of Ca^{2+} loading and also in the presence of CsA, IM had an observable effect only in loaded mitochondria, but also regardless of CsA. On the other hand, CCCP caused a release of Ca^{2+} only in the presence of CsH but not CsA, indicating that CCCP-induced Ca^{2+} release does indeed depend on the mPTP, unlike that induced by PXA. Taken together, these results indicate that PXA causes mitochondrial Ca^{2+} release largely independent from the mPTP.

PXA depolarises the mitochondria but does not uncouple cellular respiration

A change in $[Ca^{2+}]_{mito}$ likely correlates with changes in other mitochondrial ion gradients. Uptake of Ca^{2+} into the mitochondrial matrix is driven by $\Delta\Psi_m$. We thus analysed the effect of PXA on $\Delta\Psi_m$. Indeed, PXA caused immediate mitochondrial depolarisation similar to CCCP, both in whole cells and isolated mitochondria (Fig. 3a, b). The EC_{50} for PXA-induced loss of $\Delta\Psi_m$ in Ramos cells was determined to be 1.1 ± 0.3 μM (Fig. S3). The key contributor to $\Delta\Psi_m$ is ΔpH_m, which is maintained via cellular respiration by consumption of O_2. If the PXA-induced loss of $\Delta\Psi_m$ was caused by loss of ΔpH_m downstream of the ETC, as in case of CCCP, it would be accompanied by an increase in respiration to compensate for the loss. Therefore, we measured cellular O_2 consumption upon increasing concentrations of either PXA or CCCP. As expected, CCCP caused a dose-dependent increase in O_2 consumption. However, in contrast to CCCP, PXA caused no increase but rather a slight decrease in O_2 consumption (Fig. 3c). An overview of the kinetics of the effects of PXA on $[Ca^{2+}]_{cyt}$, $[Ca^{2+}]_{mito}$, O_2 consumption and $\Delta\Psi_m$ is presented in Fig. 3d.

PXA inhibits cellular respiration by disrupting the electron transport chain

Since PXA had a moderate inhibitory effect on cellular O_2 consumption under basal conditions, we next measured O_2 consumption after the respiration rate was first increased by CCCP. Here, treatment with PXA caused a strong decrease in O_2 consumption to levels below baseline (Fig. 4a). It thus appeared likely that PXA, unlike CCCP, is not an inducer but rather an inhibitor of cellular respiration and of the ETC. We, therefore, compared PXA to known ETC inhibitors: rotenone (complex I), thenoyltrifluoroacetone (TTFA; complex II), antimycin A (complex III), sodium azide (NaN_3; complex IV) and

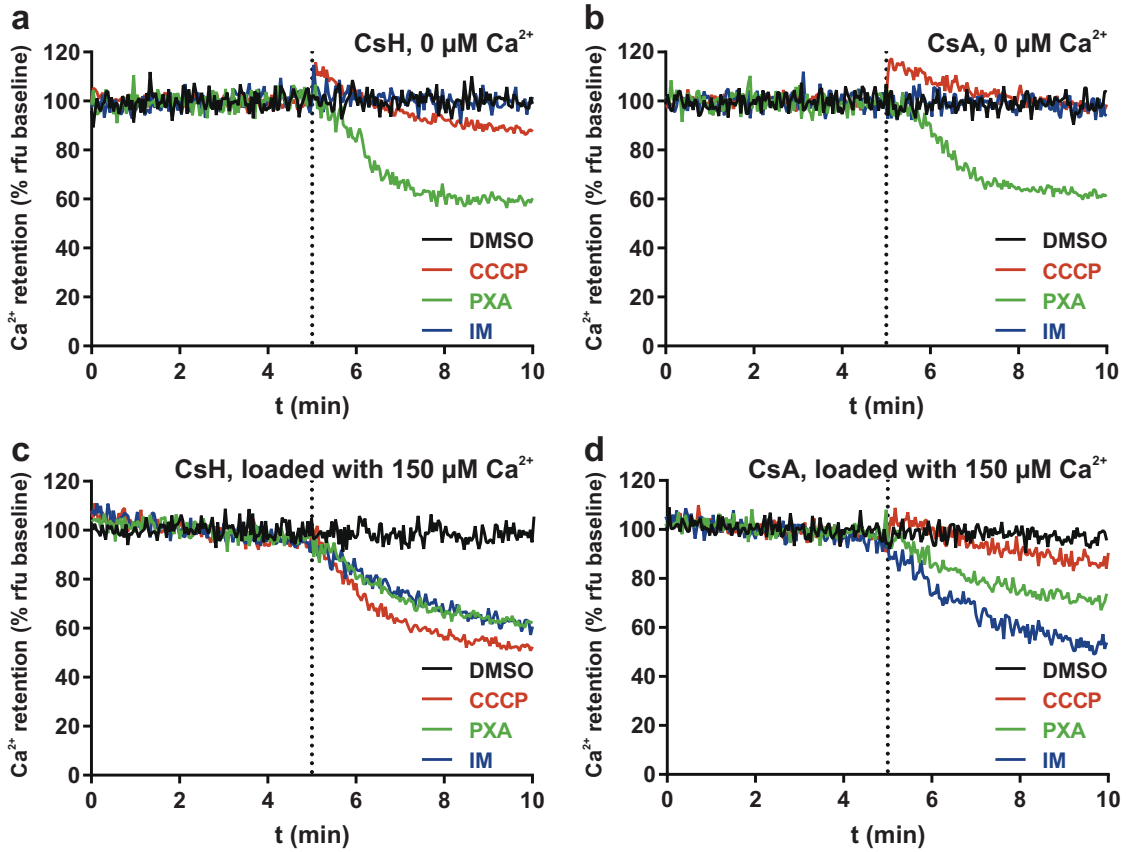

Fig. 2 Live measurement of the effect of PXA on mitochondrial Ca^{2+} retention capacity. Isolated mitochondria were stained with calcium green AM and maintained in the presence of either (**a**, **c**) CsH or (**b**, **d**) CsA, and fluorescence was measured either (**a**, **b**) directly after staining or (**c**, **d**) after first loading the mitochondria with 150 µM Ca^{2+}

oligomycin A (complex V / ATP synthase). In an O_2 consumption assay, PXA caused a strong decrease in cellular respiration, both after CCCP treatment and under basal conditions, similar to that caused by rotenone, antimycin A and azide (Fig. 4b). Oligomycin A expectedly inhibited respiration under basal conditions but not after CCCP treatment since CCCP uncouples respiration from ATP synthesis. TTFA did not have a significant effect, probably because complex II is not involved in respiration if complex I substrates are available[19].

Since a functional ETC is required for ATP synthesis by OXPHOS, we also compared PXA to known ETC inhibitors in this context. Indeed, PXA as well as all tested ETC inhibitors strongly reduced cellular ATP levels if galactose was the only available sugar and ATP had to be synthesised via OXPHOS instead of glycolysis (Fig. 4c). Thus assuming that PXA targets the ETC, we tried to determine if it specifically inhibits one of the ETC complexes. This experiment was performed in permeabilized cells, comparing PXA to rotenone. Succinate, which induces complex II-dependent respiration only if complex I is inhibited, alleviated rotenone-induced inhibition of O_2 consumption but had only a marginal effect in PXA-treated cells. In contrast, duroquinol, which induces complex III-dependent respiration, increased O_2 consumption in both PXA-treated as well as rotenone-treated cells back to levels before inhibition (Fig. 4d). These data suggest that PXA might either affect both complex I and II or the shuttling of electrons between complex I/II and III.

Comparison of PXA with other ETC inhibitors

While PXA inhibits the ETC as well as ATP synthesis, it differs from the other ETC inhibitors used in this study concerning its effects on Ca^{2+} and $\Delta\Psi_m$. Unlike PXA, neither CCCP nor any of the tested ETC inhibitors with the exception of antimycin A caused a noticeable release of Ca^{2+} (Fig. S4a), and that caused by antimycin A was much weaker and had an earlier but slower onset than the one caused by PXA. Similarly, while both CCCP and PXA induced a strong and immediate decrease in $\Delta\Psi_m$, none of the other ETC inhibitors except antimycin A had any effect on $\Delta\Psi_m$, and that of antimycin A was much slower and weaker (Fig. S4b). Since we previously

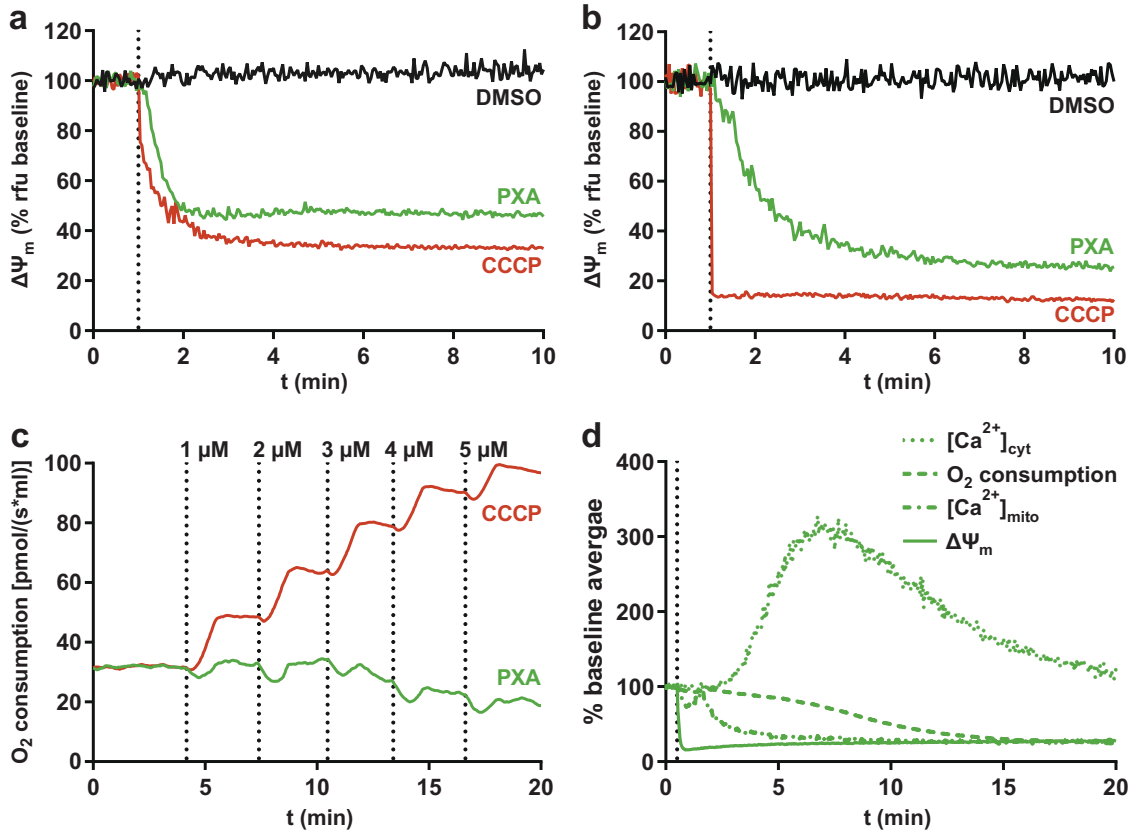

Fig. 3 PXA dissipates the mitochondrial membrane potential ($\Delta\Psi_m$) but does not increase cellular respiration. a Live measurement of the effect of PXA (10 µM) on $\Delta\Psi_m$ in Ramos cells. Measurements were performed by flow cytometry using the $\Delta\Psi_m$-sensitive fluorescent probe TMRE (Ex 488 nm, Em 575 ± 26 nm). A decrease in TMRE fluorescence corresponds to a decrease in $\Delta\Psi_m$. The protonophore carbonyl cyanide *m*-chlorophenyl hydrazone (CCCP; 10 µM) was used as positive control for mitochondrial depolarisation. **b** Live measurement of the effect of PXA (10 µM) $\Delta\Psi_m$ in isolated mitochondria. Measurements were performed by flow cytometry using the $\Delta\Psi_m$-sensitive fluorescent probe TMRM (Ex 488 nm, Em 575 ± 26 nm). The mitochondria were maintained in the presence of 1.6 µM CsH to prevent passive TMRM leakage. **c** Titration of PXA to determine the effect on cellular respiration in Ramos cells as measured by oxygen consumption. CCCP was used as positive control for increase of respiration. Measurement of extracellular [O_2] was performed using an oxygraph. **d** Comparison of the kinetics of the effects of PXA on $[Ca^{2+}]_{cyt}$ (as measured by Fluo-4-AM fluorescence), $[Ca^{2+}]_{mito}$ (as measured by mito-Pericam fluorescence), O_2 consumption (as measured by changes in extracellular [O_2]) and $\Delta\Psi_m$ (as measured by TMRE fluorescence). Graphs were partially adapted from other figures

showed that PXA is cytotoxic and induces apoptosis, we also compared it to CCCP, ETC inhibitors, IM (control for Ca^{2+} release) and staurosporine (control for cytotoxicity/apoptosis) in these regards. PXA, staurosporine and CCCP strongly induced apoptosis, while the ETC inhibitors and IM were much weaker inducers in Ramos cells and did not noticeably induce apoptosis at all in Jurkat cells (Fig. 5a, b). Dependency on OXPHOS for ATP synthesis, which considerably increased the toxicity of the ETC inhibitors, appeared to have no effect on the toxicity of PXA or staurosporine (Fig. 5c, d). These observations indicate that PXA probably causes cytotoxicity in general and apoptosis in particular not via its effects on the ETC, $\Delta\Psi_m$, or $[Ca^{2+}]_{mito}$, but rather that all of these events might have a common cause further upstream.

PXA causes irreversible cleavage of OPA1 mediated by OMA1 but not YME1L1

Several stress conditions including loss of $\Delta\Psi_m$ and low levels of ATP can induce cleavage of the IMM fusion regulator OPA1 by the protease OMA1 (ref. [20]). Additionally, OPA1 is also cleaved by the protease YME1L1, resulting in fragments of different size. We treated MEF cells deficient for either one or both of these proteases with either PXA or CCCP. We observed that PXA, like CCCP, caused stress-induced OPA1 cleavage that was dependent on OMA1, whereas expression of YME1L1 did not have any visible effect on PXA-induced OPA1 cleavage (Fig. 6a). Similarly to their effect in MEF cells, PXA and CCCP-induced cleavage of OPA1 in Ramos and Jurkat cells within minutes. Interestingly, and unlike CCCP, removal of PXA did not enable recovery of the

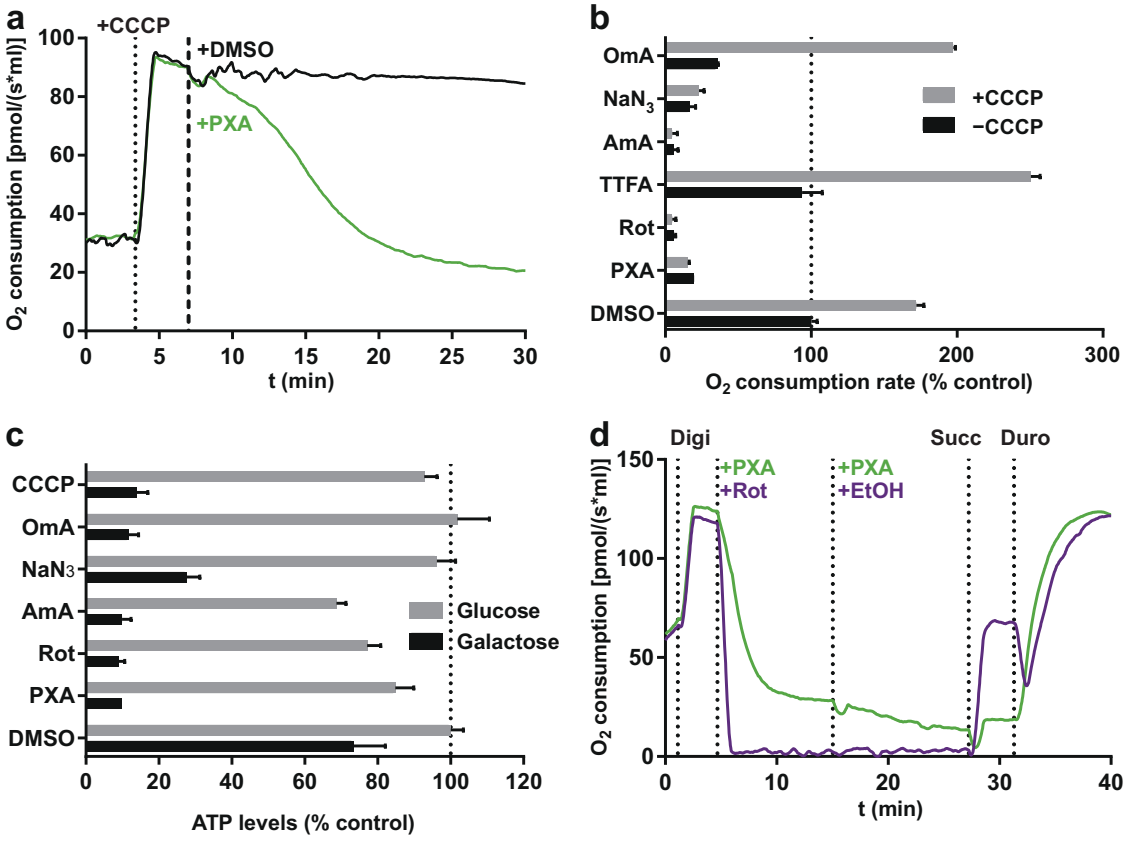

Fig. 4 Effect of PXA on electron transport chain and OXPHOS. a Live measurement of the effect of PXA on uncoupled cellular respiration in intact Ramos cells. Cells were first treated with 1 µM CCCP to uncouple respiration and then with either 10 µM PXA or 0.1% v/v DMSO (vehicle control) to test for inhibition. Measurement of extracellular [O_2] was performed using an oxygraph. **b** Comparative measurements of the effect of PXA and other compounds on basal and uncoupled respiration in Ramos cells. Respiration was uncoupled by CCCP (1 µM). PXA (10 µM) was compared to the complex-specific ETC inhibitors rotenone (Rot; complex I; 10 µM), thenoyltrifluoroacetone (TTFA; complex II; 10 µM), antimycin A (AmA; complex III; 10 µM), azide (NaN_3; complex IV; 1 mM) and oligomycin A (OmA; complex V; 10 µM). Measurement was performed in a microplate reader using the fluorescence-based *MITO-ID® Extracellular O2 Sensor Kit (High Sensitivity)* (Enzo). **c** Comparative measurements of the effect of PXA and other compounds on ATP levels in Ramos cells after 120 min of treatment. PXA (10 µM) was compared to complex-specific ETC inhibitors (see above) as well as CCCP (1 µM). Measurement was performed in a microplate reader using the luminescence-based *Mitochondrial ToxGlo™ Assay* (Promega). Cells were incubated in full growth medium containing either glucose or galactose as the only available sugar. Galactose alone forces the cells to resort exclusively to OXPHOS for ATP synthesis. **d** Live measurement of mitochondrial respiration in Ramos cells permeabilized by digitonin (Digi; 5 µg/ml). The effect of PXA (first 1 µM, then increased to 10 µM as indicated) was compared to that of the known complex I inhibitor rotenone (Rot; 1 µM). To specifically induce complex II and III of the electron transport chain, succinate (Succ; 10 mM) and duroquinol (Duro; 1 mM) were used, respectively. Measurement of extracellular [O_2] was performed using an oxygraph

long OPA1 forms (Fig. 6b). This prompted us to also investigate the effects of removal of PXA on cytotoxicity. Indeed, though PXA was about fivefold less toxic if removed after a few minutes, it still irreversibly primed the cells for death (Fig. 6c). It, thus, appears that at least some of the effects of PXA on the cells are irreversible.

PXA induces fragmentation of the inner but not of the outer mitochondrial membrane independently of OMA1, OPA1 and DRP1

Excessive processing of OPA1 by OMA1 changes mitochondrial cristae morphology, resulting in the release of pro-apoptotic factors such as CYCS and SMAC. We, therefore, investigated the effects of PXA on SMAC localisation and on recruitment of BAX to the OMM. We observed that PXA indeed induced recruitment of GFP-BAX to the mitochondria, with concurrent release of SMAC-mCherry into the cytosol, within about 2–3 h (Fig. 7a and Supplementary Movie S4; quantification shown in Fig. S5). OPA1 processing by OMA1 also prevents IMM fusion and, if excessive, results in mitochondrial fragmentation. Intriguingly, PXA caused rapid fragmentation of the mitochondrial network within minutes (Fig. 7b), and independent of the cells' OMA1 or YME1L1 status (Fig. 7c, left panels; Supplementary Movies S5–S7). The persistence of PXA-induced

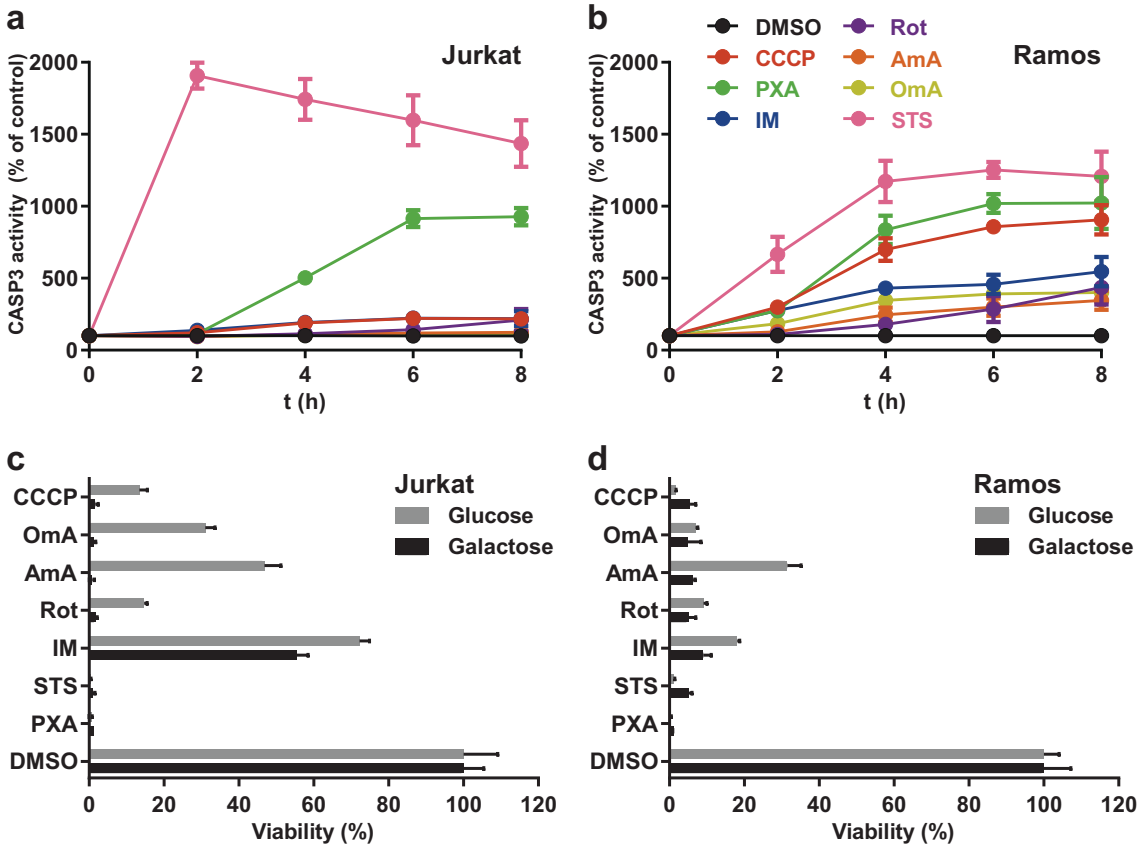

Fig. 5 Comparative measurements of the effect of PXA and other compounds on apoptosis induction and cytotoxicity in Jurkat and Ramos cells. PXA (10 µM) was compared to the protonophore carbonyl cyanide *m*-chlorophenyl hydrazone (CCCP; 10 µM), the Ca^{2+} ionophore ionomycin (IM; 10 µM), the apoptosis inducer staurosporine (STS; 10 µM), and the complex-specific ETC inhibitors rotenone (Rot; complex I; 10 µM), antimycin A (AmA; complex III; 10 µM) and oligomycin A (OmA; complex V; 10 µM). Data shown are the means of three independent experiments; error bars = SD. **a**, **b** Measurement of apoptosis induction based on cleavage of the pro-fluorescent CASP3 substrate Ac-DEVD-AMC, which results in release of AMC (Ex 360 nm, Em 450 nm), as an indicator of apoptosis. **c**, **d** Measurement of cytotoxicity after 24 h of treatment in the presence of either glucose or galactose as the only available sugar. Galactose alone forces the cells to resort exclusively to OXPHOS for ATP synthesis. Measurement was performed in a microplate reader using the MTT viability assay

mitochondrial fragmentation in OMA1-YME1L1 DKO cells indicates that this process is independent of OPA1 cleavage.

Mitochondrial fission is also regulated by the dynamin DRP1, which mediates OMM fission. We, thus, tested the effect of PXA on the mitochondrial morphology in DRP1-deficient MEF cells. Again, fragmentation was observed within minutes after treatment (Fig. 7c, right panel; Supplementary Movie S8). We next used dual staining of both the matrix (via HSP60) as well as the OMM (via TOMM20) to determine whether both or only one of these structures are affected by PXA. CCCP was used as a positive control for fragmentation. As expected, CCCP could not induce fragmentation in DRP1-KO cells, and in WT cells it induced fragmentation of both the IMM and OMM together (Fig. 8a, b). In contrast, in the WT cells treated with PXA, fragmentation was much stronger and resulted in smaller fragments. More intriguingly, in DRP1-KO cells treated with PXA, only the matrix appeared to have fragmented, whereas the OMM appeared to have shrunken around the matrix fragments but otherwise remained connected (Fig. 8a, b). This effect could also be observed in cells deficient for both DRP1 and OPA1 (Fig. S6) demonstrating that PXA acts independently of canonical regulators of mitochondrial fission. Finally, a close examination of the mitochondrial ultrastructure by transmission electron microscopy (TEM) revealed that PXA causes OMA1-independent disruption of mitochondrial matrix morphology, complete loss of cristae, and condensation of IMM structures at the OMM (Fig. 8c).

Taken together, our results show that PXA disturbs mitochondrial form and function in several ways. Some effects, such as the rapid inhibition of both $\Delta\Psi_m$ and the ETC at the same time, the delayed release of mitochondrial Ca^{2+}, and the fragmentation of the inner but not the

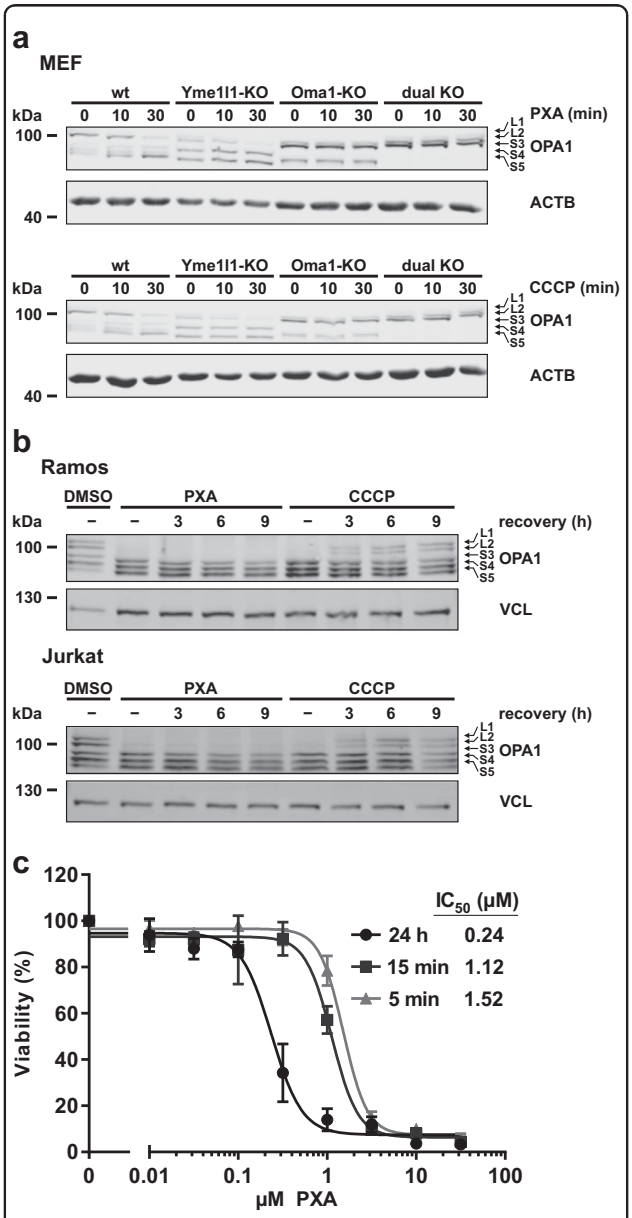

Fig. 6 PXA causes irreversible OMA1-dependent OPA1 processing and primes cells for death. a Effect of PXA (10 μM) and of the protonophore carbonyl cyanide *m*-chlorophenyl hydrazone (CCCP; 10 μM) on OPA1 processing in cells deficient for the OPA1 protease OMA1 and/or YME1L1. Proteins were detected by immunoblot. Beta-actin (ACTB) was used as loading control. **b** Examination of the recovery of long OPA1 forms in Ramos or Jurkat cells after 5 min of treatment with either PXA (10 μM) or CCCP (10 μM) followed by removal of the substance and a recovery period of up to 9 h. Proteins were detected by immunoblot. Vinculin (VCL) was used as loading control. **c** Comparison of the effect of PXA on cell viability if the stimulus was removed after treatment. Measurement was performed in a microplate reader using the MTT viability assay. Data shown are the means of three independent experiments; error bars = SD

outer mitochondrial membrane, are unique and indicate a mode of action that is distinct from all other compounds to which it was compared in this study.

Discussion

The mycotoxin PXA is a toxic natural product whose mechanism of action has so far remained elusive. We provide evidence that PXA disrupts mitochondrial function and causes IMM fragmentation and cristae disruption independently of DRP1 and OPA1, leading to the release of pro-apoptotic factors and ultimately to apoptosis.

PXA, just like CCCP, dissipates $\Delta\Psi_m$ within seconds. In the case of CCCP, respiration increases to compensate this, whereas PXA has the opposite effect and blocks respiration. Conversely, respiration is also blocked by ETC inhibitors, yet in contrast to PXA, these do not strongly affect $\Delta\Psi_m$. This suggests an entirely different mode of action for PXA. Additionally, unlike any of these compounds, PXA causes a strong mitochondrial release of Ca^{2+} and rapid fragmentation of the IMM but not the OMM.

Release of mitochondrial Ca^{2+} and loss of $\Delta\Psi_m$ can be results of persistent mPTP opening, yet we showed that PXA does not strongly affect the mPTP. Since mitochondrial ion gradients are interdependent through various antiporters that are generally linked to $\Delta\Psi_m$ (ref. [2]), one might assume that loss of $\Delta\Psi_m$ disturbs these gradients sufficiently to induce a net Ca^{2+} efflux from the mitochondria. For CCCP, contradictory results have been reported—in some cases it caused Ca^{2+} release[21], in some cases it did not[22]. We observed no effect of CCCP and most ETC inhibitors on $[Ca^{2+}]_{cyt}$, and in fact both ETC-deficient (ρ^0) mitochondria[23] and depolarised mitochondria[24] can still facilitate a net uptake of Ca^{2+}. It, thus, appears that the mitochondrial Ca^{2+} release induced by PXA is not necessarily a result of its effects on the ETC and $\Delta\Psi_m$, but rather that all of these effects might have a common cause.

The delay between addition of PXA and the first observable increase in $[Ca^{2+}]_{cyt}$ and decrease in $[Ca^{2+}]_{mito}$ contrasts with the immediate change in $\Delta\Psi_m$ (Fig. 3d). This discrepancy could possibly be explained by the hypothesis that mitochondria release Ca^{2+} mainly into the cristae, and that the cristae junctions may function as bottlenecks for mitochondrial Ca^{2+} transport[8,25]. Cristae junctions are regulated by OPA1, which is cleaved by OMA1 in response to mitochondrial stress, leading to cristae disruption[26]. We not only showed that OPA1 is irreversibly cleaved by OMA1 upon PXA treatment, but that PXA also causes cristae disruption independently of OMA1. Thus, PXA-induced cristae disruption might cause the release of Ca^{2+} from the cristae and thus eventually into the cytosol. In addition, irreversible cristae

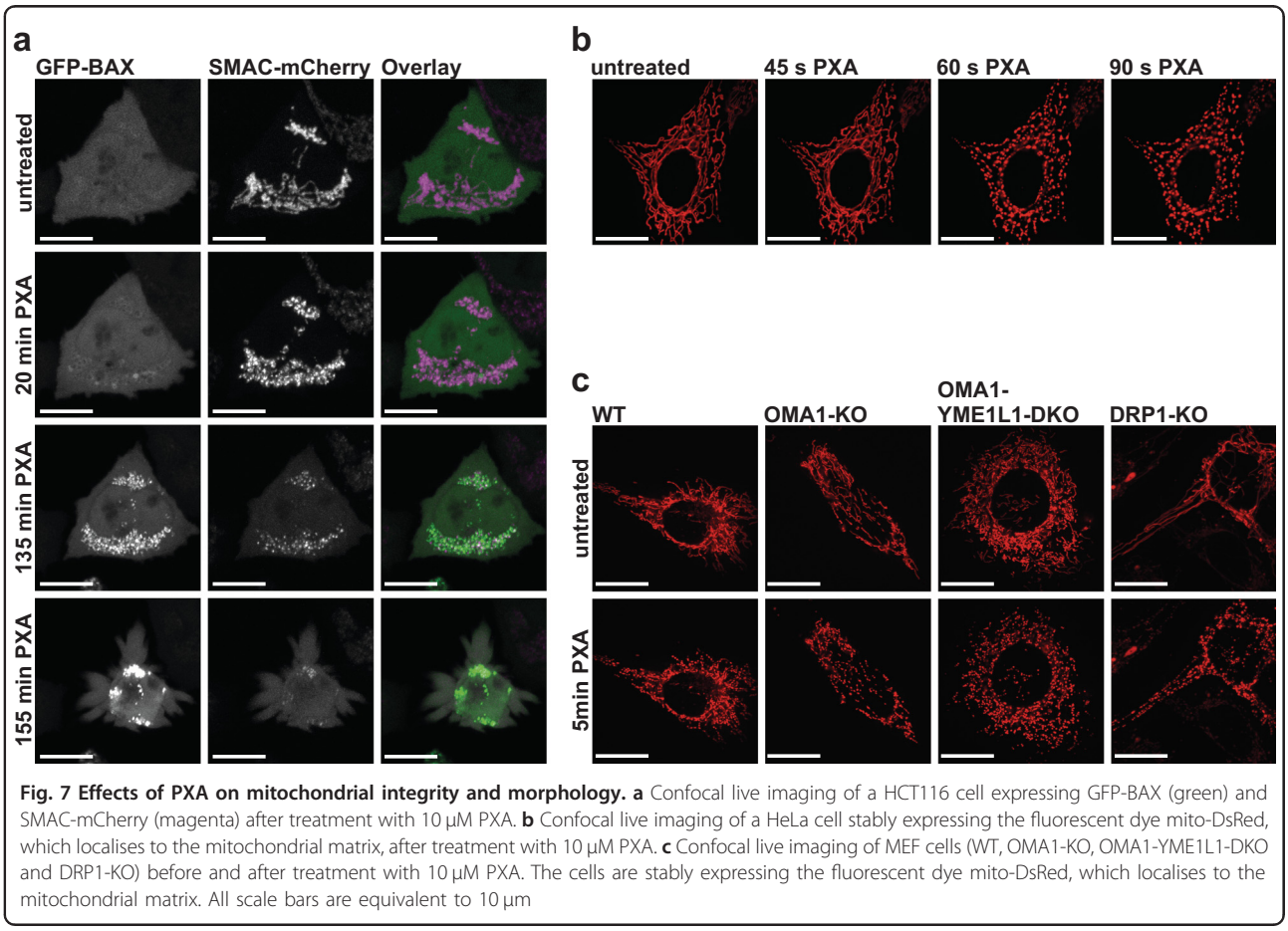

Fig. 7 Effects of PXA on mitochondrial integrity and morphology. a Confocal live imaging of a HCT116 cell expressing GFP-BAX (green) and SMAC-mCherry (magenta) after treatment with 10 µM PXA. **b** Confocal live imaging of a HeLa cell stably expressing the fluorescent dye mito-DsRed, which localises to the mitochondrial matrix, after treatment with 10 µM PXA. **c** Confocal live imaging of MEF cells (WT, OMA1-KO, OMA1-YME1L1-DKO and DRP1-KO) before and after treatment with 10 µM PXA. The cells are stably expressing the fluorescent dye mito-DsRed, which localises to the mitochondrial matrix. All scale bars are equivalent to 10 µm

disruption could well be a sufficient condition for the release of pro-apoptotic factors and thus the induction of apoptosis[26–28].

OPA1 also affects the fragmentation of mitochondrial network structures, which can be induced by PXA as well as CCCP. In the case of CCCP, this is commonly explained by the excessive activation of DRP1 after increased OPA1 processing by OMA1, which in turn is a response to several kinds of cellular stress including impaired ATP production and loss of $\Delta\Psi_m$ (ref. [4,6,20,29–32]). Since PXA dissipates $\Delta\Psi_m$, inhibits ATP production and consequently induces OMA1-mediated OPA1 cleavage, one might assume that it induces fragmentation via the same mechanism, yet we observed PXA-induced fragmentation events that were independent of DRP1, OMA1 and even OPA1.

Mitochondrial fragmentation independent of DRP1 is an unusual phenomenon but has been reported in cells undergoing apoptosis after pro-apoptotic factors had already been released[33,34]. In the case of PXA, however, fragmentation occurs within minutes after treatment, whereas pro-apoptotic factors are released only after several hours. In addition, whereas both the OMM and IMM are divided together during DRP1-dependent fragmentation, PXA can cause exclusive fragmentation of the IMM while the OMM remains intact. This is surprising since no active mechanism for exclusive IMM fission is known in higher eukaryotes, and there are only few reports documenting this phenomenon[6,35,36].

The OMA1-processed short OPA1 forms play a role in IMM fission and cristae morphology[5,29,35]. However, since PXA-induced IMM fragmentation and cristae disruption are independent of both OMA1 and OPA1, this implies that OPA1 may well be an IMM fission regulator but not necessarily a fission executor. It has been recently proposed that OPA1 is dispensable for cristae junction biogenesis but may still be required for cristae junction remodelling[37]. Our results suggest that excessive OPA1 processing may be sufficient but not necessary for inner membrane remodelling and cristae disruption and for the consequent release of pro-apoptotic factors.

The independence of PXA-induced IMM fragmentation from DRP1, OMA1 and OPA1, as well as its very fast onset, suggest that it might not depend on the fission/fusion machinery at all, but could work via a completely separate mechanism. Since no such mechanism is known

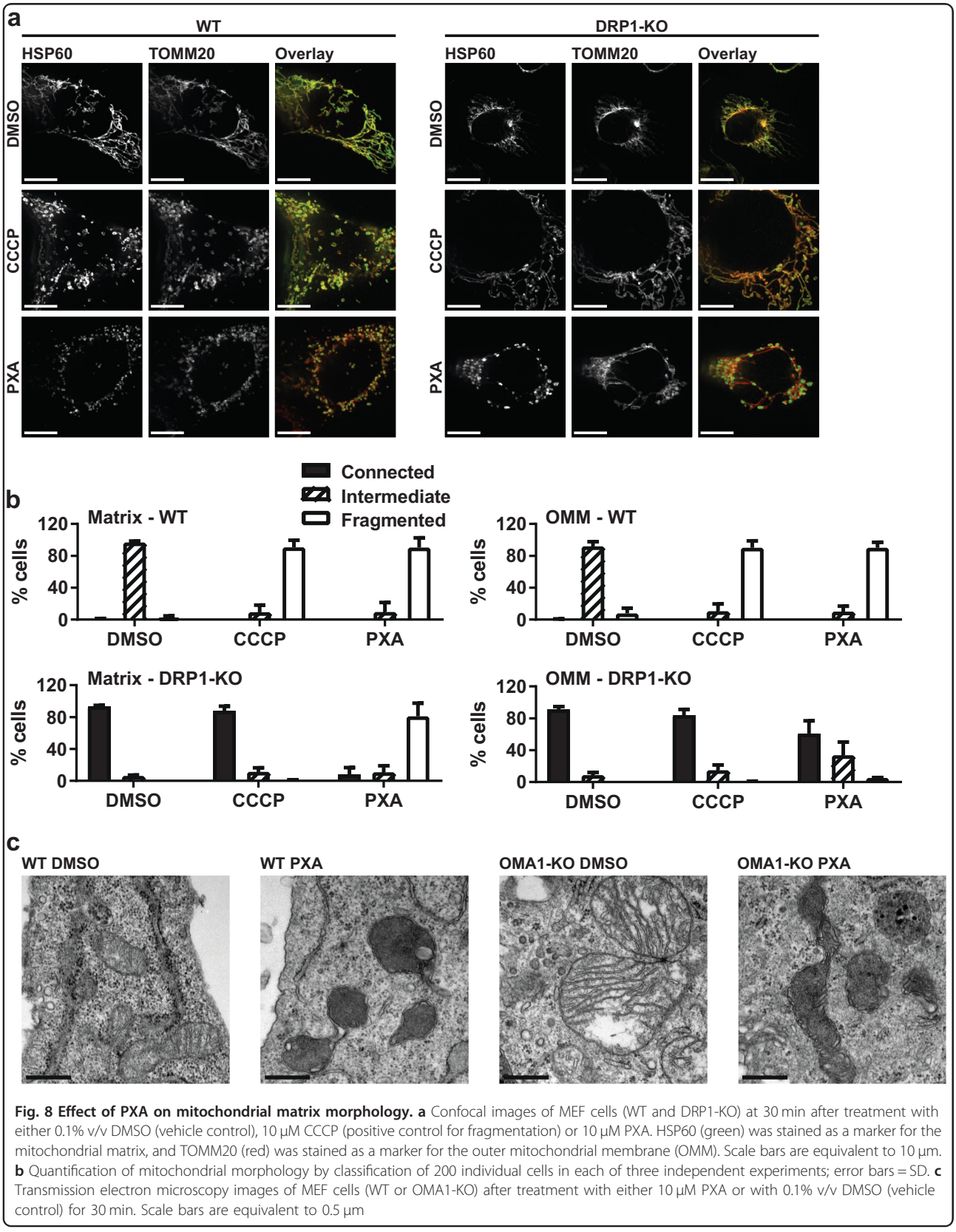

Fig. 8 Effect of PXA on mitochondrial matrix morphology. a Confocal images of MEF cells (WT and DRP1-KO) at 30 min after treatment with either 0.1% v/v DMSO (vehicle control), 10 µM CCCP (positive control for fragmentation) or 10 µM PXA. HSP60 (green) was stained as a marker for the mitochondrial matrix, and TOMM20 (red) was stained as a marker for the outer mitochondrial membrane (OMM). Scale bars are equivalent to 10 µm. **b** Quantification of mitochondrial morphology by classification of 200 individual cells in each of three independent experiments; error bars = SD. **c** Transmission electron microscopy images of MEF cells (WT or OMA1-KO) after treatment with either 10 µM PXA or with 0.1% v/v DMSO (vehicle control) for 30 min. Scale bars are equivalent to 0.5 µm

in higher eukaryotes, any attempt at explaining this effect remains speculative. One explanation could be a change in IMM fluidity or matrix architecture, causing an immediate and strong retraction of the IMM. This could result from interference with the tethering of IMM and OMM at mitochondrial contact sites. If this is the case, a possible mechanistic target of PXA could be the mitochondrial phospholipid cardiolipin, which is present almost exclusively in the IMM and especially at mitochondrial contact sites[38,39]. Cardiolipin serves as a membrane anchor for many proteins that are implicated in mitochondrial contact site formation, mitochondrial ultrastructure and the ETC, such as MIC27 (APOOL)[40,41], F_1F_O ATP synthase[41,42], CYCS[41], and ETC complexes III and IV[41,43,44]. A disruptive interaction between PXA and either cardiolipin or cardiolipin-binding proteins might thus explain several of the effects induced by PXA.

In summary, we identified PXA as a mitochondrial toxin with a mode of action distinct from known ETC inhibitors, OXPHOS uncouplers, and ionophores. Its effects, such as the rapid inhibition of both ETC and $\Delta\Psi_m$, the release of mitochondrial Ca^{2+}, and the induction of DRP1- and OPA1-independent cristae disruption and fission of the inner but not the outer mitochondrial membrane, might render it a useful tool in studying these phenomena. Further studies may reveal the molecular target of PXA and the mechanisms through which it induces mitochondrial Ca^{2+} release and IMM fission.

Material and methods

Cell lines and cell culture

Jurkat cells were obtained from DSMZ (#ACC-282). Ramos cells were kindly provided by Michael Engelke (Institute of Cellular and Molecular Immunology, University Hospital Göttingen, Göttingen, Germany). HeLa cells stably expressing mito-DsRed were kindly provided by Aviva M. Tolkovsky (Department of Clinical Neurosciences, University of Cambridge, England, UK) and have been described previously[45]. MEF cells deficient for OMA1 and/or YME1L1 as well as the corresponding wild-type cells were generated by Ruchika Anand and kindly provided by Thomas Langer (Institute for Genetics, University of Cologne, Germany) and have been described previously[29]. MEF cells deficient for DRP1 as well as the corresponding wild-type cells used for live imaging were kindly provided by Hiromi Sesaki (Department of Cell Biology, Johns Hopkins University, Baltimore, MD, USA) and have been described previously[33]. MEF cells deficient for DRP1 used for imaging of fixed cells were generated using the CRISPR/Cas9 system as described previously[46]. The DNA target sequence for the guide RNA was 5'-CAGTGGGAAGAGCTCAGTGC-3'. HCT116 cells were kindly provided by Frank Essmann (Interfaculty Institute of Biochemistry, Eberhard Karls University Tübingen, Germany). Transient expression of SMAC-mCherry and GFP-BAX was achieved by lipofection at 70–80% confluence using Lipofectamine 2000 (Life Technologies, Darmstadt, Germany). Cells were incubated with 0.15 µl Lipofectamine 2000, 50 ng pcDNA3-Smac(1-60)mCherry (Addgene ID 40880; this plasmid was kindly provided by Stephen Tait (Beatson Institute, University of Glasgow, Scotland, UK) and has been described previously[47]), and 50 ng pGFP-Bax (kindly provided by Nathan R. Brady, Department of Molecular Microbiology and Immunology, Johns Hopkins University, Baltimore, MD, USA) per well in glass bottom 8-well chambers (Ibidi, Planegg, Germany) for 16 h. HeLa cells used for Ca^{2+} measurements were cultured in Dulbecco's modified Eagle's medium supplemented with 10% fetal calf serum (FCS) and 4 mM L-glutamine, 100 U/ml penicillin and 100 µg/ml streptomycin at 37 °C and 5% CO_2. They were authenticated using autosomal STR profiling performed by the University of Arizona Genetics Core and they fully matched the DNA fingerprint present in reference databases. Cell lines stably expressing either mito-DsRed (except HeLa; see above) or ratiometric mito-Pericam were generated by retroviral transfection using the Platinum-E (Plat-E) packaging cell line (kindly provided by Toshio Kitamura, Institute of Medical Science, University of Tokyo, Japan) and the retroviral vectors pMSCVpuro-mito-DsRed1 (Addgene ID 87379) or pMSCVpuro-mito-Pericam (Addgene ID 87381). The medium used for the cultivation of Jurkat cells and Ramos cells was RPMI 1640 medium, and the medium used for cultivation of HCT116 cells was McCoy's 5A medium. All other cells were cultivated in high-glucose Dulbecco's Modified Eagle's medium (DMEM). All media were supplemented with 10% FCS, 100 U/ml penicillin, and 100 µg/ml streptomycin. All cell lines were maintained at 37 °C and 5% CO_2 in a humidity-saturated atmosphere.

Reagents

Phomoxanthone A was isolated and purified as described previously[16]. We found that PXA becomes unstable if dissolved in dimethyl sulfoxide (DMSO) and readily isomerises into the essentially non-toxic compound dicerandrol C (data not shown), in a process similar to the one previously described for the structurally related secalonic acids[48]. However, PXA is barely soluble in EtOH and not soluble in H_2O. Therefore, PXA was prepared in small lyophilised aliquots and only dissolved in DMSO immediately before usage.

The tyrosine phosphatase inhibitor pervanadate (VO_4^{3-}) was freshly prepared by mixing 30 mM sodium orthovanadate with 60 mM H_2O_2 in phosphate-buffered saline (PBS) and incubating at room temperature (RT) in the dark for 10 min; sodium orthovanadate was purchased from Sigma (Munich, Germany), #450243; IM from

Sigma, #I9657; thapsigargin (TG) from Sigma, #T9033; carbonyl cyanide *m*-chlorophenyl hydrazone (CCCP) from Sigma, #C2759; rotenone from Sigma, #45656; thenoyltrifluoroacetone (TTFA) from Sigma, #88300; antimycin A from Sigma, #A8674; sodium azide (NaN_3) from Sigma, #S2002; oligomycin A from Toronto Research Chemicals (Toronto, Canada), #O532970; staurosporine (STS) from LC Laboratories (Woburn, MA, USA), #9300. All cell culture reagents were purchased from Life Technologies, and all other reagents where no manufacturer is explicitly mentioned were purchased from Carl Roth GmbH (Karlsruhe, Germany).

Replicates and statistical analysis

Experiments were replicated at least three times, and representative data are shown. Error bars indicate standard deviation. All statistical analysis was performed using Prism v7.01 (GraphPad Software, La Jolla, CA, USA).

In vitro kinase activity screening

The effect of PXA on the activity of 141 protein kinases was assessed by the International Centre for Kinase Profiling (Dundee, Scotland, UK) using a radioactive filter binding assay with ^{33}P ATP[49,50].

Live measurement of $[Ca^{2+}]_{cyt}$ by Fluo-4-AM

Cells were stained by incubation in growth medium containing 1 µM Fluo-4-AM (Life Technologies; #F14201), 0.005% w/v Pluronic F-127 (Sigma, #540025), 10 mM HEPES and 5% v/v FCS at 30 °C. After 25 min, an equal volume of full growth medium was added, the temperature was increased to 37 °C, and the cells were incubated for another 10 min. After that, the cells were washed and resuspended in Krebs-Ringer buffer (10 mM HEPES pH 7.0, 140 mM NaCl, 4 mM KCl, 1 mM $MgCl_2$, 10 mM glucose) supplemented with 1 mM $CaCl_2$. The cells were kept at RT in the dark until measurement. Just before measurement, the cells were washed and resuspended in Krebs-Ringer buffer supplemented with 0.5 mM EGTA. Fluo-4-AM fluorescence was measured live using an LSRFortessa flow cytometer (BD, Franklin Lakes, NJ, USA) recording fluorescence in the FITC channel (Ex 488 nm, Em 530 ± 30 nm). For each sample, after at least 30 s of baseline measurement, the stimulus was added and measurement was continued for at least 10 min.

Live measurement of $[Ca^{2+}]_{mito}$ and $[Ca^{2+}]_{ER}$ by CEPIA

Measurements of $[Ca^{2+}]_{mito}$ and $[Ca^{2+}]_{ER}$ in HeLa single cells were performed as described previously[51,52], using the genetically-encoded Ca^{2+} indicators CEPIA3mt (Addgene ID 58219) and G-CEPIA1er (Addgene ID 58215), respectively, which were developed by Dr. M. Iino (The University of Tokyo, Japan)[53]. The constructs were introduced into HeLa cells utilising the X-tremeGENE HP DNA transfection reagent (Roche, Mannheim, Germany) according to the manufacturer's protocol. The $[Ca^{2+}]$ measurements were performed 48 h after transfection using a Zeiss Axio Observer Z1 Inverted Microscope equipped with a 20 × air objective and a high-speed digital camera (Axiocam Hsm, Zeiss, Jena, Germany). Changes in fluorescence were monitored in the GFP channel (Ex 480 nm, Em 520 nm). Extracellular Ca^{2+} was chelated with 3 mM EGTA, and PXA (10 µM) or thapsigargin (1 µM) were added as indicated on the figures. All traces were normalised (F/F_0) where F_0 is the starting fluorescence of each trace.

Live measurement of $[Ca^{2+}]_{mito}$ by ratiometric mito-Pericam

Ramos cells stably transfected with ratiometric mito-Pericam as described above were used for this measurement. Ratiometric mito-Pericam is a Ca^{2+}-sensitive fluorescent protein and was described previously[54,55]. An increase in $[Ca^{2+}]$ causes a shift of the Pericam excitation maximum from ~410 to ~495 nm while the emission peak remains at ~515 nm. Pericam fluorescence was measured live using an LSRFortessa flow cytometer recording fluorescence in both the FITC channel (Ex 488 nm, Em 530 ± 30 nm) and the AmCyan channel (Ex 405 nm, Em 525 ± 50 nm). For each sample, after at least 30 s of baseline measurement, the stimulus was added and measurement was continued for at least 10 min. The ratio of fluorescence with excitation at 488 to 405 nm was calculated.

Live measurement of mPTP opening by cobalt-calcein assay

This method was adapted from previously published protocols[10,18,56]. The cells were stained by incubation in Krebs-Ringer buffer supplemented with 1 mM $CaCl_2$, 1 mM $CoCl_2$, and 1 µM calcein-AM (Life Technologies, #65-0853-78) at 37 °C for 30 min. After that, the cells were washed and maintained in Krebs-Ringer buffer supplemented with 1 mM $CaCl_2$ and 1.6 µM cyclosporin H (CsH) to prevent passive efflux of calcein. For live measurement by confocal microscopy, imaging and quantification were performed using a Perkin Elmer Spinning Disc microscope with a 60× objective (oil-immersion and NA = 1.49) at an excitation wavelength of 488 nm. The videos were obtained at 1000 × 1000 pixel resolution with a Hamamatsu C9100 camera. Additional live measurement by flow cytometry was performed using an LSRFortessa flow cytometer recording fluorescence in the FITC channel (Ex 488 nm, Em 530 ± 30 nm). For each sample, after at least 30 s of baseline measurement, the stimulus was added and measurement was continued for at least 10 min.

Isolation of live mitochondria

Adherent cells were harvested by a cell scraper. All cells were pelletised by centrifugation at 600 rcf, resuspended in ice-cold mitochondria isolation buffer (210 mM mannitol, 70 mM sucrose, 1 mM K_2EDTA, 20 mM HEPES), and passed through a 23 G needle ten times. The resulting suspension was centrifuged at 600 rcf and the supernatant was transferred to a new tube and centrifuged at 6500 rcf and 4 °C for 15 min. The resulting mitochondrial pellet was resuspended in sodium-free mitochondrial respiration buffer MiR05 (0.5 mM EGTA, 3 mM $MgCl_2$, 60 mM lactobionic acid, 20 mM taurine, 10 mM KH_2PO_4, 20 mM HEPES, 110 mM D-sucrose, 0.1% w/v fatty-acid-free bovine serum albumin [BSA]) supplemented with 10 mM succinate and 5 mM malate.

Live measurement of mitochondrial Ca^{2+} retention capacity by calcium green

Live mitochondria isolated as described above were stained by incubation in MiR05 buffer supplemented with 10 mM succinate, 5 mM malate, and 1 µM calcium green AM (Life Technologies, #C3012) for 20 min on a shaker at 37 °C. Before measurement, the mitochondria were pelletised at 6500 rcf for 5 min, washed and resuspended in MiR05 supplemented with 10 mM succinate, 5 mM malate, and 5 µM of either CsH or CsA. In experiments where the mitochondria were loaded with Ca^{2+} before measurement, this was achieved by incubation in MiR05 additionally supplemented with 150 µM $CaCl_2$ on a shaker at 37 °C for 10 min after the first washing step and followed by a second washing step.

Measurement of mitochondrial membrane potential by TMRE and TMRM

For measurement in whole cells, the cells were stained by incubation in full growth medium containing 100 nM tetramethylrhodamine ethyl ester (TMRE; AAT Bioquest, Sunnyvale, CA, USA; #22220) and 10 mM HEPES at 37 °C in the dark for 15 min. After that, the cells were washed and resuspended in full growth medium containing 10 mM HEPES and were incubated at 37 °C in the dark for another 15 min. The cells were maintained at these conditions until measurement. For measurement in live mitochondria, these were isolated as described above, resuspended in sodium-free mitochondrial respiration buffer MiR05 supplemented with 10 mM succinate, 5 mM malat, and 1 mM ADP, stained with 50 nM tetramethylrhodamine methyl ester (TMRM; Life Technologies, #T668) at 37 °C for 15 min, and washed and resuspended in MiR05 additionally supplemented with 1.6 µM cyclosporin H (CsH) to prevent passive TMRM leakage. For live measurement, TMRE or TMRM fluorescence was measured using an LSRFortessa flow cytometer recording fluorescence in the PE channel (Ex 488 nm, Em 575 ± 26 nm). For each sample, after at least 30 s of baseline measurement, the stimulus was added and measurement was continued for at least 10 min. For the titration of the EC_{50} for mitochondrial depolarisation, TMRE fluorescence was measured using a Synergy Mx microplate reader (BioTek, Bad Friedrichshall, Germany) recording fluorescence at Ex 549 ± 9 nm, Em 575 ± 9 nm. TMRE fluorescence was measured right before and 10 min after addition of PXA. EC_{50} values were calculated using Prism v7.01.

Live O_2 respirometry measurements

This method was adapted from previously published protocols[19,57]. All measurements were performed using an OROBOROS Oxygraph-2k (Oroboros Instruments, Innsbruck, Austria). For measurement of total cellular respiration, intact cells (2×10^6 cells/ml) were used and maintained in full growth medium supplemented with 20 mM HEPES during measurement. For direct measurement of mitochondrial respiration, digitonin-permeabilised cells (2×10^6 cells/ml) were used and maintained in mitochondrial respiration buffer MiR05 during measurement. To induce respiration, 10 mM glutamate, 5 mM malate, 1 mM ADP, and 5 µg/ml digitonin were added. The following complex-specific ETC inducers were used: For complex II, 10 mM succinate (from Sigma, #S3674); for complex III, 1 mM tetramethylhydroquinone / duroquinol (from TCI Germany, Eschborn, Germany; #T0822); for complex IV, 50 µM tetramethyl-*p*-phenylenediamine (TMPD; from Sigma, #87890) supplemented with 200 µM ascorbate.

Fluorimetric O_2 consumption assay

This measurement was performed using the *MITO-ID® Extracellular O2 Sensor Kit (High Sensitivity)* (Enzo Life Sciences, Lörrach, Germany; #51045) according to manufacturer's instructions. Fluorescence was measured using a Synergy Mx microplate reader (Ex 340–400 nm, Em 630–680 nm; time-resolved fluorescence, delay time 30 µs, integration time 100 µs).

Measurement of cellular ATP levels

This measurement was performed using the *Mitochondrial ToxGlo™ Assay* (Promega, Mannheim, Germany; #G8000) according to manufacturer's instructions. Since most cancer cells prefer ATP synthesis by glycolysis over OXPHOS if glucose is present, this experiment was conducted in the presence of either glucose or galactose as the only available sugar, the latter of which reduces the net ATP yield of glycolysis to zero and forces the cells to resort to OXPHOS for ATP production[58,59].

Fluorimetric caspase-3 activity assay

Caspase-3 activity was measured as described previously[60]. Briefly, cells were harvested by centrifugation at

600 rcf and lysed with 50 µl of ice-cold lysis buffer (20 mM HEPES, 84 mM KCl, 10 mM, $MgCl_2$, 200 µM EDTA, 200 µM EGTA, 0.5% NP-40, 1 µg/ml leupeptin, 1 µg/ml pepstatin, 5 µg/ml aprotinin) on ice for 10 min. Cell lysates were transferred to a black flat-bottom microplate and mixed with 150 µl of ice-cold reaction buffer (50 mM HEPES, 100 mM NaCl, 10% sucrose, 0.1% CHAPS, 2 mM $CaCl_2$, 13.35 mM DTT, 70 µM Ac-DEVD-AMC). The kinetics of AMC release were monitored by measuring AMC fluorescence intensity (Ex 360 nm, Em 450 nm) at 37 °C in intervals of 2 min over a time course of 150 min, using a Synergy Mx microplate reader. The slope of the linear range of the fluorescence curves (Δrfu/min) was considered as corresponding to caspase-3 activity.

Measurement of cell viability by MTT assay

Cell viability was determined by the ability to convert the yellow MTT substrate (Roth, #4022) into a blue formazan product. MTT solution (5 mg/ml MTT in PBS) was added to cells to a final concentration of 1 mg/ml, and the cells were then incubated at 37 °C for 60 min and pelletised at 600 rcf. The supernatant was discarded and replaced with DMSO. After the formazan crystals were fully dissolved, absorption was measured (test wavelength 570 nm, reference wavelength 650 nm). Reference absorbance was subtracted from test absorbance. Cell-free medium samples were considered as having 0% viability and the average of the control samples was considered as having 100% viability. IC_{50} values were calculated using Prism v7.01.

Immunoblotting

Cells were harvested by centrifugation at 11,000 rcf in 4 °C for 10 s, quick-frozen in liquid nitrogen, thawed on ice, incubated in lysis buffer (20 mM Tris-HCl, 150 mM NaCl, 1% v/v Triton X-100, 0.5 mM EDTA, 1 mM Na_3VO_4, 10 mM NaF, 2.5 mM $Na_4P_2O_7$, 0.5% sodium deoxycholate, protease inhibitor (Sigma, #P2714)) for 30 min and vortexed repeatedly. The cell lysates were then cleared from cell debris by centrifugation at 20,000 rcf for 15 min. Sodium dodecyl sulfate-polyacrylamide gel electrophoresis and western blot were performed according to standard protocol. The antibodies used for protein detection were mouse anti-phospho-tyrosine (Merck-Millipore, Darmstadt, Germany; clone 4G10, #05-1050); rabbit anti-OPA1 (described previously[37]); mouse anti-ACTB (Sigma; clone AC-74, #A5316); and mouse anti-VCL (Sigma; clone hVIN-1, #V9131).

Confocal microscopy

Live imaging of HCT116 cells transiently expressing GFP-BAX and SMAC-mCherry was performed using a Zeiss LSM 710 ConfoCor3 microscope (Carl Zeiss, Jena, Germany) with a C-Apochromat × 40 N.A. 1.2 water immersion objective (Zeiss). Excitation light came from argon ion (488 nm) and DPSS (561 nm) lasers. The cells were maintained in full growth medium at 37 °C and 5% CO_2 during imaging. Images were recorded every 5 min and were processed with Fiji[61]. For each time frame, the standard deviation (SD) of the fluorescence intensity was measured for each channel. A low SD was considered as corresponding to homogenous distribution, whereas a high SD was considered as corresponding to accumulation.

Live imaging of HeLa cells stably expressing mito-DsRed was performed using a Cell Observer SD Dual Cam spinning disc confocal microscope (Zeiss) equipped with a C-Apochromat 63×, N.A. of 1.45 oil-immersion objective. Excitation light came from an argon ion (488 nm) and DPSS (561 nm) laser. The cells were maintained in full growth medium supplemented with 10 mM HEPES at 37 °C during imaging. Images were recorded every 5 s.

Live imaging of MEF cells stably expressing mito-DsRed was performed using a Perkin Elmer Spinning Disc microscope with a 60 × objective (oil-immersion and NA = 1.49) at an excitation wavelength of 561 nm. The videos were obtained at 1000 × 1000 pixel resolution with a Hamamatsu C9100 camera. The cells were maintained in full growth medium supplemented with 10 mM HEPES at 37 °C during imaging.

For imaging of fixed HeLa and MEF cells, the cells were seeded on glass coverslips and grown to 60–90% confluence prior to experiments. Cells were treated with either 10 µM PXA, 10 µM CCCP or 0.1% v/v DMSO for 30 min, and were fixed by incubation with pre-warmed 4% paraformaldehyde in PBS at 37 °C for 10 min. Coverslips were then washed once with PBS, followed by incubation with PBS supplemented with 0.5% Triton X-100 for 10 min at RT. The coverslips were washed three times for 3–5 min with PBS supplemented with 0.2% Tween-20 (PBS-T). The coverslips were then incubated at RT for 30 min with blocking buffer (PBS-T supplemented with 0.2% fish gelatin and 5% goat serum) in a humidified box, followed by 1 h incubation with primary antibodies (anti-HSP60 clone N-20, #sc-1052 and anti-TOMM20 clone FL-145, #sc-11415 both from Santa Cruz, Dallas, TX, USA) diluted in blocking buffer. The coverslips were then washed three times with PBS-T, and incubated with blocking buffer for 30 min before adding secondary antibodies (Alexa Fluor 488-labelled donkey anti-goat and Alexa Fluor 594-labelled donkey anti-rabbit). Immunofluorescence images were acquired with a Marianas spinning disc confocal microscope (Intelligent Imaging Innovations, Denver, CO, USA).

Transmission electron microscopy

TEM samples were fixed for a minimum of 4 h in 2.5% v/v glutaraldehyde (GA) and 4% w/v paraformaldehyde

(PFA) in 0.1 M cacodylate buffer (pH 7.4) at 4 °C. Then, samples were incubated in 1% osmium tetroxide in 0.1 M cacodylate buffer for 2 h. Dehydration was achieved using acetone (50%, 70%, 90% and 100%) and block contrast was applied (1% phosphotungstic acid/0.5% uranylacetate in 70% acetone). A SPURR embedding kit (Serva, Heidelberg, Germany) was used to embed samples, which were polymerised overnight at 70 °C, before cutting into 80 nm sections using an Ultracut EM UC7 (Leica, Wetzlar, Germany). Images were captured using an H600 TEM (Hitachi, Tokyo, Japan) at 75 kV.

Acknowledgements
We thank Michael Engelke for providing Ramos B lymphocytes, Hiromi Sesaki for providing wild-type and DRP1-KO MEFs, Frank Essmann for providing HCT116 cells, and Aviva M. Tolkovsky for providing mito-DsRed-expressing HeLa cells. We are furthermore indebted to Thomas Langer for providing wild-type, OMA1-KO, YME1L1 KO and OMA1/YME1L1 DKO MEFs. We thank Stephen Tait for providing the plasmid pcDNA3-Smac(1-60)mCherry, Nathan R. Brady for providing the plasmid pGFP-Bax, and Toshio Kitamura for providing Plat-E cells. This study was supported by the Deutsche Forschungsgemeinschaft STO 864/3-1, STO 864/4-1, STO 864/5-1 (to B.S.), GRK 2158 (to P.P., to S.W. and to B. S.), and SFB 974 Project B09 (to A.S.R.), the Research Committee of the Medical Faculty of the Heinrich Heine University Düsseldorf 22/2015 (to B.S.) and 02/2015 (to A.S.R and R.A.) and 37/2015 (to A.K.K), and the Düsseldorf School of Oncology (to S.W. and B.S.; funded by the Comprehensive Cancer Centre Düsseldorf/Deutsche Krebshilfe and the Medical Faculty of the Heinrich Heine University Düsseldorf).

Author details
[1]Institute of Molecular Medicine I, Medical Faculty, Heinrich Heine University Düsseldorf, 40225 Düsseldorf, Germany. [2]Institute of Biochemistry and Molecular Biology I, Medical Faculty, Heinrich Heine University Düsseldorf, 40225 Düsseldorf, Germany. [3]Institute of Pharmaceutical Biology and Biotechnology, Faculty of Mathematics and Natural Sciences, Heinrich Heine University Düsseldorf, 40225 Düsseldorf, Germany. [4]Institute of Anatomy I, Medical Faculty, Heinrich Heine University Düsseldorf, 40225 Düsseldorf, Germany. [5]Laboratory of Molecular and Cellular Signaling, Department of Cellular and Molecular Medicine, KU Leuven, 3000 Leuven, Belgium. [6]Center for Advanced Imaging, Faculty of Mathematics and Natural Sciences, Heinrich Heine University Düsseldorf, 40225 Düsseldorf, Germany. [7]Interfaculty Institute of Biochemistry, Eberhard Karls University Tübingen, 72076 Tübingen, Germany. [8]Department of Biological Chemistry, David Geffen School of Medicine at UCLA, Los Angeles, CA 90095, USA

Conflict of interest
The authors declare that they have no conflict of interest.

Supplementary Information accompanies this paper at (https://doi.org/10.1038/s41419-018-0312-8).

Received: 1 December 2017 Accepted: 4 January 2018
Published online: 19 February 2018

References

1. Vyas, S., Zaganjor, E. & Haigis, M. C. Mitochondria and Cancer. *Cell* **166**, 555–566 (2016).
2. Rizzuto, R., De Stefani, D., Raffaello, A. & Mammucari, C. Mitochondria as sensors and regulators of calcium signalling. *Nat. Rev. Mol. Cell Biol.* **13**, 566–578 (2012).
3. Nunnari, J. & Suomalainen, A. Mitochondria: in sickness and in health. *Cell* **148**, 1145–1159 (2012).
4. Mishra, P. & Chan, D. C. Metabolic regulation of mitochondrial dynamics. *J. Cell Biol.* **212**, 379–387 (2016).
5. Youle, R. J. & van der Bliek, A. M. Mitochondrial fission, fusion, and stress. *Science* **337**, 1062–1065 (2012).
6. van der Bliek, A. M., Shen, Q., Kawajiri, S. Mechanisms of mitochondrial fission and fusion. *Cold Spring Harb. Perspect. Biol.* **5**, a011072 (2013).
7. Demaurex, N., Poburko, D. & Frieden, M. Regulation of plasma membrane calcium fluxes by mitochondria. *Biochim. Biophys. Acta* **1787**, 1383–1394 (2009).
8. Palty, R. et al. NCLX is an essential component of mitochondrial Na+/Ca2+ exchange. *Proc. Natl Acad. Sci. USA* **107**, 436–441 (2010).
9. Jiang, D., Zhao, L. & Clapham, D. E. Genome-wide RNAi screen identifies Letm1 as a mitochondrial Ca2+/H+ antiporter. *Science* **326**, 144–147 (2009).
10. Bonora, M. et al. Comprehensive analysis of mitochondrial permeability transition pore activity in living cells using fluorescence-imaging-based techniques. *Nat. Protoc.* **11**, 1067–1080 (2016).
11. Rao, V. K., Carlson, E. A. & Yan, S. S. Mitochondrial permeability transition pore is a potential drug target for neurodegeneration. *Biochim. Biophys. Acta* **1842**, 1267–1272 (2014).
12. Chipuk, J. E. & Green, D. R. Dissecting p53-dependent apoptosis. *Cell Death Differ.* **13**, 994–1002 (2006).
13. Wallace, K. B. & Starkov, A. A. Mitochondrial targets of drug toxicity. *Annu. Rev. Pharmacol. Toxicol.* **40**, 353–388 (2000).
14. Isaka, M. et al. Phomoxanthones A and B, novel xanthone dimers from the endophytic fungus *Phomopsis* Species. *J. Nat. Prod.* **64**, 1015–1018 (2001).
15. Elsässer, B. et al. X-ray structure determination, absolute configuration and biological activity of phomoxanthone A. *Eur. J. Org. Chem.* **2005**, 4563–4570 (2005).
16. Rönsberg, D. et al. Pro-apoptotic and immunostimulatory tetrahydroxanthone dimers from the endophytic fungus *Phomopsis longicolla*. *J. Org. Chem.* **78**, 12409–12425 (2013).
17. Frank, M. et al. Phomoxanthone A - from mangrove forests to anticancer therapy. *Curr. Med. Chem.* **22**, 3523–3532 (2015).
18. Petronilli, V. et al. Transient and long-lasting openings of the mitochondrial permeability transition pore can be monitored directly in intact cells by changes in mitochondrial calcein fluorescence. *Biophys. J.* **76**, 725–734 (1999).
19. Salabei, J. K., Gibb, A. A. & Hill, B. G. Comprehensive measurement of respiratory activity in permeabilized cells using extracellular flux analysis. *Nat. Protoc.* **9**, 421–438 (2014).
20. Baker, M. J. et al. Stress-induced OMA1 activation and autocatalytic turnover regulate OPA1-dependent mitochondrial dynamics. *EMBO J.* **33**, 578–593 (2014).
21. de la Fuente, S., Fonteriz, R. I., de la Cruz, P. J., Montero, M. & Alvarez, J. Mitochondrial free [Ca(2+)] dynamics measured with a novel low-Ca(2+) affinity aequorin probe. *Biochem. J.* **445**, 371–376 (2012).
22. Hoth, M., Fanger, C. M. & Lewis, R. S. Mitochondrial regulation of store-operated calcium signaling in T lymphocytes. *J. Cell Biol.* **137**, 633–648 (1997).
23. de Andrade, P. B. et al. Diabetes-associated mitochondrial DNA mutation A3243G impairs cellular metabolic pathways necessary for beta cell function. *Diabetologia* **49**, 1816–1826 (2006).
24. Trenker, M., Malli, R., Fertschai, I., Levak-Frank, S. & Graier, W. F. Uncoupling proteins 2 and 3 are fundamental for mitochondrial Ca2+ uniport. *Nat. Cell Biol.* **9**, 445–452 (2007).
25. Fülöp, L., Szanda, G., Enyedi, B., Várnai, P. & Spät, A. The effect of OPA1 on mitochondrial Ca2+ signaling. *PLoS ONE* **6**, e25199 (2011).
26. MacVicar, T. & Langer, T. OPA1 processing in cell death and disease - the long and short of it. *J. Cell Sci.* **129**, 2297–2306 (2016).
27. Zick, M., Rabl, R. & Reichert, A. S. Cristae formation-linking ultrastructure and function of mitochondria. *Biochim. Biophys. Acta* **1793**, 5–19 (2009).
28. Scorrano, L. et al. A distinct pathway remodels mitochondrial cristae and mobilizes cytochrome c during apoptosis. *Dev. Cell* **2**, 55–67 (2002).
29. Anand, R. et al. The i-AAA protease YME1L and OMA1 cleave OPA1 to balance mitochondrial fusion and fission. *J. Cell Biol.* **204**, 919–929 (2014).
30. Head, B., Griparic, L., Amiri, M., Gandre-Babbe, S. & van der Bliek, A. M. Inducible proteolytic inactivation of OPA1 mediated by the OMA1 protease in mammalian cells. *J. Cell Biol.* **187**, 959–966 (2009).
31. Ishihara, N., Fujita, Y., Oka, T. & Mihara, K. Regulation of mitochondrial morphology through proteolytic cleavage of OPA1. *EMBO J.* **25**, 2966–2977 (2006).

32. Duvezin-Caubet, S. et al. Proteolytic processing of OPA1 links mitochondrial dysfunction to alterations in mitochondrial morphology. *J. Biol. Chem.* **281**, 37972–37979 (2006).
33. Wakabayashi, J. et al. The dynamin-related GTPase Drp1 is required for embryonic and brain development in mice. *J. Cell Biol.* **186**, 805–816 (2009).
34. Ishihara, N. et al. Mitochondrial fission factor Drp1 is essential for embryonic development and synapse formation in mice. *Nat. Cell Biol.* **11**, 958–966 (2009).
35. Suen, D. F., Norris, K. L. & Youle, R. J. Mitochondrial dynamics and apoptosis. *Genes Dev.* **22**, 1577–1590 (2008).
36. Labrousse, A. M., Zappaterra, M. D., Rube, D. A. & van der Bliek, A. M. *C. elegans* dynamin-related protein DRP-1 controls severing of the mitochondrial outer membrane. *Mol. Cell* **4**, 815–826 (1999).
37. Barrera, M., Koob, S., Dikov, D., Vogel, F. & Reichert, A. S. OPA1 functionally interacts with MIC60 but is dispensable for crista junction formation. *FEBS Lett.* **590**, 3309–3322 (2016).
38. van Meer, G. & de Kroon, A. I. Lipid map of the mammalian cell. *J. Cell Sci.* **124**, 5–8 (2011). (Pt 1).
39. Ardail, D. et al. Mitochondrial contact sites. Lipid composition and dynamics. *J. Biol. Chem.* **265**, 18797–18802 (1990).
40. Weber, T. A. et al. APOOL is a cardiolipin-binding constituent of the Mitofilin/MINOS protein complex determining cristae morphology in mammalian mitochondria. *PLoS ONE* **8**, e63683 (2013).
41. Planas-Iglesias, J. et al. Cardiolipin interactions with proteins. *Biophys. J.* **109**, 1282–1294 (2015).
42. Acehan, D. et al. Cardiolipin affects the supramolecular organization of ATP synthase in mitochondria. *Biophys. J.* **100**, 2184–2192 (2011).
43. Pfeiffer, K. et al. Cardiolipin stabilizes respiratory chain supercomplexes. *J. Biol. Chem.* **278**, 52873–52880 (2003).
44. Zhang, M., Mileykovskaya, E. & Dowhan, W. Gluing the respiratory chain together. Cardiolipin is required for supercomplex formation in the inner mitochondrial membrane. *J. Biol. Chem.* **277**, 43553–43556 (2002).
45. Bampton, E. T. W., Goemans, C. G., Niranjan, D., Mizushima, N. & Tolkovsky, A. M. The dynamics of autophagy visualised in live cells: from autophagosome formation to fusion with endo/lysosomes. *Autophagy* **1**, 23–36 (2014).
46. Ran, F. A. et al. Genome engineering using the CRISPR-Cas9 system. *Nat. Protoc.* **8**, 2281–2308 (2013).
47. Tait, S. W. et al. Resistance to caspase-independent cell death requires persistence of intact mitochondria. *Dev. Cell* **18**, 802–813 (2010).
48. Qin, T., Iwata, T., Ransom, T. T., Beutler, J. A. & Porco, J. A. Jr. Syntheses of dimeric tetrahydroxanthones with varied linkages: Investigation of "Shape-shifting" properties. *J. Am. Chem. Soc.* **137**, 15225–15233 (2015).
49. Hastie, C. J., McLauchlan, H. J. & Cohen, P. Assay of protein kinases using radiolabeled ATP: a protocol. *Nat. Protoc.* **1**, 968–971 (2006).
50. Bain, J. et al. The selectivity of protein kinase inhibitors: a further update. *Biochem. J.* **408**, 297–315 (2007).
51. Vervloessem, T., Ivanova, H., Luyten, T., Parys, J. B., Bultynck, G. The selective Bcl-2 inhibitor venetoclax, a BH3 mimetic, does not dysregulate intracellular Ca2+ signaling. *Biochim. Biophys. Acta* **1864**, 968–976 (2017).
52. Bittremieux, M. et al. DPB162-AE, an inhibitor of store-operated Ca2+ entry, can deplete the endoplasmic reticulum Ca2+ store. *Cell Calcium* **62**, 60–70 (2017).
53. Suzuki, J. et al. Imaging intraorganellar Ca2+ at subcellular resolution using CEPIA. *Nat. Commun.* **5**, 4153 (2014).
54. Nagai, T., Sawano, A., Park, E. S. & Miyawaki, A. Circularly permuted green fluorescent proteins engineered to sense Ca2+. *Proc. Natl Acad. Sci. USA* **98**, 3197–3202 (2001).
55. Filippin, L. et al. Improved strategies for the delivery of GFP-based Ca2+ sensors into the mitochondrial matrix. *Cell Calcium* **37**, 129–136 (2005).
56. Petronilli, V., Penzo, D., Scorrano, L., Bernardi, P. & Di Lisa, F. The mitochondrial permeability transition, release of cytochrome c and cell death. Correlation with the duration of pore openings in situ. *J. Biol. Chem.* **276**, 12030–12034 (2001).
57. Kuznetsov, A. V. et al. Analysis of mitochondrial function in situ in permeabilized muscle fibers, tissues and cells. *Nat. Protoc.* **3**, 965–976 (2008).
58. Warburg, O. On the origin of cancer cells. *Science* **123**, 309–314 (1956).
59. Marroquin, L. D., Hynes, J., Dykens, J. A., Jamieson, J. D. & Will, Y. Circumventing the Crabtree effect: replacing media glucose with galactose increases susceptibility of HepG2 cells to mitochondrial toxicants. *Toxicol. Sci.* **97**, 539–547 (2007).
60. Czugala, M. et al. Efficient and safe gene delivery to human corneal endothelium using magnetic nanoparticles. *Nanomedicine (Lond.)* **11**, 1787–1800 (2016).
61. Schindelin, J. et al. Fiji: an open-source platform for biological-image analysis. *Nat. Methods* **9**, 676–682 (2012).

Publication 5

Carbamoyl-phosphate synthase 1 as a novel target of phomoxanthone A, a bioactive fungal metabolite

Sara Ceccacci, Jana Deitersen, Matteo Mozzicafreddo, Elva Morretta, Peter Proksch, Sebastian Wesselborg, Björn Stork, Maria Chiara Monti

Manuscript under revision at Biomolecules.

biomolecules

MDPI

Article

Carbamoyl-phosphate synthase 1 as a novel target of phomoxanthone A, a bioactive fungal metabolite.

Sara Ceccacci [1,2], Jana Deitersen [3], Matteo Mozzicafreddo [4], Elva Morretta [1], Peter Proksch [5], Sebastian Wesselborg [3], Björn Stork [3] and Maria Chiara Monti [1,*]

[1] Dept. of Pharmacy, Università di Salerno, Via Giovanni Paolo II 132, 84084 Fisciano (Salerno, Italy); sceccacci@unisa.it; emorretta@unisa.it; mcmonti@unisa.it
[2] PhD Program in Drug Discovery and Development, Dept. of Pharmacy, Università di Salerno, Via Giovanni Paolo II 132, 84084 Fisciano (Salerno, Italy); sceccacci@unisa.it
[3] Institute of Molecular Medicine I, Medical Faculty, Heinrich Heine University Düsseldorf, Universitätsstr. 1, 40225 Düsseldorf, Germany; jana.deitersen@uni-duesseldorf.de; sebastian.wesselborg@uni-duesseldorf.de; bjoern.stork@uni-duesseldorf.de
[4] School of Biosciences and Veterinary Medicine, University of Camerino, Via Gentile III da Varano, 62032 Camerino, Italy; matteo.mozzicafreddo@unicam.it
[5] Institute of Pharmaceutical Biology and Biotechnology, Heinrich Heine University, Universitätsstr. 1, 40225 Düsseldorf, Germany; Peter.Proksch@hhu.de
* Correspondence: mcmonti@unisa.it;

Abstract: Phomoxanthone A, a bioactive xanthone dimer isolated from the endophytic fungus *Phomopsis* sp., is a mitochondrial toxin weakening cellular respiration and electron transport chain activity by a fast breakup of the mitochondrial assembly. Here, a multi-disciplinary strategy has been developed and applied for identifying phomoxanthone A target(s) to fully address its mechanism of action, based on drug affinity response target stability and targeted limited proteolysis. Both approaches point to the identification of carbamoyl-phosphate synthase 1 as a major phomoxanthone A target in mitochondria cell lysates, giving also detailed insights into the ligand/target interaction sites by molecular docking and assessing an interesting phomoxanthone A stimulating activity on carbamoyl-phosphate synthase 1. Thus, phomoxanthone A can be regarded as an inspiring molecule for the development of new leads in counteracting hyperammonemia states.

Keywords: Proteomics; Drug Affinity Responsive Target Stability; Targeted-Limited Proteolysis; Bioactive Xanthone; Molecular Docking.

1. Introduction

Phomoxanthone A (PXA, Figure 1A) is a xanthone dimer, isolated from the endophytic fungus *Phomopsis* sp., known as a wealthy source of bioactive secondary metabolites endowed with a broad range activity against *Plasmodium falciparum* and *Mycobacterium tuberculosis* [1]. In particular, PXA shows a widespread bioactivity and, along years, it has been tested on a large variety of cellular systems and pathways. Initially, PXA showed significant pro-apoptotic properties when tested on

human cancer cell lines, whereas it was inactive on healthy normal cells. Interestingly, PXA was also an effective activator of Natural Killer cells, murine T lymphocytes and macrophages, coding for a stimulation of the immune system together with its pro-apoptotic activity. This dual effect could help in counteracting resistance phenomena during chemotherapy [2,3]. More recently, PXA also displayed robust cytotoxicity against different solid tumor cells and their cisplatin-resistant sub-cells, with IC_{50} values in the high nanomolar/low micromolar range, as in ovarian cancer and bladder cancer cell pairs [4].

Besides, PXA has been considered a mitochondrial toxin since its action selectively induces Ca^{2+} release from the mitochondria, but not from the endoplasmic reticulum, as reported by Böhler *et al* [5]. This event depolarizes the mitochondria diminishing cellular respiration and electron transport chain activity, and is accompanied by a rapid fragmentation (fission) of the mitochondrial network structure. This breakup solely includes the inward mitochondrial membrane, leading to cristae breakdown, release of pro-apoptotic proteins and apoptosis. Thus, mitochondrial ion homoeostasis and membrane dynamics seem to be affected by PXA [5]. On the basis of this broad biological profile and due to the limited information about the macromolecular targets involved in PXA action, a multi-disciplinary strategy has been developed and applied for identifying PXA target(s) to fully address its mechanism of action. In the early past, the mass spectrometry-based affinity purification approach (AP-MS) was one of the most recognized strategies for target identification of the so-called small molecules [6–9]: the indispensable requirement for *fishing out* protein interactors from a complex mixture is the covalent binding of the compound to a solid matrix, to create the fishing bait. Thus, this method is limited to molecules standing with one or more functional groups with proper reacting outlines. Clearly, the compound under analysis has to be stable during the reaction with its matrix in the chosen solvent and, unfortunately, this is not the case for PXA. Indeed, PXA becomes unstable when dissolved in dimethyl sulfoxide, since it isomerizes into dicerandrol C [5]. To overcome these restrictions, many strategies have newly been developed for the target protein(s) detection of unmodified small molecules, such as DARTS (Drug Affinity Responsive Target Stability) [10–13]. DARTS is based on the ability of the tested compound to protect the interacting protein(s) against enzymatic proteolysis, as easily revealed by gel electrophoresis (SDS-PAGE). Later on, high resolution MS can identify the targets by proteomics [12,13]. Furthermore, a more detailed depiction of the molecular mechanism of binding between a small molecule and its putative targets can be accomplished by t-LiP-MRM (targeted-Limited Proteolysis-Multiple Reaction Monitoring), which is a *gel-free* DARTS-like strategy based on a double-protease action and Multiple Reaction Monitoring-Mass Spectrometry (MRM-MS) detection. T-LiP-MRM points to the discovery of the local protein structural alterations due to complex formation with the small molecule [13–15]. Since PXA is unsuited for AP-MS analysis as reported above, DARTS and t-LIP-MRM were chosen to reveal its cellular targets in mitochondrial protein mixtures, isolated from HeLa cells. Mitochondria were selected as protein source since previously described PXA activities are related to this organelle. Next, the identified targets were validated by Western Blotting analysis, *in silico* and *in vitro* biochemical experiments. More in details, the gathered data led to the identification of Carbamoyl-phosphate synthase 1 (CPS1) as a major PXA target, giving also detailed insights into the ligand/target interaction site and assessing an interesting PXA stimulating activity on CPS1. Thus, PXA and its analogues can be regarded as inspiring molecules for the development of new leads in counteracting hyperammonemia states.

2. Materials and Methods

2.1. Purification of mitochondria from HeLa cells.

HeLa wild type cells were cultivated on 150 mm diameter tissue culture treated dishes (Sarstedt) and ~$3.6x10^8$ cells were harvested the next day via scraping. Cells were pelleted at 500 × g for 5 min and washed twice with PBS (Gibco). The pellet was re-suspended in 10 ml mitochondria isolation buffer (210 mM mannitol, 70 mM sucrose, 1 mM EDTA, 20 mM HEPES and protease inhibitor cocktail [Sigma-Aldrich, #P2714]) for 5 min on ice before rupturing by seven strokes through a 26 G canule.

The cell lysate was then centrifuged at 1000 × g and 4°C for 5 min and the supernatant was collected. The remaining pellet of non-lysed cells was re-suspended in 2 ml mitochondria isolation buffer and ruptured again before centrifugation, and the two fractions were pooled. The pooled lysate was centrifuged again at 1000 × g and 4°C for 5 min and the pellet was discarded. The remaining lysate was centrifuged at 8000 × g and 4°C for 10 min. The supernatant (cytosolic fraction) was collected and centrifuged again before transferring into a new tube and freezing in liquid nitrogen. The pellet (mitochondrial fraction) was washed three times at 8000 × g for 10 min in 250 µl mito isolation buffer. The pellet was finally centrifuged at 10,000 × g and 4°C for 10 min. The supernatant was discarded and the pellet containing isolated mitochondria was frozen in liquid nitrogen and stored at -80°C.

2.2 Identification of PXA cellular target(s) through DARTS.

Mitochondria were lysed in a buffer composed of 1,5 % digitonin, a protease inhibitor cocktail (Sigma Aldrich), 150mM NaCl, 10mM Tris/HCl (pH 7.5) and 5mM EDTA. After 15 min at 4°C, debris were removed by centrifugation at 20,000 × g (30 min at 4°C). Protein concentration of the obtained supernatant was determined by Bradford assay (BioRad Laboratoties, Hercules, CA) and subsequently adjusted at 3 mg/ml. DARTS experiments were carried out as reported by Morretta *et al.* [13]. Briefly, 300 µg proteins aliquots were either incubated with DMSO (vehicle control) or with PXA (1, 10 and 100 µM final concentrations) for 1h at room temperature and under agitation. The obtained samples were then treated with the unspecific protease subtilisin (enzyme to proteins ratio of 1:1000 w/w) and leaved shaking for 30 min at 25°C. One aliquot of the DMSO treated sample went a mock proteolysis, to be kept as a reference. The protease was then quenched by adding PMSF (phenylmethylsulfonyl fluoride, Sigma–Aldrich, St. Louis, U.S.A., 1 mM final concentration) to each sample. Subsequently, all of the samples were boiled in SDS-PAGE loading buffer (60 mM Tris/HCl pH 6.8, 2% SDS, 0.001% bromophenol blue, 10% glycerol, 2% 2-mercaptoethanol) and 20 µg were loaded on a 4-12% Bis-Tris Criterion™ XT Precast Gel (BioRad Laboratoties, Hercules, CA), which was then stained with a Comassie solution and submitted to a densitometric analysis through ImageJ. This experiment was carried out in duplicate. Thus, protein bands whose intensity raised at increasing PXA amounts were excised from the gels and submitted to an *in situ* tryptic digestion protocol [16]. Briefly, gel slices were reduced (6.5 mM 1,4-dithiothreitol-DTT), alkylated (54 mM iodoacetamide-IAA), washed and rehydrated, on ice for 1 h, in a 12 ng/µl trypsin/LysC solution (Promega, Madison, Wisconsin). The enzymes excess was then removed and replaced with ammonium bicarbonate (AmBic, 40 µl, 50 mM, pH 8.5), allowing protein digestion to proceed overnight at 37°C. Subsequently, supernatants were collected and peptides were extracted from each gel slice, shrinking them in 100% CH_3CN. The obtained peptides mixtures were dried under vacuum and dissolved in formic acid (FA, 10%) for the MS analysis.

5 µl of each sample were injected into a nano-ACQUITY UPLC system (Waters, Milford, MA, USA), separating peptides on a 1.7 µm BEH C18 column (Waters) at a flow rate of 280 nl/min. Peptide elution was achieved with a linear gradient of mobile phase B from 20% to 90% in 65 min (mobile phase A: 95% H_2O, 5% CH_3CN, 0.1% acetic acid; mobile phase B: 95% CH_3CN, 5% H_2O, 0.1% acetic acid). MS and MS/MS data were acquired on an LTQ Orbitrap XL high-performance liquid chromatography MS system (Thermo-Scientific, Waltham, MA, USA), provided with an electrospray (ESI) source. The ten most intense doubly and triply charged peptide ions were fragmented. MS data were then processed by the MS Converter General User Interface software (ProteoWizard; http://proteowizard.sourceforge.net/project.html) to generate peak lists for protein identifications. Subsequently, database searches were carried out on Mascot Deamon (version 5.1, Matrix Science, London, UK), employing the SwissProt database (release November 2019, 561344 entries) and the following settings: two missed cleavages; carbamidomethyl (C) as fixed modification; oxidation (M) and phosphorylation (ST) as variable modifications; peptide tolerance 30 ppm; MS/MS tolerance 0.8 Da.

144
145 *2.3 Western Blotting.*
146
147 5 µg of samples from the duplicate experiments were analyzed by a 12% SDS-PAGE and
148 transferred onto a nitrocellulose membrane, incubated for 1 h in a blocking solution (30 mM Tris pH
149 8, 170 mM NaCl, 3.35 mM KCl, 0.05% Tween-20, 5% non-fat dried milk) and left for 16h at 4°C with
150 monoclonal antibodies against CPS-1, ACON, HS71A and THIL (1:1000, Proteintech). Then, a mouse
151 peroxidase-conjugated secondary antibody (1:2500; Thermo-Scientific) was added and the signal was
152 detected using an enhanced chemiluminescent substrate and LAS 4000 (GE Healthcare, Waukesha,
153 WI, USA) digital imaging system. Finally, an antibody against GAPDH (1:2000 in 5% milk;
154 Invitrogen) has been tested as a loading normalizer.
155
156 *2.4 T-LiP-MRM analysis.*
157
158 CPS1 peptides previously detected by MS were selected through the proteomics data resource
159 Peptide Atlas (http://www.peptideatlas.org/). They were subsequently queried in the complete
160 human SRM Atlas (https://db.systemsbiology.net/sbeams/cgi/PeptideAtlas/GetTransitions) to get a
161 list consisting of 52 precursors, each one presenting the three most intense daughter ions. T-LiP-MRM
162 experiments were carried out as reported by Morretta *et al*. [13].
163
164 *2.5 In silico prediction of the PXA/CPS1 complex.*
165
166 The molecular docking analysis between PXA and CPS1 was performed to predict the best
167 complexes and it included the ligand and protein preparation, the genetic algorithm (GA) execution,
168 the data analysis and the final image preparation. PXA was designed, including the addition of
169 tautomeric states, partial charges and protonation, and finally minimized using the Avogadro
170 software (version 1.2.0) [17] with a universal force field, UFF, and a conjugate gradient algorithm until
171 a ΔE lower than 0.001 kJ/mol, as previously reported [18]. The Universal Force Field (UFF) was
172 developed to provide a set of rules and procedures for producing appropriate parameters across the
173 entire periodic table. The CPS1 three-dimensional structure were obtained from the Protein Data
174 Bank [19] (pdbID: 5DOU) [20] and prepared, using the Hermes software (version 1.10.0) [21]
175 incorporating the Gasteiger(Marsili) partial charges, adding polar protons and removing crystal
176 waters and extra co-crystallized ligands (see also Figure S3). Moreover, all planar R-NR1R2 were
177 made available for the cis/trans flipping and the tautomeric states of Asp, Glu and His residues were
178 adjusted. GOLD (version 5.7.0) [21] was performed to achieve the molecular docking using the
179 ChemScore as scoring function, search efficiency at 200% (very flexible), selecting all atoms within
180 20Å from three centroids (namely the residues used as centroid were Leu134, Val647 and Leu778) to
181 completely cover the whole protein, 20 GA runs and other parameters as default. The resulting
182 ChemScore ΔG, the total free energy change of the system upon ligand binding, and the relationship
183 between this score and experimental free energy of binding, previously obtained [22], were used to
184 calculate the predicted equilibrium dissociation constant K_D. The best complex geometry, on the base
185 of the ChemScore and the ChemScore ΔG, was rendered using PyMol software (The PyMOL
186 Molecular Graphics System, Version 2.3.4 Schrödinger, LLC.) whereas the 2D representation was
187 created using PoseView server [23].
188
189 *2.6 CPS-1 in vitro activity assay.*
190
191 The reaction mixture consisted of 50 mM NH_4HCO_3, 10 mM $Mg(C_2O_2H_3)_2$, 5 mM ATP, 5mM
192 NAG, 1 mM dithiothreitol, 50 mM triethanolamine, 50 µg/ml of CPS1 in a final volume of 20 µl. The
193 reaction was run for 10 min at 37°C and the resulting carbamoyl phosphate was converted to
194 hydroxyurea by the addition of 100 mM hydroxylamine and incubation for 10 min at 95°C. To
195 measure the concentration of hydroxyurea, 80 µl of chromogenic reagent was added to the reaction

tubes followed by heating for 15 min at 95°C. The chromogenic reagent consisted of equal volumes of solutions A and B, mixed immediately before use. Solution A consisted of 8 mg of antipyrine dissolved in 1 ml of 40% (v/v) H_2S0_4. Solution B contained 6 mg of diacetyl monoxime in 1 ml of 5% (v/v) acetic acid. After cooling to room temperature, 30 µl were loaded in triplicate in a 384-multiwell plate and the absorbance was measured at 458 nm on MultiskanGO Spectrophotometer. Opportune controls were performed such as the measure of PXA absorbance at the different used concentrations. The same experiment has been carried out using Serratol (also diluted in DMSO), a component of the frankincense essential oil, as negative control. Indeed, Serratol did not affect CPS1 activity at tested concentrations from 100 to 500 µM (Figure S2).

3. Results and Discussion

Due to its intrinsic instability, PXA has not been considered appropriate for AP-MS strategy and the subsequent covalent modification. For this reason, both DARTS and t-LiP-MRM approaches were applied and improved for the detection of unmodified PXA targets in an unbiased way: DARTS-MS has been used to identify the main targets of the molecule, confirmed or not by Western Blotting analysis. Then, t-LiP-MRM and molecular docking have been performed to shed light on the molecule putative interaction site(s). Finally, *in vitro* assays to evaluate PXA biological properties were performed.

3.1 Identification of PXA cellular target(s) through DARTS.

In a pseudo-physiological environment, a protein is in dynamic equilibrium with multiple conformations but, upon ligand binding, the equilibrium will move to the bound state stabilized by possible hydrogen bonding, hydrophobic and/or electrostatic interactions. This drives to a thermodynamically more stable state in which the protein breathing is lowered and the target resistance to proteolysis is definitely enlarged [24,25].

Thus, the limited proteolysis of a total (not fractionated) native cellular lysate, in presence or in absence of PXA, has been carried out using an unspecific enzyme as subtilisin and the digestion profile has been compared by SDS-PAGE: in principle, the bands of the protein targets should be more colored in the samples pre-treated with PXA compared to the control ones and they can be identified through classical proteomic approaches [16]. Here, non-denatured mitochondrial lysates from HeLa cells were incubated with PXA for 1 h (from 1 to 100 µM), and then treated with subtilisin in controlled conditions of pH, time and temperature. The samples were resolved by SDS-PAGE and revealed by *Coomassie* (Figure 1B and Figure S1): following the densitometric analysis in Figure 1C, those bands whose intensity enhanced in the lanes containing increasing concentration of PXA were cut (see red dotted lines, Figure 1B) and digested as reported by Shevchenko [16]. The entire experimental flowchart has been repeated twice and all of the samples were analyzed through nano-ultra performance liquid chromatography coupled to high resolution tandem mass spectrometry (nano-UPLC-MS/MS), followed by Mascot database search, to obtain protein identification. In order to estimate, in a semi-quantitative way, the PXA protection levels calculating a protection percentage, Mascot protein matches outputs (Table S1) were compared for all identified proteins at their own molecular weight. The proteins whose protection was clearly dependent on PXA were comprised in the list of its putative interacting partners (Figure 1D); namely they are acetyl-CoA acetyltransferase (THIL), aconitate hydratase (ACON), carbamoyl-phosphate synthase-1 (CPS1) and heat shock 70 kDa protein 1A (HSP71A). The direct contact of PXA with its putative targets, and accordingly their low susceptibility from subtilisin, was then verified by Western Blotting analysis: the partially digested samples were mixed with appropriate antibodies to have a better quantitative measurement of the PXA protection grade, independent by mass spectrometry (Figure 1E). Indeed, the comparison of PXA treated samples showed increasing intensities (from left to right) of both CPS1 and HSP71A corresponding bands (MW of 160 and 70 kDa, respectively), while a significant variation of signal intensity was evident neither for ACON nor for THIL. A densitometric analysis has been carried out, using GAPDH (Glyceraldehyde 3-phosphate dehydrogenase) as loading control (Figure S2). Since

HSP71A is principally localized in the cellular nucleus and cytoplasm, the characterization of PXA binding to the mitochondrial enzyme CPS1 has been carried out.

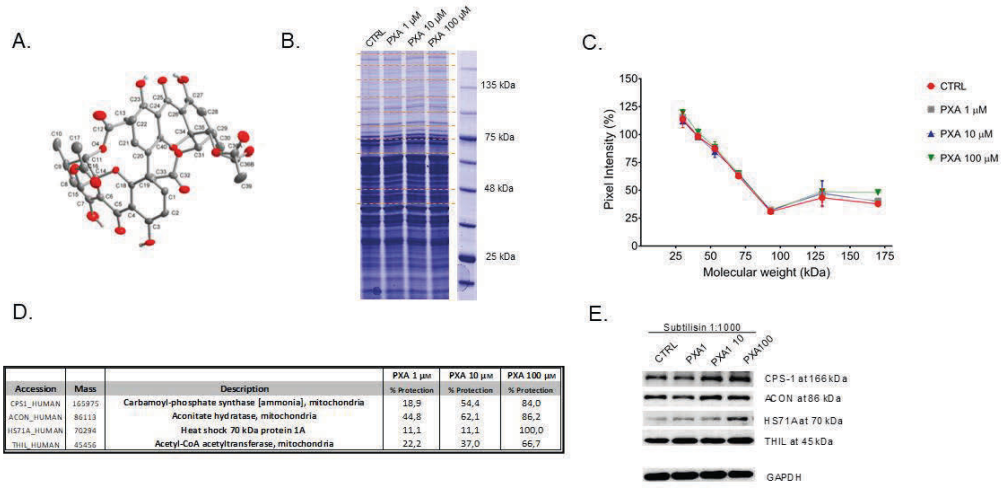

Accession	Mass	Description	PXA 1 µM % Protection	PXA 10 µM % Protection	PXA 100 µM % Protection
CPS1_HUMAN	165975	Carbamoyl-phosphate synthase [ammonia], mitochondria	18,9	54,4	84,0
ACON_HUMAN	86113	Aconitate hydratase, mitochondria	44,8	62,1	86,2
HS71A_HUMAN	70294	Heat shock 70 kDa protein 1A	11,1	11,1	100,0
THIL_HUMAN	45456	Acetyl-CoA acetyltransferase, mitochondria	22,2	37,0	66,7

Figure 1. (A) Phomoxanthone A (PXA) structure. (B) Coomassie stained gel of samples treated without (CTRL) or with 1 µM, 10 µM or 100 µM of PXA and subtilisin at 1:1000 (w/w). Red lines indicate gel regions digested on one SDS-PAGE, as an example. (C) Densitometric analysis of the SDS-PAGE gels in Figure S1 reported, through GraphPad Prism, as pixel intensity of each gel region vs molecular weight. The major variation of pixel intensity of PXA treated samples can be observed at MW higher than 75 kDa. For some points, the error bars would be shorter than the height of the symbol, thus Prism does not draw them. (D) List of putative PXA interacting proteins together with % of protection calculated as (matches of PXA treated sample – matches of control sample)/(matches of undigested lysate – matches of control sample)*100. (E) Immunoblotting analysis with opportune antibodies using subtilisin at 1:1000 (w/w). GAPDH has been used as a loading normalizer.

3.2 Analysis of PXA/targets interaction area by t-LiP-MRM.

DARTS allows to identify the putative interactome of PXA; following t-LiP-MRM has been applied on CPS1 in order to go in the deep in the interaction features. Indeed, t-LiP-MRM allows the identification of the target/ligand interaction peptides due to the protein structural changes induced by the small molecule, without any purification of the protein itself in a whole cell lysate.

This protocol is based on a double-protease digestion procedure: in a first step the proteolysis by an unspecific enzyme is carried out in limited conditions on native samples; afterwards, the sample are denatured and fully hydrolysed by trypsin. Thus, a mixture of semi-tryptic and fully tryptic peptides is produced, the latter suitable for targeted MRM-MS and quantification analysis. Definitely, fully tryptic peptide abundances are related to the target local conformational changes due to ligand binding. More in the deep, an *in silico* search using the bio-informatics tool Peptide Atlas allows to write the MRM methods, setting the best MRM transitions of the theoretical CPS1 fully tryptic peptides to map the protein sequences.

Next, mitochondria lysate samples were incubated with 1 and 10 µM PXA or vehicle (negative control) and treated with subtilisin at 1:1500 w:w enzyme to proteins ratio, under non-denaturing conditions. Then, samples were denatured and submitted to a complete tryptic digestion, giving peptides mixtures suitable for UPLC-MRM-MS analysis. Comparison of intensities of the fully tryptic peptides of PXA treated and untreated runs revealed the interaction regions between PXA and CPS1, namely the peptides protected from subtilisin action. Peptides whose intensity raised up in the samples exposed to the molecule were selected as symptomatic of protection on specific CPS1 regions (Figure 2A). In particular, peptides mapping for CPS1 interaction sites were identified around different regions: peptides G-[275-286]-K, V-[491-505]-R, I-[519-533]-K, A-[534-545]-R, I-[699-709]-K,

I-[1033-1043]-R, S-[1048-1058]-K, F-[1109-1115]-R resulted to be protected by both concentrations of PXA in three experiments. The first peptide resides in the so called S2 region and the following four peptides belong to the active bicarbonate phosphorylation site (L1 region, Figure 2B). Moreover, the latter three peptides belong to the so-called carbamate phosphorylation site, the other CPS1 catalytic site (L3 region, Figure 2B). Thus, even though no data about the stoichiometry of the complex between CPS1 and PXA were obtained, it seems that PXA can interact on the protein surface within different sites, promoting the protection of several peptides in L1, L3 and S2 (Figure 2B).

A.

Q1_m/z	Peptide	rt	Fold change at PXA 1 µM	pvalue	Fold change at PXA 10 µM	pvalue
663,36	G-[275-286]-K	6,7 min	1,73	0,0001	1,74	0,0003
804,4	V-[491-505]-R	9,58 min	1,77	0,0013	1,84	0,0008
795,43	I-[519-533]-K	12,45 min	2,57	0,0338	2,40	0,0473
653,85	A-[534-545]-R	9,13 min	1,30	0,0016	1,25	0,0033
582,37	I-[699-709]-K	11,24 min	1,23	0,0179	1,20	0,0422
615,83	I-[1033-1043]-R	8,04 min	1,44	0,0011	1,41	0,0013
611,34	S-[1048-1058]-K	13,44 min	1,88	0,0001	1,85	0,0001
433,22	F-[1109-1115]-R	5,05 min	1,34	0,0235	1,28	0,0315

B.

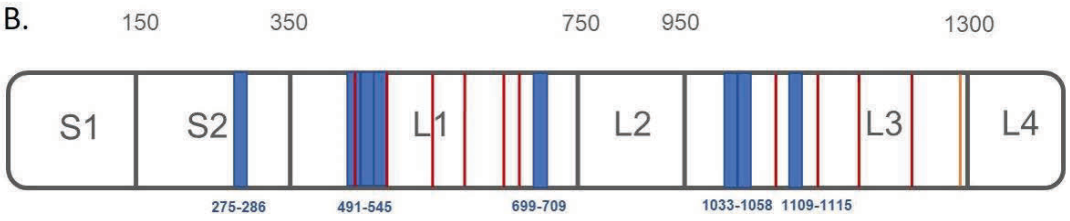

Figure 2. (A) Selected CPS1peptides reported with their Q1 m/z value, their length, the retention time in UPLC-MS and the calculated fold changes. The fold change represents the ratio between the area of the tryptic peptide in PXA treated sample and the area of the tryptic peptide in untreated sample. The same experiments have been repeated three times and the fold changes were calculated over the means of peptides area. P-values have been calculated and only tryptic peptides with a p value <0.05 are reported. (B) A schematic CPS1 cartoon covering different domains is depicted in gray, with the LiP protected peptides highlighted in blue, ADP binding sites residues in red (T502, E503, R505, M543, R545, E581, K582, V584, E589, M614, H617, Q658, E672, N674, R676 and R679, R1087, K1126, V1128, E1133, H1160, Q1201, E1213, R1217, R1220) and T'-loop in orange (P1269-G1291).

3.3 Molecular docking analysis of PXA/CPS1 complex.

In parallel, a molecular docking analysis of PXA on CPS1 protein has been performed using the 3D structure of the human protein with a resolved crystallographic structure (pdb ID 5DOU) [17–20]. On the basis of the predicted affinity, PXA shows best interaction poses into three different protein binding sites: in particular, as reported in Figure 3A, PXA interacts with the aminoacids R738, H775, I944, N1021, R1195, into the interspace between the L2 and L3 region, with a K_D of 27.2 µM; with the aminoacids N894, W898 and Q923, in the L2 region, with a K_D of 4.42 µM; and with the aminoacids K77, Y78, N188, M666 into the interspace between S2 and L1 region, with a K_D of 2.84 µM. Comparing

the t-LIP-MRM data with those obtained by molecular docking, it seems clear that the L3 region of CPS1 undergoes a conformational variation, identified as a protection from proteolysis by t-LIP-MRM namely the peptides I-[1033-1043]-R, S-[1048-1058]-K, F-[1109-1115]-R, due to a direct interaction within PXA, inferred by molecular docking (Figure 3B). In addition, the L1 region seems to be sheltered from proteolysis by t-LIP-MRM even if, accordingly to molecular docking data, PXA doesn't lie in close proximity of this region but, possibly, inducing a middle term conformational variation (Figure 3B). On the other side, no experimental t-LIP-MRM evidences corroborate the molecular docking-based interaction of PXA in between L2 and S1 cavity. In Figure 2B, the aminoacids of two active sites of the protein (in L1 and L3 domains) are reported in red: those of the L1 domain involved in the binding of the nucleotide and phosphate are T502, E503, R505, M543, R545, E581, K582, V584, E589, M614, H617, Q658, E672, N674, R676 and R679, those of L3 domain are R1087, K1126, V1128, E1133, H1160, Q1201, E1213, R1217, R1220. Looking at the putative PXA interaction sites disclosed by docking analysis or t-LIP-MRM (Figure 3A and B), it seems that two of them (in proximity of L3 and L2) are allosteric binding sites whereas the PXA binding site reported in L1 domain (K_D of 2.84 uM) can be considered orthosteric since the residues T502, E503, R505, M543, R545 of the active sites are in two peptides protected in t-LIP experiments. [20].

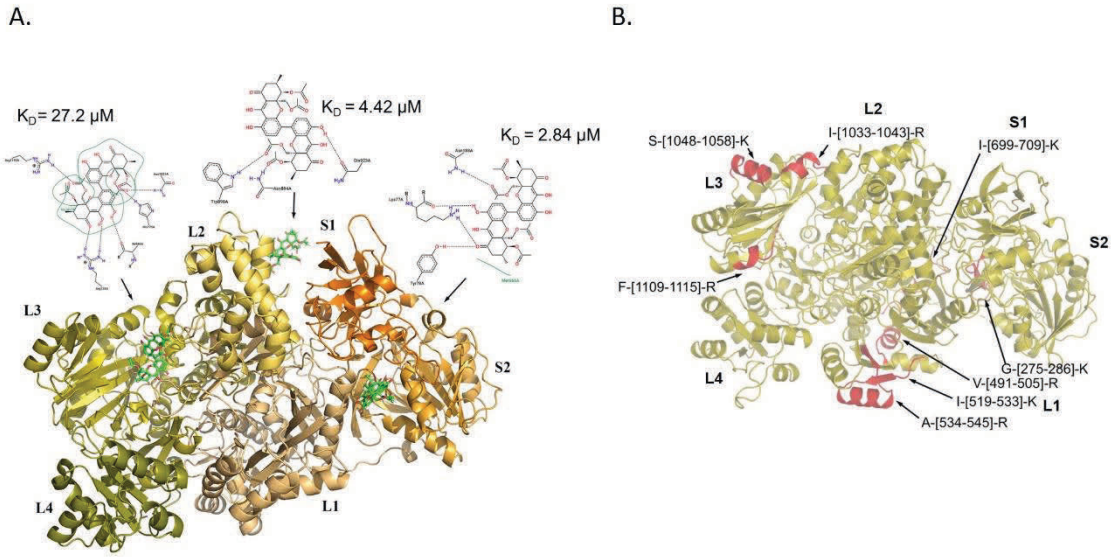

Figure 3. (A) The three best predicted complexes between PXA and CPS1 obtained using the molecular docking. CPS1 regions, showed in cartoon mode, are labelled and reported with different colors. Equilibrium dissociation constants K_D for each binding pose and the aminoacids involved in the interaction with PXA (showed as green sticks) are reported in the 2D pose depictions. (B) CPS1 3D structure is depicted in gold and the PXA protected peptides identified by t-LiP-MRM in red and marked with the corresponding identifiers.

3.4 CPS-1 in vitro activity assay.

Finally, *in vitro* activity assays were performed to monitor the effect of PXA on CPS1 activity. Human CPS1 is a 1462 amino acids, 160-kDa multi-domain mitochondrial, liver and intestinal enzyme. It catalyzes the biosynthesis of carbamoyl phosphate (the first reaction of the urea cycle) in a multi-components reaction ($2ATP + NH_3 + HCO_3^- \rightarrow 2ADP + Pi +$ carbamoyl phosphate), which

takes place in these sequential steps: bicarbonate phosphorylation, synthesis of carbamate and its phosphorylation. CPS1 is inactive in its apo-form and requires N-acetyl-L-glutamate (NAG) to reach an active conformation [26]. Its activity is correlated with many cellular functions and its dysfunction or deficit leads to many pathological conditions. In mammals, surplus nitrogen, mainly from protein catabolism, is mainly detoxified in the urea cycle: this pathway is responsible for ammonia detoxification and for endogenous arginine synthesis [26]. On the other side, CPS1 deficiency (CPS1D) generates urea cycle disorders (UCDs), a set of inborn diseases linked to nitrogen detoxification, which can undergo to hyperammonemia [27–29]. Unless promptly treated, it can generate encephalopathy, coma and death. Current treatment of CPS1D includes the use of N-carbamyl-L-glutamate, the commercial analogue of NAG, improving *in vitro* and *in vivo* the function of the enzyme. In order to test the effect of PXA on CPS-1 activity, an *in vitro* colorimetric assay has been developed. The reaction mixture containing CPS1, ATP and NAG was run for 10 min at 37°C [30] in presence and in absence of PXA at concentrations from 7.5 μg/ml to 375 μg/ml. The resulting carbamyl phosphate was converted to hydroxyurea by the addition of hydroxylamine and the reaction was stopped by heating the samples. To evaluate the hydroxyurea concentration, a chromogenic reagent was added and the mixtures were loaded, in triplicate, in a 384-multiwell plate to measure the absorbance at 458 nm. As it is clearly shown in Figure 4, high PXA concentrations are able to significantly increase CPS1 enzymatic activity up to threefold. Since the peptide F-[1109-1115]-R, whose protease susceptibility has been altered by PXA, is in spatial proximity to the so-called T'-loop which undergoes to a conformational variation upon NAG binding 'opening' a tunnel channel for carbamate translocation, [20] it may be speculated that PXA favours this opening acting positively on CPS1 activity.

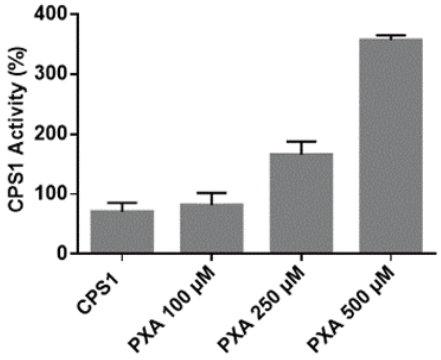

Figure 4. CPS1 activity measured as reported above in presence of different PXA concentrations. The data are shown as % of CPS1 activity. The experiments have been repeated three times and S.D. has been calculated. Opportune controls were carried out as the measurement of the signal of PXA alone at different concentrations (see also Figure S4).

4. Conclusions

PXA and other phomoxanthones are secondary metabolites typical for the fungal genus *Phomopsis* [2]. Chemically, PXA is a homodimer of two tetrahydroxanthones with the two units covalently linked to each other via a biaryl bond with four hydroxy groups replaced by acetyl groups and four free alcoholic (phenolic) functions. The site of the bond between the two dimer subunits is the only structural difference between PXA and its less toxic isomers phomoxanthone B and dicerandrol C: in PXA, the two xanthonoid monomers are symmetrically linked at the position C-4,4'. Notably, PXA is unstable in polar solvents for medium time with the covalent bond between the two monomers shifting between 2,2'-, 2,4'-, and 4,4'-linkage [31,32]. It is interesting that PXA was first identified as an antimalarial compound, revealing its strong antibiotic activity against the protozoan parasite *Plasmodium falciparum*, then against *Mycobacterium tuberculosis* and against two human cancer

cells lines [1] Furthermore, its reported antibiotic activity has been investigated against the alga *Chlorella fusca*, the fungus *Ustilago violacea* and the bacterium *Bacillus megaterium*. This broad range of activity against bacteria, protozoans, fungi, plants and animal cells banned it as a specific antibiotic, promoting, on the other side, its anti-cancer profile since it was more toxic against human cancer cells than non-cancer cells [2–5]. More recently, it has been enlightened that PXA might have an application as a tool in the study of mitochondrial membrane dynamics, particularly non-canonical mitochondrial fission and remodeling of the mitochondrial matrix. Indeed, PXA mainly causes cristae disruption and fragmentation of the matrix [3–5]. Intrigued by its spread biological profile, our MS-based proteomics research moved to the target(s) discovery of this natural compound through a combined strategy consisting of MS-based DARTS and t-LiP-MRM. All the gathered proteomics data, together with molecular docking analysis and biochemical *in vitro* assays, pointed to the unexpected discovery of CPS1 as one of the most reliable PXA partners, together with mitochondrial aconitate hydratase, heat shock 70 kDa protein 1A and mitochondrial acetyl-CoA acetyltransferase. We pointed out our main interest on CPS1 since this mitochondrial enzyme acts a decisive task in get rid of ammonia in excess into cells (mainly in intestinal epithelial cells and hepatocytes) by producing carbamoyl phosphate from ammonium, increasing arginine content and substrate of pyrimidine synthesis in the so called urea cycle. It is also expressed in several types of cancer cells including liver, colorectal, stomach, cervical, and pancreatic cancer cell lines [20]. On the other side, CPS1 deficiency is a rare autosomal genetics-based disease belonging to urea cycle disorders (UCD), producing reduced metabolism of proteins and nitrogen and elevated ammonia levels in the cell. Ammonia is extremely toxic, especially for the nervous system, and high NH_3 levels can result in retardation and convulsions. Moreover, hyperammonemia can happen after birth causing vomiting, hypothermia, seizures and coma. Activation of CPS1 as detoxifying by NAG or its analogues is actually employed as pharmacological strategy, since they improved *in vitro* and *in vivo* the function of CPS1 and mutated isoforms [33]. It is very interesting that low CPS1 expression and hyperammonemia have been measured in Non-Alcoholic Steato Hepatitis (NASH) and Non-Alcoholic Fatty Liver Disease (NAFLD), very common diseases worldwide. Indeed, CPS1 can be considered as a potential novel target for prevention of progression of both diseases: mainly, when the liver is affected, the enzymes converting nitrogen into urea are inhibited, leading to the growth of toxic ammonia that determines scratch of tissue development, increasing the risk of disease progression [34,35]. Moreover, it has been reported that chemotherapy might induce hyperammonemia by CPS1 deficiency and, consequently, there is the need for urgent therapeutic strategies addressing a possible secondary urea cycle failure in patients affected by hyperammonemia during chemotherapy and stem cell transplantation [29]. Actually, a natural compound called fisetin, a plant polyphenol from the flavonoid group, has been tested in the treatment of induced hyperammonemic rats showing an increase of expression of several enzymes as CPS1 and a decrease of iNOS and NF-κB p65. It was observed that fisetin normalized ammonia levels, transaminases and alkaline phosphatase in circulation, glutamate and glutamine in brain, and stabilized the circadian locomotor rhythm [36]. On the basis of this study, PXA could be considered an interesting probe for further investigations on the development of a new class of CPS1 positive modulators playing a pharmacological role in the therapy of several human diseases and metabolic disorders.

Supplementary Materials: The following are available online at www.mdpi.com/xxx/s1, **Table S1.** All proteins identified in two independent DARTS experiments together with the mean of their Mascot scores and matches **Figure S1.** DARTS replicate experiments exploited for the densitometric analysis reported in Figure 1C. The left panel of this figure is reported in the manuscript as Figure 1B. Figure S2. Densitometric analysis of immunoblotting reported in Figure 1E was performed through ImageJ and the histograms are the results of the quantitation of the signals from two independent experiments (standard deviations are reported). The undigested protein was rated as 100% in each analysis and GAPDH was exploited as a loading normalizer. **Figure S3**: ADP has been chosen as a known CPS1 ligand. The docking analysis of ADP on CPS1 has been carried out using the identical experimental parameters employed in PXA one. The superimposition is now reported in Figure S3: the light blue cartoon ADP from 5dou is comparable with the green cartoon of ADP conformation obtained by us. Root-mean-square deviation (RMSD) has also been reported. **Figure S4.** CPS1 activity measured by the reported assay in presence of another natural compound (Serratol) as control.

Author Contributions: Conceptualization, B.S., P.P, M.C.M.; methodology, S.C., E.M., J.D., M.M formal analysis, S.C., E.M., J.D., M.M. P.P, B.S., S.W. M.C.M; resources, M.C.M.; data curation, S.C., E.M., M.M.; writing—original draft preparation, S.C., M.C.M; writing—review and editing, P.P, S.W, B.S, M.C.M; funding acquisition, M.C.M, P.P, B.S., P.W. All authors have read and agreed to the published version of the manuscript.

Funding: This research was funded by "MIUR ITALY PRIN 2017 "Intestinal microbiota, bile acids activated receptors and metabolism: development of novel therapeutic targets in the treatment of steato-hepatitis (NASH)." (grant number 2017FJZZRC)". PP, SW and BS are supported by the Deutsche Forschungsgemeinschaft (DFG) within the research training school GRK 2158.

Conflicts of Interest: The authors declare no conflict of interest.

References

1. Isaka, M.; Jaturapat, A.; Rukseree, K.; Danwisetkanjana, K.; Tanticharoen, M.; Thebtaranonth, Y. Phomoxanthones A and B, novel xanthone dimers from the endophytic fungus Phomopsis species. *J. Nat. Prod.* **2001**, *64*, 1015–1018.
2. Rönsberg, D.; Debbab, A.; Mándi, A.; Vasylyeva, V.; Böhler, P.; Stork, B.; Engelke, L.; Hamacher, A.; Sawadogo, R.; Diederich, M.; et al. Pro-apoptotic and immunostimulatory tetrahydroxanthone dimers from the endophytic fungus Phomopsis longicolla. *J. Org. Chem.* **2013**, *78*, 12409–12425.
3. Pavão, G.B.; Venâncio, V.P.; de Oliveira, A.L.L.; Hernandes, L.C.; Almeida, M.R.; Antunes, L.M.G.; Debonsi, H.M. Differential genotoxicity and cytotoxicity of phomoxanthone A isolated from the fungus Phomopsis longicolla in HL60 cells and peripheral blood lymphocytes. *Toxicol. In Vitro* **2016**, *37*, 211–217.
4. Wang, C.; Engelke, L.; Bickel, D.; Hamacher, A.; Frank, M.; Proksch, P.; Gohlke, H.; Kassack, M.U. The tetrahydroxanthone-dimer phomoxanthone A is a strong inducer of apoptosis in cisplatin-resistant solid cancer cells. *Bioorg. Med. Chem.* **2019**, *27*, 115044.
5. Böhler, P.; Stuhldreier, F.; Anand, R.; Kondadi, A.K.; Schlütermann, D.; Berleth, N.; Deitersen, J.; Wallot-Hieke, N.; Wu, W.; Frank, M.; et al. The mycotoxin phomoxanthone A disturbs the form and function of the inner mitochondrial membrane. *Cell Death Dis.* **2018**, *9*, 286.
6. Rix, U.; Superti-Furga, G. Target profiling of small molecules by chemical proteomics. *Nat. Chem. Biol.* **2009**, *5*, 616–624.
7. Margarucci, L.; Monti, M.C.; Tosco, A.; Riccio, R.; Casapullo, A. Chemical Proteomics Discloses Petrosapongiolide M, an Antiinflammatory Marine Sesterterpene, as a Proteasome Inhibitor. *Angew. Chemie Int. Ed.* **2010**, *49*, 3960–3963.
8. Margarucci, L.; Monti, M.C.; Cassiano, C.; Mozzicafreddo, M.; Angeletti, M.; Riccio, R.; Tosco, A.; Casapullo, A. Chemical proteomics-driven discovery of oleocanthal as an Hsp90 inhibitor. *Chem. Commun. (Camb).* **2013**, *49*, 5844–5846.
9. Del Gaudio, F.; Pollastro, F.; Mozzicafreddo, M.; Riccio, R.; Minassi, A.; Monti, M.C. Chemoproteomic fishing identifies arzanol as a positive modulator of brain glycogen phosphorylase. *Chem. Commun. (Camb).* **2018**, *54*, 12863–12866.
10. Chang, J.; Kim, Y.; Kwon, H.J. Advances in identification and validation of protein targets of natural products without chemical modification. *Nat. Prod. Rep.* **2016**, *33*, 719–730.
11. Hwang, H.-Y.; Kim, T.Y.; Szász, M.A.; Dome, B.; Malm, J.; Marko-Varga, G.; Kwon, H.J. Profiling the Protein Targets of Unmodified Bio-Active Molecules with Drug Affinity Responsive Target Stability and Liquid Chromatography/Tandem Mass Spectrometry. *Proteomics* **2020**, e1900325.
12. Morretta, E.; Esposito, R.; Festa, C.; Riccio, R.; Casapullo, A.; Monti, M. Discovering the Biological Target of 5-epi-Sinuleptolide Using a Combination of Proteomic Approaches. *Mar. Drugs* **2017**, *15*, 312.
13. Morretta, E.; Tosco, A.; Festa, C.; Mozzicafreddo, M.; Monti, M.C.; Casapullo, A. Crellastatin A, a PARP-1 Inhibitor Discovered by Complementary Proteomic Approaches. *ChemMedChem* **2020**, *15*, 317–323.
14. Feng, Y.; De Franceschi, G.; Kahraman, A.; Soste, M.; Melnik, A.; Boersema, P.J.; de Laureto, P.P.; Nikolaev, Y.; Oliveira, A.P.; Picotti, P. Global analysis of protein structural changes in complex proteomes. *Nat. Biotechnol.* **2014**, *32*, 1036–1044.
15. Schopper, S.; Kahraman, A.; Leuenberger, P.; Feng, Y.; Piazza, I.; Müller, O.; Boersema, P.J.; Picotti, P. Measuring protein structural changes on a proteome-wide scale using limited proteolysis-coupled mass spectrometry. *Nat. Protoc.* **2017**, *12*, 2391–2410.
16. Shevchenko, A.; Tomas, H.; Havlis, J.; Olsen, J. V; Mann, M. In-gel digestion for mass spectrometric characterization of proteins and proteomes. *Nat. Protoc.* **2006**, *1*, 2856–2860.

17. Hanwell, M.D.; Curtis, D.E.; Lonie, D.C.; Vandermeersch, T.; Zurek, E.; Hutchison, G.R. Avogadro: an advanced semantic chemical editor, visualization, and analysis platform. *J. Cheminform.* **2012**, *4*, 17.
18. Mozzicafreddo, M.; Cuccioloni, M.; Bonfili, L.; Cecarini, V.; Palermo, F.A.; Cocci, P.; Mosconi, G.; Capone, A.; Ricci, I.; Eleuteri, A.M.; et al. Environmental pollutants directly affect the liver X receptor alpha activity: Kinetic and thermodynamic characterization of binding. *J. Steroid Biochem. Mol. Biol.* **2015**, *152*, 1–7.
19. Berman, H.M.; Westbrook, J.; Feng, Z.; Gilliland, G.; Bhat, T.N.; Weissig, H.; Shindyalov, I.N.; Bourne, P.E. The Protein Data Bank. *Nucleic Acids Res.* **2000**, *28*, 235–242.
20. de Cima, S.; Polo, L.M.; Díez-Fernández, C.; Martínez, A.I.; Cervera, J.; Fita, I.; Rubio, V. Structure of human carbamoyl phosphate synthetase: deciphering the on/off switch of human ureagenesis. *Sci. Rep.* **2015**, *5*, 16950.
21. Jones, G.; Willett, P.; Glen, R.C.; Leach, A.R.; Taylor, R. Development and validation of a genetic algorithm for flexible docking. *J. Mol. Biol.* **1997**, *267*, 727–748.
22. Verdonk, M.L.; Cole, J.C.; Hartshorn, M.J.; Murray, C.W.; Taylor, R.D. Improved protein-ligand docking using GOLD. *Proteins Struct. Funct. Genet.* **2003**, *52*, 609–623.
23. Stierand, K.; Maass, P.C.; Rarey, M. Molecular complexes at a glance: automated generation of two-dimensional complex diagrams. *Bioinformatics* **2006**, *22*, 1710–1716.
24. Lomenick, B.; Hao, R.; Jonai, N.; Chin, R.M.; Aghajan, M.; Warburton, S.; Wang, J.; Wu, R.P.; Gomez, F.; Loo, J.A.; et al. Target identification using drug affinity responsive target stability (DARTS). *Proc. Natl. Acad. Sci. U. S. A.* **2009**, *106*, 21984–21989.
25. Lomenick, B.; Olsen, R.W.; Huang, J. Identification of Direct Protein Targets of Small Molecules. *ACS Chem. Biol.* **2011**, *6*, 34–46.
26. Diez-Fernandez, C.; Häberle, J. Targeting CPS1 in the treatment of Carbamoyl phosphate synthetase 1 (CPS1) deficiency, a urea cycle disorder. *Expert Opin. Ther. Targets* 2017, *21*, 391–399.
27. Moonen, R.M.J.; Paulussen, A.D.C.; Souren, N.Y.P.; Kessels, A.G.H.; Rubio-Gozalbo, M.E.; Villamor, E. Carbamoyl phosphate synthetase polymorphisms as a risk factor for necrotizing enterocolitis. *Pediatr. Res.* **2007**, *62*, 188–190.
28. Pekkala, S.; Martínez, A.I.; Barcelona, B.; Yefimenko, I.; Finckh, U.; Rubio, V.; Cervera, J. Understanding Carbamoyl-phosphate Synthetase I (CPS1) deficiency by using expression studies and structure-based analysis. *Hum. Mutat.* **2010**, *31*, 801–808.
29. Laemmle, A.; Hahn, D.; Hu, L.; Rüfenacht, V.; Gautschi, M.; Leibundgut, K.; Nuoffer, J.M.; Häberle, J. Fatal hyperammonemia and carbamoyl phosphate synthetase 1 (CPS1) deficiency following high-dose chemotherapy and autologous hematopoietic stem cell transplantation. *Mol. Genet. Metab.* **2015**, *114*, 438–444.
30. Pierson, D.L. A rapid colorimetric assay for carbamyl phosphate synthetase I. *J. Biochem. Biophys. Methods* **1980**, *3*, 31–37.
31. Qin, T.; Iwata, T.; Ransom, T.T.; Beutler, J.A.; Porco, J.A. Syntheses of Dimeric Tetrahydroxanthones with Varied Linkages: Investigation of "Shapeshifting" Properties. *J. Am. Chem. Soc.* **2015**, *137*, 15225–15233.
32. Elsässer, B.; Krohn, K.; Flörke, U.; Root, N.; Aust, H.-J.; Draeger, S.; Schulz, B.; Antus, S.; Kurtán, T. X-ray Structure Determination, Absolute Configuration and Biological Activity of Phomoxanthone A. *European J. Org. Chem.* **2005**, *2005*, 4563–4570.
33. Kim, J.; Raushel, F.M. Access to the carbamate tunnel of carbamoyl phosphate synthetase. *Arch. Biochem. Biophys.* **2004**, *425*, 33–41.
34. De Chiara, F.; Heebøll, S.; Marrone, G.; Montoliu, C.; Hamilton-Dutoit, S.; Ferrandez, A.; Andreola, F.; Rombouts, K.; Grønbæk, H.; Felipo, V.; et al. Urea cycle dysregulation in non-alcoholic fatty liver disease. *J. Hepatol.* **2018**, *69*, 905–915.
35. Eriksen, P.L.; Vilstrup, H.; Rigbolt, K.; Suppli, M.P.; Sørensen, M.; Heebøll, S.; Veidal, S.S.; Knop, F.K.; Thomsen, K.L. Non-alcoholic fatty liver disease alters expression of genes governing hepatic nitrogen conversion. *Liver Int.* **2019**, *39*, 2094–2101.
36. Subramanian, P.; Jayakumar, M.; Jayapalan, J.J.; Hashim, O.H. Chronotherapeutic effect of fisetin on expression of urea cycle enzymes and inflammatory markers in hyperammonaemic rats. *Pharmacol. Rep.* **2014**, *66*, 1037–1042.

539